Vibration Serviceability of Cold-Formed Steel Floor Systems

by

Sigong Zhang

A thesis
presented to the University of Waterloo
in fulfillment of the
thesis requirement for the degree of
Doctor of Philosophy
in
Civil Engineering

Waterloo, Ontario, Canada, 2017

Author's Declaration

I hereby declare that I am the sole author of this thesis. This is a true copy of the thesis, including any required final revisions, as accepted by my examiners.

I understand that my thesis may be made electronically available to the public.

Abstract

Excessive vibration in response to human activities has been a significant problem associated with lightweight steel floor systems, especially cold-formed steel (CFS) floors. Methods for accurately predicting these vibrations and evaluating floor systems are not readily available to the design community. The limited amount and complexity of research on the vibration serviceability of lightweight steel floor systems have shown an urgent need for further investigation.

The objective of this research is to evaluate how human walking affects the performance of lightweight steel floor systems. Four important aspects that influence floor vibration performance are investigated: rotationally restrained floor joist ends, structural properties of CFS floors, human-structure interactions, and the applicable design guidelines.

The investigation was carried out using an analytical approach in which CFS floor systems are modelled by equivalent orthotropic plates, and the equivalent structural properties are determined by using the Rayleigh method. The method of finite integral transform is extended to obtain the exact series solutions of the bending and vibration of orthotropic plates with rotationally restrained edges. The analytical/numerical results are compared to the results obtained in previous methods and experimental investigations. Then, the significant effects of human occupants on the dynamic properties and responses of lightweight steel floors are examined through the proposed damped plate-oscillator model, which determines frequencies and damping ratios through analytical analysis of coupled floor-occupant systems. The predicted results are compared with previous test results. Three loading models–moving force, moving damped-oscillator, and moving and stationary damped-oscillators are subsequently proposed to obtain the dynamic responses of floor systems to human walking. The analytical results from the three models are compared with the previous test results. After that, parametric studies are conducted on the effects of step frequency, damping ratio, human-to-structure mass ratio, and walking path. The foregoing investigations provide a comprehensive understanding of the dynamic performance of lightweight steel floors affected by human walking. Finally, design guidelines are developed for lightweight CFS steel floors in residential constructions. The floors are classified into three categories based on their fundamental frequencies,

i.e. low-, mid-, and high-frequency floors. For each category, the corresponding design criterion and method are proposed.

It is the author's desire that the contributions made in this thesis research help engineering practitioners better understand the dynamic responses and vibrational characteristics of lightweight CFS floor systems, particularly on human-structure interactions and ultimately lead to the efficient design of lightweight CFS floor systems that resisting the vibration induced by human walking.

Acknowledgements

I would like take this opportunity to extend my deepest gratitude to my professors, friends, and family for their constant support.

First, I must thank my supervisor, Professor Lei Xu. His encouragement and patience have allow me to explore my interests and his guidance ensured that I have the opportunity of challenging myself, improving myself, and becoming mature as a researcher. Working with Professor Xu is such a great pleasure and I have learned so much experience and wisdom from him.

Dr. Lin J. Hu of FPInnovations generously offered enormous suggestions, discussions and help last four years. Her willingness and professional assistance is grateful acknowledged. Thanks also to Professor Ying Hei Chui at the University of Alberta (former professor at the University of New Brunswick) for scanning his thesis and providing valuable suggestions.

I would also like to thank Professor Giovanni Cascante for helping me on the signal processing. Thanks Professor Wei-Chau Xie for providing the TA position of Differential Equation, which inspired me a lot.

I have to thank those made this thesis possible for me. To Jane Russwurm and Mary Mcpherson of Writing Center for they were always there to help my writing and studies. To all my friends and colleagues, including Dr. Bo Li, Dr. Xiaoli Yuan, Dr. Yi Zhuang, Dr. Wei Jiang, Zhen Cai, Jingnan Liu, Wenfu Wang, Shijun Yang and Yang Zhou.

Last but not least, I dedicate this thesis to my love Judy Liu. You are my muse.

To *Judy*

Table of Contents

List of Tables

List of Figures

Nomenclature

2-DOF	Two Degree-of-Freedom
AISC	American Institute of Steel Construction
AISI	American Iron and Steel Institute
ATC	Applied Technology Council
CCFSRG	Canadian Cold-Formed Steel Research Group
CFS	Cold-Formed Steel
CISC	Canadian Institute of Steel Construction
CWC	Canadian Wood Council
HSI	Human-Structure Interaction
MDOF	Multiple Degrees-of-Freedom
OSB	Oriented Strand Board
RMS	Root Mean Square
SCI	Steel Construction Institute, UK
SDOF	Single Degree of Freedom
SJI	Steel Joist Institute
SSMA	Steel Stud Manufacturers Association

1

Introduction

1.1 Background

Cold-formed steel (CFS) floor systems (Fig. 1.1) generally comprise a series of equally spaced CFS joists sheathed with different subfloors such as plywood, oriented strand board (OSB), cementitious board, or corrugated steel deck with lightweight gypsum-based underlayment. They are also referred to as lightweight steel floors, light-gauge steel framings or lightweight steel framings. Throughout the past few decades, CFS floor systems have been increasingly used in residential construction and other light frame construction in North America as a cost-effective alternative to traditional wood-framed floors. Compared to this counterpart, CFS floors are relatively lighter in weight, have less damping and allow for longer spans. However, similar to that of wood-framed floors in residential construction, CFS floor systems are also prone to vibration induced by human activities, typically walking (Fig. 1.2).

Design against perceptible vibrations disturbing the floor occupants is referred as the vibration serviceability in this research. If special design considerations are not taken, this longer span and lighter structure can unfortunately result in vibration serviceability problems that may affect occupant comfort. Furthermore, if this issue is not seriously taken into consideration, there is a risk that the potential market share growth of residential buildings with lightweight structures will diminish (Hagberg et al., 2009).

Over the last half century, vibration serviceability of floors has attracted interest

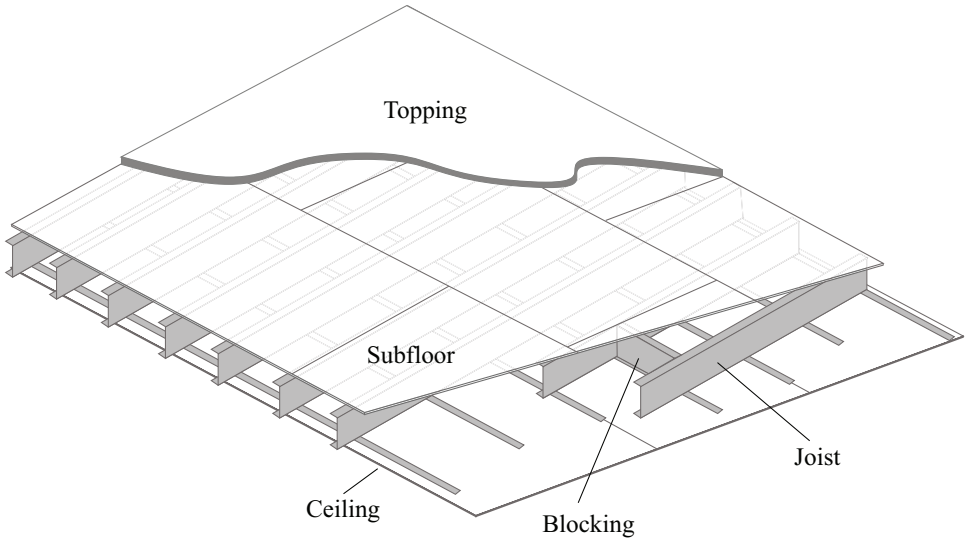

Figure 1.1 Typical CFS floor systems.

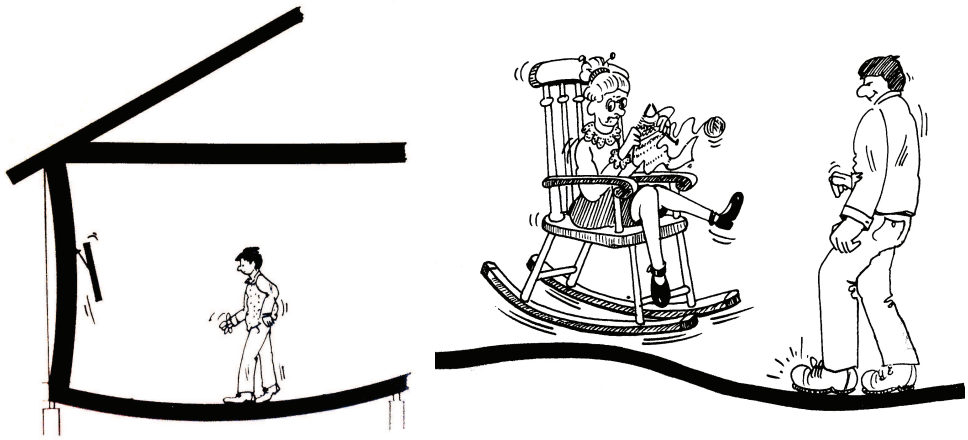

Figure 1.2 Vibration serviceability problem in residential buildings (Ohlsson, 1988a).

from researchers, engineers and regulators. Several design methods were published to enable engineers to ensure human comfort in daily life such as Steel Design Guide 11 (Murray et al., 1997) of the American Institute of Steel Construction/Canadian Institute of Steel Construction (AISC/CISC) for structural steel-framed floor systems, CWC et al. (1997) of Canadian Wood Council for wood-framed floors, and Applied Technology Council (ATC) Design Guide 1 (Allen et al., 1999) for lightweight floor systems. However, although significant developments in CFS joist products and sheathing have occurred, research on vibration serviceability for CFS floor systems is limited. The current design procedures for CFS floor systems are primarily based on that is developed either for wood-framed floors or structural steel floors. The American Institute of Steel Construction (AISI) standards on CFS building construction have been silent on the performance and serviceability requirements of floor vibration due to the limited research. Current AISI S100 (2012) shifts the burden of floor vibration serviceability to other design guides such as AISC/CISC Design Guide 11 and ATC Design Guide 1. However, comparing to the floor systems outlined in both design guides, the nature of being the lighter weight and less damping of CFS floors may alter the dynamic responses of floors and complete buildings, resulting in greater instances of vibration serviceability problems. As a result, vibration serviceability of such floor systems needs separate investigation. An easier and more economical approach is to limit the possibility of this problem in the design stage.

Vibration serviceability of CFS floor systems consists of two aspects: a design criterion related to human acceptability of floors, and a design method to determine the criterion parameters. Currently, the analytical background of vibrations is well developed and understood. Detailed and rigorous computational tools are available to analyze static and dynamic responses of both simple and complex structures. These complex approaches, however, may be beyond the scope of engineers in their daily practice. A simple, practical and comprehensive design criterion and method are desirable for engineers to prevent floor vibration problems in design practice.

1.2 Objectives and Scope of Research

Initiated in 1999, multi-phase tests were carried out at the University of Waterloo by Canadian Cold-Formed Steel Research Group (CCFSRG) for evaluating vibration performance of CFS floor systems (Xu et al., 2000; Xu, 2000, 2001a; Tangorra et al., 2002; Xu,

2005; Xu and Tangorra, 2007; Parnell et al., 2009; Xu, 2011). Full-scale floor systems with different framing configurations were constructed and tested in both laboratory and in situ conditions. The vibration performances of CFS floor systems constructed in current practice were evaluated; critical parameters/details that contribute to the reduction of floor vibrations were identified and discussed; and existing design methods and criteria were examined by test results. Although comprehensive test results have been made towards achieving a better understanding of the performance of CFS floor systems, there is still a lack of reliable theoretical models and adequate design guideline pertinent to vibration serviceability of CFS floor systems due to human occupant activities. The objective of this study is, therefore, to conduct theoretical analyses for investigating the structural properties and vibration performance of lightweight steel floor systems with occupants.

The research has focused on a number of key aspects such as rotational restraints at the joist ends, structural properties of CFS floors, human-structure interactions, and the applicable design criteria as summarised in following:

- Developing a unified and simple method to obtain the exact series solutions of the bending and vibration of orthotropic plates with rotationally restrained edges;
- Determining the structural properties of CFS floor systems in consideration of rotational restraints at the joist ends for vibration analysis;
- Proposing a coupled floor-occupant model to evaluate the dynamic properties of lightweight steel floor systems with occupants and predicting the response of such floor systems under human activities;
- Providing design criteria and methods for CFS floor systems in residential construction.

This research provides better theoretical tools for vibration serviceability of lightweight steel floor systems with a focus on rotationally restrained edges and human-structure interaction. Moreover, the methods developed will not only improve structural analysis of floor structures but also have helped to develop applicable design criteria and approaches to lightweight steel floor systems.

1.3 Thesis Organization

This thesis is divided into seven chapters. The current chapter introduces the research topic. Chapter 2 summarizes the previous studies on vibration serviceability of lightweight steel floor systems, particularly CFS floors. Design criteria, vibration tests and design methods are reviewed. Chapters 3 to 6 discuss the various aspects of vibration serviceability for lightweight steel floor systems. Chapter 3 presents a method of finite integral transform to determine the exact series solutions of the bending and vibration of orthotropic plates with rotationally restrained edges. Chapter 4 models CFS floor systems by equivalent orthotropic plates, and the equivalent structural properties are determined using the Rayleigh method. In Chapter 5, the significant effects of human occupants on dynamic properties and responses of lightweight steel floors (i.e., Human-structure interaction) are examined through the proposed damped plate-oscillator model. The important effects of human occupants on the dynamic properties of flooring systems are addressed by determining the frequencies and damping ratios obtained through analysis of the coupled floor-occupant systems. Three loading models, i.e., the models of moving force, moving damped-oscillator, and moving and stationary damped-oscillators, are subsequently proposed to obtain the dynamic responses of floor systems to human walking. Chapter 6 discusses existing design criteria and proposes design criteria and methods for CFS floor systems in residential construction with demonstrated examples. The final chapter concludes this thesis and provides recommendations for further research.

2

Literature Review

2.1 Introduction

Floor vibration serviceability has been studied extensively from the 1970s in a number of countries, including Australia, Canada, Finland, New Zealand, Norway, Sweden, the United Kingdom, and the USA. Significant progress has been made towards a better understanding of the parameters influencing human perception of vibrations, design approaches for vibration control, floor response to static and dynamic loads, and the influence of components and construction details on vibration performance (Hu et al., 2001). However, the vibration serviceability concerns about lightweight steel floors have not been well addressed in current construction practice. Extensive reviews of floor vibration serviceability are available (Pavic and Reynolds, 2002; Sachse et al., 2003; Ebrahimpour and Sack, 2005). The following review is limited to lightweight floor systems, particularly CFS floor systems, for the design criteria, vibration tests, and design methods.

2.2 Design Criteria

Several design criteria have been proposed for lightweight floor systems (Ohlsson, 1988a; Onysko, 1988a; Smith and Chui, 1988; Allen et al., 1999; Toratti and Talja, 2006) based on long-standing historical practice in wood-framed building construction. Although a general consensus has not been reached, many approaches still have merit.

One of the most widely used criteria–limiting the static deflection of a floor under 1 kN concentrated load– is based on extensive field and laboratory studies of solid sawn lumber joist floors in Canada in the 1970s (Onysko, 1988a,b; Onysko et al., 2000). This criterion was adopted by ATC Design Guide 1 (Allen et al., 1999) for light-frame floors with a natural frequency greater than 8 Hz. The criterion is shown in Fig. 2.1 and is expressed in the international system of units as:

$$\Delta_P \leqslant \begin{cases} 2.0\ mm & for\ L \leqslant 3.0\ m \\ 8.0/L^{1.3} & for\ 3.0\ m < L \leqslant 9.9\ m \end{cases} \tag{2.1}$$

where L is the joist span and Δ_P is the maximum deflection of the floor under a 1 kN concentrated load. It should be noted that the ATC criterion was adjusted in accordance with CWC et al. (1997):

$$\Delta_P \leqslant \begin{cases} 2.0\ mm & for\ L \leqslant 3.0\ m \\ 8.0/L^{1.3} & for\ 3.0\ m < L \leqslant 5.5\ m \\ 2.55/L^{0.63} & for\ 5.5\ m < L \leqslant 9.9\ m \\ 0.6\ mm & for\ L > 9.9\ m \end{cases} \tag{2.2}$$

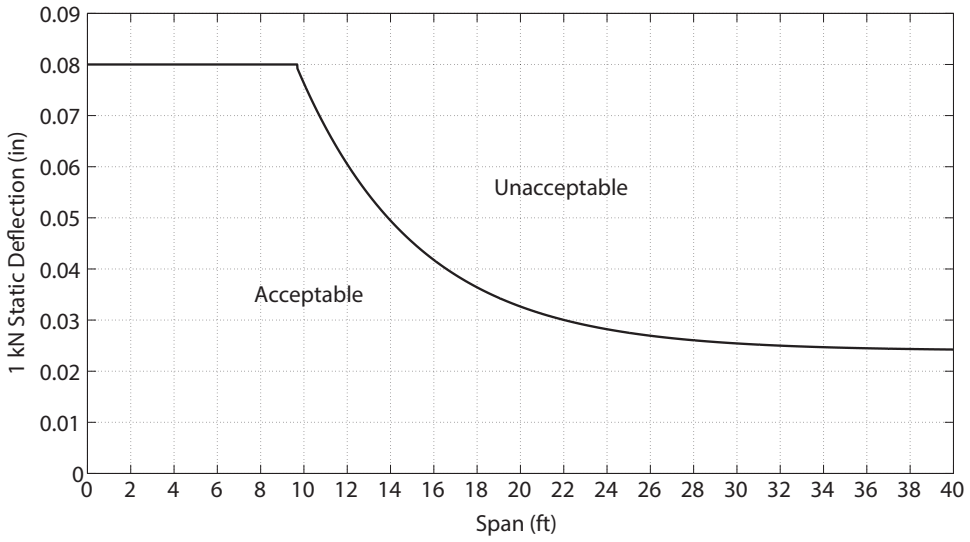

Figure 2.1 ATC design criterion for light-frame floors (Allen et al., 1999).

Ohlsson (1986, 1988a,b) developed a design approach for lightweight floor systems with a fundamental frequency of no less than 8 Hz. The design procedure is independent of the construction material and made relatively simple through the use of several design aids such as flow-charts and diagrams. Four design parameters for stiffness criteria and dynamic serviceability were developed:

1) static deflection w under a point load of 1 kN at mid-span not exceeding 1.5 mm,

2) initial impulse velocity response h'_{max} form a unit impulse = 1 Ns,

3) damping coefficient $\sigma_o = (c/c_{cr}) \cdot f_1$,

4) stationary vibration velocity w'_{RMS} from the force spectrum.

These parameters were presented by Ohlsson (1988a) in detail. This criterion was also adopted by the Australian Standard for Domestic Metal Framing (AS 3623, 1993), with slight modification.

Hu (2002) considered that vibration serviceability will likely involve multiple parameters rather than a single parameter only. Based on the field investigation conducted by the Eastern Laboratory of Forintek Canada Corp., several forms for a tentative criterion were generated by using logistic regression. The proposed forms are the fundamental frequency with 1kN static deflection, fundamental frequency with peak velocity, fundamental frequency with peak acceleration, and fundamental frequency with root mean square (RMS) acceleration. Although some of these combinations showed good potential for use as design criteria, the combination containing fundamental frequency and 1 kN static deflection is easier to calculate and for designers to adopt (Hu et al., 2001). The proposed design criterion was derived from a database of 112 field floors by using logistic regression and is represented as follows

$$\frac{f}{d^{0.39}} > 15.3 \tag{2.3}$$

where d is the calculated maximum static deflection under 1 kN concentrated load at the floor center, and f is the fundamental natural frequency of a wood-framed floor. A further validation study was also conducted by Hu (2002) to assess the robustness of this criterion by using a database of 58 lightweight floors, of which 21 were field floors studied by Forintek and 37 were floor specimens tested and subjectively evaluated by five

Canadian and overseas research laboratories. In particular, 13 of the 37 laboratory floors were built with CFS joists. The comparison of acceptance predicted using the proposed criterion with subjective ratings of the floors in the second database is shown in Fig. 2.2. Similarly, a new design criterion was proposed by Hu and Chui (2004) for wood floors as

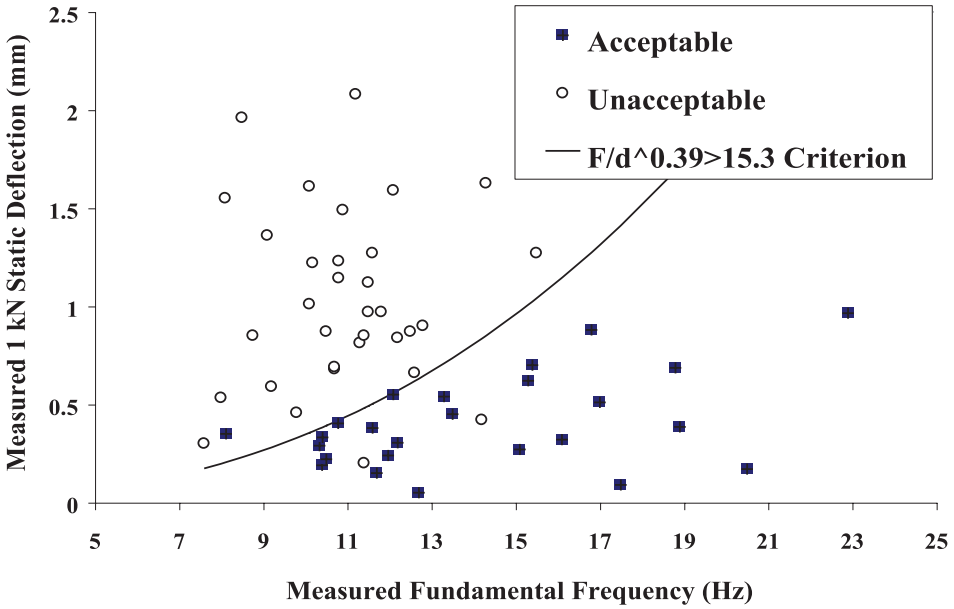

Figure 2.2 Comparison between subjective rating and their predicted acceptance (Hu, 2002).

follows:

$$\frac{f}{d^{0.44}} > 18.7 \tag{2.4}$$

Toratti and Talja (2006) classified floors in residential and office buildings into five categories for floor acceptance based on test data collected over ten years for timber, steel and concrete floors. Table. 2.1 gives their tentative criteria and limiting values to be applied in either the design or testing of floors for the following parameters: the fundamental frequency f_0, the RMS for weighted acceleration $a_{w.rms}$ and for velocity v_{rms} during one second period, the peak vertical displacement $|u_{max}|$, the peak vertical velocity v_{max}, the global displacement of load bearing member δ_0 due to 1 kN point load, and the local displacement δ_l due to 1 kN point load. It was recognized that only the global deflection (δ_0) and the fundamental natural frequency (f_0) can be expected to be estimated accurately by engineers using formulas. The other parameters related to acceptability of a floor performance ($a_{w.rms}$, $|u_{max}|$ and v_{max}) have to be obtained

by testing. In particular, the local deflection δ_l might be the first attempt to consider vibration serviceability caused by soft toppings, floating and raised floors, although the corresponding design methods were not given.

Table 2.1 Tentative acceptance limits for vibration classes (Toratti and Talja, 2006).

Classes	Dynamic vibration values				Static deflection values	
	$f_0 < 10$ Hz		$f_0 > 10$ Hz		$f_0 > 10$ Hz	Floor plate or superstructure
	$a_{w.rms}$ (m/s^2)	v_{max} (mm/s)	v_{rms} (mm/s)	$\|u_{max}\|$ (mm)	δ_0 (mm/kN)	δ_1 (mm/kN)
A	$\leqslant 0.03$	$\leqslant 4$	$\leqslant 0.3$	$\leqslant 0.05$	$\leqslant 0.12$	$\leqslant 0.12$
B	$\leqslant 0.05$	$\leqslant 6$	$\leqslant 0.6$	$\leqslant 0.1$	$\leqslant 0.25$	$\leqslant 0.25$
C	$\leqslant 0.075$	$\leqslant 8$	$\leqslant 1.0$	$\leqslant 0.2$	$\leqslant 0.5$	$\leqslant 0.5$
D	$\leqslant 0.12$	$\leqslant 10$	$\leqslant 1.5$	$\leqslant 0.4$	$\leqslant 1.0$	$\leqslant 1.0$
E	> 0.12	> 10	> 1.5	> 0.4	> 1.0	> 1.0

2.3 Floor Tests

One of the earliest studies on the vibration serviceability of CFS floor systems was those by Wiss et al. (1977).In order to determine the static and dynamic properties of cold-formed steel-joist (CFSJ) floor systems, twelve laboratory floor systems were tested and rated subjectively for the perceptibility of vibration due to human walking. It was found that span length has a notable effect on the human rating but a superimposed live load has no significant effect. No significant difference was found in the human rating between the control wood-framed floor and the CFSJ floors with plywood decks for spans of 16 ft (4.88 m). Dynamic deflection during human walking was considered as the best empirical indicator for the human rating. CFSJ floors with a peak amplitude of dynamic deflection less than approximately 0.005 in. (0.13 mm) were rated in the mid-span, comparable to or better than the control wood-joist floor in terms of human rating.

Since it is known that human acceptance criteria of floor vibration are independent of construction material, the earlier studies for design criteria of CFS floor systems started from adoption or verification of the existing design criteria of wood floors. Kraus (1997) conducted a series of tests on residential floor systems supported by C-shaped CFS members. Dynamic impact and static loading tests were conducted on twelve full-size

laboratory floors and five two-joist line laboratory floors to determine what properties influenced vibration in light-gauge steel framed floors (i.e., CFS floors). The test results were compared with four design criteria:

1) Australian Standard for Domestic Metal Framing (AS 3623, 1993);

2) Swedish Design Guide (Ohlsson, 1988a);

3) American Timber Floor Vibration Criterion proposed by Johnson (1994);

4) Canadian Timber Floor Criterion developed by Onysko et al. (Onysko, 1988a; Onysko et al., 2000).

All laboratory test floors were classified by each criterion, and the results were compared to the subjective evaluation. As a result, the Onysko criterion was recommended for use as a possible criterion for CFS joist residential floors because of its simplicity and satisfactory agreement with test results.

Three different lightweight steel-joist floors were tested by Kullaa and Talja (1999) to study vibration induced by human walking. Experimental modal analysis was applied to identify the dynamic properties of the structures. Walking tests and subjective evaluation were conducted to compare with design criteria proposed by Ohlsson (1988a), Onysko (1988a) and AISC/CISC Design Guide 11 by Murray et al. (1997). They concluded that the deflection criterion proposed by Onysko (1988a) was more satisfactory. Although AISC/CISC method is actually not intended for lightweight floors, this criterion also agrees with the subjective evaluation. The test details can be found in Kullaa and Talja (1998) and Talja and Kullaa (1998) as well.

The Swedish Institute of Steel Construction in cooperation with VTT Building Technology, Steel and Composite Structures summarized six test series with a total of 38 tests on cold-formed C-section supported residential floors and wood-framed floors by sense rating and dynamic measurements (Burstrand and Talja, 2001). The maximum peak displacement of the vibration due to walking was found to correlate best with the rating of floor vibration acceptability and was much better than a static deflection under 1 kN concentrated load. A peak amplitude of 0.2 mm measured from the top surface of the floor was proposed as an acceptance criterion when CFS floors are tested with a walking test.

From 1999 to 2005, six CFS floor systems were tested in the Structures Lab at the University of Waterloo by CCFSRG (Xu, 2000, 2001a, 2005; Liu, 2001; Xu and Tangorra, 2007). In addition, five CFS floor systems were also tested in situ near Toronto, Ontario, in 2002 (Tangorra, 2005), and a wood floor for comparison. In addition to the four design criteria evaluated by Kraus (1997), ATC Design Guide 1 (Allen et al., 1999) was also investigated. The tested CFS floors were evaluated based on these criteria. Onysko method, ATC method, and Johnson's method yielded the same results while the Australian and the Swedish methods were too lax in their respective serviceability criteria (Tangorra, 2005). In the end, a design method based on the ATC Design Guide 1 was proposed. Further experimental studies in the laboratory and the field were conducted by CCFSRG to investigate dynamic characteristics of CFS floor systems and assess the influence of different construction details on those characteristics (Parnell et al., 2009). The actual design and performance of the in-situ floor systems was evaluated by Parnell (2008) based on the RMS heel-drop acceleration criterion developed by Smith and Chui (1988), the ISO acceleration limit for residential occupancy proposed by AISC/CISC Design Guide 11 (Murray et al., 1997), and Onysko's static stiffness criterion defined in ATC Design Guide 1 (Allen et al., 1999).

Rack and Lange (2009) built two types of CFS floor systems in the laboratory, by using C-shaped CFS joists with OSB subfloors. Static and dynamic tests were conducted to obtain the maximum deflection, load sharing capacity and dynamic characteristics. Acceptance limits and construction details were discussed to draw the conclusion that limiting the fundamental frequencies and the dead load and point load deflections do not adequately quantify acceleration and velocity. For a practice-oriented solution, increasing the damping ratio and reducing the dynamic response for a broad spectrum of adaptability are recommended.

Rehman (2014) presented the test results of laboratory and field studies on the vibration of a CFS I-shape joist called "iSPAN" and compared the experimental results with available serviceability design codes. Experimental findings show that the CWC et al. (1997) underestimates 1-kN load deflection but provides accurate results for floor natural frequency. On the other hand, ATC Design Guide 1 does not show general trend in estimating the 1-kN load deflection and floor frequency.

2.4 Design Methods

2.4.1 Deflection under 1 kN concentrated load

In previous studies, the maximum deflection under 1 kN concentrated load was acknowledged as one of the best indicators of floor performance for lightweight floors. Different methods were developed to predict this 1 kN deflection in design practice. Among them, Talja and Kullaa (1998) and Toratti and Talja (2006) developed a method based on the deflection of an orthotropic plate with all edges simply supported. The maximum deflection can be approximated by

$$\delta_{max} = \gamma \cdot \frac{Fl^2}{(EI)_l} \tag{2.5}$$

where

$$\gamma = \frac{4}{\alpha\pi^4} \sum_m \sum_n \frac{1}{(2m-1)^4 + \beta\left(\frac{2n-1}{\alpha}\right)^4} \tag{2.6}$$

In Eq. (2.6), α is the ratio of floor width to length, and β is the ratio of transverse to longitudinal stiffness of the floor. They can be expressed as

$$\alpha = \frac{b}{l},\ \beta = \frac{(EI)_b}{(EI)_l} \tag{2.7}$$

ATC Design Guide 1 (Allen et al., 1999) suggests that the equation for calculating deflection under a concentrated load by adjusting the equivalent beam model in accordance with CWC et al. (1997) should be

$$\Delta_p = \frac{C_{pd}}{N_{eff}} \frac{PL^3}{48EI_{eff}} \tag{2.8}$$

where P is the concentrated load (1kN or 225 lb), L is the joist span length, EI_{eff} is the effective flexural stiffness of a joist panel, N_{eff} is the number of effective joists, and C_{pd} is a joist continuity factor (0.7 for continuous span and 1.0 for single span). The partial composite action was considered in Eq. (2.8) by determining the effective flexural stiffness based on the method in CWC et al. (1997). Meanwhile, ATC Design Guide 1

provides two methods for calculating the number of effective joists, which needed account for load sharing action when determining the coefficient N_{eff}. The first method follows the method of CWC et al. (1997) for wood floors. The second method adopts the design equation in AISC/CISC Design Guide 11 (Murray et al., 1997), which is applicable for open-web steel joists or structural steel beams supporting ribbed concrete decks. The design equation was proposed by Kitterman (1994), who used linear regression analysis for the SAP90 models of 240 floors: 103 open-web steel-joist supported floors and 137 structural-steel-beam-supported floors.

Based on ATC Design Guide 1 with modifications, a design method was proposed by CCFSRG (Tangorra, 2005). First, an end-fixity factor, r, was introduced to account for the partial restraining effects on the joist-end rotations from partitions and load-bearing walls. Therefore, the maximum deflection due to 1 kN concentrated load at mid-span is determined by

$$\Delta_p = \frac{1}{N_{eff}} \frac{L^2}{48EI_{eff}} \left[3\left(M_1 + M_2\right) - PL\right] \tag{2.9}$$

where EI_{eff} is the effective flexural stiffness, N_{eff} is the effective number of joists, and M_1 and M_2 are end moments expressed as

$$\begin{aligned} M_1 &= \frac{3r_1}{8\left(4 - r_1 r_2\right)} \left[2 - r_2\right] PL \\ M_2 &= \frac{3r_2}{8\left(4 - r_1 r_2\right)} \left[2 - r_1\right] PL \end{aligned} \tag{2.10}$$

in which r_1 and r_2 are end-fixity factors associated with the two ends of a floor joist (Xu, 2001b). In the case that $r_1 = r_2 = 0$, the joist ends are simply supported while $r_1 = r_2 = 1$ indicates the joist ends are fully clamped. The joist ends are considered to be semi-rigidly supported when the values of the end-fixity factors are between 0 and 1. Tangorra (2005) also indicated that the method of calculating N_{eff} in ATC Design Guide 1 is not applicable for the calculation of the effective number of CFS floor systems because the design equation was calibrated with test results obtained from lightweight floors supported by wood joists. Then, a new equation for determining the effective number of joists, N_{eff}, was developed as

$$N_{eff} = 3.6e^{\alpha} \tag{2.11}$$

$$\alpha = -\left\{\alpha_0 + \alpha_1 \frac{L}{D} + \alpha_2 \left[1 - \left(\frac{254}{D}\right)^{0.5}\right] - 2\left[1 - \left(\frac{s}{400}\right)^{0.4}\right]\right\} \tag{2.12}$$

where D is depth of floor joist (mm); L is floor span (mm); s is joist spacing (mm); and α_0, α_1 and α_2 are coefficients calibrated with the laboratory test results. Eq. (2.11) was based on the assumption that the concentrated load was primarily resisted by the four joists located near the center of the floors. A modified formulation for the calculation of the effective flexural stiffness, EI_{eff}, was developed for considering the presence of ceiling material.

2.4.2 Fundamental frequency

The method proposed by Ohlsson (1988a) was suggested by Talja and Kullaa (1998) to calculate the fundamental natural frequency of lightweight steel floors. The frequency can be approximated by

$$f_0 = \frac{\pi}{2l^2}\sqrt{\frac{(EI)_l}{m}} \tag{2.13}$$

where m is the floor mass per unit area, l is the length of the floor, and $(EI)_l$ is the longitudinal floor stiffness per unit length. In many cases, the edge condition parallel to the floor joist may be neglected (Toratti and Talja, 2006).

Kraus (1997) recommended the method proposed by Johnson (1994) to predict the fundamental frequency of a CFS floor. The fundamental frequency is obtained by calculating the frequency of a representative T-beam in the floor system as follows:

$$f = 1.57\sqrt{\frac{386EI}{WL^3}} \tag{2.14}$$

where E is the modulus of elasticity (lb/in^2), I is the transformed moment of inertia of the T-beam model (in^4), L is the span (in), and W is the weight supported by the T-beam (lb), calculated based on the tributary width of the beam.

Liu (2001) developed the equivalent orthotropic plate to evaluate the maximum deflection of a floor system and compared the results with those of finite element modelling and ATC Design Guide 1. However, no corresponding design method was proposed. Tangorra (2005) proposed a modification method based on ATC Design Guide 1 by introducing the end-fixity factor, r , to model the restraints provided by walls on joist end-

rotations. The fundamental frequency can be expressed in terms of mid-span deflection by

$$f = 0.18\sqrt{\frac{g}{\Delta_j}} \tag{2.15}$$

where g is acceleration due to gravity and Δ_j is a static deflection of a beam under a uniformly distributed load (UDL), which can be determined similar to Eq. (2.9) as

$$\Delta_{j,r} = \frac{L^2}{8EI_{eff}}\left[(M_1 - M_2) - \frac{5WL^2}{48}\right] \tag{2.16}$$

in which

$$\begin{aligned} M_1 &= (WL^2/12)\left[3r_1\left(2 - r_2\right)/\left(4 - r_1r_2\right)\right] \\ M_2 &= -\left(WL^2/12\right)\left[3r_2\left(2 - r_1\right)/\left(4 - r_1r_2\right)\right] \end{aligned} \tag{2.17}$$

Parnell (2008) examined the methods of evaluating floor frequency in ATC Design Guide 1 and AISC/CISC Design Guide 11, which were both derived based on a single degree of freedom (SDOF) beam model. In addition, a frequency-evaluation method proposed by Chui and Hu (2004) based on a ribbed plate from Timoshenko and Woinowsky-Krieger (1959) was also studied. As shown in Table 5-4 in Parnell (2008), floor frequencies evaluated by all of the three methods were found to be significantly over-predicted. However, the methods are generally more accurate when the estimated frequency does not exceed approximately 13 Hz, indicating that the methods tend to be more accurate for long-span floors.

2.4.3 Dynamic response

Occupants' perception of vibration was correlated with vibration magnitude, a frequency component, and vibration damping. However, although a number of dynamic tests were conducted on CFS floor systems, very few research studies have investigated dynamic criteria of CFS floor systems affected by human walking. For residential construction, both AISC/CISC Design Guide 11 and ATC Design Guide 1 suggested that a minimum floor stiffness is needed for a floor subjected to a 1 kN concentrated load when the fundamental frequency of a floor is greater than 9-10 Hz. This requirement is in addition to the resonance criterion proposed for steel construction with a fundamental frequency less than 8 Hz.

Parnell (2008) proposed to check the resonant RMS acceleration from walking excitation by using the method provided in ATC Design Guide 1 (the same as AISC/CISC Design Guide 11). The response threshold for residential construction is $0.5\%g$. However, this acceleration limit was proposed for peak acceleration based on the experience of various investigators with long-span steel and concrete floors. The limit is highly questionable when it is used for RMS acceleration of CFS floor systems.

2.5 Summary

Accumulated studies have been carried out during the last 20 years on the vibration serviceability of CFS floor systems. Extensive research on wood-framed floors has promoted better understanding of the vibration performance of lightweight floor systems. Limiting static deflection under concentrated load has been proved one of the best evaluation methods for CFS floor systems. However, the method of predicting this deflection still needs further investigation focusing on transverse flexural stiffness and various boundary conditions.

Although many attempts have been made to develop a dynamic response-based method for ensuring vibration serviceability of lightweight floors, a widely accepted method and criteria have not been provided. Moreover, complex issues such as damping evaluation and human-structure interaction are still puzzling researchers and engineering practitioners.

3

Orthotropic Plates with Rotationally Restrained Edges

3.1 Introduction

Among the different proposed design criteria, limiting the centre deflection of the floors under a static concentrated load has been found to be a successful predictor of the vibration performance of lightweight floor systems (Allen et al., 1999; Chui, 2002). Generally, the effectiveness of static deflection criteria depends on factors such as how floors are supported and whether they have significant flexural stiffness in the direction perpendicular to the span (Weckendorf et al., 2015). Furthermore, the fundamental frequency plays a major role in characterizing the dynamic response of a floor system, and needs to be manually calculated in design practice. Design equations for lightweight floor systems (Allen et al., 1999; Dolan et al., 1999) were developed based on the equivalent beam theory. Although this theory is relatively simple and practical, the obtained fundamental frequency may not be accurate, depending on the configuration and support conditions of the floor. Alternatively, lightweight steel floor systems (i.e., CFS floor systems) can be regarded as a thin plate reinforced by a series of equidistant stiffeners on one side with various transverse elements such as strapping, blocking and strongback. In other words, the floor can be simulated as an orthotropic plate. Thus, the orthotropic plate model is adopted to simulate the behaviour of lightweight floor systems.

Experimental investigations reveal that the boundary conditions of lightweight floor

systems in current practice are neither simply-supported nor fully clamped. The common boundary condition of the floor can be best described as elastically restrained against rotation (Xu and Tangorra, 2007). Although bending and vibration of rectangular orthotropic thin plates with various combinations of boundary conditions have been investigated extensively, most previous methods are suitable only for specific boundary conditions. Unlike the large number of investigations on orthotropic plates with either simply-supported and/or clamped boundary conditions, fewer solutions are available for plates with elastically restrained edges. Furthermore, to this author's knowledge, no closed-form solution is available for bending of rectangular orthotropic thin plates with rotationally restrained edges.

In the present chapter, the method of finite integral transforms is employed to solve the bending and vibration of rectangular orthotropic thin plates with rotationally restrained edges (i.e., R-R-R-R). A rotational fixity factor is introduced to define elastic restraints against rotation along edges, and a general boundary condition is presented. The effects of rotational restraints, load patterns and aspect ratios are investigated. The results obtained from the proposed solutions are compared with previously reported results. Furthermore, numerical issues associated with the application of finite integral transform method for the flexure and vibration of orthotropic plates with rotationally restrained edges are discussed. In addition, existing analytical methods are briefly compared and discussed.

3.1.1 Exact series solutions

Over the last few decades, boundary value problems of beams and plates with general boundary conditions have been studied extensively. Among the studies, considerable efforts have been made to obtain the exact analytical solutions for structures with general boundary conditions. Exact series solutions have been derived from different mathematical principles with various procedures. The first notable method was proposed by Wang and Lin (1996) who applied Fourier series to the vibration analysis of beams with general boundary conditions. Subsequently, Wang and Lin (1999) extended the use of the Fourier series to obtain the exact solutions of several structural mechanics problems with arbitrary boundary conditions by transforming the governing differential equations into integral form with sinusoidal weighting functions. Hurlebaus et al. (2001) broadened the use

of the method by Wang and Lin (1996, 1999) to calculate an exact series solution for the free vibration of a completely free orthotropic plate. Other works based on Fourier series were presented in references (Green, 1944; Greif and Mittendorf, 1976; Kim and Kim, 2001; Khalili et al., 2005) and a short review can be found in Maurizi and Robledo (1998). In order to remedy the slow convergence problem of the Fourier series method, an improved (or modified) Fourier series method was proposed by Li et al. (Li, 2000; Li and Daniels, 2002; Li, 2004; Du et al., 2007; Li et al., 2009b; Zhang and Li, 2009; Khov et al., 2009), in which the displacement functions comprise a Fourier series and an auxiliary function (polynomial function or one-dimensional Fourier series), resulting in remarkable convergence and accuracy.

The method of superposition was thoroughly studied by Gorman (1999). In this method, boundary conditions are decomposed into a set of "build blocks" such that analytical solutions can be obtained by means of the generalized Levy method (Gorman and Yu, 2012). Recently, Bhaskar et al. (Bhaskar and Kaushik, 2004; Bhaskar and Sivaram, 2008; Kshirsagar and Bhaskar, 2008) simplified the method of superposition with use of the so-called untruncated infinite Fourier series instead of conventional Levy-type closed-form expressions to obtain accurate results.

Another remarkable analytical tool is the method of finite integral transform. Various types of integral transform were employed to obtain the solutions of a wide variety of boundary value and initial value problems several decades ago. Brown (1943) made a short survey of the applicability of the finite Fourier transformation to engineering problems. Jaramillo (1950) applied a Fourier integral to solve deflections and moments due to a concentrated load on a cantilever plate of infinite length. Amba-Rao (1964) employed a double finite sine transform to investigate the vibration of simply supported rectangular plates carrying a concentrated mass. Magrab (1968) extended Amba-Rao's solution to plates simply supported on two opposite edges with the remaining two edges being simply supported, clamped, or free by using the combination of the finite sine transform and the Laplace transform. Sharp (1967a,b) and Anderson (1969) applied Hankel-type finite integral transforms to vibration analysis of annular membranes and circular plates, respectively. Using finite integral transform, Cobble and Fang (1967) determined the motion of an elastically supported cantilever beam whose wall edge elastically restrained against rotation. Notably, various researchers have recently adopted the double finite

integral transforms to acquire exact series solutions for plates with different complicated boundary conditions, using various integral kernels, such as fully clamped orthotropic plates (Li et al., 2009a), free orthotropic rectangular plates (Zhong and Yin, 2008; Li et al., 2013; Tian et al., 2015), and rectangular cantilever thin plates (Tian et al., 2011). However, flexural and dynamic analysis of a plate with rotationally restrained edges has not been explored with use of the method of finite integral transform.

It should be recognised that even though the aforementioned methods are derived from different mathematical principles with various procedures, the methods are all Fourier-series-based analytical methods. The inversion formulas of finite Fourier transforms are exactly Fourier sine/cosine series. Accordingly, Fourier series expansion and finite Fourier-integral transform are equivalent, but the finite integral transform method is more convenient and automatically involves boundary conditions in the process of conversion. It also can be found that the improved superposition method proposed by Bhaskar et al. (Bhaskar and Kaushik, 2004; Bhaskar and Sivaram, 2008; Kshirsagar and Bhaskar, 2008) literally adopted the same concept by using Fourier series expansion to replace conventional Levy-type expressions in the forms of trigonometric and hyperbolic functions. Nevertheless, the superposition process requires skillful decomposition of the original boundary value problems as well as different formulations for each kind of boundary condition (Li et al., 2009b). Furthermore, in the comparison of the Fourier expansion and finite integral transform method, the improved Fourier series methods developed by Li et al. (Li, 2000; Li and Daniels, 2002; Li, 2004; Du et al., 2007; Li et al., 2009b; Zhang and Li, 2009; Khov et al., 2009) can be quite complicated for some boundary conditions (except classical cases) such as edges elastically restrained against rotations, although the solutions provide accurate results with rapid convergence for arbitrary boundary conditions.

3.1.2 Method of finite integral transform

Over last several decades, integral transformation has been employed to obtain solutions of a wide variety of boundary value and initial value problems (Sneddon, 1972, 1975). This technique simply transforms partial or ordinary differential equations into reduced ordinary differential equations or simple algebraic equations, although a substantial difficulty is present regarding the inversion process (Watanabe, 2014). Various types of integral

transform method have been used successfully to solve many kinds of mixed boundary value problems in engineering. For finite domains, the suitable integral transforms are the finite (Fourier) sine transform and the finite (Fourier) cosine transform.

In the present study, integral transform methods such as finite sine/cosine transform is applied to solve the bending and vibration of orthotropic plates with rotationally restrained edges. An introduction to and details about finite sine/cosine transform, although omitted here, can be found in Debnath and Bhatta (2014) and Churchill (1972). The application of the method of finite integral transform for the solution of vibration problems is considered in Rao (2007). The pair of finite Fourier sine transforms is defined as

$$\bar{f}(m) = \int_0^a f(x) \sin \frac{m\pi x}{a} dx \tag{3.1a}$$

$$f(x) = \frac{2}{a} \sum_{m=1}^{\infty} \bar{f}(m) \sin \frac{m\pi x}{a} \tag{3.1b}$$

Similarly, the pair of finite Fourier cosine transforms is expressed as

$$\bar{f}(n) = \int_0^a f(x) \cos \frac{n\pi x}{a} dx \tag{3.2a}$$

$$f(x) = \frac{\bar{f}(0)}{a} + \frac{2}{a} \sum_{n=1}^{\infty} \bar{f}(n) \cos \frac{n\pi x}{a} \tag{3.2b}$$

Firstly, the application of finite sine/cosine transform in the bending and vibration of orthotropic plates is illustrated by a simple problem in which all sides of Plates are simply supported (i.e., S-S-S-S) as shown in Fig. 3.1. The governing equation for bending of a rectangular orthotropic plate is found in Timoshenko and Woinowsky-Krieger (1959)

$$\nabla_o^4 w = q(x, y) \tag{3.3}$$

where $w(x, y)$ is the transverse flexural displacement, $q(x, y)$ is an arbitrary transverse load, and ∇_o^4 is the biharmonic operator for orthotropic plate, which can be expressed as

$$\nabla_o^4 = D_x \frac{\partial^4}{\partial x^4} + 2H \frac{\partial^4}{\partial x^2 \partial y^2} + D_y \frac{\partial^4}{\partial y^4} \tag{3.4}$$

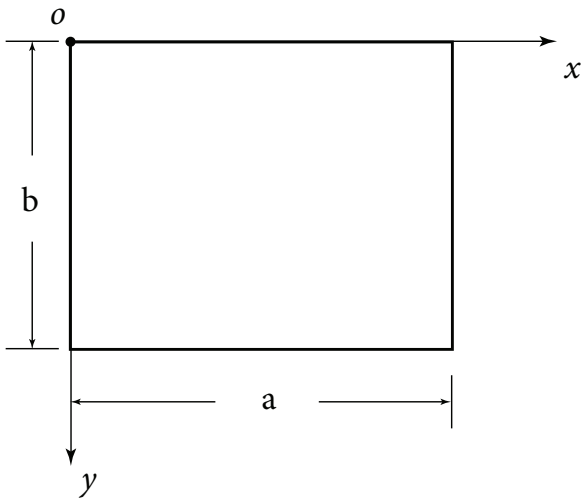

Figure 3.1 Simply supported orthotropic plate.

in which D_x is the flexural rigidity in the x-direction, D_y is the flexural rigidity in the y-direction, $H = D_1 + 2D_{xy}$ is effective torsional rigidity where $D_{xy} = G_{xy}h^3/12$ is torsional rigidity and $D_1 = \nu_x D_y = \nu_y D_x$ is defined in terms of the Poisson's ratios ν_x and ν_y, respectively. For a simply supported plate, boundary conditions are

$$w = 0,\ D_x \left[\frac{\partial^2 w}{\partial x^2} + \nu_y \frac{\partial^2 w}{\partial y^2} \right] = 0, for\ x = 0, a \tag{3.5a}$$

$$w = 0,\ D_y \left[\frac{\partial^2 w}{\partial y^2} + \nu_x \frac{\partial^2 w}{\partial x^2} \right] = 0, for\ y = 0, b \tag{3.5b}$$

It may be noted that if $w = 0$ along the edges $y = 0$ and $y = b$, this guarantees that all derivatives of w in the x-direction ($\partial w/\partial x$, $\partial^2 w/\partial x^2$, etc.) along those edges are zero (Timoshenko and Woinowsky-Krieger, 1959). Then, the boundary conditions can also be expressed as

$$w = 0,\ \frac{\partial^2 w}{\partial x^2} = 0, for\ x = 0, a \tag{3.6a}$$

$$w = 0,\ \frac{\partial^2 w}{\partial y^2} = 0, for\ y = 0, b \tag{3.6b}$$

A concentrated load P at the point (ξ, η) is expressed as

$$q(x,y) = P\delta(x-\xi)\delta(y-\eta) \tag{3.7}$$

where δ is the Dirac delta function. The pair of the double finite sine transforms is defined as

$$\bar{\bar{w}}(m,n) = \int_0^a \int_0^b w(x,y)\sin\alpha_m x \sin\beta_n y dxdy \tag{3.8a}$$

$$w(x,y) = \frac{4}{ab}\sum_{m=1}^{\infty}\sum_{n=1}^{\infty}\bar{\bar{w}}(m,n)\sin\alpha_m x \sin\beta_n y \tag{3.8b}$$

where

$$\alpha_m = \frac{m\pi}{a},\ \beta_n = \frac{n\pi}{b}\ (m=1,2,3,...,n=1,2,3,...) \tag{3.9}$$

Using integration by parts and the boundary conditions of Eqs. (3.6), the double finite sine transforms of the fourth derivatives in Eq. (3.3) can be obtained by

$$\int_0^a \int_0^b \frac{\partial^4 w}{\partial x^4}\sin\alpha_m x \sin\beta_n y dxdy = \alpha_m^4 \bar{\bar{w}}(m,n) \tag{3.10a}$$

$$\int_0^a \int_0^b \frac{\partial^4 w}{\partial x^2 \partial y^2}\sin\alpha_m x \sin\beta_n y dxdy = \alpha_m^2\beta_n^2 \bar{\bar{w}}(m,n) \tag{3.10b}$$

$$\int_0^a \int_0^b \frac{\partial^4 w}{\partial y^4}\sin\alpha_m x \sin\beta_n y dxdy = \beta_n^4 \bar{\bar{w}}(m,n) \tag{3.10c}$$

Taking double finite sine transforms to both sides of Eq. (3.3) and using the property that

$$\int_0^a \int_0^b \delta(x-\xi)\delta(y-\eta)\sin\alpha_m x \sin\beta_n y dxdy = \sin\alpha_m\xi \sin\beta_n\eta \tag{3.11}$$

it can be derived that

$$\bar{\bar{w}}(m,n)\Big[D_x\alpha_m^4 + 2H\alpha_m^2\beta_n^2 + D_y\beta_n^4\Big] = P\sin\alpha_m\xi\sin\beta_n\eta \tag{3.12}$$

or

$$\bar{\bar{w}}(m,n) = \frac{1}{\Omega_{mn}}P\sin\alpha_m\xi\sin\beta_n\eta \tag{3.13}$$

where

$$\Omega_{mn} = D_x\alpha_m^4 + 2H\alpha_m^2\beta_n^2 + D_y\beta_n^4 \tag{3.14}$$

The inverse transform of Eq. (3.13) gives the solution

$$w(x,y) = \frac{4P}{ab} \sum_{m=1}^{\infty} \sum_{n=1}^{\infty} \frac{\sin \alpha_m \xi \sin \beta_n \eta \sin \alpha_m x \sin \beta_n y}{\Omega_{mn}} \tag{3.15}$$

For an arbitrary load of density $f(x,y)$ distributed over an area A inside the region of plates, the corresponding deflection can easily be obtained. Assuming an elementary load $f(\xi,\eta)d\xi d\eta$ at $x=\xi,\ y=\eta$ and using the principle of superposition, the deflection is obtained and has the form

$$w(x,y) = \frac{4}{ab} \sum_{m=1}^{\infty} \sum_{n=1}^{\infty} \frac{\sin \alpha_m x \sin \beta_n y}{\Omega_{mn}} \iint_A f(\xi,\eta) \sin \alpha_m \xi \sin \beta_n \eta d\xi d\eta \tag{3.16}$$

3.1.3 Stokes's transformation

If a function is expanded in a Fourier sine series, the end values of the function are forced to be zero. As a result, the sine series may not actually converge to the true end values of the function. However, if two end points are excluded and defined separately, the end values are released and the function is not forced to be zero at the end points even if it is being represented by a Fourier sine series (Greif and Mittendorf, 1976). In this manner, the function is defined in two separate regions, one involving the end points and the other involving the intermediate region between these end points as

$$f(0) = f_0, \quad f(a) = f_a, \quad f(x) = \sum_{m=1}^{\infty} A_m \sin \alpha_m x \quad (0 < x < a) \tag{3.17}$$

where

$$A_m = \frac{2}{a} \int_0^a f(x) \sin \alpha_m x dx \tag{3.18}$$

After that, the derivative of functions must be handled carefully because term-by-term differentiation may not be valid. Mathematical discussions and proofs on this topic can be found on pages 137-139 in Tolstov (1962) and on pages 375-377 in Bromwich (1965). This differentiation procedure is called Stokes's transformation as shown below.

First, an independent cosine series is formulated for $f'(x)$:

$$f'(x) = B_0 + \sum_{m=1}^{\infty} B_m \cos \alpha_m x \tag{3.19}$$

in which

$$B_0 = \frac{1}{a}\int_0^a f'(x)dx = \frac{f(a) - f(0)}{a} = \frac{f_a - f_0}{a} \tag{3.20a}$$

$$B_m = \frac{2}{a}\int_0^a f'(x)\cos \alpha_m x dx \tag{3.20b}$$

Applying integration by parts gives

$$\int_0^a f(x)\sin \alpha_m x dx = -\frac{1}{\alpha_m} f(x)\cos \alpha_m x\Big|_0^a + \frac{1}{\alpha_m}\int_0^a f'(x)\cos \alpha_m x dx \tag{3.21}$$

and substituting Eq. (3.18) and Eq. (3.20b) into Eq. (3.21) yields

$$\frac{a}{2}A_m = -\frac{1}{\alpha_m}\Big[(-1)^m f_a - f_0\Big] + \frac{1}{\alpha_m}\frac{a}{2}B_m \tag{3.22}$$

Therefore,

$$B_m = \frac{2}{a}\Big[(-1)^m f_a - f_0\Big] + \alpha_m A_m \tag{3.23}$$

Similarly, the second derivative can be defined as

$$f''(x) = \sum_{m=1}^{\infty} C_m \sin \alpha_m x \quad (0 < x < a) \tag{3.24}$$

where

$$C_m = \frac{2}{a}\int_0^a f''(x)\sin \alpha_m x dx \tag{3.25}$$

Applying integration by parts results in

$$\int_0^a f(x)\sin \alpha_m x dx = -\frac{1}{\alpha_m} f(x)\cos \alpha_m x\Big|_0^a + \frac{1}{\alpha_m^2} f'(x)\sin \alpha_m x\Big|_0^a - \frac{1}{\alpha_m^2}\int_0^a \sin \alpha_m x f''(x)dx \tag{3.26}$$

Then, it can be obtained that

$$C_m = -\frac{2}{a}\alpha_m\Big[(-1)^m f_a - f_0\Big] - \alpha_m^2 A_m \tag{3.27}$$

Once the values of $f''(0)$ and $f''(a)$ are known, the coefficient in the Fourier-series for

the fourth derivative $f''''(x)$ can be determined by using the formula

$$E_m = -\frac{2}{a}\alpha_m\Big[(-1)^m f''(a) - f''(0)\Big] - \alpha_m^2 C_m \tag{3.28}$$

The results are summarized below:

$$f'(x) = \frac{f_a - f_0}{a} + \sum_{m=1}^{\infty}\left[\frac{2}{a}\Big[(-1)^m f_a - f_0\Big] + \alpha_m A_m\right]\cos\alpha_m x, \quad (0 \leqslant x \leqslant a) \tag{3.29}$$

$$\begin{aligned} &f''(0) = f_0'', \quad f''(a) = f_a'' \\ &f''(x) = -\sum_{m=1}^{\infty}\alpha_m\left[\frac{2}{a}\Big[(-1)^m f_a - f_0\Big] + \alpha_m A_m\right]\sin\alpha_m x, \quad (0 < x < a) \end{aligned} \tag{3.30}$$

$$\begin{aligned} f'''(x) = \frac{f_a'' - f_0''}{a} + \sum_{m=1}^{\infty}\Bigg\{&\frac{2}{a}\Big[(-1)^m f_a'' - f_0''\Big] \\ &- \alpha_m^2\left[\frac{2}{a}\Big[(-1)^m f_a - f_0\Big] + \alpha_m A_m\right]\Bigg\}\cos\alpha_m x, \\ &(0 \leqslant x \leqslant a) \end{aligned} \tag{3.31}$$

$$\begin{aligned} f''''(x) = -\sum_{m=1}^{\infty}\alpha_m\Bigg\{&\frac{2}{a}\Big[(-1)^m f_a'' - f_0''\Big] \\ &- \alpha_m^2\left[\frac{2}{a}\Big[(-1)^m f_a - f_0\Big] + \alpha_m A_m\right]\Bigg\}\sin\alpha_m x, \\ &(0 < x < a) \end{aligned} \tag{3.32}$$

If the function is expanded in a Fourier cosine series, it yields

$$f(x) = \sum_{n=0}^{\infty} B_n \cos\beta_n y, \qquad (0 \leqslant y \leqslant b) \tag{3.33}$$

$$f'(0) = f_0', \quad f'(b) = f_b', \quad f'(y) = -\sum_{n=0}^{\infty}\beta_n B_n \sin\beta_n y \quad (0 < y < b) \tag{3.34}$$

$$f''(x) = \frac{f_b' - f_0'}{b} + \sum_{n=1}^{\infty} \left[\frac{2}{b} \Big[(-1)^n f_b' - f_0' \Big] - \beta_n^2 B_n \right] \cos \beta_n y, \qquad (0 \leqslant y \leqslant b) \tag{3.35}$$

$$\begin{aligned} &f'''(0) = f_0''', \quad f'''(b) = f_b''' \\ &f'''(x) = -\sum_{n=1}^{\infty} \beta_n \left[\frac{2}{b} \Big[(-1)^n f_b' - f_0' \Big] - \beta_n^2 B_n \right] \sin \beta_n y, \quad (0 < y < b) \end{aligned} \tag{3.36}$$

$$\begin{aligned} f''''(x) = \frac{f_b''' - f_0'''}{b} + \sum_{m=1}^{\infty} \Bigg\{ &\frac{2}{b} \Big[(-1)^n f_b''' - f_0''' \Big] - \\ &\beta_n^2 \left[\frac{2}{b} \Big[(-1)^n f_b' - f_0' \Big] - \beta_n^2 B_n \right] \Bigg\} \cos \beta_n y, \\ &(0 \leqslant y \leqslant b) \end{aligned} \tag{3.37}$$

3.1.4 Rotational fixity factors

In the present research, the rotational restraints are assumed to be proportional to the rotations, and the restraint stiffness may have any value in the range between simply supported (i.e., perfectly hinged) and fully clamped (i.e., completely fixed) conditions. Although the stiffness of such restraints may vary from point to point, the values of restraints are assumed to be uniform along a given boundary for the sake of simplicity .

The rotational spring constant or stiffness, R, is commonly defined to account for the effects of rotational restraints along edges in previous analyses (Li, 2004). Although these constants are straightforward in analyses, they actually have little practical use in determining the flexibility at the edges, because they are not related to the stiffness of a plate. It is difficult to answer “How large a spring constant can represent zero flexibility (i.e., clamped edges) and how small a constant for infinite flexibility (i.e., simply supported edges)?" Bapat et al. (1988) raised this question and attempted to provide the answer, but without signifying that the flexibility does not solely depend on the restraints but also involves the flexural stiffness of plates.

On the other hand, non-dimensional restraint ratios of Ra/D and Rb/D ($R_x a/D_x$

and $R_y b/D_y$ for orthotropic plates) were applied to evaluate the relative stiffness of the plate and the rotational elastic restraints (Laura et al., 1978; Warburton and Edney, 1984). However, as can be seen from the variation of frequencies with the restraint ratios demonstrated in Warburton and Edney (1984), slight changes in frequencies would require significant increases of the restraint ratios when the magnitudes of the ratios are greater than 10^3. Conversely, if the magnitudes of the ratios range between 1 and 10^2, small increases of the ratios would lead to appreciable increases in the frequencies. This highly nonlinear feature associated with the directly use of the ratios is unfavorable in design practice as the structural response, such as frequency in this case, is not proportional to the selected design parameters (i.e., the non-dimensional ratios Ra/D and Rb/D). A similar issue was reported in the design of semi-rigid beam-column members in the framed structures (Cunnigham, 1990; Xu, 2001b).

In this matter, a “fixity factor" was developed for semi-rigid beam-column members to characterise the relative stiffness between the member and the rotational spring of the end-connection, as in Monforton and Wu (1963)

$$r = \frac{1}{1 + 3\dfrac{EI}{RL}} \tag{3.38}$$

in which R is the end-connection spring stiffness and EI/L is the flexural stiffness of the beam-column member. The physical meaning of the fixity factor, r, can be interpreted as the ratio of the beam end's rotation under a unit end moment divided by the rotation of the beam plus the connection spring, for the same unit end moment as that shown in Fig. 3.2. The far end of the beam is simply supported.

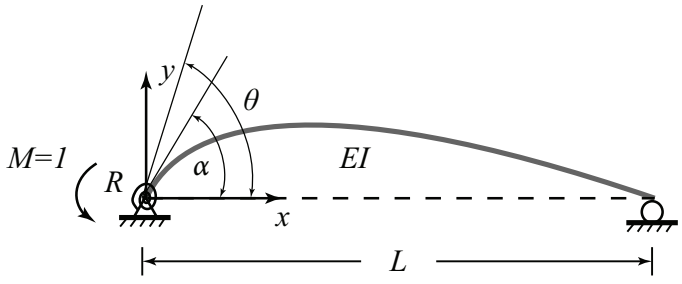

Figure 3.2 Definition of the end-fixity factor.

From the illustration of Fig. 3.2, this factor can be derived as

$$r = \frac{\alpha}{\vartheta} = \frac{\alpha}{1/R + \alpha} = \frac{1}{1 + 3\dfrac{EI}{RL}} \tag{3.39}$$

The factor can vary from 0 to 1. The simply-supported or fully clamped condition will be the limiting case with the value of 0 or 1, respectively. This range of values from 0 to 1 provides to engineers an intuitive manner for the extent of fixity available in a connection (Cunnigham, 1990). Moreover, this factor is insensitive to R, and a simple linear model will produce satisfactory results for design practice (Xu, 2001b).

Similar to Eq. (3.38), the rotational fixity factors can also be defined for plates with rotationally restrained edges as

$$r_x = \frac{1}{1 + 3\dfrac{D_x}{R_x a}} \tag{3.40a}$$

$$r_y = \frac{1}{1 + 3\dfrac{D_y}{R_y b}} \tag{3.40b}$$

where D_x and D_y are the flexural rigidities of an orthotropic plate in the x and y - directions, respectively; R_x and R_y are the rotational stiffness along the edges. Thus, the following can be obtained:

$$3 r_x D_x = (1 - r_x) R_x a \tag{3.41a}$$

$$3 r_y D_y = (1 - r_y) R_y b \tag{3.41b}$$

3.2 Bending of R-R-R-R Orthotropic Plates

3.2.1 Formulation and methodology

Consider now an orthotropic rectangular thin plate of span a, width b and thickness h, as shown in Fig. 3.3. The plate is assumed to be rigidly supported against transverse displacement around all the edges and these edges are rotationally restrained (i.e., elastically restrained against rotation).

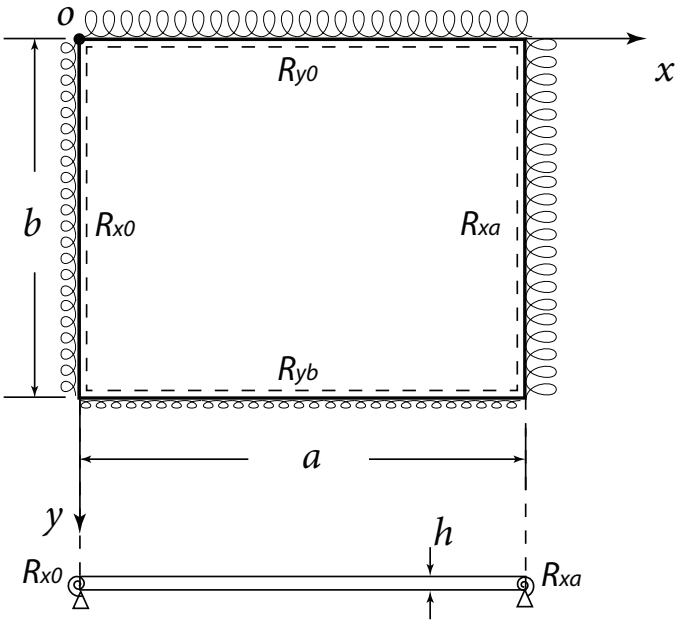

Figure 3.3 Orthotropic plate with four edges rotationally restrained.

The governing equation is Eq. (3.3). Denoting partial differentiation by a comma, the boundary conditions can be written as

$$w = 0,\ M_x = -D_x\left(w_{,xx} + \nu_y w_{,yy}\right) = -R_{x0} w_{,x} \ \ at\ x = 0 \tag{3.42a}$$

$$w = 0,\ M_x = -D_x\left(w_{,xx} + \nu_y w_{,yy}\right) = R_{xa} w_{,x} \ \ at\ x = a \tag{3.42b}$$

$$w = 0,\ M_y = -D_y\left(w_{,yy} + \nu_x w_{,xx}\right) = -R_{y0} w_{,y} \ \ at\ y = 0 \tag{3.42c}$$

$$w = 0,\ M_y = -D_y\left(w_{,yy} + \nu_x w_{,xx}\right) = R_{yb} w_{,y} \ \ at\ y = b \tag{3.42d}$$

It can be noted that the second terms in bending moment M_x and M_y are zero because $w = 0$ along the edges (Timoshenko and Woinowsky-Krieger, 1959). After taking finite sine transform, the boundary conditions in Eqs. (3.42) becomes

$$D_x \bar{w}_{,xx}(0,n) = R_{x0} \bar{w}_{,x}(0,n) \tag{3.43a}$$

$$D_x \bar{w}_{,xx}(a,n) = -R_{xa} \bar{w}_{,x}(a,n) \tag{3.43b}$$

$$D_y \bar{w}_{,yy}(m,0) = R_{y0} \bar{w}_{,y}(m,0) \tag{3.43c}$$

$$D_y \bar{w}_{,yy}(m,b) = -R_{yb} \bar{w}_{,y}(m,b) \tag{3.43d}$$

Applying Eqs. (3.41), Eqs. (3.43) can be rewritten as

$$(1 - r_{x0}) a \bar{w}_{,xx}(0,n) = 3 r_{x0} \bar{w}_{,x}(0,n) \tag{3.44a}$$

$$(1 - r_{xa}) a \bar{w}_{,xx}(a,n) = -3 r_{xa} \bar{w}_{,x}(a,n) \tag{3.44b}$$

$$(1 - r_{y0}) b \bar{w}_{,yy}(m,0) = 3 r_{y0} \bar{w}_{,y}(m,0) \tag{3.44c}$$

$$(1 - r_{yb}) b \bar{w}_{,yy}(m,b) = -3 r_{yb} \bar{w}_{,y}(m,b) \tag{3.44d}$$

Taking double finite sine transforms on both sides of Eq. (3.3) gives

$$\int_0^a \int_0^b \nabla_o^4 w \sin \alpha_m x \sin \beta_n y dx dy = \int_0^a \int_0^b q(x,y) \sin \alpha_m x \sin \beta_n y dx dy \tag{3.45}$$

Using integration by parts and considering the boundary conditions of Eqs. (3.42), the double finite sine transforms of the fourth derivatives in Eq. (3.45) can be obtained (Meirovitch, 1967):

$$\begin{aligned} \int_0^a \int_0^b w_{,xxxx} \sin \alpha_m x \sin \beta_n y dx dy = \alpha_m^4 \bar{\bar{w}}(m,n) \\ - \alpha_m \Big[(-1)^m \bar{w}_{,xx}(a,n) - \bar{w}_{,xx}(0,n) \Big] \end{aligned} \tag{3.46a}$$

$$\int_0^a \int_0^b w_{,xxyy} \sin \alpha_m x \sin \beta_n y dx dy = \alpha_m^2 \beta_n^2 \bar{\bar{w}}(m,n) \tag{3.46b}$$

$$\int_0^a \int_0^b w_{,yyyy} \sin\alpha_m x \sin\beta_n y dxdy = \beta_n^4 \bar{\bar{w}}(m,n) - \beta_n \Big[(-1)^n \bar{w}_{,yy}(m,b) - \bar{w}_{,yy}(m,0) \Big] \tag{3.46c}$$

where coefficients $\bar{w}_{,xx}(0,n)$, $\bar{w}_{,xx}(a,n)$, $\bar{w}_{,yy}(m,0)$ and $\bar{w}_{,yy}(m,b)$ are determined from the finite-sine transformed boundary conditions at four edges by

$$\bar{w}_{,xx}(0,n) = \int_0^b w_{,xx}(0,y) \sin\beta_n y dy \tag{3.47a}$$

$$\bar{w}_{,xx}(a,n) = \int_0^b w_{,xx}(a,y) \sin\beta_n y dy \tag{3.47b}$$

$$\bar{w}_{,yy}(m,0) = \int_0^a w_{,xx}(x,0) \sin\beta_n x dx \tag{3.47c}$$

$$\bar{w}_{,yy}(m,b) = \int_0^a w_{,xx}(x,b) \sin\beta_n x dx \tag{3.47d}$$

Substituting Eqs. (3.46) into Eq. (3.45), the following is obtained

$$\bar{\bar{w}}(m,n) = \frac{1}{\Omega_{mn}} \Bigg\{ \bar{\bar{q}}(m,n) + \alpha_m D_x \Big[(-1)^m \bar{w}_{,xx}(a,n) - \bar{w}_{,xx}(0,n) \Big] + \beta_n D_y \Big[(-1)^n \bar{w}_{,yy}(m,b) - \bar{w}_{,yy}(m,0) \Big] \Bigg\} \tag{3.48}$$

where

$$\Omega_{mn} = D_x \alpha_m^4 + 2H \alpha_m^2 \beta_n^2 + D_y \beta_n^4 \tag{3.49}$$

$$\bar{\bar{q}}(m,n) = \int_0^a \int_0^b q(x,y) \sin\alpha_m x \sin\beta_n y dxdy \tag{3.50}$$

Taking the inverse finite sine transform on Eq. (3.48) with respect to variable x yields

$$\bar{w}(x,n) = \frac{2}{a} \sum_{m=1}^{\infty} \bar{\bar{w}}(m,n) \sin\alpha_m x \tag{3.51}$$

Taking the derivative of Eq. (3.51) with respect to x and using Stokes's transformation, it is found

$$\bar{w}_{,x}(x,n) = \frac{2}{a} \sum_{m=1}^{\infty} \alpha_m \bar{\bar{w}}(m,n) \cos\alpha_m x \tag{3.52}$$

Substituting Eq. (3.44) and (3.48) into Eq. (3.52), the following can be obtained

$$\begin{aligned} a^2(1-r_{x0})\bar{w}_{,xx}(0,n) =& 6r_{x0}\sum_{m=1}^{\infty}\frac{\alpha_m}{\Omega_{mn}}\Bigg\{\bar{\bar{q}}(m,n) \\ &+\alpha_m D_x\Big[(-1)^m\bar{w}_{,xx}(a,n)-\bar{w}_{,xx}(0,n)\Big] \\ &+\beta_n D_y\Big[(-1)^n\bar{w}_{,yy}(m,b)-\bar{w}_{,yy}(m,0)\Big]\Bigg\} \end{aligned} \tag{3.53a}$$

$$\begin{aligned} a^2(1-r_{xa})\bar{w}_{,xx}(a,n) =& -6r_{xa}\sum_{m=1}^{\infty}\frac{(-1)^m\alpha_m}{\Omega_{mn}}\Bigg\{\bar{\bar{q}}(m,n) \\ &+\alpha_m D_x\Big[(-1)^m\bar{w}_{,xx}(a,n)-\bar{w}_{,xx}(0,n)\Big] \\ &+\beta_n D_y\Big[(-1)^n\bar{w}_{,yy}(m,b)-\bar{w}_{,yy}(m,0)\Big]\Bigg\} \end{aligned} \tag{3.53b}$$

Similarly, it is obtained

$$\begin{aligned} b^2(1-r_{y0})\bar{w}_{,yy}(m,0) =& 6r_{y0}\sum_{n=1}^{\infty}\frac{\beta_n}{\Omega_{mn}}\Bigg\{\bar{\bar{q}}(m,n) \\ &+\alpha_m D_x\Big[(-1)^m\bar{w}_{,xx}(a,n)-\bar{w}_{,xx}(0,n)\Big] \\ &+\beta_n D_y\Big[(-1)^n\bar{w}_{,yy}(m,b)-\bar{w}_{,yy}(m,0)\Big]\Bigg\} \end{aligned} \tag{3.54a}$$

$$\begin{aligned} b^2(1-r_{yb})\bar{w}_{,yy}(m,b) =& -6r_{yb}\sum_{n=1}^{\infty}\frac{(-1)^n\beta_n}{\Omega_{mn}}\Bigg\{\bar{\bar{q}}(m,n) \\ &+\alpha_m D_x\Big[(-1)^m\bar{w}_{,xx}(a,n)-\bar{w}_{,xx}(0,n)\Big] \\ &+\beta_n D_y\Big[(-1)^n\bar{w}_{,yy}(m,b)-\bar{w}_{,yy}(m,0)\Big]\Bigg\} \end{aligned} \tag{3.54b}$$

Rearranging Eqs. (3.53) and (3.54) yields

$$\sum_{m=1}^{\infty} A_m^0 \bar{\bar{q}}(m,n) = \beta_n D_y \sum_{m=1}^{\infty} A_m^0 \bar{w}_{,yy}(m,0) - (-1)^n \beta_n D_y \sum_{m=1}^{\infty} A_m^0 \bar{w}_{,yy}(m,b)$$
$$+ \left[a^2(1-r_{x0}) + D_x \sum_{m=1}^{\infty} \alpha_m A_m^0\right] \bar{w}_{,xx}(0,n) - D_x \sum_{m=1}^{\infty} (-1)^m \alpha_m A_m^0 \bar{w}_{,xx}(a,n) \tag{3.55a}$$

$$\sum_{m=1}^{\infty} (-1)^m A_m^a \bar{\bar{q}}(m,n) = \beta_n D_y \sum_{m=1}^{\infty} (-1)^m A_m^a \bar{w}_{,yy}(m,0)$$
$$- \beta_n D_y \sum_{m=1}^{\infty} (-1)^{m+n} A_m^a \bar{w}_{,yy}(m,b) \tag{3.55b}$$
$$+ D_x \sum_{m=1}^{\infty} (-1)^m \alpha_m A_m^a \bar{w}_{,xx}(0,n) - \left[a^2(1-r_{xa}) + D_x \sum_{m=1}^{\infty} \alpha_m A_m^a\right] \bar{w}_{,xx}(a,n)$$

$$\sum_{n=1}^{\infty} B_n^0 \bar{\bar{q}}(m,n) = \left[b^2(1-r_{y0}) + D_y \sum_{n=1}^{\infty} \beta_n B_n^0\right] \bar{w}_{,yy}(m,0)$$
$$- D_y \sum_{n=1}^{\infty} (-1)^n \beta_n B_n^0 \bar{w}_{,yy}(m,b) \tag{3.55c}$$
$$+ \alpha_m D_x \sum_{n=1}^{\infty} B_n^0 \bar{w}_{,xx}(0,n) - (-1)^m \alpha_m D_x \sum_{n=1}^{\infty} B_n^0 \bar{w}_{,xx}(a,n)$$

$$\sum_{n=1}^{\infty} (-1)^n B_n^0 \bar{\bar{q}}(m,n) = D_y \sum_{n=1}^{\infty} (-1)^n \beta_n B_n^b \bar{w}_{,yy}(m,0)$$
$$- \left[b^2(1-r_{ya}) + D_y \sum_{n=1}^{\infty} \beta_n B_n^b\right] \bar{w}_{,yy}(m,b) \tag{3.55d}$$
$$+ \alpha_m D_x \sum_{n=1}^{\infty} (-1)^n B_n^b \bar{w}_{,xx}(0,n) - \alpha_m D_x \sum_{n=1}^{\infty} (-1)^{m+n} B_n^b \bar{w}_{,xx}(a,n)$$

where

$$A_m^0 = 6 r_{x0} \frac{\alpha_m}{\Omega_{mn}} \tag{3.56a}$$

$$A_m^a = 6 r_{xa} \frac{\alpha_m}{\Omega_{mn}} \tag{3.56b}$$

$$B_n^0 = 6 r_{y0} \frac{\beta_n}{\Omega_{mn}} \tag{3.56c}$$

$$B_n^b = 6r_{yb}\frac{\beta_n}{\Omega_{mn}} \tag{3.56d}$$

Eqs. (3.55) are four infinite systems of linear equations with respect to coefficients $\bar{w}_{,xx}(0,n)$, $\bar{w}_{,xx}(a,n)$, $\bar{w}_{,yy}(m,0)$, and $\bar{w}_{,yy}(m,b)$. For each combination of m and n, Eqs. (3.53) and (3.54) produce $2m+2n$ equations with $2m+2n$ unknown coefficients. This set of equations can be solved to find the coefficients in Eq. (3.48). Once these coefficients have been computed, the deflection $w(x,y)$ can be obtained by substituting Eq. (3.48) into Eq. (3.8b). It should be noted that the limiting cases of simply-supported and fully clamped can also be obtained from Eqs. (3.55) by setting $r_{x0} = r_{xa} = r_{y0} = r_{yb} = 0$ and $r_{x0} = r_{xa} = r_{y0} = r_{yb} = 1$, respectively. The corresponding equations for a fully clamped plate are exactly equal to equations presented in Li et al. (2009a).

Furthermore, the bending moments along the edges can be obtained from the following:

$$M_x\Big|_{x=0} = -D_x\left(w_{,xx} + \nu_y w_{,yy}\right)\Big|_{x=0} = -\frac{2}{b}D_x\sum_{n=1}^{\infty}\bar{w}_{,xx}(0,n)\sin\beta_n y \tag{3.57a}$$

$$M_x\Big|_{x=a} = -D_x\left(w_{,xx} + \nu_y w_{,yy}\right)\Big|_{x=a} = -\frac{2}{b}D_x\sum_{n=1}^{\infty}\bar{w}_{,xx}(a,n)\sin\beta_n y \tag{3.57b}$$

$$M_y\Big|_{y=0} = -D_y\left(w_{,yy} + \nu_x w_{,xx}\right)\Big|_{y=0} = -\frac{2}{a}D_y\sum_{m=1}^{\infty}\bar{w}_{,yy}(m,0)\sin\alpha_m x \tag{3.57c}$$

$$M_y\Big|_{y=b} = -D_y\left(w_{,yy} + \nu_x w_{,xx}\right)\Big|_{y=b} = -\frac{2}{a}D_y\sum_{m=1}^{\infty}\bar{w}_{,yy}(m,b)\sin\alpha_m x \tag{3.57d}$$

For any position not located along the edges, the bending moments can be expressed by

$$M_x = -D_x\left(w_{,xx} + \nu_y w_{,yy}\right) \tag{3.58a}$$

$$M_y = -D_y\left(w_{,yy} + \nu_x w_{,xx}\right) \tag{3.58b}$$

where $w_{,xx}$ can be given by using Stokes's transformation as

$$w_{,xx} = -\frac{4}{ab}\sum_{m=1}^{\infty}\sum_{n=0}^{\infty}\alpha_m^2\varepsilon_n\bar{\bar{w}}(m,n)\sin\alpha_m x\cos\beta_n y \tag{3.59}$$

and $w_{,yy}$ can be expressed as

$$w_{,yy} = \frac{2}{a}\sum_{m=1}^{\infty} \bar{w}_{,yy}\,(m,y)\sin\alpha_m x \tag{3.60}$$

The foregoing method is valid for arbitrary loads by various $\bar{\bar{q}}(m,n)$. A concentrated load P at the point (ξ,η), for instance, will have the expression of $\bar{\bar{q}}(m,n)$ as

$$\bar{\bar{q}}(m,n) = P\sin\alpha_m\xi\sin\beta_n\eta \tag{3.61}$$

This is obtained by using the property that

$$\int_0^a\int_0^b \delta(x-\xi)\delta(y-\eta)\sin\alpha_m x\sin\beta_n y dxdy = \sin\alpha_m\xi\sin\beta_n\eta \tag{3.62}$$

Similarly, any one, two or three rotational fixity factors of r_{x0}, r_{xa}, r_{y0}, r_{yb} equal to zero will produce corresponding edges simply supported. For instance, for $r_{y0} = r_{yb} = 0$, plate only have two opposite edges rotationally restrained and the other two edges simply supported. Thus, Eq. (3.48) becomes

$$\bar{\bar{w}}(m,n) = \frac{1}{\Omega_{mn}}\left\{\bar{\bar{q}}(m,n) + \alpha_m D_x\Big[(-1)^m\bar{w}_{,xx}\,(a,n) - \bar{w}_{,xx}\,(0,n)\Big]\right\} \tag{3.63}$$

in which $\bar{w}_{,xx}\,(0,n)$ and $\bar{w}_{,xx}\,(a,n)$ can be determined from a system of linear equations as follows:

$$\begin{aligned} a^2(1-r_{x0})\bar{w}_{,xx}\,(0,n) = 6r_{x0}\sum_{m=1}^{\infty}\frac{\alpha_m}{\Omega_{mn}}\Bigg\{&\bar{\bar{q}}(m,n) \\ &+ \alpha_m D_x\Big[(-1)^m\bar{w}_{,xx}\,(a,n) - \bar{w}_{,xx}\,(0,n)\Big]\Bigg\} \end{aligned} \tag{3.64a}$$

$$\begin{aligned} a^2(1-r_{xa})\bar{w}_{,xx}\,(a,n) = -6r_{xa}\sum_{m=1}^{\infty}\frac{(-1)^m\alpha_m}{\Omega_{mn}}\Bigg\{&\bar{\bar{q}}(m,n) \\ &+ \alpha_m D_x\Big[(-1)^m\bar{w}_{,xx}\,(a,n) - \bar{w}_{,xx}\,(0,n)\Big]\Bigg\} \end{aligned} \tag{3.64b}$$

In addition, the foregoing results for orthotropic plates also apply to the special case of isotropic plates just by replacing the orthotropic constants by their corresponding isotropic values as listed

$$\nu_x = \nu_y = \nu,\ D_x = D_y = H = D,\ D_1 = \nu D \text{ and } D_{xy} = \frac{1-\nu}{2}D \tag{3.65}$$

where D is the flexural rigidity and ν is Poisson's ratio.

3.2.2 Numerical results and discussion

Comprehensive numerical results are presented in this section to validate the foregoing derived analytical procedure. Results of the proposed analytical procedure for both isotropic and orthotropic plates are compared with previously published results. Deflection and bending moments under three types of loading are examined:

1) a uniform distributed load of intensity q;

2) hydrostatic pressure with the intensity qx;

3) a concentrated load P at the center of the plate.

Numerical results associated with the proposed analytical procedure for the foregoing cases are obtained using the MATLAB® software package. For the sake of convenience, the numbers of terms in double series are chosen to be same and denoted by N (i.e., $m,\ n = 1, 2, 3, ..., N$) and four edges have the same values for the rotational fixity factors (i.e., $r_{x0} = r_{xa} = r_{y0} = r_{yb} = r$). The results are theoretically exact when $N \to \infty$, while convergent solutions with satisfactory accuracy can be acquired by a finite number of terms. The convergence rates of the displacement at the plate center ($x = a/2$ and $y = b/2$) and bending moment at the center along the edge of $x = 0$ with respect to N are respectively shown in Fig. 3.4(a) and 3.4(b), for the case of an isotropic plate with four edges rotationally restrained and subjected to a uniform distributed load. The rotational fixity factors are the same along the four edges and set as 0.9. From the results of a convergence study, N is taken as 200 in this study.

The proposed analytical approach to plates with rotationally restrained edges can be applied for plates with general boundary conditions ranging from simply supported to fully clamped with use of appropriate rotational fixity factors. However, for the fully

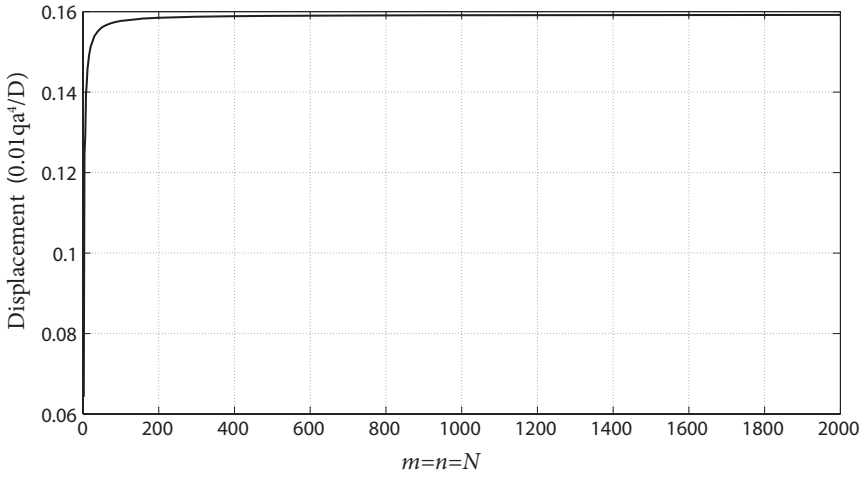

(a) Displacement at $x = a/2$, $y = b/2$

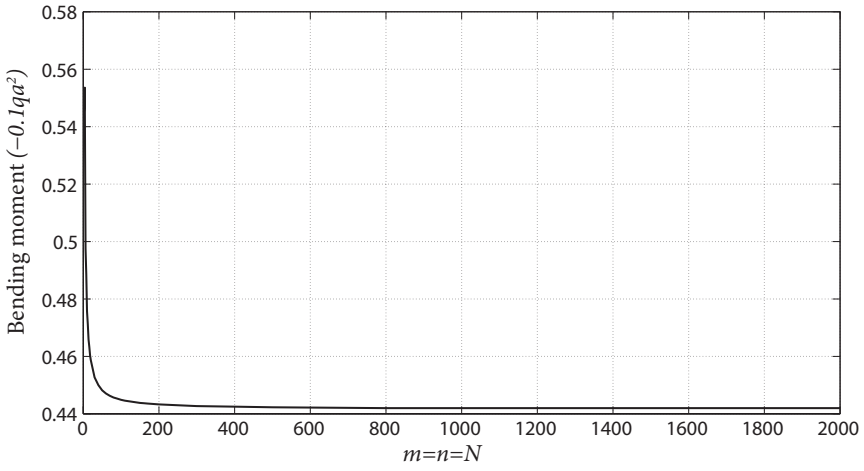

(b) Bending moment at $x = 0$, $y = b/2$

Figure 3.4 Convergence of results for an isotropic plate under a uniform distributed load.

clamped plates $r = 1$, it can be found that the coefficient matrix of Eqs. (3.55) becomes singular for any combination of m and n, making the system of equations unsolvable. A technique reported in Li et al. (2009a) was to evaluate the summations of the coefficients of $\bar{w}_{,xx}(0,n)$ and $\bar{w}_{,xx}(a,n)$ in Eqs. (3.55a) and (3.55b) without truncation; a similar process was applied for $\bar{w}_{,yy}(m,0)$ and $\bar{w}_{,yy}(m,b)$ in Eqs. (3.55c) and (3.55d) as well. This technique can be performed by symbolic mathematical computation programs such as *MATHEMATICA* Wolfram Research, Inc. (2016). The infinite series in Eqs. (3.55) can be summed without much difficulty for isotropic plates but the process is very complicated for orthotropic plates. Alternatively, given that no singularity issue occurs in the presented approach for plates with any values of rotational fixity factors except $r = 1.0$, the results of clamped plates can be approximately obtained by setting rotational fixity factors as 0.999 or 0.9999 according to the required accuracy.

Figs. 3.5 and 3.6 illustrate the effects of rotational restraints on the displacement and bending moment of the plate. Both the rotational fixity factor, r, and the restraint ratio, Ra/D_x, are employed to evaluate the corresponding displacement and bending moment. From Eq. (3.40), it can be obtained that

$$\frac{Ra}{D_x} = \frac{3r}{1-r} \tag{3.66}$$

The range of r is from 0 to 0.99 and the corresponding Ra/D_x varies between 0 and 297. It can be observed from Figs. 3.5 and 3.6 that the correlations of the moment and deflection to the restraint ratio are highly nonlinear, whereas the relationship between the moment or deflection and the rotational fixity factor is approximately linear. Thus, in practice, it is more favorable to characterize the edge rotational restraints with use of the rotational fixity factor rather than the restraint ratio.

Tables 3.1 and 3.2 tabulate the present results of the displacement and bending moment of an isotropic plate under a uniform distributed load, which agree well with those in Timoshenko and Woinowsky-Krieger (1959), Mbakogu and Pavlović (2000) and Li et al. (2009a). Similarly, the numerical results of flexural displacement and bending moment of an isotropic plate under a hydrostatic pressure qx are tabulated in Table. 3.3. Excellent agreement can be observed, except in the results of M_x at $x = 0$, $y = b/2$. The highlighted values of present results in Table. 3.3 are considerably less than those

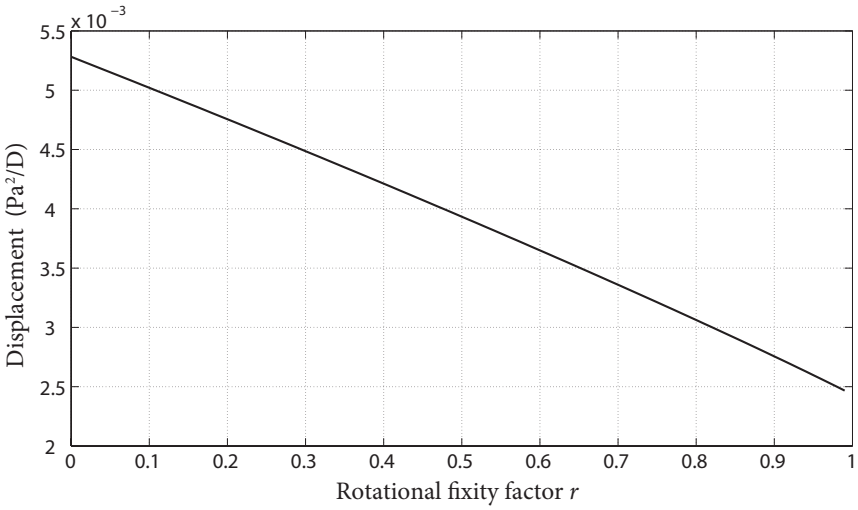

(a) Displacement Vs. Rotational fixity factor

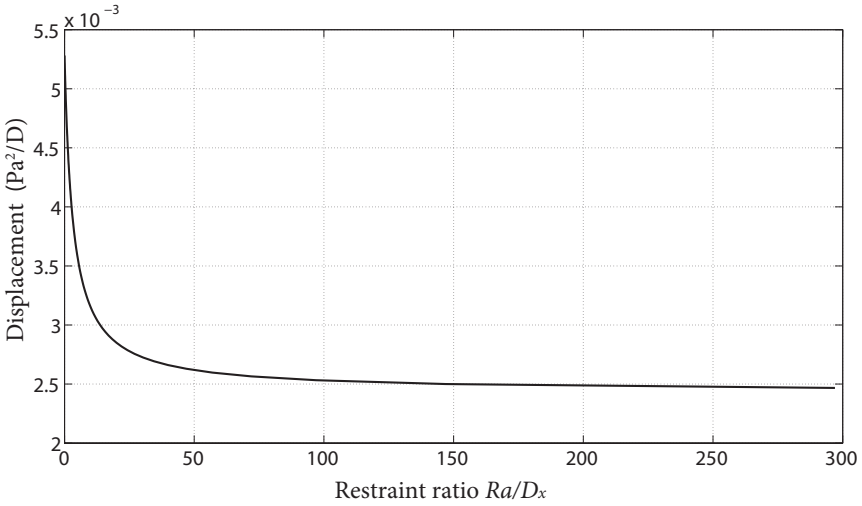

(b) Displacement Vs. Restraint ratio

Figure 3.5 Significance of rotational restraints to the displacement at $x = a/2$, $y = b/2$ for an orthotropic plate under a concentrated load.

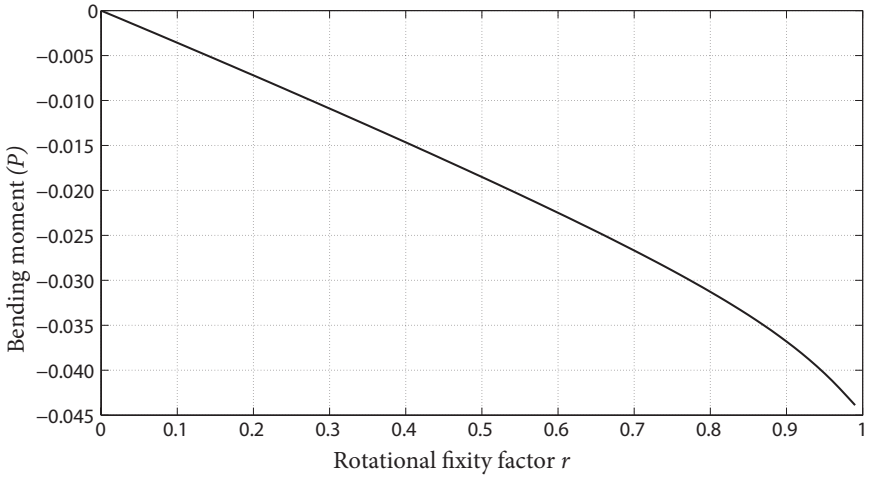

(a) Bending moment Vs. Rotational fixity factor

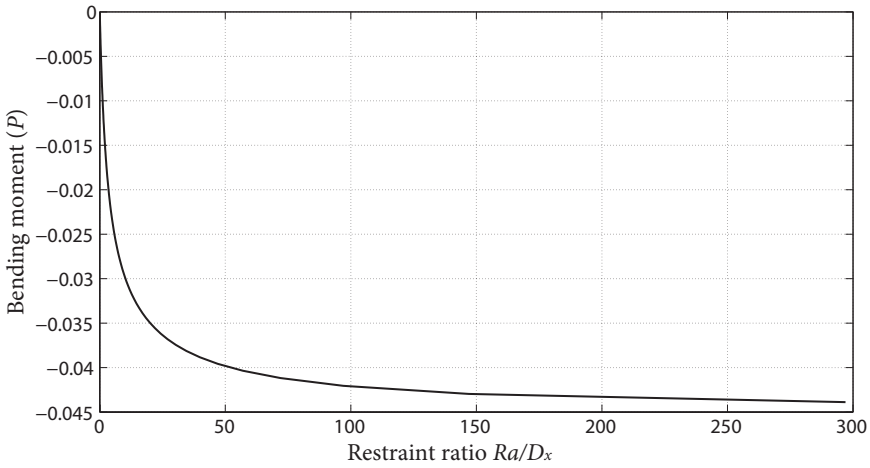

(b) Bending moment Vs. Restraint ratio

Figure 3.6 Significance of rotational restraints to the bending moment at $x = 0$, $y = b/2$ for an orthotropic plate under a concentrated load.

of Timoshenko and Woinowsky-Krieger (1959) and Li et al. (2009a). However, further comparison shows that the present results agree fairly well with the results of Odley (1947), as shown in Table. 3.4. Therefore, the discrepancies between the present results and those of Timoshenko and Woinowsky-Krieger (1959) and Li et al. (2009a) need further validation in the future.

Other disagreements can be found in the results for the bending moment for an isotropic rectangular plate with four edges rotationally restrained under a concentrated load, as marked values listed in Table. 3.5. It is noted that the present results of M_x agree with M_y in Timoshenko and Woinowsky-Krieger (1959) and Li et al. (2009a); and the present results of M_y agree with M_x in Li et al. (2009a). Nonetheless, the present results agree very well with Li et al. (2009a) in Table. 3.7 for the orthotropic plate. The accuracy of the results of Li et al. (2009a) are inconsistent. The values of bending moments from Timoshenko and Woinowsky-Krieger (1959) and Li et al. (2009a) for a fully clamped isotropic plate under a concentrated load are doubtful. These facts may suggest typos in Timoshenko and Woinowsky-Krieger (1959) and Li et al. (2009a) for the bending moment of an isotropic rectangular clamped plate under a concentrated load.

For future comparison, the bending solutions of rectangular orthotropic plates with edges rotationally restrained at varying degrees are also included in Tables. 3.6, 3.7 and 3.8. The material properties for an orthotropic plate have been taken to be

$$D_y = 4D_x,\ D_{xy} = 0.85D_x,\ \nu_x = 0.075,\ \nu_y = 0.3 \tag{3.67}$$

Table. 3.6 presents the results for an orthotropic plate under a uniform distributed load and compares them with the results of An et al. (2016). Numerical results for a rectangular orthotropic plate with four edges rotationally restrained and subjected to a concentrated load at the center of the plate are compared with those of a fully clamped plate in Li et al. (2009a) as shown in Tables. 3.7 and 3.8. Both comparisons are shown excellent agreement between the results of this study and those of Li et al. (2009a) and An et al. (2016), respectively.

Additionally, plates with any of one, two and three edges being rotationally restrained and other edges being simply supported can also be easily obtained by setting the rotational fixity factor of the simply supported edge to equal 0. Table. 3.9 illustrates the

displacement results of an isotropic plate with two opposite edges ($y = 0$ and $y = b$) rotationally restrained and the remaining edges simply supported under a uniform distributed load.

The comparison show that, overall, the results determined in this research agree very well with the results for fully clamped plates when rotational fixity factors are approaching 1 (i.e., 0.999, 0.9999). It can also be observed that the results of displacement when $r = 0.9999$ are slightly less than those for fully clamped plates and a little higher for values of bending moments. In consideration of the singular problem in the coefficient matrix for fully clamped plate (i.e., $r = 1$) when applying finite integral transform, the results for plates with rotational fixity factors approaching 1 are more applicable for clamped plates. Thus, it can be concluded that the present approach to bending of plates with rotationally restrained edges can be applied for plates with general boundary conditions from simply supported to fully clamped, by using various rotational fixity factors.

Table 3.1 Displacement $w(0.01qa^4/D)$ at the center ($x = a/2,\ y = b/2$) for an isotropic rectangular plate with four edges rotationally restrained under uniform distributed load q ($\nu = 0.3$).

b/a	rotational fixity factor $r_{x0} = r_{xa} = r_{y0} = r_{yb}$								References*		
	0	0.05	0.1	0.5	0.9	0.99	0.999	0.9999	I	II	III
1.0	0.406	0.394	0.382	0.277	0.158	0.129	0.126	0.126	0.126	0.127	0.127
1.1	0.487	0.472	0.457	0.332	0.189	0.154	0.150	0.150	0.150	0.151	0.151
1.2	0.565	0.548	0.530	0.381	0.216	0.176	0.172	0.171	0.172	0.173	0.172
1.3	0.639	0.619	0.598	0.427	0.240	0.195	0.190	0.190	0.191	0.191	0.191
1.4	0.708	0.685	0.662	0.467	0.260	0.211	0.206	0.205	0.207	0.207	0.207
1.5	0.772	0.746	0.719	0.502	0.276	0.224	0.218	0.218	0.220	0.220	0.220
1.6	0.831	0.801	0.771	0.531	0.289	0.234	0.229	0.228	0.230	0.230	0.230
1.7	0.884	0.851	0.818	0.557	0.300	0.243	0.237	0.236	0.238	0.238	0.238
1.8	0.932	0.895	0.859	0.578	0.308	0.249	0.243	0.242	0.245	0.245	0.245
1.9	0.974	0.935	0.896	0.596	0.315	0.254	0.248	0.248	0.249	0.250	0.250
2.0	1.013	0.971	0.929	0.611	0.320	0.258	0.252	0.251	0.254	0.254	0.253

note: $*$ results of fully clamped plates

reference I: Timoshenko and Woinowsky-Krieger (1959)

reference II: Mbakogu and Pavlović (2000)

reference III: Li et al. (2009a)

Table 3.2 Bending moment $M_x(-0.1qa^2)$ at $(x = 0,\ y = b/2)$ for an isotropic rectangular plate with four edges rotationally restrained under uniform distributed load q ($\nu = 0.3$).

b/a	rotational fixity factor $r_{x0} = r_{xa} = r_{y0} = r_{yb}$							References*		
	0.05	0.1	0.5	0.9	0.99	0.999	0.9999	I	II	III
1.0	0.020	0.041	0.221	0.443	0.508	0.515	0.516	0.513	0.515	0.513
1.1	0.024	0.049	0.260	0.509	0.575	0.582	0.583	0.581	0.582	0.581
1.2	0.028	0.056	0.295	0.566	0.633	0.641	0.641	0.639	0.640	0.639
1.3	0.031	0.063	0.328	0.614	0.682	0.689	0.689	0.687	0.688	0.687
1.4	0.035	0.069	0.356	0.654	0.721	0.727	0.728	0.726	0.726	0.726
1.5	0.037	0.075	0.380	0.685	0.752	0.758	0.759	0.757	0.756	0.757
1.6	0.040	0.080	0.401	0.711	0.775	0.782	0.782	0.780	0.779	0.780
1.7	0.043	0.085	0.419	0.730	0.794	0.799	0.800	0.799	0.796	0.798
1.8	0.045	0.089	0.434	0.746	0.807	0.813	0.814	0.812	0.809	0.812
1.9	0.047	0.093	0.446	0.757	0.817	0.823	0.824	0.822	0.817	0.822
2.0	0.048	0.096	0.457	0.765	0.824	0.830	0.830	0.825	0.823	0.829

note: $*$ results of fully clamped plates

reference I: Timoshenko and Woinowsky-Krieger (1959)

reference II: Mbakogu and Pavlović (2000)

reference III: Li et al. (2009a)

Table 3.3 Deflection and bending moment for an isotropic rectangular plate with four edges rotationally restrained under hydrostatic pressure qx ($\nu = 0.3$).

b/a	rotational fixity factor $r_{x0} = r_{xa} = r_{y0} = r_{yb}$								References*	
	0	0.05	0.1	0.5	0.9	0.99	0.999	0.9999	I	II
	$w(0.01qa^4/D)$ at $x = a/2,\ y = b/2$									
0.5	0.032	0.03	0.029	0.019	0.01	0.00806	0.00787	0.00785	0.008	0.00788
2/3	0.076	0.074	0.071	0.0495	0.0272	0.0221	0.0216	0.0215	0.0217	0.0217
1.0	0.203	0.197	0.191	0.139	0.0792	0.0644	0.0629	0.0628	0.063	0.0629
1.5	0.386	0.373	0.359	0.251	0.138	0.112	0.109	0.109	0.11	0.11
	$M_x(-0.1qa^3)$ at $x = 0,\ y = b/2$									
0.5	0	0.0011	0.0022	0.0104	0.0211	0.0272	0.0281	**0.0282**	**0.115**	**0.115**
2/3	0	0.0029	0.0058	0.0288	0.0549	0.0653	0.0667	**0.0668**	**0.187**	**0.187**
1	0	0.0085	0.017	0.0873	0.1596	0.1775	0.1794	**0.1796**	**0.334**	**0.334**
1.5	0	0.0167	0.0335	0.1632	0.2749	0.2939	0.2956	**0.2957**	**0.462**	**0.461**
	$M_y(-0.1qa^3)$ at $x = a/2,\ y = 0$									
0.5	0	0.006	0.012	0.057	0.096	0.103	0.104	0.104	0.104	0.104
2/3	0	0.0083	0.017	0.084	0.152	0.167	0.168	0.168	0.168	0.168
1	0	0.01	0.021	0.111	0.222	0.254	0.257	0.258	0.257	0.257
1.5	0	0.009	0.018	0.1	0.226	0.28	0.287	0.287	0.285	0.285

note: $*$ results of fully clamped plates

reference I: Timoshenko and Woinowsky-Krieger (1959)

reference II: Li et al. (2009a)

Table 3.4 Deflection and bending moment for a clamped isotropic rectangular plate under hydrostatic pressure qx ($\nu = 0.3$).

	b/a							
	0.6	0.8	1	1.2	1.4	1.6	1.8	2
	$w(0.01qa^4/D)$ at $x = a/2,\ y = b/2$							
Odley (1947)	0.0146	0.0433	0.066	0.0893	0.104	0.111	0.115	0.116
Present ($r = 0.9999$)	0.0152	0.037	0.0628	0.0855	0.102	0.114	0.121	0.125
	$M_x(-0.1qa^3)$ at $x = 0,\ y = b/2$							
Odley (1947)	0.034	0.083	0.150	0.208	0.247	0.269	0.280	0.285
Present ($r = 0.9999$)	0.049	0.110	0.179	0.239	0.281	0.307	0.323	0.331
	$M_y(-0.1qa^3)$ at $x = a/2,\ y = 0$							
Odley (1947)	0.143	0.222	0.272	0.293	0.302	0.308	0.313	0.318
Present ($r = 0.9999$)	0.143	0.213	0.258	0.279	0.286	0.288	0.288	0.288

Table 3.5 Deflection and bending moment for an isotropic rectangular plate with four edges rotationally restrained under a concentrated load P ($\nu = 0.3$).

b/a	rotational fixity factor $r_{x0} = r_{xa} = r_{y0} = r_{yb}$								References*	
	0	0.05	0.1	0.5	0.9	0.99	0.999	0.9999	I	II
	$w(0.01Pa^2/D)$ at $x = a/2,\ y = b/2$									
1	1.1600	1.1345	1.1085	0.8862	0.6311	0.5664	0.5596	0.5589	0.560	0.561
1.2	1.3556	1.3246	1.2933	1.0277	0.7285	0.6535	0.6458	0.6450	0.647	0.648
1.4	1.4866	1.4502	1.4135	1.1092	0.7793	0.6985	0.6902	0.6894	0.691	0.692
1.6	1.5700	1.5287	1.4872	1.1516	0.8023	0.7188	0.7102	0.7093	0.712	0.712
1.8	1.6214	1.5760	1.5307	1.1722	0.8117	0.7269	0.7182	0.7173	0.720	0.720
2	1.6524	1.6038	1.5556	1.1815	0.8151	0.7297	0.7210	0.7201	0.722	0.723
	$M_x(-0.1P)$ at $x = 0,\ y = b/2$									
1	0	0.0448	0.0904	0.4943	1.0445	1.2385	1.2593	**1.2591**	N.A.	**1.2560**
1.2	0	0.0540	0.1090	0.5941	1.2486	1.4706	1.4948	**1.4959**	N.A.	**0.9351**
1.4	0	0.0601	0.1212	0.6511	1.3505	1.5830	1.6086	**1.6104**	N.A.	**0.6466**
1.6	0	0.0640	0.1286	0.6805	1.3947	1.6301	1.6563	**1.6585**	N.A.	**0.4217**
1.8	0	0.0663	0.1330	0.6947	1.4119	1.6476	1.6742	**1.6766**	N.A.	**0.2603**
2	0	0.0676	0.1355	0.7010	1.4178	1.6534	1.6801	**1.6826**	N.A.	**0.1511**
	$M_y(-0.1P)$ at $x = a/2,\ y = 0$									
1	0	0.0448	0.0904	0.4943	1.0445	1.2385	1.2593	**1.2591**	**1.257**	**1.256**
1.2	0	0.0344	0.0693	0.3721	0.7727	0.9213	0.9370	**0.9347**	**1.490**	**1.490**
1.4	0	0.0257	0.0516	0.2679	0.5336	0.6368	0.6470	**0.6427**	**1.604**	**1.604**
1.6	0	0.0190	0.0379	0.1875	0.3500	0.4154	0.4209	**0.4145**	**1.651**	**1.651**
1.8	0	0.0139	0.0276	0.1287	0.2196	0.2569	0.2585	**0.2504**	**1.667**	**1.669**
2	0	0.0101	0.0200	0.0871	0.1317	0.1498	0.1486	**0.1389**	**1.674**	**1.674**

note: $*$ results of fully clamped plates

reference I: Timoshenko and Woinowsky-Krieger (1959)

reference II: Li et al. (2009a)

N.A.: Not Available

Table 3.6 Deflection and bending moment for an orthotropic rectangular plate with four edges rotationally restrained under a uniform distributed load q with $N = 200$.

b/a	rotational fixity factor $r_{x0} = r_{xa} = r_{y0} = r_{yb}$					References*
	0	0.1	0.5	0.99	0.9999	
	$w(0.01qa^4/D)$ at $x = a/2,\ y = b/2$					
1	0.179477158	0.167512605	0.118007975	0.053175615	0.051790351	0.052239018
1.2	0.284370124	0.266917312	0.192466802	0.088755641	0.086444444	0.087223947
1.4	0.398068014	0.374292071	0.271870190	0.126292735	0.123004495	0.123982330
1.6	0.511766718	0.480722097	0.347731553	0.160862718	0.156674086	0.157928260
1.8	0.619497474	0.580336215	0.415073010	0.189863668	0.184918907	0.186629070
2	0.717908634	0.670050421	0.472031900	0.212702462	0.207161405	0.208807100
	$M_x(-0.1qa^2)$ at $x = 0,\ y = b/2$					
1	0	0.01910395	0.10401693	0.27930060	0.28636592	0.28415356
1.2	0	0.02935664	0.15936679	0.39165037	0.39924677	0.39689187
1.4	0	0.04032832	0.21711586	0.50058840	0.50838627	0.50606117
1.6	0	0.05115019	0.27155217	0.59479747	0.60253700	0.60024615
1.8	0	0.06125028	0.31941970	0.66965647	0.67717686	0.67505836
2	0	0.07033046	0.35961026	0.72565299	0.73288007	0.73074900

note: $*$ results of fully clamped plates in An et al. (2016)

Table 3.7 Bending moment for an orthotropic rectangular plate with four edges rotationally restrained under a concentrated load P with $N = 100$.

b/a	rotational fixity factor $r_{x0} = r_{xa} = r_{y0} = r_{yb}$							References*
	0.05	0.1	0.5	0.9	0.99	0.999	0.9999	
	$M_x(-0.1P)$ at $x = 0,\ y = b/2$							
1	0.0178	0.0357	0.1851	0.368	0.4388	0.4417	0.4356	0.4436
1.1	0.0215	0.0433	0.2299	0.4714	0.5626	0.5684	0.564	0.569
1.2	0.025	0.0505	0.2724	0.5687	0.6779	0.6863	0.6833	0.6852
1.3	0.0283	0.0571	0.3112	0.6562	0.7805	0.791	0.7892	0.7885
1.4	0.0313	0.0631	0.3456	0.7318	0.8684	0.8806	0.8797	0.8768
1.5	0.0339	0.0685	0.3753	0.7951	0.9411	0.9548	0.9545	0.95
1.6	0.0362	0.0732	0.4004	0.8466	0.9997	1.0146	1.0147	1.009
1.7	0.0383	0.0772	0.4213	0.8875	1.0458	1.0615	1.062	1.055
1.8	0.04	0.0807	0.4384	0.9194	1.0813	1.0977	1.0984	1.091
1.9	0.0415	0.0837	0.4512	0.9437	1.1081	1.125	1.126	1.118
2	0.0428	0.0862	0.4631	0.962	1.128	1.1453	1.1465	1.137
	$M_y(-0.1P)$ at $x = a/2,\ y = 0$							
1	0.0855	0.1723	0.9263	1.924	2.2561	2.2907	2.2931	2.275
1.1	0.0806	0.1626	0.8822	1.8487	2.1735	2.2065	2.2082	2.192
1.2	0.0752	0.1519	0.8296	1.75	2.0635	2.0943	2.0951	2.082
1.3	0.0697	0.1407	0.771	1.6325	1.9305	1.9589	1.9596	1.948
1.4	0.0641	0.1295	0.7092	1.5023	1.7813	1.8068	1.8052	1.799
1.5	0.0587	0.1184	0.6464	1.3655	1.623	1.6453	1.6422	1.639
1.6	0.0534	0.1078	0.5846	1.2277	1.462	1.4809	1.4762	1.477
1.7	0.0485	0.0977	0.5254	1.0932	1.3036	1.3192	1.3127	1.318
1.8	0.0438	0.0883	0.4695	0.9652	1.1518	1.164	1.1557	1.165
1.9	0.0395	0.0795	0.4177	0.8458	1.0093	1.0182	1.0079	1.021
2	0.0356	0.0715	0.3701	0.7361	0.8777	0.8834	0.8711	0.8887

note: $*$ results of fully clamped plates in Li et al. (2009a)

Table 3.8 Displacement $w(0.01Pa^2/D_x)$ at the center $(x = a/2,\ y = b/2)$ for an orthotropic rectangular plate with four edges rotationally restrained under a concentrated load P with $N = 100$.

b/a	rotational fixity factor $r_{x0} = r_{xa} = r_{y0} = r_{yb}$								References*
	0	0.05	0.1	0.5	0.9	0.99	0.999	0.9999	
1	0.5282	0.5152	0.5021	0.3933	0.2756	0.2467	0.2437	0.2434	0.2454
1.1	0.6069	0.5926	0.5782	0.4569	0.322	0.2884	0.2849	0.2846	0.2869
1.2	0.6811	0.6657	0.65	0.5168	0.3659	0.3278	0.3239	0.3235	0.3261
1.3	0.7497	0.7331	0.7162	0.5715	0.4057	0.3636	0.3592	0.3587	0.3617
1.4	0.8119	0.794	0.7759	0.62	0.4405	0.3948	0.3901	0.3896	0.3928
1.5	0.8676	0.8485	0.8289	0.6619	0.4701	0.4213	0.4162	0.4157	0.4191
1.6	0.9167	0.8962	0.8753	0.6975	0.4945	0.4432	0.4378	0.4373	0.4409
1.7	0.9597	0.9377	0.9155	0.7271	0.5142	0.4607	0.4552	0.4546	0.4583
1.8	0.9969	0.9736	0.95	0.7513	0.5298	0.4745	0.4688	0.4683	0.4721
1.9	1.0289	1.0042	0.9793	0.771	0.5419	0.4853	0.4794	0.4788	0.4828
2	1.0563	1.0303	1.0041	0.7867	0.5511	0.4934	0.4874	0.4868	0.4909

note: $*$ results of fully clamped plates in Li et al. (2009a)

Table 3.9 Displacement $w(0.01qa^4/D)$ at the center $(x = a/2,\ y = b/2)$ for an isotropic rectangular plate with two opposite edges rotationally restrained ($y = 0$ and $y = b$) and remaining edges simply supported under an uniform distributed load q ($\nu = 0.3$).

b/a	rotational fixity factor $r_{x0} = r_{xa} = r_{y0} = r_{yb}$								Reference*
	0	0.05	0.1	0.5	0.9	0.99	0.999	0.9999	
1	0.4062	0.4001	0.3937	0.3293	0.2265	0.1944	0.1909	0.1906	0.192
1.1	0.4869	0.4809	0.4746	0.4090	0.2946	0.2560	0.2518	0.2514	0.251
1.2	0.5650	0.5594	0.5534	0.4891	0.3673	0.3232	0.3183	0.3178	0.319
1.3	0.6392	0.6340	0.6285	0.5672	0.4423	0.3939	0.3883	0.3878	0.388
1.4	0.7085	0.7037	0.6987	0.6417	0.5173	0.4659	0.4599	0.4593	0.46
1.5	0.7724	0.7682	0.7637	0.7115	0.5906	0.5375	0.5312	0.5305	0.531
1.6	0.8308	0.8271	0.8231	0.7761	0.6607	0.6072	0.6007	0.6000	0.603
1.7	0.8838	0.8805	0.8770	0.8350	0.7268	0.6739	0.6673	0.6666	0.668
1.8	0.9316	0.9287	0.9257	0.8885	0.7883	0.7367	0.7302	0.7295	0.732
1.9	0.9745	0.9720	0.9694	0.9367	0.8448	0.7953	0.7889	0.7882	0.79
2	1.0128	1.0107	1.0084	0.9798	0.8963	0.8492	0.8431	0.8424	0.844

note: $*$ results of fully clamped plates in Timoshenko and Woinowsky-Krieger (1959)

3.3 Vibration of R-R-R-R Orthotropic Plates

Although a number of studies have investigated the vibration of plates with uniform or non-uniform elastic boundary restraints (Carmichael, 1959; Laura and Romanelli, 1974; Laura et al., 1978; Laura and Grossi, 1979; Leissa et al., 1980; Mukhopadhyay, 1979, 1989; Warburton and Edney, 1984; Bapat et al., 1988; Li, 2004), most of those studies use approximate methods such as the Rayleigh-Ritz method, which is inconvenient compared to the method of finite integral transform (Wang and Lin, 1999). The study presented in this section is the first to examine whether the method of finite integral transform can be applied to plates with different boundary conditions other than the completely free conditions reported in Hurlebaus et al. (2001). Its universal application was questioned by Li et al. (2009b).

3.3.1 Free vibration

Consider an orthotropic rectangular thin plate with rotationally restrained edges as shown in Fig. 3.3. The governing equation of the free vibration is (Leissa, 1969)

$$D_x \frac{\partial^4 w}{\partial x^4} + 2H \frac{\partial^4 w}{\partial x^2 \partial y^2} + D_y \frac{\partial^4 w}{\partial y^4} + \rho h \frac{\partial^2 w}{\partial t^2} = 0 \tag{3.68}$$

in which ρ is the density of the plate; D_x, D_y, and H are the same as those defined in Section 3.1.2. The displacement function $w(x, y, t)$ can be expressed as the product of two functions, one involving only the coordinates x and y, called a mode shape function $W(x, y)$, and the other involving the variable time *T(t)*. Denoting the frequency of sinusoidal oscillations by ω, the displacement function can be expressed as

$$w(x, y, t) = W(x, y)e^{i\omega t} \tag{3.69}$$

Substituting Eq. (3.69) into Eq. (3.68) yields

$$D_x \frac{\partial^4 W}{\partial x^4} + 2H \frac{\partial^4 W}{\partial x^2 \partial y^2} + D_y \frac{\partial^4 W}{\partial y^4} - \omega^2 \rho h W = 0 \tag{3.70}$$

The boundary conditions of the plates are described in Eqs. (3.42) and (3.43). The pair of double finite sine transforms is defined in Eqs. (3.8) as (Sneddon, 1972):

$$\bar{\bar{W}}(m,n) = \int_0^a \int_0^b W(x,y) \sin\alpha_m x \sin\beta_n y dx dy \tag{3.71a}$$

$$W(x,y) = \frac{4}{ab} \sum_{m=1}^{\infty} \sum_{n=1}^{\infty} \bar{\bar{W}}(m,n) \sin\alpha_m x \sin\beta_n y \tag{3.71b}$$

Taking double finite sine transforms on both sides of Eq. (3.70) gives

$$\int_0^a \int_0^b \nabla_o^4 W(x,y) \sin\alpha_m x \sin\beta_n y dx dy - \omega^2 \rho h \bar{\bar{W}}(m,n) = 0 \tag{3.72}$$

Using integration by parts and considering the boundary conditions of Eqs. (3.42), the double finite sine transforms of the fourth derivatives in Eq. (3.72) can be obtained (Meirovitch, 1967):

$$\begin{aligned} \int_0^a \int_0^b W_{,xxxx} \sin\alpha_m x \sin\beta_n y dx dy &= \alpha_m^4 \bar{\bar{W}}(m,n) \\ &\quad - \alpha_m \Big[(-1)^m \bar{W}_{,xx}(a,n) - \bar{W}_{,xx}(0,n) \Big] \end{aligned} \tag{3.73a}$$

$$\int_0^a \int_0^b W_{,xxyy} \sin\alpha_m x \sin\beta_n y dx dy = \alpha_m^2 \beta_n^2 \bar{\bar{W}}(m,n) \tag{3.73b}$$

$$\begin{aligned} \int_0^a \int_0^b W_{,yyyy} \sin\alpha_m x \sin\beta_n y dx dy &= \beta_n^4 \bar{\bar{W}}(m,n) \\ &\quad - \beta_n \Big[(-1)^n \bar{W}_{,yy}(m,b) - \bar{W}_{,yy}(m,0) \Big] \end{aligned} \tag{3.73c}$$

where coefficients $\bar{W}_{,xx}(0,n)$, $\bar{W}_{,xx}(a,n)$, $\bar{W}_{,yy}(m,0)$ and $\bar{W}_{,yy}(m,b)$ are determined from the finite-sine transformed boundary conditions at the four edges. Substituting Eq. (3.73) into Eq. (3.72), the following is obtained

$$\begin{aligned} \bar{\bar{W}}(m,n) = \frac{1}{\Omega_{mn} - \omega^2 \rho h} \Bigg\{ & \alpha_m D_x \Big[(-1)^m \bar{W}_{,xx}(a,n) - \bar{W}_{,xx}(0,n) \Big] \\ & + \beta_n D_y \Big[(-1)^n \bar{W}_{,yy}(m,b) - \bar{W}_{,yy}(m,0) \Big] \Bigg\} \end{aligned} \tag{3.74}$$

Taking the inverse finite sine transform of Eq. (3.74) with respect to the spatial variable x and y, separately, results in

$$\bar{W}(x,n) = \frac{2}{a}\sum_{m=1}^{\infty}\bar{\bar{W}}(m,n)\sin\alpha_m x \tag{3.75a}$$

$$\bar{W}(m,y) = \frac{2}{b}\sum_{n=1}^{\infty}\bar{\bar{W}}(m,n)\sin\beta_n y \tag{3.75b}$$

Using Stokes's transformation and taking the derivative of Eq. (3.75a) with respect to x and Eq. (3.75b) to y, respectively, yields

$$\bar{W}_{,x}(x,n) = \frac{2}{a}\sum_{m=1}^{\infty}\alpha_m\bar{\bar{W}}(m,n)\cos\alpha_m x \tag{3.76a}$$

$$\bar{W}_{,y}(m,y) = \frac{2}{b}\sum_{n=1}^{\infty}\beta_n\bar{\bar{W}}(m,n)\cos\beta_n y \tag{3.76b}$$

Applying Eqs. (3.43) and Eqs. (3.74), four infinite systems of equations with respect to $\bar{W}_{,xx}(0,n)$, $\bar{W}_{,xx}(a,n)$, $\bar{W}_{,yy}(m,0)$, and $\bar{W}_{,yy}(m,b)$ can be obtained.

$$\begin{aligned}\bar{W}_{,xx}(0,n) = \frac{2}{a}\frac{R_{x0}}{D_x}\sum_{m=1}^{\infty}\frac{\alpha_m}{\Omega_{mn}-\omega^2\rho h}\Bigg\{&\alpha_m D_x\Big[(-1)^m\bar{W}_{,xx}(a,n)-\bar{W}_{,xx}(0,n)\Big]\\&+\beta_n D_y\Big[(-1)^n\bar{W}_{,yy}(m,b)-\bar{W}_{,yy}(m,0)\Big]\Bigg\}\end{aligned} \tag{3.77a}$$

$$\begin{aligned}\bar{W}_{,xx}(a,n) = -\frac{2}{a}\frac{R_{xa}}{D_x}\sum_{m=1}^{\infty}\frac{(-1)^m\alpha_m}{\Omega_{mn}-\omega^2\rho h}\Bigg\{&\alpha_m D_x\Big[(-1)^m\bar{W}_{,xx}(a,n)-\bar{W}_{,xx}(0,n)\Big]\\&+\beta_n D_y\Big[(-1)^n\bar{W}_{,yy}(m,b)-\bar{W}_{,yy}(m,0)\Big]\Bigg\}\end{aligned} \tag{3.77b}$$

$$\begin{aligned}\bar{W}_{,yy}(m,0) = \frac{2}{b}\frac{R_{y0}}{D_y}\sum_{n=1}^{\infty}\frac{\beta_n}{\Omega_{mn}-\omega^2\rho h}\Bigg\{&\alpha_m D_x\Big[(-1)^m\bar{W}_{,xx}(a,n)-\bar{W}_{,xx}(0,n)\Big]\\&+\beta_n D_y\Big[(-1)^n\bar{W}_{,yy}(m,b)-\bar{W}_{,yy}(m,0)\Big]\Bigg\}\end{aligned} \tag{3.77c}$$

$$\bar{W}_{,yy}(m,b) = -\frac{2}{b}\frac{R_{yb}}{D_y}\sum_{n=1}^{\infty}\frac{(-1)^n\beta_n}{\Omega_{mn}-\omega^2\rho h}\Bigg\{\alpha_m D_x\Big[(-1)^m\bar{W}_{,xx}(a,n)-\bar{W}_{,xx}(0,n)\Big] + \beta_n D_y\Big[(-1)^n\bar{W}_{,yy}(m,b)-\bar{W}_{,yy}(m,0)\Big]\Bigg\} \tag{3.77d}$$

For each combination of m and n, Eqs. (3.77) produce $2m+2n$ equations with $2m+2n$ unknown variables. Non-trivial solutions require the determinant of the coefficient matrix to vanish. Then, the eigenfrequencies of the plate can be calculated as well as the associated vibration modes. This approach was also reported in Green (1944), Hurlebaus et al. (2001) and Zhong and Yin (2008). However, such a procedure involves solving a highly non-linear equation, which requires quite laborious computation even for small m and n. This problem cannot be remedied through reducing the $2m+2n$ equations to $m+n$ equations by using the symmetry conditions of modes in the case with symmetric boundary conditions, i.e., $R_{x0}=R_{xa}$ and $R_{y0}=R_{yb}$. For the purpose of illustration, consider the doubly symmetric modes of a clamped plate, from which it can be obtained

$$0 = \sum_{m=1}^{\infty}\frac{\alpha_m}{\Omega_{mn}-\omega^2\rho h}\Bigg\{\alpha_m D_x\Big[(-1)^m\bar{W}_{,xx}(a,n)-\bar{W}_{,xx}(0,n)\Big] + \beta_n D_y\Big[(-1)^n\bar{W}_{,yy}(m,b)-\bar{W}_{,yy}(m,0)\Big]\Bigg\} \tag{3.78a}$$

$$0 = \sum_{m=1}^{\infty}\frac{(-1)^m\alpha_m}{\Omega_{mn}-\omega^2\rho h}\Bigg\{\alpha_m D_x\Big[(-1)^m\bar{W}_{,xx}(a,n)-\bar{W}_{,xx}(0,n)\Big] + \beta_n D_y\Big[(-1)^n\bar{W}_{,yy}(m,b)-\bar{W}_{,yy}(m,0)\Big]\Bigg\} \tag{3.78b}$$

$$0 = \sum_{n=1}^{\infty}\frac{\beta_n}{\Omega_{mn}-\omega^2\rho h}\Bigg\{\alpha_m D_x\Big[(-1)^m\bar{W}_{,xx}(a,n)-\bar{W}_{,xx}(0,n)\Big] + \beta_n D_y\Big[(-1)^n\bar{W}_{,yy}(m,b)-\bar{W}_{,yy}(m,0)\Big]\Bigg\} \tag{3.78c}$$

$$0 = \sum_{n=1}^{\infty} \frac{(-1)^n \beta_n}{\Omega_{mn} - \omega^2 \rho h} \Bigg\{ \alpha_m D_x \Big[(-1)^m \bar{W}_{,xx}(a,n) - \bar{W}_{,xx}(0,n) \Big] + \beta_n D_y \Big[(-1)^n \bar{W}_{,yy}(m,b) - \bar{W}_{,yy}(m,0) \Big] \Bigg\} \tag{3.78d}$$

Using the symmetric boundary conditions, it can be found that

$$\begin{aligned} \bar{W}_{,xx}(a,n) &= \bar{W}_{,xx}(0,n) \\ \bar{W}_{,yy}(m,b) &= \bar{W}_{,yy}(m,0) \end{aligned} \tag{3.79}$$

Thus, terms with even m or n in Eqs. (3.78) will vanish. After that, Eqs. (3.78) turn into

$$\sum_{m=1,3,\ldots}^{\infty} \frac{\alpha_m^2 D_x}{\Omega_{mn} - \omega^2 \rho h} \bar{W}_{,xx}(a,n) + \sum_{m=1,3,\ldots}^{\infty} \frac{\alpha_m \beta_n D_y}{\Omega_{mn} - \omega^2 \rho h} \bar{W}_{,yy}(m,b) = 0 \tag{3.80a}$$

$$\sum_{n=1,3,\ldots}^{\infty} \frac{\alpha_m \beta_n D_x}{\Omega_{mn} - \omega^2 \rho h} \bar{W}_{,xx}(a,n) + \sum_{n=1,3,\ldots}^{\infty} \frac{\beta_n^2 D_y}{\Omega_{mn} - \omega^2 \rho h} \bar{W}_{,yy}(m,b) = 0 \tag{3.80b}$$

It can be observed that even for the simplified Eqs. (3.80), the highly non-linear equation must still be solved. The infinite series of the first term in Eq. (3.80a) or the second term in Eq. (3.80b) can be summed without much difficulty in the case of isotropic plates, as it will benefit the numerical computation. However, the sum of the infinite series will be complex for orthotropic plates. In addition, it can also be recognised that Eqs. (3.80) are coincidentally identical to Eqs. (16) in Kshirsagar and Bhaskar (2008), in which the improved superposition method is applied for isotropic plates. This verifies that the finite integral transform method is essentially the same as the improved superposition method.

Alternatively, instead of solving non-linear equations, Li et al. (Li, 2000; Li et al., 2009b) proposed a simple procedure to obtain the natural frequency. This procedure is also adopted herein for the method of finite integral transform. Combining Eqs. (3.43) and Eqs. (3.76) yields

$$\bar{W}_{,xx}(0,n) = \frac{2}{a} \frac{R_{x0}}{D_x} \sum_{m=1}^{\infty} \alpha_m \bar{\bar{W}}(m,n) \tag{3.81a}$$

$$\bar{W}_{,xx}(a,n) = -\frac{2}{a}\frac{R_{xa}}{D_x}\sum_{m=1}^{\infty}(-1)^m\alpha_m\bar{\bar{W}}(m,n) \tag{3.81b}$$

$$\bar{W}_{,yy}(m,0) = \frac{2}{b}\frac{R_{y0}}{D_y}\sum_{n=1}^{\infty}\beta_n\bar{\bar{W}}(m,n) \tag{3.81c}$$

$$\bar{W}_{,yy}(m,b) = -\frac{2}{b}\frac{R_{yb}}{D_y}\sum_{n=1}^{\infty}(-1)^n\beta_n\bar{\bar{W}}(m,n) \tag{3.81d}$$

Substituting Eqs. (3.81) into Eq. (3.74) produces

$$\begin{aligned}&\Omega_{mn}\bar{\bar{W}}(m,n) + \frac{2\alpha_m}{a}\sum_{i=1}^{\infty}\left[(-1)^{i+m}R_{xa} + R_{x0}\right]\alpha_i\bar{\bar{W}}(i,n)\\ &+\frac{2\beta_n}{b}\sum_{j=1}^{\infty}\left[(-1)^{j+n}R_{yb} + R_{y0}\right]\beta_j\bar{\bar{W}}(m,j) - \omega^2\rho h\bar{\bar{W}}(m,n) = 0\end{aligned} \tag{3.82}$$

where

$$\alpha_i = \frac{i\pi}{a},\ \beta_j = \frac{j\pi}{b}\ (i = 1,2,3,...,j = 1,2,3,...) \tag{3.83}$$

Based on Eqs. (3.40), rotational fixity factors are introduced to define elastic restraints along edges and can be expressed as

$$\frac{R_{x0}a}{D_x} = \frac{3r_{x0}}{1-r_{x0}} \tag{3.84a}$$

$$\frac{R_{xa}a}{D_x} = \frac{3r_{xa}}{1-r_{xa}} \tag{3.84b}$$

Similarly,

$$\frac{R_{y0}b}{D_y} = \frac{3r_{y0}}{1-r_{y0}} \tag{3.85a}$$

$$\frac{R_{yb}b}{D_y} = \frac{3r_{yb}}{1-r_{yb}} \tag{3.85b}$$

Substituting Eqs. (3.84) and Eqs. (3.85) into Eq. (3.82) yields

$$\Omega_{mn}\bar{\bar{W}}(m,n)+\frac{2\alpha_m D_x}{a^2}\sum_{i=1}^{\infty}\left[(-1)^{i+m}\frac{3r_{xa}}{1-r_{xa}}+\frac{3r_{x0}}{1-r_{x0}}\right]\alpha_i\bar{\bar{W}}(i,n)$$
$$+\frac{2\beta_n D_y}{b^2}\sum_{j=1}^{\infty}\left[(-1)^{j+n}\frac{3r_{yb}}{1-r_{yb}}+\frac{3r_{y0}}{1-r_{y0}}\right]\beta_j\bar{\bar{W}}(m,j)-\omega^2\rho h\bar{\bar{W}}(m,n)=0 \tag{3.86}$$

Eq. (3.86) can be conveniently expressed in the following matrix form:

$$\mathbf{AW}=\omega^2\rho h\mathbf{W} \tag{3.87}$$

where $\mathbf{W}=[\bar{\bar{W}}(1,1),\bar{\bar{W}}(1,2)...\bar{\bar{W}}(1,N),\bar{\bar{W}}(2,1)...\bar{\bar{W}}(2,N)...\bar{\bar{W}}(M,N)]$ and $\mathbf{A}$ is the corresponding coefficient matrix which can be obtained from Eq. (3.86). It is assumed that all the series expansions are truncated to finite number M for m and N for n while the upper limit of summation may be theoretically specified as infinity. It can be observed that Eq. (3.87) is a standard characteristic equation for a matrix, and the corresponding eigenfrequencies ω can be conveniently determined. As a result, a complex non-linear problem of Eqs. (3.77) is now converted to the simple eigenvalue problem of Eq. (3.87). For any obtained eigenfrequency, the corresponding eigenvector can be directly determined by substituting the eigenfrequency into Eq. (3.87). Subsequently, the corresponding mode shape can be derived by substituting the eigenvector of $\bar{\bar{W}}(m,n)$ into Eq. (3.71b) for each natural frequency.

3.3.2 Forced vibration

The classical method of analyzing the forced vibration response of a plate is the method of modal analysis (i.e., eigenfunction expansion) by expanding the forcing function into a series of eigenfunctions and taking advantage of their orthogonality relation. Instead of using classical modal analysis to analyse the forced vibration response, a straightforward unified approach by applying the finite integral transform is also presented. Theoretically, any loading function can be expanded into a Fourier series (Wang and Lin, 1996). Thus, for illustration, only forced vibrations induced by harmonic excitations are studied.

A forced vibration of the orthotropic plate is governed by

$$D_x\frac{\partial^4 w}{\partial x^4}+2H\frac{\partial^4 w}{\partial x^2\partial y^2}+D_y\frac{\partial^4 w}{\partial y^4}+\rho h\frac{\partial^2 w}{\partial t^2}=f(x,y,t) \tag{3.88}$$

in which $f(x,y,t) = p(x,y)\sin\omega t$ where $p(x,y)$ is the spatial distribution and ω is the angular frequency of force. Eq. (3.88) admits a solution of the form

$$w(x,y,t) = W(x,y)\sin\omega t \tag{3.89}$$

Therefore, w must satisfy the equation

$$D_x\frac{\partial^4 W}{\partial x^4} + 2H\frac{\partial^4 W}{\partial x^2\partial y^2} + D_y\frac{\partial^4 W}{\partial y^4} - \omega^2\rho h W = p(x,y) \tag{3.90}$$

By applying the same procedure illustrated in Section 3.3.1, forced vibration responses can be determined.

3.3.3 Numerical results and comparison

Several representative examples are presented in this section to validate the foregoing proposed analytical procedure and the corresponding numerical results are obtained by using built-in *eigs* function in the MATLAB® software package. For the sake of convenience, the numbers of double series items are chosen to be the same and denoted by N (i.e., $m,\ n = 1,2,3,...,N$) and the four edges have the same values for the rotational fixity factors (i.e., $r_{x0} = r_{xa} = r_{y0} = r_{yb} = r$). The results are theoretically exact when $N \to \infty$, while convergent solutions with satisfactory accuracy can be acquired by a finite number of items.

First of all, the convergence of the fundamental frequency is shown in Fig. 3.7 for the case of a square isotropic plate with four edges rotationally restrained with $r = 0.999$. The exact value of the fundamental frequency parameter of the fully clamped plate is 35.985 in Li et al. (2009b) with use of improved Fourier series method. It can be observed from Fig. 3.7 that the parameter converges to the exact value quite slowly. Since the computation time becomes very long when $N > 150$ on a standard PC, the values are examined by truncating the series up to $N = 150$. From the results of convergence study, N is taken to be 100 for all numerical results presented in the present study. Figs. 3.8 illustrate the first six mode shapes of a square isotropic plate with $r = 0.25$. Figs. 3.9 show the influence of rotational stiffness on the mode shapes of plate. Square isotropic plates with four different values of rotational fixity factors (0, 0.25, 0.5 and 0.999) are

examined. The results indicate that the rotational stiffness may alter the mode shapes, as shown in Figs. 3.9.

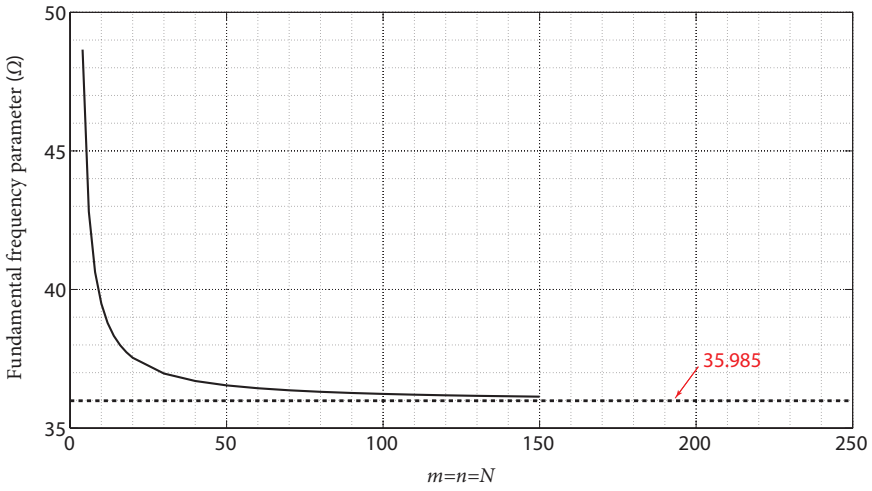

Figure 3.7 Convergence of the fundamental frequency parameter $\Omega = \omega a^2\sqrt{\rho h/D}$ of a square isotropic plate with $r = 0.999$.

The next example involves a square isotropic plate with four edges rotationally restrained. Various rotational fixity factors from 0.0323 to 0.997 are investigated, and the results are shown in Table. 3.10. The present results are compared with those of Mukhopadhyay (1979) and Li et al. (2009b). The differences between the present results and those of Mukhopadhyay (1979) are calculated with respect to the exact solutions of Li et al. (2009b), separately. It is found that the proposed method provides better predictions than those of Mukhopadhyay (1979) in general, with differences from the exact solutions of Li et al. (2009b) being less than 0.9 percent. Furthermore, the frequencies obtained from the proposed method are more accurate when the rotational restraint is flexible, say when $r < 0.25$.

Last, rectangular orthotropic plates with three edges simply supported ($r_{x0} = r_{xa} = r_{yb} = 0$) and one edge rotationally restrained are considered. The effect of aspect ratios and rotational fixity factors are investigated. The obtained fundamental frequency parameters are tabulated in Table. 3.11 and compared with the results of Laura and Grossi (1979) using the material properties of $D_x/H = D_y/H = 0.5$. The comparisons shown in Table. 3.11 indicate good agreement in the results, with difference less than 0.8 percent.

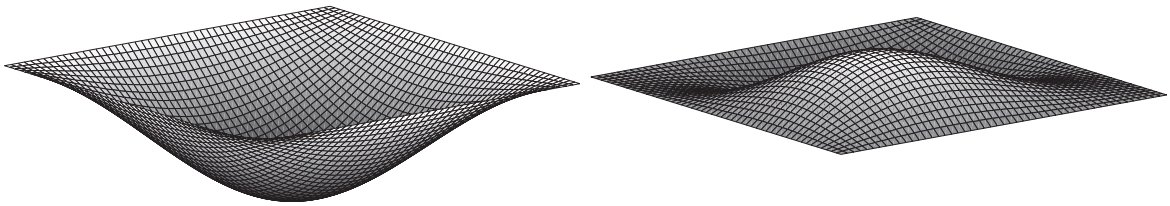

(a) First mode

(b) Second mode

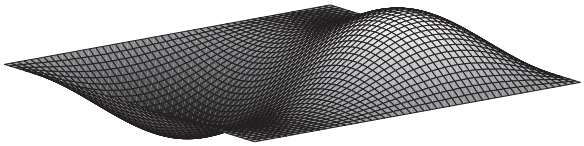

(c) Third mode

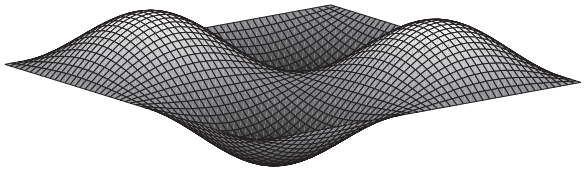

(d) Fourth mode

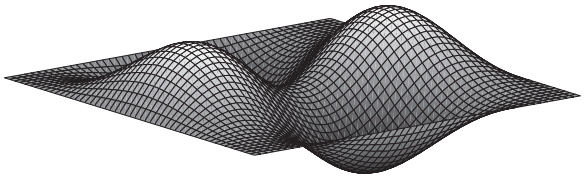

(e) Fifth mode

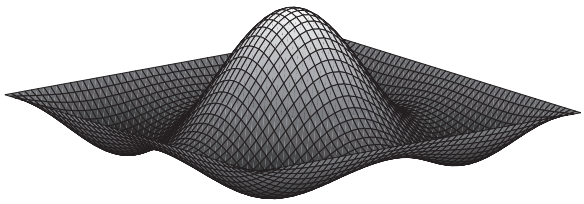

(f) Sixth mode

Figure 3.8 First six mode shapes of a square isotropic plate with $r = 0.25$.

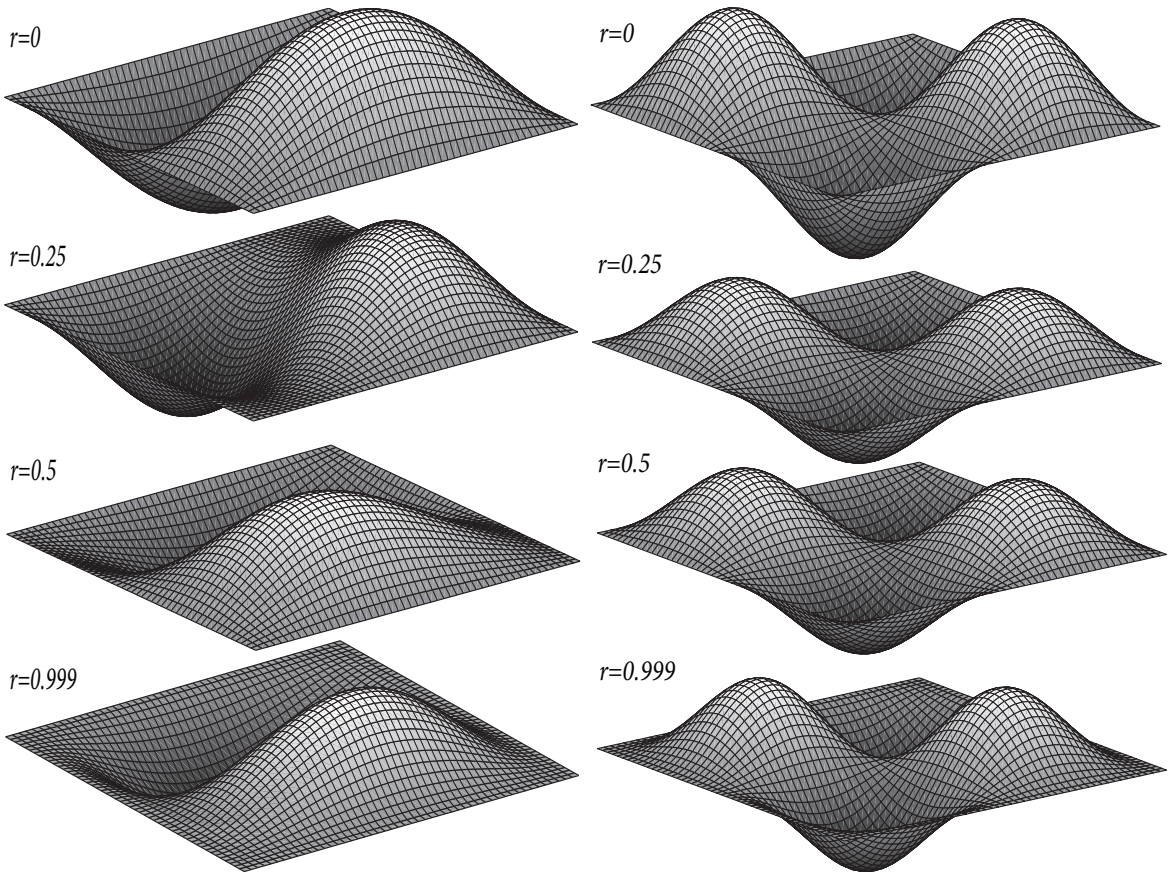

(a) Third mode (b) Fourth mode

Figure 3.9 The effect of rotational restraints on the mode shapes of a square isotropic plate with rotational restrained edges.

Table 3.10 First six frequency parameters Ω for a square isotropic plate with four edges rotationally restrained.

r	Ka/D		$\Omega = \omega a^2\sqrt{\rho h/D}$					
			1	2	3	4	5	6
0.0323	0.1	Mukhopadhyay (1979)	19.839	48.894	49.629	79.04	95.678	99.211
		Present	19.936	49.546	49.546	79.155	98.895	98.895
0.25	1	Li et al. (2009b)	21.5	51.187	51.187	80.816	100.58	100.59
		Mukhopadhyay (1979)	20.511	49.116	50.927	79.851	95.777	100.727
		(%)^a	-4.60	-4.05	-0.51	-1.19	-4.78	0.14
		Present	21.505	51.195	51.195	80.831	100.587	100.594
		(%)^b	0.02	0.02	0.02	0.02	0.01	0.00
0.7692	10	Li et al. (2009b)	28.501	60.215	60.215	90.808	111.19	111.41
		Present	28.583	60.337	60.337	90.957	111.352	111.578
		(%)^b	0.29	0.20	0.20	0.16	0.15	0.15
0.8696	20	Li et al. (2009b)	31.08	64.31	64.31	95.85	116.8	117.2
		Mukhopadhyay (1979)	31.111	64.342	64.861	95.85	117.029	118.214
		(%)^a	0.10	0.05	0.86	0.00	0.20	0.87
		Present	31.219	64.535	64.535	96.112	117.181	117.566
		(%)^b	0.45	0.35	0.35	0.27	0.33	0.31
0.9709	100	Li et al. (2009b)	34.671	70.78	70.78	104.45	127.02	127.61
		Mukhopadhyay (1979)	34.753	69.319	70.929	103.377	120.047	127.616
		(%)^a	0.24	-2.06	0.21	-1.03	-5.49	0.00
		Present	34.918	71.259	71.259	105.128	127.845	128.439
		(%)^b	0.71	0.68	0.68	0.65	0.65	0.65
0.997	1000	Li et al. (2009b)	35.842	73.103	73.103	107.79	131.06	131.68
		Present	36.134	73.694	73.694	108.658	132.129	132.756
		(%)^b	0.81	0.81	0.81	0.81	0.82	0.82

note: a–percentage difference of results between Mukhopadhyay (1979) and Li et al. (2009b)
b–percentage difference of results between the present study and Li et al. (2009b)
Ka/D–rotational stiffness coefficient defined in Li et al. (2009b)

Table 3.11 Fundamental frequency parameter Ω_1 for rectangular orthotropic plates with three edges simply supported ($r_{x0} = r_{xa} = r_{yb} = 0$) and one edge rotationally restrained r_{y0}.

k_3	$\frac{R_{y0}b}{D_y}$	r_{y0}	$\Omega_1 = \omega_1 a^2\sqrt{\rho h/D_x}$								
			b/a=0.5			b/a=1			b/a=1.5		
			Ref.*	Present	(%)	Ref.*	Present	(%)	Ref.*	Present	(%)
0	0	0	56.5685	56.6966	0.23	24.1831	24.1755	-0.03	16.9706	17.0242	0.32
0.5	1	0.25	58.8313	59.1302	0.51	24.4659	24.5448	0.32	17.0963	17.1301	0.20
5	10	0.7692	67.8823	68.0681	0.27	26.1630	26.1534	-0.04	17.7248	17.6557	-0.39
∞	∞	0.9999	75.2362	75.7808	0.72	28.0014	27.9691	-0.12	18.5419	18.4179	-0.67

note: k_3–rotational stiffness coefficient defined in Laura and Grossi (1979)
$*$–Laura and Grossi (1979)
(%)–percentage difference between reference and present results

3.4 Discussion and remarks

The flexural and vibration analysis of rectangular orthotropic plates with rotationally restrained edges has been carried out by means of double finite sine transforms in preceding sections. This method is essentially the same as the Fourier series expansion (Wang and Lin, 1996, 1999) and the improved superposition method (Bhaskar and Kaushik, 2004; Bhaskar and Sivaram, 2008; Kshirsagar and Bhaskar, 2008). Compared to these equivalent methods, the finite integral transform method is more convenient and can be routinely applied to more complex boundary value problems by choosing different integral kernels. However, due to slow convergence, these so-called theoretical-exact series solutions normally produce only approximate results for vibration analysis of plates. The larger the value of rotational fixity factors, the greater the time needed to achieve a high degree of accuracy. In such cases, the improved Fourier series method developed by Li et al. (Li, 2004; Li et al., 2009b) can be applied to improve convergence and as well as accuracy.

3.4.1 Formulations

The method of finite integral transform presented in this study is straightforward in concept and systematic in formulation. First, the governing differential equation is converted into an algebraic equation in terms of the integral form of the solution by applying an appropriate integral kernel. The initial or boundary conditions will be accounted for automatically in the process of conversion. The resulting algebraic equation can be solved without much difficulty. If the algebraic equation involves variables that are unknown, the boundary conditions can be applied to determine the variables eventually. Through this procedure, a system of linear algebraic equations will be obtained for unknown variables. Once the integral form of the solution is known, the original function can be derived by using the inverse integral transform (Rao, 2007).

As discussed in Section 3.3.1, two different formulations (i.e., Eqs. (3.77) and (3.86)) can be generated. For the case investigated in this present research, the first formulation leads to Eq. (3.74) and then to four infinite systems of equations, Eqs. (3.77), with respect to $\bar{W}_{,xx}(0,n)$, $\bar{W}_{,xx}(a,n)$, $\bar{W}_{,yy}(m,0)$, and $\bar{W}_{,yy}(m,b)$. For each combination of m and n, Eqs. (3.77) produce $2m+2n$ equations with $2m+2n$ unknown variables. As a

results, frequencies can be acquired by solving a highly nonlinear equation representing the determinant of the coefficient matrix with dimensions of $(2m + 2n) \times (2m + 2n)$. This approach was employed by Hurlebaus et al. (2001) and Zhong and Yin (2008). However, the number of terms used in the numerical computations (size of the matrix) and the corresponding numerical method are not reported in Hurlebaus et al. (2001). Zhong and Yin (2008) computed the eigenfrequencies and corresponding mode shapes by truncating the series up to 13 terms. It would be quite difficult to solve the non-linearly equation resulting from the determinant to obtain the frequency when large values of m and n are selected. The other formulation results in Eq. (3.82) or Eq. (3.86) by expressing $\bar{W}_{,xx}(0,n)$, $\bar{W}_{,xx}(a,n)$, $\bar{W}_{,yy}(m,0)$, and $\bar{W}_{,yy}(m,b)$ in terms of $\bar{\bar{W}}(m,n)$ and substituting them into Eq. (3.74). A system of linear equations about $\bar{\bar{W}}(m,n)$ with dimensions of $(m \times n) \times (m \times n)$ is obtained. Natural frequencies can be easily obtained by determining the eigenvalues of the coefficient matrix. As shown in Section 3.3.3, the numerical results can be calculated without much difficulty by selecting $m = n = 150$. The second formulation is more efficient than the first one for the case of free vibration analysis for either one-dimensional elements or two-dimensional elements.

For the flexural analysis carried out in Section 3.2, the first formulation leads to a coefficient matrix with dimensions of $(2m + 2n) \times (2m + 2n)$, but the second one has dimensions of $(m \times n) \times (m \times n)$. The first formulation is more computationally efficient for flexural analysis, and also more efficient for forced vibration analysis as well because their procedure are same.

3.4.2 Convergence

A convergence study has been conducted to analyze the free vibration of a square isotropic plate with four edges rotationally restrained with $r = 0.999$ in Section 3.3.3, using the MATLAB program on a desktop computer equipped with a 3.40 GHz Intel Core i7-2600 processor and 8 GB of memory. Similarly, the rate of convergence was examined during flexural analysis of plates with edges rotationally restrained in Section 3.2. It was observed that the results converged slowly. However, during the flexural analysis in Section 3.2, numerical results were easily obtained for a series of up to 2000 terms. Thus, the exact solutions were acquired. On the other hand, overflow problems occurred shortly when m and n were greater than 200 on the computer program carried out for the free vibration

analysis in this research. Therefore, only approximate values are obtained by applying the method of finite integral transform for free vibration analysis, whereas exact solutions can be theoretically determined by using an infinite series.

However, the convergence of the solutions is significantly accelerated by adopting the improved Fourier series methods developed by Li et al. (Li, 2000; Li and Daniels, 2002; Li, 2004; Du et al., 2007; Li et al., 2009b; Zhang and Li, 2009; Khov et al., 2009) through introducing the supplementary terms to Fourier series. Highly accurate results can be obtained by setting $M = N = 6$ as reported in Li (2004). This improvement seems to be unnecessary for flexural analysis of beams or plates with arbitrary boundary conditions, because the issue of the convergence is not significant in flexural analysis.

3.4.3 Untruncated and truncated

For numerical calculations, the series solution has to be truncated to a finite number of terms. However, as pointed out in Section 3.2, the coefficient matrix will become singular when applying this method for fully clamped plates (i.e., $r = 1.0$); therefore, the infinite summations should first be evaluated without truncation. This step might be required because the infinite summations are the counterparts of the derivatives of the closed-form Levy-type expressions (Kshirsagar and Bhaskar, 2008). Nevertheless, there is no issue of singularity in applying the proposed method for plates with rotationally restrained edges. Alternatively, fully clamped plates can be treated as a limiting cases by specifying the rotational fixity factor to be either 0.999 or 0.9999.

3.4.4 Broad applicability

The broad generality of the method of finite integral transform in solving plate flexural problems was summarized by Li et al. (2013). Selecting appropriate integral transform kernels based on boundary conditions will improve the accuracy and convergence. Li (2000, 2002) proved that the cosine series expansion would converge faster than its sine counterpart for beams with arbitrary elastic restraints, but the convergence speed of the sine series solution will be greatly increased when beams are simply supported with only rotational restraints. This fact might explain why the kernels $\sin \alpha_m x \sin \beta_n y$ are applied in this research for an orthotropic plate with rotationally restrained edges. Similarly, Hurlebaus et al. (2001) employed $\cos \alpha_m x \cos \beta_n y$ for free orthotropic plates.

In general, the sinusoidal kernel (i.e., $\sin \alpha_m x$) is taken for edges that are simply supported, clamped or rotationally restrained (i.e., elastically restrained against rotation). The co-sinusoidal kernel (i.e., $\cos \alpha_m x$) is recommended for free or translational restrained (i.e., elastically restrained against translation) edges, as presented in Appendix A. Alternatively, if for a pair of opposite edges, one is fully clamped or simply supported and the other is free, a half-sinusoidal kernel (i.e., $\sin \frac{\alpha_m}{2} x$) can be chosen (Li et al., 2013). The half-sinusoidal kernel is also defined as the modified finite sine transformation as demonstrated by Churchill (1972).

3.5 Summary

In the present research, the method of finite integral transform has been applied to the flexural and vibration analysis of a rectangular orthotropic plate with rotationally restrained edges. A rotational fixity factor is introduced to define elastic restraints along edges against rotations, thereby reflecting the relative stiffness of the plate and the rotational elastic restraints. Thus, the approach used in this thesis for plates with rotationally restrained edges can be applied for plates with general boundary conditions from simply supported to fully clamped by using various rotational fixity factors. Two formulations are developed for flexural and vibration analysis, separately. The validation of the present method is conducting by comparing the results with different exact solutions and approximate solutions reported from other researchers. The effects of rotational restraints, load distributions and aspect ratios on plate bending and vibration are investigated using comprehensive numerical results. In addition, various exact analytical methods for beams and plates with general boundary conditions have been reviewed, such as Fourier series expansion, improved Fourier series method, improved superposition method, and finite integral transform method. Brief comparisons and discussions are summarized for these exact analytical methods. Although the present research focuses on investigating orthotropic plates, conclusions obtained from the research are also applicable for isotropic plates.

It can be concluded that the finite integral transform method is simple and straightforward, can be calculated with the desired accuracy, and has general applicability. However, due to its slow convergence, this unified and systematic method only provides approximate values for vibration analysis of plates.

4

Equivalent Orthotropic Plates of CFS Floor Systems

4.1 Introduction

CFS floor systems can be regarded as a thin plate (i.e., subfloor) reinforced by a series of equidistant stiffeners (i.e., CFS joists) on one side in one direction with various transverse elements such as strapping and blocking. These floor systems can be idealized as equivalent orthotropic plates as discussed in Chapter 3. Analysing CFS floors as equivalent orthotropic plates is often sufficiently accurate and usually less complicated than an approach that considers the stiffeners discretely. Thus, it is necessary to determine the four elastic rigidities D_x, D_y, D_{xy}, D_1 and the mass of the equivalent orthotropic plate.

With the determination of the equivalent rigidities, the equivalent orthotropic plates can simulate the desired behavior of original CFS floor systems. For instance, in free vibration analysis, the equivalent orthotropic plates should provide the accurate solution on natural frequencies and modal shapes of original structures (Iyengar and Iyengar, 1967). Considerable efforts have been devoted to obtaining the rigidities of an equivalent orthotropic plate (Troitsky, 1976). Nevertheless, most existing methods have been developed in the context of static problems, such as in Huffington (1956) and Timoshenko and Woinowsky-Krieger (1959). The rigidities of equivalent orthotropic plates in free vibration were proposed by Iyengar and Iyengar (1967) for stiffened plate with stiffeners in both longitudinal and transverse directions, which is different from CFS floors with

joists running in one direction only. Moreover, considering the elastic rotational restraints along with the joist ends of CFS floors, existing equivalent rigidities based on simply supported boundaries cannot be applied directly. Therefore, it is necessary to obtain the rigidities for the equivalent orthotropic plates of CFS floors in vibration analysis with accounting for the actual boundary conditions and construction details.

This chapter presents an analytical method based on the Rayleigh method for determining the equivalent rigidities of CFS floor systems while considering elastic rotational restraints at the joist ends. Simplified design equations are developed for calculating the fundamental frequency of the floor systems. Lastly, the results obtained from the proposed equations are validated with existing test results.

4.2 Equivalent properties for vibration of CFS floors

4.2.1 Methodology

Iyengar and Iyengar (1967) employed the Rayleigh method to determine the equivalent rigidities and mass of stiffened plates in free vibration. In their study, the natural frequencies for the stiffened and the equivalent orthotropic plate were obtained by the Rayleigh method by applying eigenfunctions of beams with similar boundary conditions. The equivalent rigidities and mass were determined through equating the natural frequencies of the stiffened plates with those of the equivalent orthotropic plates. A similar method was also proposed by Smith and Chui (1988) to predict natural frequencies of lightweight wood floors.

It is well known that more accurate results can be obtained by using the Rayleigh-Ritz method with a series of admissible functions as the Rayleigh method achieves only a first approximation to a vibration frequency by using a single admissible function (Leissa, 2005). However, the Rayleigh-Ritz method can be labour intensive because the plate deflection $W(x, y)$ is expressed as the sum of a series of products of undetermined weighting coefficients and admissible functions. The one-term approximation of the Rayleigh method was applied by Warburton (1954) to derive approximate expressions for the frequencies of isotropic plates with various boundary conditions, then extended to orthotropic plates by Hearmon (1959). Its accuracy was assessed and confirmed by comparison with published

theoretical and experimental results (Warburton, 1983).

Consequently, in the context of the engineering practice, the Rayleigh method is adopted to establish the equivalent rigidities and mass of CFS floor systems. The selection of appropriate admissible functions is critical for accuracy in calculating natural frequencies of floors using the Rayleigh method. Characteristic functions for beams with similar boundary conditions are often adopted in practice as admissible functions for the various boundary conditions. Thus, to facilitate the discussion on modelling CFS floor systems with the equivalent orthotropic plates with elastically restrained edges, the free vibration of rotationally restrained beams (i.e., simply supported beams with ends elastically restrained against rotation) is investigated firstly.

4.2.2 Free vibration of rotationally restrained beams

The method of finite integral transform is applied to investigate the vibration of rotationally restrained beams. The equation of motion for the free vibrations of a Bernoulli-Euler beam with uniformly distributed mass shown in Fig. 4.1 is (Weaver Jr et al., 1990)

$$EI\frac{\partial^4 w\left(x,t\right)}{\partial x^4}+\rho A\frac{\partial^2 w\left(x,t\right)}{\partial t^2}=0 \tag{4.1}$$

where $w(x,t)$ is the displacement at distance x along the length of the beam and time t, EI is the flexural rigidity of the beam, ρ is the mass density, and A is the cross-sectional area of the beam.

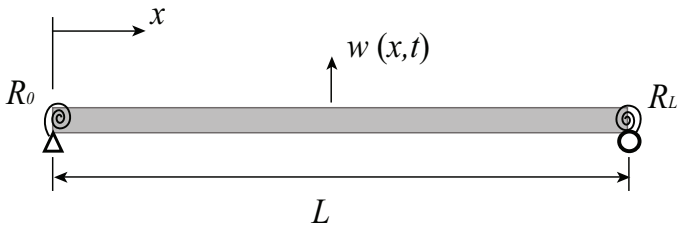

Figure 4.1 Simply supported beam with ends elastically restrained against rotation.

Upon assuming harmonic motion for the free vibration analysis, the displacement $w(x,t)$ can be expressed as

$$w\left(x,\ t\right)=\psi\left(x\right)\cos\omega t \tag{4.2}$$

where ω is the natural circular frequency and $\psi(x)$ is the modal displacement function.

Substitution of Eq. (4.2) into Eq. (4.1) will lead to

$$EI\frac{d^4\psi\,(x)}{dx^4} - \rho A\omega^2\psi\,(x) = 0 \tag{4.3}$$

Then, the boundary conditions can be expressed as

$$\psi = 0,\ \ R_0\frac{d\psi}{dx} = EI\frac{d^2\psi}{dx^2}\quad at\ x = 0 \tag{4.4a}$$

$$\psi = 0,\ \ R_L\frac{d\psi}{dx} = -EI\frac{d^2\psi}{dx^2}\quad at\ x = L \tag{4.4b}$$

in which R_0 and R_L are rotational spring constants at $x = 0$ and $x = L$, respectively. The end restraints are assumed to be proportional to the end rotations and the restraint stiffness, R_0 and R_L, may have any value in the range between simply supported (i.e., zero) and completely restrained (i.e., infinity).

The pair of the finite sine transform is defined as

$$\bar{\psi}(m) = \int_0^L \psi(x)\sin\alpha_m x dx \tag{4.5a}$$

$$\psi(x) = \frac{2}{L}\sum_{m=1}^{\infty}\bar{\psi}(m)\sin\alpha_m x \tag{4.5b}$$

where

$$\alpha_m = \frac{m\pi}{L}\ \ (m = 1, 2, 3, ...) \tag{4.6}$$

Using integration by parts and the boundary conditions of Eqs. (4.4), the finite sine transforms of the fourth derivatives in Eq. (4.3) can be obtained by

$$\int_0^L \frac{d^4\psi(x)}{dx^4}\sin\alpha_m x dx = \alpha_m^4\bar{\psi}(m) - \alpha_m\left[(-1)^m\psi_L'' - \psi_0''\right] \tag{4.7}$$

where

$$\psi_0'' = \frac{d^2\psi(0)}{dx^2},\ \ \psi_L'' = \frac{d^2\psi(L)}{dx^2} \tag{4.8}$$

Taking the finite sine transform to both sides of Eq. (4.3) and substituting Eq. (4.5a) and (4.7) yield

$$\alpha_m^4 \bar{\psi}(m) - \alpha_m \left[(-1)^m \psi_L'' - \psi_0''\right] - \beta^4 \bar{\psi}(m) = 0 \tag{4.9}$$

where

$$\beta^4 = \frac{\rho A}{EI}\omega^2 \tag{4.10}$$

From Stokes's transformation, it can be obtained from Eq. (4.5b)that

$$\frac{d\psi(x)}{dx} = \frac{2}{L}\sum_{m=1}^{\infty} \alpha_m \bar{\psi}(m) \cos \alpha_m x \tag{4.11}$$

According to the boundary conditions of Eqs. (4.4), ψ_0'' and ψ_L'' can be determined as

$$\psi''_0 = \frac{d^2\psi(0)}{dx^2} = \frac{2}{L}\frac{R_0}{EI}\sum_{m=1}^{\infty} \alpha_m \bar{\psi}(m) \tag{4.12a}$$

$$\psi''_L = \frac{d^2\psi(L)}{dx^2} = \frac{2}{L}\frac{R_L}{EI}\sum_{m=1}^{\infty} (-1)^{m+1} \alpha_m \bar{\psi}(m) \tag{4.12b}$$

Rearranging Eq. (3.38), it yields

$$\frac{R}{EI} = \frac{1}{L}\frac{3r}{1-r} \tag{4.13}$$

Substituting Eq. (4.13) into Eqs. (4.12), it gives

$$\psi''_0 = \frac{1}{L^2}\frac{6r_0}{1-r_0}\sum_{m=1}^{\infty} \alpha_m \bar{\psi}(m) \tag{4.14a}$$

$$\psi''_L = \frac{1}{L^2}\frac{6r_L}{1-r_L}\sum_{m=1}^{\infty} (-1)^{m+1} \alpha_m \bar{\psi}(m) \tag{4.14b}$$

where r_0 and r_L are rotational fixity factors at beam ends $x = 0$ and $x = L$, respectively. Substituting Eqs. (4.14) into Eq. (4.9), it produces

$$m^4 \bar{\psi}(m) + \frac{6m}{\pi^2}\sum_{i=1}^{\infty}\left[\frac{r_0}{1-r_0} + (-1)^{i+m}\frac{r_L}{1-r_L}\right] i\bar{\psi}(i) - \lambda^4 \bar{\psi}(m) = 0 \tag{4.15}$$

where

$$\lambda^4 = \frac{\rho A L^4}{EI\pi^4}\omega^2 \tag{4.16}$$

It would be convenient to expressed Eq. (4.15) in the following matrix form:

$$\mathbf{A}\boldsymbol{\Psi} = \lambda^4 \boldsymbol{\Psi} \tag{4.17}$$

where $\boldsymbol{\Psi} = [\bar{\psi}(1), \bar{\psi}(2), \ldots, \bar{\psi}(M)]$ if only the first M vibration modes of the beam is considered and $\mathbf{A}$ is the corresponding coefficient matrix of size $M \times M$ whose elements can be expressed as

$$A_{ii} = i^4 + \frac{6i^2}{\pi^2}\left[\frac{r_0}{1-r_0} + \frac{r_L}{1-r_L}\right] \tag{4.18a}$$

$$A_{ij} = \frac{2ij}{\pi^2}\left[\frac{r_0}{1-r_0} + (-1)^{i+j}\frac{r_L}{1-r_L}\right] \tag{4.18b}$$

in which $i = 1, 2, \ldots, M$, $j = 1, 2, \ldots, M$ but $i \neq j$.

The natural frequencies can be obtained by solving the eigenvalue problem of Eq. (4.17) and the corresponding mode shape can be determined in terms of Fourier sine series by substituting $\bar{\psi}(m)$ of the eigenvector into Eq. (4.5b). Numerical results for the first eight frequencies are listed and compared with those from Wang and Lin (1996) in Table 4.1. Values are easily obtained by MATLAB program for $M = 1000$. Excellent agreements can be observed in Table 4.1.

Table 4.1 Frequency parameter, λ with $r_0 = 0.9997^{\star}$.

Mode	$r_L = 0$		$r_L = 0.7692$		$r_L = 0.9709$		$r_L = 0.9712$	
	Ref*	Present	Ref*	Present	Ref*	Present	Ref*	Present
1	1.251	1.250	1.288	1.287	1.412	1.411	1.494	1.492
2	2.252	2.250	2.273	2.271	2.374	2.372	2.481	2.478
3	3.252	3.250	3.267	3.265	3.353	3.350	3.475	3.470
4	4.253	4.250	4.256	4.262	4.338	4.335	4.469	4.463
5	5.254	5.250	5.264	5.260	5.328	5.323	5.463	5.455
6	6.255	6.251	6.263	6.259	6.320	6.315	6.457	6.449
7	7.256	7.251	7.263	7.258	7.314	7.308	7.452	7.443
8	8.258	8.251	8.263	8.257	8.310	8.302	8.447	8.437

Note: $*$ Wang and Lin (1996)

$\star$ $r_0 = 0.9997$ is adapted from $\bar{K}_o = 10^5$ in Wang and Lin (1996).

4.2.3 Free vibration of orthotropic plates with rotationally restrained edges

For a rectangular orthotropic plate having one pair edges simply supported and the other pair edges elastic restrained against rotation as shown in Fig. 4.2, the determination of the natural frequencies by using the Rayleigh method applying beam characteristic functions as admissible functions is presented as follows.

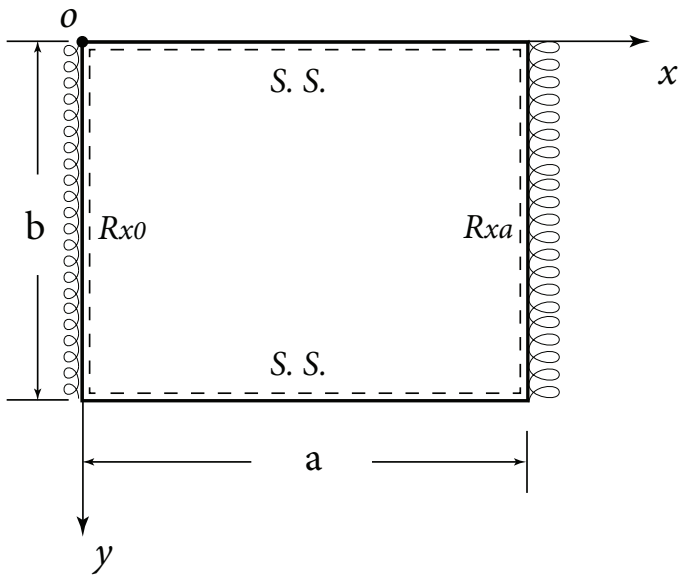

Figure 4.2 Orthotropic plate with two opposite edges rotationally restrained.

The boundary conditions of the orthotropic plate shown in Fig. 4.2 are

$$w = 0,\ \ R_{x0}\frac{\partial w}{\partial x} = D_x\left[\frac{\partial^2 w}{\partial x^2} + v_y\frac{\partial^2 w}{\partial y^2}\right],\ \ at\ \ x = 0 \tag{4.19a}$$

$$w = 0,\ \ R_{xa}\frac{\partial w}{\partial x} = -D_x\left[\frac{\partial^2 w}{\partial x^2} + v_y\frac{\partial^2 w}{\partial y^2}\right],\ \ at\ \ x = a \tag{4.19b}$$

$$w = 0,\ \ D_y\left[\frac{\partial^2 w}{\partial y^2} + v_x\frac{\partial^2 w}{\partial x^2}\right] = 0,\ \ at\ \ y = 0 \tag{4.19c}$$

$$w = 0,\ \ -D_y\left[\frac{\partial^2 w}{\partial y^2} + v_x\frac{\partial^2 w}{\partial x^2}\right] = 0,\ \ at\ \ y = b \tag{4.19d}$$

where a is the floor span; b is the floor width; R_{x0} and R_{xa} are the rotational stiffness (per unit length) along the corresponding edges $x = 0$ and $x = a$, respectively; D_x and D_y are flexural rigidities; ν_x and ν_y are Poisson's ratios. The restraint stiffness, R_{x0} and R_{xa}, can be treated the same as R_0 and R_L for the beam in the last section. For the free vibration of a plate vibrating harmonically with circular frequency ω, the deflection $w(x, y, t)$ can be expressed as

$$w\left(x,\, y,\, t\right) = W\left(x,\, y\right)\cos\omega t \tag{4.20}$$

If only the bending stresses is accounted for, the maximum strain energy (i.e. potential energy) of an orthotropic plate is given by (Timoshenko and Woinowsky-Krieger, 1959)

$$U_{pmax} = \frac{1}{2}\int_0^a\int_0^b\left[D_x\left(\frac{\partial^2 W}{\partial x^2}\right)^2 + 2D_1\frac{\partial^2 W}{\partial x^2}\frac{\partial^2 W}{\partial y^2} + D_y\left(\frac{\partial^2 W}{\partial y^2}\right)^2 + 4D_{xy}\left(\frac{\partial^2 W}{\partial x\partial y}\right)^2\right]dxdy \tag{4.21}$$

Supplementary to the plate strain energy, there is additional strain energy stored in the rotational springs along the edges (i.e. associated to the rotational restraints in the edges). The maximum strain energy associated with these boundary conditions is calculated by

$$\begin{aligned} U_{rmax} &= \frac{1}{2}D_x\left\{\int_0^b\left[\frac{\partial^2 W}{\partial x^2} + \nu_y\frac{\partial^2 W}{\partial y^2}\right]\frac{\partial W}{\partial x}\bigg|_{x=0}dy - \int_0^b\left[\frac{\partial^2 W}{\partial x^2} + \nu_y\frac{\partial^2 W}{\partial y^2}\right]\frac{\partial W}{\partial x}\bigg|_{x=a}dy\right\} \\ &= -\frac{1}{2}D_x\int_0^b\left[\frac{\partial^2 W}{\partial x^2}\frac{\partial W}{\partial x} + \nu_y\frac{\partial^2 W}{\partial y^2}\frac{\partial W}{\partial x}\right]\Bigg|_{x=0}^{x=a}dy \end{aligned} \tag{4.22}$$

The total maximum strain energy, U_{max} is obtained by summing contributions form Eqs. (4.21) and (4.22).

$$\begin{aligned} U_{max} = &\frac{1}{2}\int_0^a\int_0^b\left[D_x\left(\frac{\partial^2 W}{\partial x^2}\right)^2 + 2D_1\frac{\partial^2 W}{\partial x^2}\frac{\partial^2 W}{\partial y^2} + D_y\left(\frac{\partial^2 W}{\partial y^2}\right)^2 + 4D_{xy}\left(\frac{\partial^2 W}{\partial x\partial y}\right)^2\right]dxdy \\ &- \frac{1}{2}D_x\int_0^b\left[\frac{\partial^2 W}{\partial x^2}\frac{\partial W}{\partial x} + \nu_y\frac{\partial^2 W}{\partial y^2}\frac{\partial W}{\partial x}\right]\Bigg|_{x=0}^{x=a}dy \end{aligned} \tag{4.23}$$

The maximum kinetic energy is calculated by

$$T_{\max} = \frac{1}{2}\rho\omega^2 h\int_0^a\int_0^b W^2 dxdy \tag{4.24}$$

where ρ is the mass density of the plate and h is the thickness of the plate.

Using the Rayleigh quotient, the natural frequencies of the plate can be obtained by equating the maximum potential energy U_{max} and the maximum kinetic energy T_{max} and given as

$$\omega^2 = \frac{U_{max}}{\frac{1}{2}\rho h \int_0^a \int_0^b W^2 dxdy} \tag{4.25}$$

In order to obtain natural frequencies, $W(x, y)$ can be assumed to be separable in x and y as

$$W(x, y) = B\psi(x)\varphi(y) = B\sum_{m=1}^{\infty} A_m \sin\alpha_m x \sin\beta_n y \tag{4.26}$$

where B is a constant, $\beta_n = n\pi/b$, $\varphi(y) = \sin\beta_n y$ is the characteristic function of a simply supported beam, and

$$\psi(x) = \sum_{m=1}^{\infty} A_m \sin\alpha_m x \tag{4.27}$$

represents the characteristic function of the simply supported beam with rotational restraints, which can be obtained by Eq. (4.5b) with $A_m = \bar{\psi}(m)$.

Substituting Eq. (4.26) into Eq. (4.25) yields

$$\omega^2 = \frac{\begin{array}{l} ab\pi^4 \left[\frac{D_x}{a^4}\sum\limits_{m=1}^{\infty} m^4 A_m^2 + 2\frac{D_1+2D_{xy}}{a^2b^2} n^2 \sum\limits_{m=1}^{\infty} m^2 A_m^2 + \frac{n^4 D_y}{b^4}\right] \\ +2D_x \left[\psi_0'' \frac{\pi b}{a} \sum\limits_{m=1}^{\infty} mA_m - \psi_a'' \frac{\pi b}{a} \sum\limits_{m=1}^{\infty} (-1)^m mA_m\right] \end{array}}{\rho hab \sum\limits_{m=1}^{\infty} A_m^2} \tag{4.28}$$

where ${\psi''}_0$ and ${\psi''}_a$ can be obtained from Eq. (4.14) and (4.27) as

$${\psi''}_0 = \frac{d^2\psi(0)}{dx^2} = \frac{\pi}{a^2}\frac{3r_0}{1-r_0}\sum_{m=1}^{\infty} mA_m \tag{4.29a}$$

$${\psi''}_a = \frac{d^2\psi(a)}{dx^2} = \frac{\pi}{a^2}\frac{3r_a}{1-r_a}\sum_{m=1}^{\infty} (-1)^{m+1} mA_m \tag{4.29b}$$

Substituting Eq. (4.29) to Eq. (4.28) and rearranging the equation, it gives

$$\omega^2 = \frac{ab\pi^4\left[c_1\frac{D_x}{a^4} + 2c_2n^2\frac{H}{a^2b^2} + n^4\frac{D_y}{b^4}\right]}{\rho hab} \tag{4.30}$$

where $H = D_1 + 2D_{xy}$, c_1 and c_2 are defined as restraint coefficients which can be given by

$$c_1 = \left[\sum_{m=1}^{\infty} m^4A_m^2 + \frac{1}{\pi^2}\frac{6r_0}{1-r_0}\left(\sum_{m=1}^{\infty} mA_m\right)^2 + \frac{1}{\pi^2}\frac{6r_a}{1-r_a}\left(\sum_{m=1}^{\infty}(-1)^m mA_m\right)^2\right] \Big/ \sum_{m=1}^{\infty} A_m^2$$
$$c_2 = \sum_{m=1}^{\infty} m^2A_m^2 \Big/ \sum_{m=1}^{\infty} A_m^2 \tag{4.31}$$

The fundamental frequency can be obtained by letting $n = 1$ in Eq. (4.30) and choosing A_m of Eq. (4.31) associated to the first vibration mode of the rotationally restrained beam for the orthotropic plate with two opposite edges (i.e., $x = 0$ and $x = a$) rotationally restrained and the other two edges (i.e., $y = 0$ and $y = b$) simply supported. Numerical investigations have been performed to confirm the validity of the present equations for evaluating the fundamental frequency of rectangular orthotropic plates with rotational restraints and compared with results of Hearmon (1959) as shown in Table 4.2. The numerical results of c_1 and c_2 are obtained by setting m up to 1000 in Eq. (4.31). Hearmon (1959) applied the Rayleigh method to determine closed formulas for the natural frequencies of orthotropic plates under any combination of clamped or simply supported edges. The general equations for the natural frequencies can be expressed as

$$\rho h\omega^2 = \frac{A^4D_x}{a^4} + \frac{B^4D_y}{b^4} + \frac{2CH}{a^2b^2} \tag{4.32}$$

where the values of A, B and C of the fundamental frequency for boundary conditions of four edges simply supported (i.e., S-S-S-S) are $A = B = C = \pi^4$. For two opposite edges clamped and the others simply supported (i.e., S-C-S-C), $A = 4.730^4$, $B = \pi^4$ and $C = 12.30\pi^2$. Then, from Hearmon (1959) the restraint coefficients, $c_1 = c_2 = 1$, can be calculated for the boundary conditions of S-S-S-S and $c_1 = 5.138$ and $c_2 = 1.246$ for the boundary conditions of S-C-S-C. Table 4.2 shows that the coefficients c_1 and c_2 increase as rotational fixity factors increase as expected and approach to the value of the S-C-S-C case when r_{x0} and r_{xa} are closing to 1.

Table 4.2 Frequency coefficients for different rotational fixity factors.

	Rotational fixity factor $r_{x0} = r_{xa}$											
	0	0.1	0.2	0.3	0.4	0.5	0.6	0.7	0.8	0.9	0.999	1*
c_1	1	1.131	1.284	1.464	1.680	1.945	2.274	2.695	3.254	4.024	5.133	5.138
c_2	1	1	1.001	1.003	1.006	1.012	1.022	1.040	1.071	1.130	1.246	1.246

Note: $*$ results from Hearmon (1959).

Furthermore, the frequencies in Eq. (4.30), obtained using the Rayleigh method, are also compared with those determined by the method of finite integral transform in Section 3.3. Rearranging Eq. (4.30), the fundamental frequency parameter can be derived as

$$\Omega_1 = \omega_1 a^2 \sqrt{\frac{\rho h}{D_x}} = \pi^2 \sqrt{c_1 + 2c_2 \frac{H}{D_x} \left(\frac{a}{b}\right)^2 + \frac{D_y}{D_x} \left(\frac{a}{b}\right)^4} \tag{4.33}$$

Assuming $D_y/D_x = 4$ and $H/D_x = 2$, results of the fundamental frequency parameter obtained using both methods are listed in Table 4.3. Excellent agreements can be observed.

Table 4.3 Fundamental frequency parameter Ω_1 for different rotational fixity factors.

$r_{x0} = r_{xa}$	$\Omega_1 = \omega_1 a^2 \sqrt{\rho h / D_x}$					
	$b/a = 1$		$b/a = 1.5$		$b/a = 2$	
	FIT*	present*	FIT*	present*	FIT*	present*
0	29.609	29.609	18.643	18.643	14.804	14.804
0.100	29.825	29.824	18.983	18.982	15.230	15.229
0.200	30.078	30.079	19.375	19.367	15.714	15.714
0.300	30.379	30.382	19.832	19.831	16.271	16.268
0.400	30.742	30.745	20.372	20.367	16.919	16.911
0.500	31.190	31.200	21.020	21.016	17.684	17.675
0.600	31.756	31.770	21.814	21.805	18.603	18.585
0.700	32.493	32.517	22.810	22.794	19.732	19.702
0.800	33.492	33.525	24.099	24.071	21.158	21.110
0.900	34.921	34.956	25.836	25.780	23.026	22.943
0.999	37.099	37.083	28.278	28.156	25.561	25.411

Note: b/a Aspect ratio
$*$ Finite integral transform method
$\star$ Rayleigh method

Additionally, if edges parallel to the span (i.e., $y = 0$ and $y = b$) are free (i.e., S-F-S-F), the first mode shape $\varphi_1(y)$ in Eq. (4.26) can be defined as $\varphi_1(y) = 1$. Following the same procedure, the fundamental frequency is expressed as

$$\omega^2 = c_1 \frac{ab\pi^4}{m} \frac{D_x}{a^4} \tag{4.34}$$

where $m = \rho hab$ and c_1 is same as shown in Eq. (4.30).

4.2.4 Free vibration of CFS floor systems

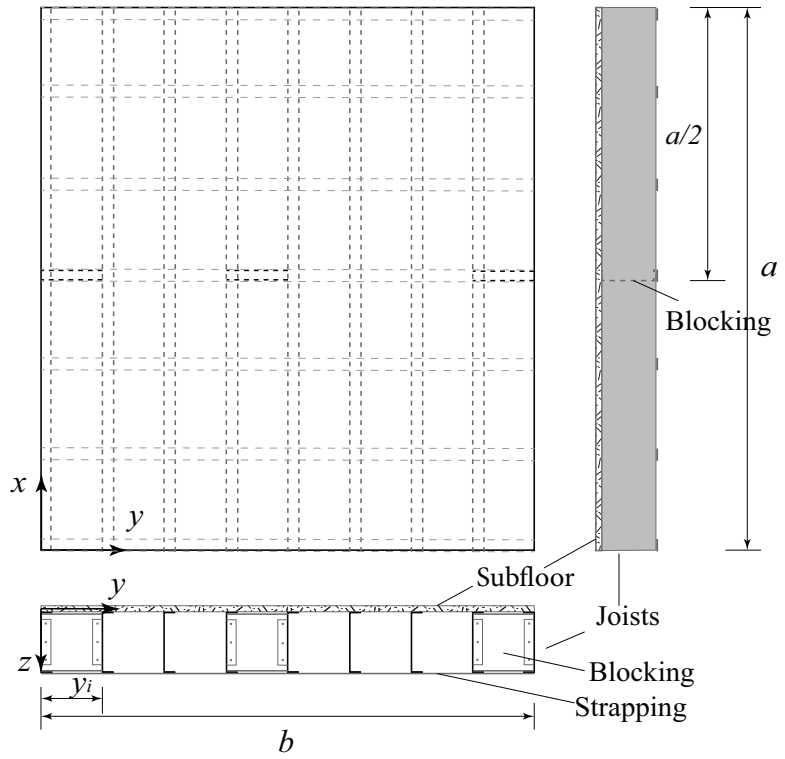

Figure 4.3 Layout of typical CFS floor systems.

Fig. 4.3 illustrates the configuration details of a typical CFS floor system. The maximum potential energy of a CFS floor system consists of the following three components.

$$U_{max} = U_{smax} + U_{jmax} + U_{tmax} \tag{4.35}$$

where U_{smax}, U_{jmax} and U_{tmax} are the maximum potential energy of subfloor, joists and

transverse elements, respectively. For the simplicity of presenting the analysis procedure, only one row of transverse elements at the mid-span is considered in the following derivation. The components of potential energy can be expressed as

$$U_{smax} = \frac{1}{2}\int_0^a \int_0^b \left[D_{sx}\left(\frac{\partial^2 W}{\partial x^2}\right)^2 + 2D_{s1}\frac{\partial^2 W}{\partial x^2}\frac{\partial^2 W}{\partial y^2} + D_{sy}\left(\frac{\partial^2 W}{\partial y^2}\right)^2 + 4D_{sxy}\left(\frac{\partial^2 W}{\partial x \partial y}\right)^2 \right] dxdy \tag{4.36a}$$

$$U_{jmax} = \frac{1}{2}EI_j \sum_{i=1}^{N_j} \int_0^a \left(\frac{\partial^2 W}{\partial x^2}\right)^2_{y=y_i} dx - \frac{1}{2}EI_j \sum_{i=1}^{N_j} \left(\frac{\partial^2 W}{\partial x^2}\frac{\partial W}{\partial x}\right)_{y=y_i}\Bigg|_{x=0}^{x=a} \tag{4.36b}$$

$$U_{tmax} = \frac{1}{2}EI_t \int_0^b \left(\frac{\partial^2 W}{\partial y^2}\right)^2_{x=a/2} dy \tag{4.36c}$$

where D_{sx}, D_{sy}, D_{s1} and D_{sxy} are the flexural and torsional rigidities of the subfloor, EI_j and EI_t are flexural rigidities of joists and transverse element at mid-span, separately, y_i represents the location of joists; and N_j is the number of joists.

The maximum kinetic energy of a CFS floor system is given by

$$T_{max} = \frac{1}{2}\omega^2 \left[\rho_s h_s \int_0^a \int_0^b W^2 dydx + \rho_j A_j \sum_{i=1}^{N_j} \int_0^a W^2_{y=y_i} dx + \rho_t A_t \int_0^b W^2_{x=a/2} dy \right] \tag{4.37}$$

where h_s is the height of the subfloor; ρ_s, ρ_j and ρ_t are the densities of the subfloor, steel joists and transverse elements, separately; A_j and A_t are the cross-sectional areas of the joists and the transverse elements, respectively.

The natural frequencies can be obtained by the Rayleigh quotient. After substituting Eq. (4.26), the natural circular frequency ω can be obtained as

$$\omega^2 = \frac{ab\pi^4 \left[\frac{c_3 D_{sx} + c_1 \frac{EI_j}{b/(N_j-1)}}{a^4} + 2c_2 n^2 \frac{(D_{s1}+2D_{sxy})}{a^2 b^2} + n^4 \frac{D_s y + 2c_4 EI_b/a}{b^4} \right]}{\rho_s h_s ab + (N_j - 1)\rho_j A_j a + 2c_4 \rho_t A_t b} \tag{4.38}$$

where restraint coefficients c_1 and c_2 can be found in Eq. (4.31); c_3 and c_4 are expressed

as

$$c_3 = \sum_{m=1}^{\infty} m^4 A_m^2 \Big/ \sum_{m=1}^{\infty} A_m^2 \tag{4.39a}$$

$$c_4 = \left(\sum_{m=1}^{\infty} A_m \sin \frac{m\pi}{2} \right)^2 \Big/ \sum_{m=1}^{\infty} A_m^2 \tag{4.39b}$$

When evaluating the integrals in Eq. (4.36b) and (4.37), a summation of the series is adopted from Chui (1987):

$$\sum_{i=1}^{N_j} \sin^2 \left(\frac{\pi y_i}{b} \right) = \sum_{i=1}^{N_j} \sin^2 \left(\frac{\pi \left(i-1 \right) s}{\left(N_j - 1 \right) s} \right) = \sum_{i=1}^{N_j} \sin^2 \left(\frac{\pi \left(i-1 \right)}{N_j - 1} \right) = \frac{N_j - 1}{2} \tag{4.40}$$

In addition, if boundary condition is S-F-S-F, the fundamental frequency can be obtained as

$$\omega^2 = \frac{ab\pi^4 \left[\dfrac{c_3 D_{sx} + c_1 \frac{EI_j}{b/N_j}}{a^4} \right]}{\rho_s h_s ab + N_j \rho_j A_j a + 2c_4 \rho_t A_t b} \tag{4.41}$$

4.2.5 Equivalent properties of CFS floor systems

If the equivalent orthotropic plate is used to predict the natural frequencies of CFS floor systems, Eq. (4.30) and Eq. (4.38) should be equal. This equality is obtained by taking

$$D_x = \frac{c_3}{c_1} D_{sx} + \frac{EI_j}{b/\left(N_j - 1 \right)} \tag{4.42a}$$

$$D_y = D_{sy} + 2c_4 EI_b / a \tag{4.42b}$$

$$H = D_{s1} + 2D_{sxy} \tag{4.42c}$$

$$\rho hab = \rho_s h_s ab + \left(N_j - 1 \right) \rho_j A_j a + 2c_4 \rho_t A_t b \tag{4.42d}$$

Therefore, Eqs. (4.42) will be used to obtain the equivalent rigidities and mass when a CFS floor system is modelled as an orthotropic plate. In addition, comparing Eq. (4.34) and Eq. (4.41), the equivalent rigidities and mass for the fundamental frequency of a CFS

floor system with boundary conditions of S-F-S-F can be expressed as

$$D_x = \frac{c_3}{c_1} D_{sx} + \frac{EI_j}{b/N_j} \tag{4.43a}$$

$$\rho hab = \rho_s h_s ab + N_j \rho_j A_j a + 2c_4 \rho_t A_t b \tag{4.43b}$$

4.3 Evaluation of the fundamental frequency of CFS floor systems

In characterizing the dynamic response of a lightweight floor system, the fundamental frequency plays a major role on the evaluation of vibration performance and it is desirable to be evaluated manually in design practice. From the preceding section, the fundamental frequency of CFS floor systems considering edges elastically restrained as shown in Eq. (4.38) (i.e., R-S-R-S) can be expressed as

$$f_1 = \frac{\pi}{2} \sqrt{\frac{ab}{m}} \sqrt{\frac{c_1 D_x}{a^4} + 2\frac{c_2 H}{a^2 b^2} + \frac{D_y}{b^4}} \tag{4.44}$$

where D_x and D_y are the equivalent flexural rigidities in $x--$ and $y--$ direction, respectively; H is the equivalent torsional rigidity; and m is the equivalent mass of a CFS floor system and is given as

$$m = \rho_s h_s ab + (N_j - 1)\, \rho_j A_j a + 2c_4 \rho_t A_t b \tag{4.45}$$

For CFS floor systems with two opposite edges elastically restrained and the other free (i.e., R-F-R-F), the fundamental frequency is obtained as

$$f_1 = \frac{\pi}{2} \sqrt{\frac{ab}{m}} \sqrt{\frac{D_x}{a^4}} \tag{4.46}$$

where

$$m = \rho_s h_s ab + N_j \rho_j A_j a + 2c_4 \rho_t A_t b \tag{4.47}$$

4.3.1 Equivalent rigidities

From Eq. (4.42a), it is found through the numerical investigation in Zhang and Xu (2016) that the coefficient c_1 and c_3 are identical for simply supported and clamped boundary conditions. For the case of rotational restrained edges, the magnitude of c_3 is comparable to but less than that of c_1. Moreover, if elastic restraints at the edges of a subfloor are considered, the restraint coefficient of D_{sx}, c_3, will be equal to c_1. Furthermore, considering the flexural stiffness of the subfloor, D_{sx}, is much less than that of the joists; for the sake of simplicity, c_3 is taken as the same value as that of c_1 regardless of whether there are restraints at the edges of the subfloor or not. Thus, Eq. (4.42a) becomes

$$D_x = \frac{1}{s}\left(D_{sx}s + EI_j\right) \tag{4.48}$$

where $s = b/(N_j - 1)$ is joist spacing, and $D_{sx}s + EI_j$ is the effective stiffness of a composite T-beam as shown in Fig. 4.4.

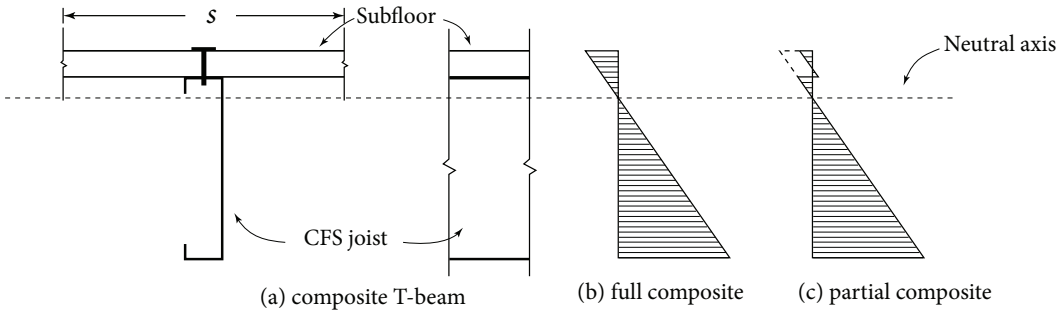

Figure 4.4 Composite T-beam and strain distribution.

The calculation of effective stiffness depends on the location of the neutral axis and the stress/strain distribution. Fig. 4.4(b) illustrates the strain distribution of a full composite T-beam in which no slip occurrs between the joist and subfloor. Otherwise, the beam becomes a partial composite beam. When a partial composite beam is subjected to a downward load, the lower extreme fibres of the subfloor tends to lengthen and the upper flange of the joist tend to shorten (Newmark et al., 1951). The shear connectors counteract these tendencies by exerting forces that produce compression in the subfloor and tension in the joist. Considering the partial composite action between the subfloor and the joists, the effective flexural stiffness, EI_{eff}, can be used in Eq. (4.48), and calculated based on

the procedure in Allen et al. (1999). Then, the flexural rigidity in the x-direction is given by

$$D_x = \frac{EI_{eff}}{s} \tag{4.49}$$

When CFS floors are modelled as orthotropic plates, difficulties are often experienced in determining the transverse flexural stiffness in the y-direction, D_y. This is because transverse elements are on only one side of the plate (i.e., underneath the subfloor), and their number may vary. An approximation was developed by Kirk (1970) assuming that the neutral plane is located at the middle plane of the plate if the plate is reinforced by a single stiffener placed along one of its centre lines. Timoshenko and Gere (1961, P. 399) claimed that the centroid of a cross section consisting of the stiffener and plate is very close to the surface of the plate when the stiffener is in the form of a channel or a bar of the Z section. The stiffness of the composite section can be evaluated by assuming the moment of inertia of the stiffener with respect to the axis coinciding with the outer surface of Z-shape stiffener's flange.

As illustrated in Figs. 4.5 and 4.6, transverse elements such as strapping, blocking, and strongback are commonly used in CFS floor systems to provide transverse floor stiffness. Since the stiffness contribution of strapping is very small, it can be ignored when calculating the stiffness of transverse elements. Given that no connection exists between the transverse elements and the subfloor, they act as independent bending members in carrying the load. The flexural stiffness in y-direction of CFS floors, D_y, is given by

$$D_y = D_{sy} + 2c_4\frac{E_tI_t}{a} = \frac{1}{a}(EI_{sy} + 2c_4EI_t) \tag{4.50}$$

with EI_{sy} and EI_t being the flexural stiffness of the subfloor in y-direction and the transverse elements, respectively.

Lastly, the Poisson's ratios in Eq. (4.48) and Eq. (4.50) are assumed to be zero for the reason of simplicity. This approximation is acceptable because the Poisson's ratios of various subfloors (i.e., OSB, Plywood, and structural concrete panel) are generally less than 0.3. Then, $D_{s1} = 0$ and H, in Eq. (4.42c) is expressed as

$$H = 2D_{sxy} = \frac{G_st_s^3}{6} \tag{4.51}$$

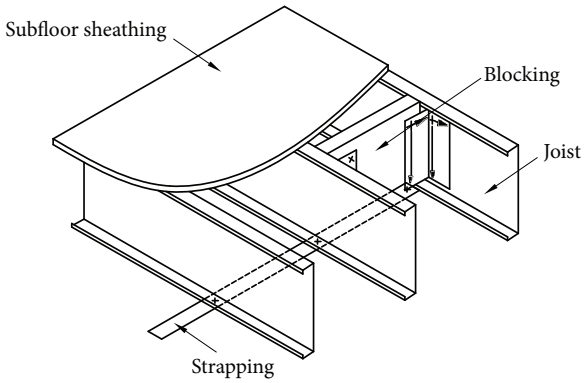

Figure 4.5 Blocking and strapping (Courtesy: ClarkDietrich).

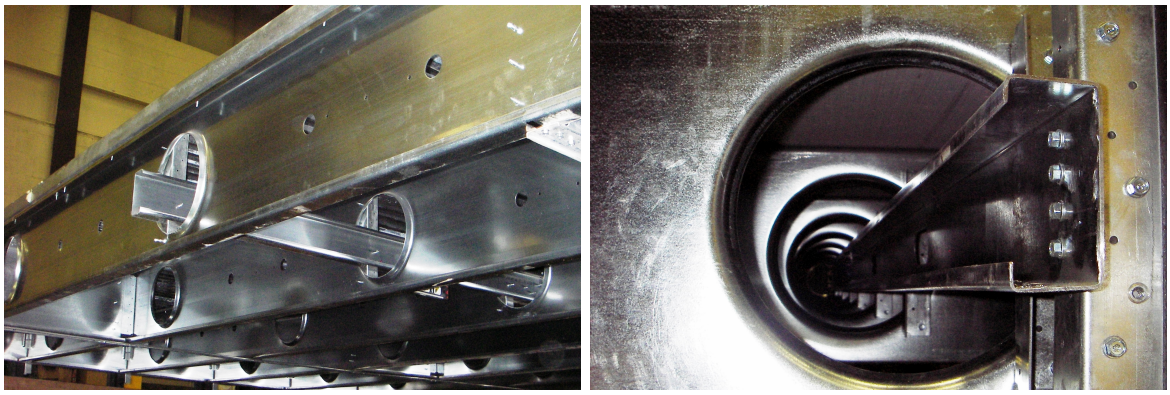

(a) Free end (b) Restrained end

Figure 4.6 Strongback of CFS floors.

where G_s is the shear modulus of the subfloor.

Thus, the fundamental frequency of a CFS floor system can be obtained by Eq. (4.44), and the corresponding equivalent rigidities are calculated based on the Eqs. (4.49), (4.50) and (4.51).

4.3.2 Simplified equations for restraint coefficients

In attempting to find simple formulas for computing restraint coefficients c_1, c_2 and c_4 for engineering practice, the coefficients can be closely approximated by

$$c_i = ar^3 + br^2 + cr + 1, \;\; i = 1, 2, 4 \tag{4.52}$$

where the rotational fixity factors $r = r_{x0} = r_{xa}$; and a, b and c are constants as shown in Table 4.4.

Table 4.4 Constant values of simple formulas for restraint coefficients.

Coefficients	a	b	c	R^2
c_1	4.619	-2.277	1.757	0.9994
c_2	0.662	-0.522	0.097	0.9929
c_4	0.284	-0.134	0.109	0.9995

Note: R^2–Coefficient of determination

A comparison of values by simplified equation Eq. (4.52) and results obtained by numerical analysis of c_1 is presented in Fig. 4.7. As can be seen, the simplified equation can provide close predictions. Comparisons of other coefficients (not presented here) also reach the same conclusion.

4.3.3 Effects of the torsional rigidity of joists

In derivation of the equivalent rigidities, the torsional effects of joists were ignored. Thus, effective torsional rigidity, H, of Eq. (4.51) does not include the torsional rigidity of joists. However, the torsional property proposed by Chui (2002) for wood floors is presented as

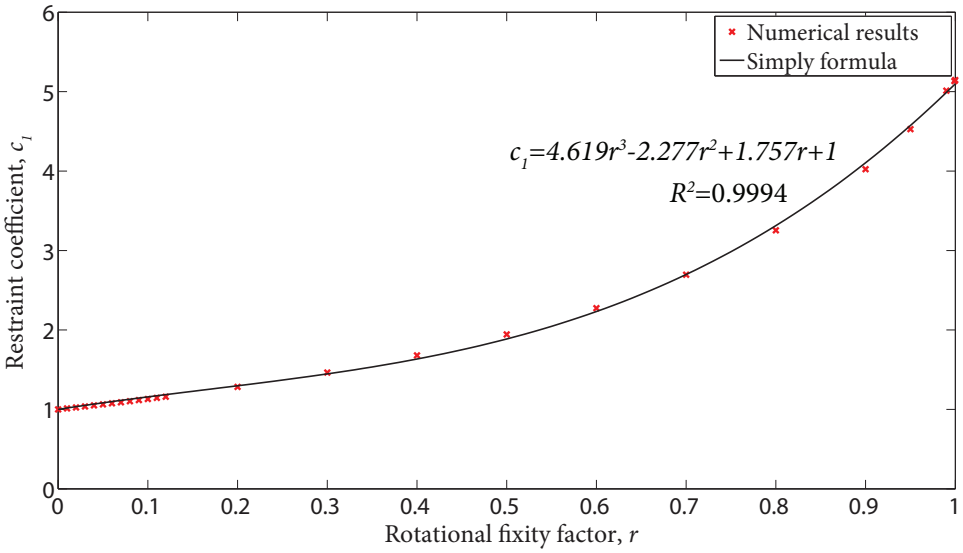

Figure 4.7 Comparison of c_1 between numerical analysis and simplified equation.

$$D_{xy} = \frac{G_s h^3}{12} + \frac{C}{2b_1} \tag{4.53}$$

in which the first term is the torsional rigidity of a subfloor, i.e., D_{sxy} in Eq. (4.51) and C is the torsional constant of the joist, provided by the joist manufacturer. This equation follows the work of Timoshenko and Woinowsky-Krieger (1959).

For the C–shape CFS joist, the torsional constant is given by (AISI S100, 2012)

$$C = \sum \frac{bt^3}{3} \tag{4.54}$$

where b represents the element plate lengths between points of intersections on their axes, and t represents the plate thicknesses. Since the thickness of C–shape CFS joists is much less than that of the wood joist, the torsional constant of the CFS joist is neglected.

4.3.4 Multiple rows of transverse elements

Chui (2002) proposed a method to determine the fundamental frequency for a wood-framed floor based on the ribbed plate theory by Timoshenko and Woinowsky-Krieger (1959). In this method, D_y is approximated by

$$D_y = \frac{EI_b}{a_1} + \frac{EI_p b_1}{b_1 - t + \alpha^3 t} \tag{4.55}$$

where t is the width of the cross-section of a timber joist, a_1 is the spacing of transverse elements, b_1 is the spacing of joists, EI_b is the stiffness of transverse elements, and EI_p is the stiffness of the floor deck. The first term of the right–hand side of Eq. (4.55) represents the stiffness of transverse elements. This method assumes that the stiffness contributions from various transverse elements (i.e., lateral-bracing elements) are the same, which is feasible if the spacing of transverse elements compared to the span is small enough. However, this approximation may not be valid for floor with only one or a few rows of transverse elements, as commonly seen in current construction practices, because the effective width of the subfloor is limited.

The coefficient c_4 is used to characterise the contribution on D_y by transverse elements such as blockings and strongbacks. In the derivation of c_4 presented in Eq. (4.39), it is assumed that there is only one row of transverse element located at mid-span, and D_y should be evaluated based on Eq. (4.50). However, if there are multiple rows of transverse elements along the span, D_y is evaluated as

$$D_y = \frac{1}{a}\left(EI_{sy} + \sum_{i=1}^{N_t} 2c_{4i} EI_{ti}\right) \tag{4.56}$$

where N_t is the number of rows of transverse elements; EI_{ti} is the flexural stiffness of the ith row of the transverse elements. It should be noted that coefficient c_{4i} is associated with locations of the transverse elements. For instance, for a floor with two rows of transverse elements located at one third and two thirds of the span (i.e., $x = a/3$, $x = 2a/3$ in Eq. (4.36c)), c_{4i} can be obtained by

$$c_{41} = c_{42} = \left(\sum_{m=1}^{\infty} A_m \sin\frac{m\pi}{3}\right)^2 \Bigg/ \sum_{m=1}^{\infty} A_m^2 \tag{4.57}$$

Values of c_{4i} for different locations of transverse elements are listed in Table 4.5.

Table 4.5 Restraint coefficient c_{4i} for different positions of transverse elements.

Position	Rotational fixity factor $r_{x0} = r_{xa}$										
x/a	0	0.1	0.2	0.3	0.4	0.5	0.6	0.7	0.8	0.9	0.999
1/2	1	1.0082	1.0179	1.0293	1.043	1.0598	1.0808	1.1076	1.1431	1.1917	1.2607
1/3 or 2/3	0.75	0.7510	0.7522	0.7536	0.7551	0.7568	0.7587	0.7607	0.7627	0.7641	0.7633
1/4 or 3/4	0.5	0.4963	0.4919	0.4867	0.4804	0.4727	0.4629	0.4500	0.4328	0.4085	0.3727

4.3.5 Continuous and discrete transverse elements

The transverse elements are assumed to be continuous in the foregoing derivation. However, in practice, only strongbacks are continuous elements and blockings are installed in several joist spaces discretely. For instance, blockings are typically installed at the first, middle and last joist space, as shown in Fig. 4.3. Taking into account the discontinuity of transverse elements, Eq. (4.36c) becomes

$$U_{t\,\max} = \frac{1}{2}\sum_{i=1}^{N_b} EI_b \int_{b_i}^{b_i+s} \left(\frac{\partial^2 W}{\partial y^2}\right)^2_{x=a/2} dy \tag{4.58}$$

where N_b is the number of blockings and b_i is the position of the ith blocking. Substituting Eq. (4.26), Eq. (4.58) can be approximated by

$$U_{t\,\max} = \frac{N_b}{N_j - 1} \cdot \frac{1}{2} EI_b \int_0^b \left(\frac{\partial^2 W}{\partial y^2}\right)^2_{x=a/2} dy \tag{4.59}$$

Thus, Eq. (4.59) will be used in Eq. (4.36c) to consider the potential energy associated with the discrete blockings.

4.3.6 Effects of ceiling

The installation of a gypsum board ceiling significantly contributes to the stiffness of a floor and increases damping as well as adds additional mass to the floor (Hu, 1998). As a result, the natural frequencies of floors are reduced accordingly. The impact of a ceiling becomes more significant with multiple layers of the ceiling. A similar conclusion can also be found in Liu (2001). The potential energy and the kinetic energy of the ceiling are in the same forms as those of the subfloor, and can be expressed as

$$U_{smax} = \frac{1}{2}\int_0^a \int_0^b \left[D_{cx}\left(\frac{\partial^2 W}{\partial x^2}\right)^2 + 2D_{c1}\frac{\partial^2 W}{\partial x^2}\frac{\partial^2 W}{\partial y^2} + D_{cy}\left(\frac{\partial^2 W}{\partial y^2}\right)^2 + 4D_{cxy}\left(\frac{\partial^2 W}{\partial x \partial y}\right)^2 \right] dxdy \tag{4.60}$$

$$T_{cmax} = \frac{1}{2}\omega^2 \rho_c h_c \int_0^a \int_0^b W^2 dxdy \tag{4.61}$$

where D_{cx}, D_{cy}, D_{c1} and D_{cxy} are the flexural and torsional rigidities of the ceiling. In Eq. (4.61), ρ_c and h_c are the density and thickness of the ceiling, respectively.

As can be found from Eqs. (4.60) and (4.61), the effect of a ceiling is similar to that of a subfloor. However, since the stiffness of the ceiling is relatively small, the effect of ceiling mass would be much more significant than the influence of ceiling stiffness provided. Therefore, for simplicity, only ceiling mass should be considered in calculating frequency and added into the Eq. (4.45).

4.4 Rotational fixity factor

In CFS construction, three framing systems are commonly used: ledger framing, platform framing, and balloon framing, as shown in Figs. 4.8 and 4.9. In design practice, a simply supported condition was traditionally assumed for all the three types of framing, including the calculation of the natural frequency and deflection of CFS floors. However, construction practice may introduce additional rotational restraints on the support condition. In platform framing, the weight of stories above is transferred to the ends of joists, which may restrain the rotation of the joist ends. For balloon framing and ledger framing, the joist-to-stud clip angle provides some degree of moment resistance at the joist end, similar to that of a semi-rigid connection. In addition, the floor sheathing in ledger framing also applies a rotational restraint on the floor joist end. The rotational restraint may influence the vibration behavior of the floor and should be accounted for in design calculations (Hernández and Chui, 2014).

Parnell et al. (2009) tested the platform framing condition by using a structural steel I-beam with steel blocks welded to the top flange (Fig. 4.10) to simulate the effect of the storey above in practice. A superimposed load of 1.9 kN/m was applied on the

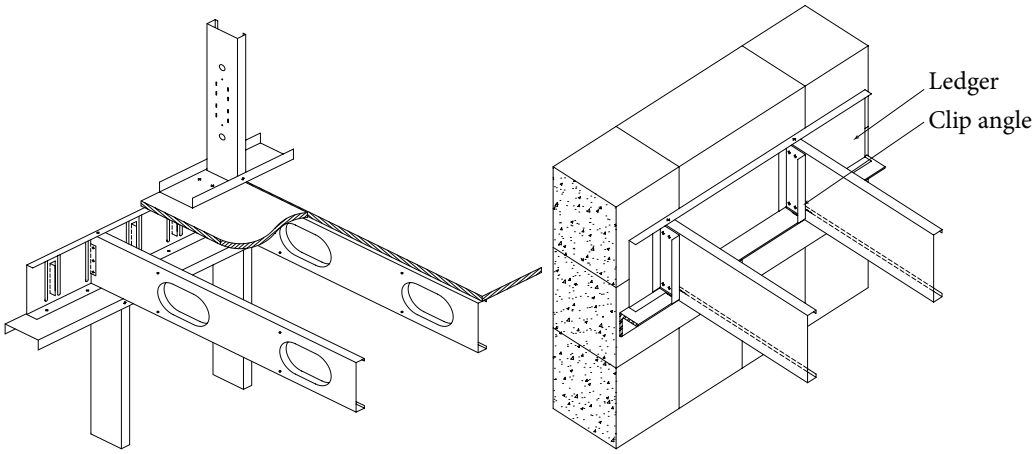

(a) Platform framing (b) Balloon framing

Figure 4.8 Details of platform framing and balloon framing (Courtesy: ClarkDietrich).

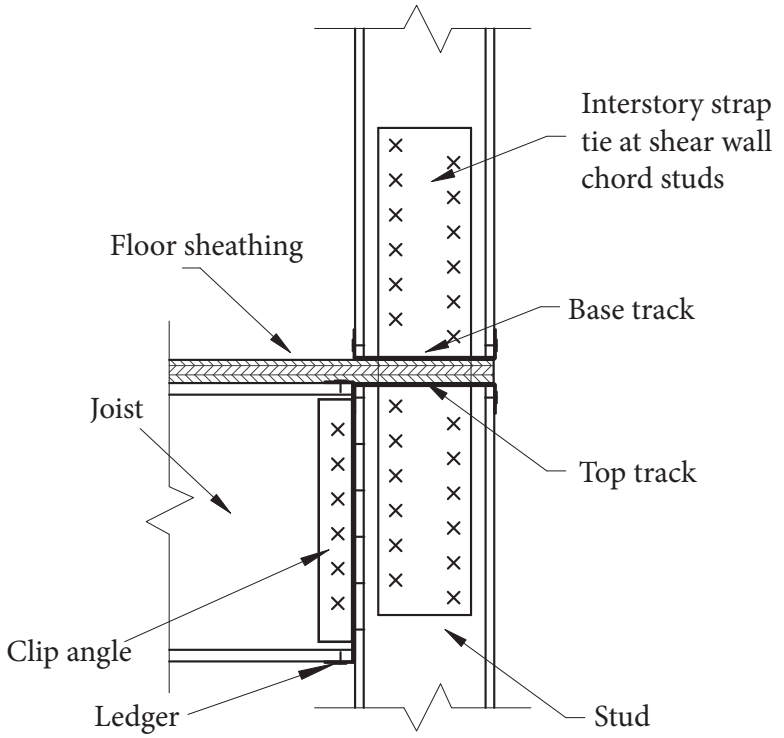

Figure 4.9 Details of ledger framing (Ayhan and Schafer, 2017).

subfloor at the end of joists. It was found that the end restraints of the platform framing have little effect on the fundamental frequency of CFS floors. In contrast, when ledger framing was tested, Parnell et al. (2009) found it had a considerable influence on the fundamental frequency as shown in Table 4.6. In this table, the restraint coefficient c_1 is calculated, and then rotational fixity factors, r, can be obtained from Eq. (4.52). In the tests reported by Hernández and Chui (2014), the end restraints of platform framing in a wood-framed floor was increased from 5 kN/m to 30 kN/m to stimulate multiple stories above. They found that the rotational stiffness significantly increased and, therefore, also the natural frequencies. Thus, it can be concluded that the effect of rotational stiffness at joist ends of platform framing is related to the weight of storeys above, while the effect of end rotational restraints of ledger framing needs to consider in the design.

Figure 4.10 Platform framing with end restraints.

Yu et al. (2015) conducted an experimental investigation aimed at determining the strength of load-bearing CFS clip angles widely used in CFS-wall and floor framing, as shown in Fig 4.11(a). A typical load-deflection curve obtained from the investigation is demonstrated in Fig. 4.11(b), in which the deflection of 1/64 in. (0.4 mm) is selected for determining the initial rotational stiffness of the clip. As can be seen from Fig. 4.11(b), the load corresponding to the deflection of 1/64 in is in the range between 300–500 lbs

Table 4.6 Fundamental frequencies of CFS floors (Parnell et al., 2009).

Floor specimen	Fundamental frequency (Hz)			c_1	r
	Platform framing†	Ledger framing	ratio		
LF14.5B	18.2*	22.5	1.236	1.112	0.086
LF14.5C	17.9*	24.8*	1.385	1.177	0.131
LF14.5D	16.2	19.7	1.216	1.103	0.079
LF17.0A	13.5	14.9	1.104	1.051	0.040
LF17.0C	12.8	14.3	1.117	1.057	0.045
LF19.5A	11.4	12	1.053	1.026	0.021
LF19.5B	10.6	11.4	1.075	1.037	0.030

Note: † No end restraints, i.e., simply supported
* Frequency revised by subsequential analysis

(1.33–2.22 kN), which corresponds to an end reaction of 300 lbs (1.33 kN) of a floor joist with a span length of 20 ft (6.1 m), 24 in (610 mm) spacing, and typical 10 psf dead and 20 psf live load. From the test results of Yu et al. (2015), the rotational stiffness or constants can be calculated by using Eq. (4.62).

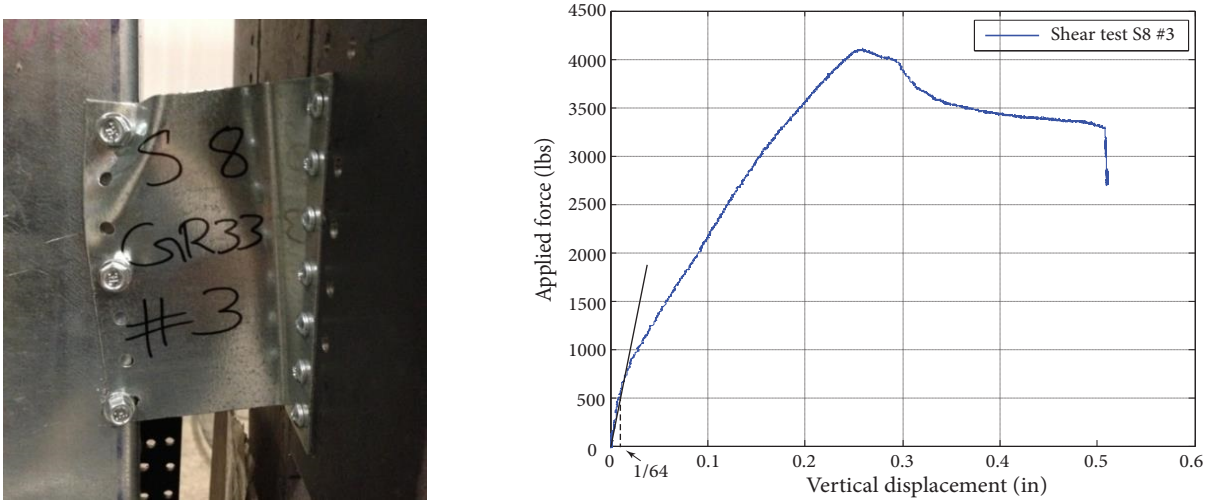

(a) Shear buckling failure

(b) Test curve

Figure 4.11 Test result of clip angle S8 #3 (Yu et al., 2015).

$$R = \frac{M}{\vartheta} = \frac{VL}{\Delta/L} = \frac{VL^2}{\Delta} \tag{4.62}$$

where $V = V_{1/64}$, $\Delta = 1/64$, and L is the the flat length of the cantilevered leg of clip angle between the center of the first line of screws and the bend line in clip tests in Yu et al. (2015). Considering the shear deflection, the values of the rotational stiffness R can be obtained and presented in Table. 4.7. Only clip angles with height B larger than 5 in. (12.7 cm) are selected with consideration of compatibility with the depth of floor joists. To evaluate the rotational fixity factor, two span lengths (i.e., 4.42 m and 5.94 m) and four C-shape CFS sections with typical floor joists depths are selected as shown in Table 4.7, in which 1200S200–54 is same as TDW $12 \times 2 \times 16$ of Dietrich TradeReady® in tests of Parnell et al. (2009), and the smallest section 800S200-54 satisfies the live load limit L/480 stipulated in the Steel Stud Manufacturers Association (SSMA) Floor Joist Span Table (SSMA, 2001) up to span length of 20 ft (6.1 m) with 24 in. (610 mm) joist spacing.

Table 4.7 Rotational stiffness and fixity factors.

Test	R	1200S250–97		1200S200–54		1000S200–54		800S200–54	
label	Nm/rad	r_1	r_2	r_1	r_2	r_1	r_2	r_1	r_2
S3†	3322.7	0.002	0.002	0.004	0.005	0.005	0.007	0.009	0.012
S4†	15682.6	0.008	0.011	0.016	0.022	0.025	0.034	0.040	0.053
S5†	4835.5	0.003	0.003	0.005	0.007	0.008	0.011	0.013	0.017
S8†	12442.0	0.007	0.009	0.013	0.018	0.020	0.027	0.032	0.042
S9†	9780.5	0.005	0.007	0.010	0.014	0.016	0.021	0.025	0.034
S10†	11659.2	0.006	0.008	0.012	0.016	0.019	0.025	0.030	0.040
T‡	74774.0	0.038	0.051	0.074	0.097	0.110	0.142	0.165	0.210

Note: R–rotational stiffness
r_1–rotational fixity factor for 4.42m span
r_2–rotational fixity factor for 5.94m span
†–tests of Yu et al. (2015)
‡–test of Ayhan and Schafer (2017)

Ayhan and Schafer (2016a,b, 2017) tested a full-scale floor-to-wall connections used in ledger-framed CFS construction to determine the moment-rotation behavior of the connections. The effects of the four parameters were investigated: i) the presence of subfloor sheathing, ii) the presence of top and bottom screws connecting the joist and ledger flanges; iii) the location of applied load, and iv) the clip angle rotation. The obtained moment-rotation behavior of the joist-to-wall connection is characterized with bilinear model with rotational stiffness k_1 and k_2 as shown in Fig. 4.12, in which k_1 is

initial stiffness corresponding to 40% of the peak load. It was concluded that the forgoing four parameters significantly influence of the initial stiffness of the connection. Specifically, initial stiffness would dramatically decrease if the subfloor sheathing was absence, the top and bottom screws connecting joist and ledger flanges were omitted or the location of the floor joist is not in line with that of the wall stud. The rotational stiffness obtained by the initial stiffness k_1 of the connection and corresponding rotational fixity factors for the foregoing joist sections are also presented in Table 4.7.

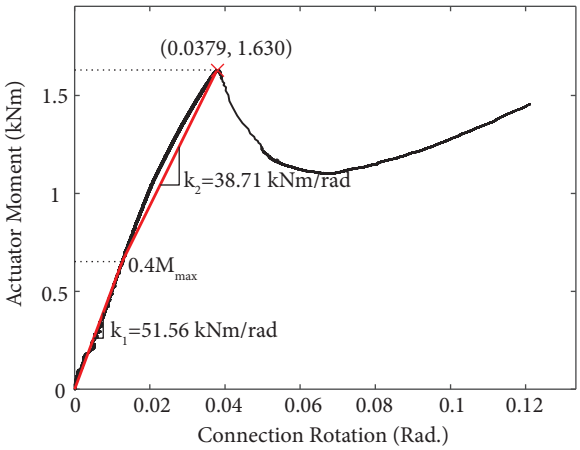

Figure 4.12 Example of stiffness degradation observed on test results (Ayhan and Schafer, 2017).

Table 4.7 shows considerable differences on the rotational fixity factors obtained from the initial stiffness between Yu et al. (2015) and Ayhan and Schafer (2016a,b, 2017). Based on Yu's tests, one may conclude that the magnitudes of the rotational fixity is quite small and can be neglected. However, it needs to point out only CFS clip angles were tested in Yu's investigation as shown in Fig. 4.11(a). Restraining effects contributed by other components of the joist end assemblage, such as subfloor sheathing and joist-to-track flange screws connections were not accounted for. In addition, there are only three screws connected the joist web and clip angle in Yu's tests. Yu subsequently confirmed that with increase number of the screws the initial stiffness of the clip angle would increase accordingly because the premature shear buckling of the clip angle was eliminated (Yu, 2016).

It should also mention that the initial stiffness obtained from tests by Yu et al. (2015) and Ayhan and Schafer (2016a,b, 2017), respectively based on joist end reaction under

the design dead plus live load and 40% peak load of the connection, are corresponding to deflection serviceability requirement in current practice. For evaluating floor vibration performance, the actual of live load 0.25 kPa should be used instead of the design load 1.9 kPa as stipulated in ATC Design Guide 1 by Allen et al. (1999) and AISC/CISC Design Guide 11 by Murray et al. (1997). With that in mind, the initial stiffness selected for evaluation of floor vibration performance can be higher than that of shown in Table 4.7.

Table 4.8 shows restraint coefficients corresponding to the rotational fixity factors in the range of 0 to 0.1. It is found that the trivial increase of the restraint coefficients associated with the rotational fixity factor being in the range 0 to 0.1 results in a negligible influence on the fundamental frequency in Eq. (4.44). Therefore, in this research, the rotational fixity factor for CFS floor systems with balloon or ledger framing is approximately taken as 0.1 and the corresponding restraint coefficients can be obtained roughly as $c_1 = 1.13$; $c_2 = 1$; and $c_4 = 1, 0.75, and\ 0.5$ for transverse elements located at 1/2, 1/3 and 1/4 span, respectively.

Table 4.8 Restraint coefficients for rotational fixity factor in the range of 0 to 0.1.

r	c_1	c_2	c_4		
			1/2*	1/3*	1/4*
0	1	1	1	0.75	0.5
0.01	1.0122	1	1.0008	0.7501	0.4996
0.02	1.0247	1	1.0015	0.7502	0.4993
0.03	1.0372	1	1.0023	0.7503	0.4989
0.04	1.0501	1	1.0031	0.7504	0.4986
0.05	1.0630	1	1.0040	0.7505	0.4982
0.06	1.0762	1	1.0048	0.7506	0.4978
0.07	1.0896	1	1.0056	0.7507	0.4974
0.08	1.1031	1	1.0065	0.7508	0.4971
0.09	1.1169	1	1.0074	0.7509	0.4967
0.1	1.1310	1	1.0082	0.7510	0.4963

Note: $*$ transverse elements located at 1/2, 1/3 and 1/4 of span, respectively

4.5 Design method for fundamental frequency of CFS floor systems

4.5.1 Proposed method

The procedure for evaluating fundamental frequency of CFS floor systems based on the proposed equivalent orthotropic plates is summarized as follows:

the fundamental frequency is expressed as

$$f_1 = \frac{\pi}{2}\sqrt{\frac{ab}{m}}\sqrt{\frac{c_1 D_x}{a^4} + 2\frac{c_2 H}{a^2 b^2} + \frac{D_y}{b^4}} \tag{4.63}$$

where

- a is the span and b is the width.
- $D_x = EI_{eff}/s$
  s is the spacing of the joists;
  EI_{eff} is the effective flexural stiffness, which can be calculated based on ATC Design Guide 1 by Allen et al. (1999).
- $D_y = \frac{1}{a}\left(EI_{sy} + \sum_{i=1}^{N_t} 2c_{4i}EI_{ti}\right)$
  N_t is the number of rows of transverse elements;
  EI_{sy} and EI_{ti} are the flexural stiffness of the subfloor in y-direction and the ith row of the transverse elements, respectively;
  c_{4i} is restraint coefficient associated with locations of the ith row of the transverse elements;
  For discrete transverse elements such as blockings, the stiffness contribution is reduced through multiplying by a constant of $N_b/(N_j - 1)$, in which N_b is the number of blockings per row and N_j is the number of joists.
- $H = G_s t_s^3/6$
  G_s and t_s is the shear modulus and thickness of the subfloor, respectively.
- $m = m_s + m_c + (N_j - 1)m_j + 2m_t$

m_s, m_c, m_j and m_t are mass of subfloor, ceiling, single joist and transverse elements,respectively.

- c_1, c_2 and c_4 are restraint coefficients, and can be obtained roughly as $c_1 = 1.13$; $c_2 = 1$; and $c_4 = 1, 0.75, and\ 0.5$ for transverse elements located at 1/2, 1/3 and 1/4 span, respectively, for CFS floor systems with balloon or ledger framing. For platform framing, $c_1 = c_2 = 1$ and c_4 is same as that of balloon or ledger framing.

For CFS floor systems with two opposite edges being free, the design equation of fundamental frequency is expressed as

$$f_1 = \frac{\pi}{2}\sqrt{\frac{ab}{m}}\sqrt{\frac{D_x}{a^4}} \tag{4.64}$$

where $m = m_s + m_c + N_j m_j + 2m_t$.

4.5.2 Comparison with test results

The fundamental frequencies obtained from the proposed method and two existing methods (Allen et al., 1999; Chui, 2002) are compared with available test results in this section. The method adopted in ATC Design Guide 1 by Allen et al. (1999), known as ATC method, evaluates the fundamental frequency of the floor based on the model of a simply-supported beam. Chui (2002) simulated lightweight wood floors by using the ribbed-plate theory of Timoshenko and Woinowsky-Krieger (1959) and provided a procedure to evaluate the corresponding equivalent rigidities. Test results of CFS floor systems obtained from the investigations at Virginia Polytechnic Institute and State University (VT) (Kraus, 1997) and CCFSRG at the University of Waterloo (UW) (Parnell et al., 2009) are selected for the comparison.

VT tests

Kraus (1997) conducted a series of tests on residential floor systems constructed by OSB decking supported by C-shaped CFS joists at VT. Twelve full-scale laboratory floors were built and tested. Each floor system was simply supported on four edges and only one row of bridging with C-shape blockings was placed at mid-span. Thus, restraint coefficients $c_1 = c_2 = c_4 = 1$ are applied. The structural properties of floor specimens were

also provided in Kraus (1997). As shown in Table 4.9, test results of the fundamental frequency of the floor specimens with blockings are compared with predicted values by the proposed method in this study, the ATC method (Allen et al., 1999), and Chui's method (Chui, 2002).

It can be observed from Table 4.9 that the predictions obtained from all three methods for floor specimens with short spans (i.e., 8B, 8D, 8E, and 12E) are considerably greater than test results. Both plate-based methods (the proposed and Chui's method) provide a better predictions than that of the beam-based method, i.e., the ATC method. As CFS floors with OSB subfloor and one row of bridging with C-shape blockings lack of the transverse stiffness, such floors behave similar to one-way floor systems. For one-way floor systems, the plate-based methods may not necessarily provide more accurately predictions.

Table 4.9 Comparison test results of Kraus (1997) with the results predicted by using different methods.

Floor	Span	Test	ATC		Chui		Proposed	
specimens	(m)	(Hz)	(Hz)	(%)	(Hz)	(%)	(Hz)	(%)
8A	4.19	20.3	19.11	-5.88	19.19	-5.47	19.27	-5.05
8B	3.73	17.4	24.07	38.34	24.15	38.77	24.22	39.20
8C	3.28	29.0	31.26	7.79	31.32	8.01	31.39	8.24
8D	2.69	31.4	39.07	24.42	39.14	24.64	39.20	24.86
8E	2.16	35.6	60.76	70.67	60.81	70.82	60.87	70.97
10C	4.65	22.0	19.10	-13.18	19.53	-11.23	19.95	-9.31
10D	3.99	25.0	25.95	3.80	26.32	5.28	26.69	6.74
12B	5.33	20.6	18.33	-11.02	18.68	-9.34	19.02	-7.69
12C	4.93	22.6	21.48	-4.97	21.80	-3.55	22.11	-2.15
12D	4.29	26.5	26.31	-0.72	26.64	0.52	26.96	1.75
12E	3.43	28.5	41.23	44.67	41.50	45.60	41.76	46.52
Mean				13.99		14.91		15.82
Standard deviation				27.08		26.66		26.26

Note: % – the difference between test results and calculated values

UW tests

Parnell et al. (2009) investigated vibration performance of lightweight CFS floor systems with different subfloors such as OSB, FORTACRETE®, and CFS steel deck with and without lightweight concrete topping (i.e., LevelRock® 3500). The floor specimens were supported on edges of joist ends and were free on the other two edges. Each floor specimen was tested in three different joist-end boundary conditions: ledger framing, platform framing and simply supported. It can be found from the test results of the fundamental frequency in Parnell et al. (2009) that the effect of the restraints in platform framing is negligible comparing with the simply supported condition. Then in this research, only test results in the simply supported condition and the ledger framing condition are compared with the predictions obtained by ATC and proposed methods.

First, Table 4.10 tabulates comparisons among test results of floor specimens with ledger framing and the predicted values of the proposed methods and ATC method. Four types of subfloor configurations were tested, namely, OSB, FORTACRETE® (FC), FORTACRETE® with LevelRock ® topping (LR), and steel deck (UFS of Dietrich) with LevelRock ® topping. As discussed in Section 4.4, the rotational fixity factor associated with ledger framing is taken as 0.1 and the corresponding restraint coefficients $c_1 = 1.13$; $c_2 = 1$; and $c_4 = 1$ and 0.5 for transverse elements located at 1/2 and 1/4 span, respectively. Partial composite action is considered for connections between CFS joists and OSB or FC, and the slip modulus between joists with OSB or FC is assumed as $4.14 \times 10^6 N/m^2$ from Allen et al. (1999). However, since lacking of research on composite action between CFS joists with steel deck, fully composite action is assumed for them in this research.

It can be observed from Table 4.10 that both the ATC method and the proposed methods provide predictions with excellent accuracy for floor specimens with FC subfloor. For these floors, the results of $r = 0$ provide more accurate predictions than those of $r = 0.1$. It means that the influence of the rotational restraints at joist ends of ledger framing may be overestimated if $r = 0.1$. For floors with subfloor of FC & LR (LF14.5E, LF17.0A and LF19.5A), the predictions are considerably less than the test results, while calculated results for those with UFS & LR (LF14.5F, LF17.0C and LF19.5B) are significantly greater than the tested values. For LF14.5E, LF17.0A and LF19.5A, transverse stiffness provided by subfloor and transverse elements could be comparable to

the flexural stiffness parallel to the joists, and then two-way behavior occurs although the edges parallel to joists are free. By using the design equations for boundary conditions of R–S–R–S shown in Eq. (4.63), prediction errors as shown in Table 4.10 are reduced notably. For subfloor of UFS & LR (LF14.5F, LF17.0C and LF19.5B), the large differences may be caused by the assumption of fully composite action.

Second, Table 4.11 illustrates test results of floor specimens in simply supported condition and the corresponding predictions by the proposed methods and ATC method. It is noticed that predictions for floor specimens with FC subfloor (LF14.5B and LF14.5D) do not agree well with the test results.

In summary, the effect of subfloor materials can be significant on transverse stiffness of the floor. CFS floor systems with OSB subfloor behave similar to that of one-way systems whereas the floors with lightweight concrete topping may are similar to two-way systems. Thus the plate-based method proposed in this research should provide better predicted results for CFS floor systems with lightweight concrete topping.

4.6 Summary

An analytical approach based on the Rayleigh method has been presented for calculating the fundamental frequency of a CFS floor system while considering the effect of the rotational restraints along two opposite edges by using the beam characteristic function as the admission function. The equivalent rigidities and mass of equivalent orthotropic plates for CFS floor systems were developed. The effects of transverse elements such as strapping, blocking and strongback are taken into accounted in the proposed method. In addition, the rotational fixity factors were introduced to evaluate the restraint coefficients for calculating the fundamental frequency of the CFS floor system in design practice. Lastly, the fundamental frequencies obtained by proposed method were validated using the test results and other existing methods. For ledger-framed CFS floor systems, the rotational fixity factor being 0.1 is recommended for evaluating the floor fundamental frequency.

Table 4.10 Comparison test results of CCFSRG with different predicted values.

Floor	Span	Subfloor	Test	ATC		Proposed					
						r=0		r=0.1			
specimen	(m)		(Hz)	(Hz)	(%)	RFRF (Hz)	(%)	RFRF (Hz)	(%)	RSRS (Hz)	(%)
LF14.5B	4.42	FC	22.5	23.16	2.93	22.80	1.33	24.23	7.71	/	/
LF14.5C	4.42	OSB	24.8†	28.69	15.67	28.03	13.03	29.80	20.15	/	/
LF14.5D	4.42	FC	19.7	20.01	1.57	19.79	0.44	21.03	6.76	/	/
LF14.5Di	4.42	FC	23.6	23.28	-1.37	22.93	-2.86	24.37	3.26	/	/
LF14.5E	4.42	FC & LR	17.7	14.86	-16.04	14.77	-16.53	15.70	-11.27	16.23	-8.29
LF14.5F	4.42	UFS & LR	16.1	22.42	39.28	22.30	38.53	23.71	47.26	/	/
LF17.0A	5.19	FC & LR	14.9	12.09	-18.88	12.00	-19.46	12.76	-14.39	13.39	-10.11
LF17.0C	5.19	UFS & LR	14.3	17.53	22.60	17.49	22.32	18.59	30.03	/	/
LF19.5A	5.95	FC & LR	12	9.37	-21.88	9.31	-22.44	9.89	-17.55	10.62	-11.50
LF19.5B	5.95	UFS & LR	11.4	13.49	18.33	13.37	17.30	14.22	24.69	/	/
Mean					4.22		3.17		9.67		
Standard deviation					19.89		19.77		21.02		

Note: % – the difference between test results and calculated values

/ – not available

† – frequency revised by reprocessing

Table 4.11 Comparison test results of CCFSRG with different predicted values.

Floor	Span	Subfloor	Test	ATC		Proposed					
						r=0		r=0.1			
specimen	(m)		(Hz)	(Hz)	(%)	RFRF (Hz)	(%)	RFRF (Hz)	(%)	RSRS (Hz)	(%)
LF14.5B	4.42	FC	18.2†	23.16	21.42	21.45	17.85	22.80	25.27	/	/
LF14.5C	4.42	OSB	17.9†	28.69	37.61	26.37	47.31	28.03	56.59	/	/
LF14.5D	4.42	FC	16.2	20.01	19.04	18.62	14.92	19.79	22.16	/	/
LF17.0A	5.19	FC & LR	13.5	12.09	-11.66	11.29	-16.38	12.00	-11.11	12.60	4.22
LF17.0C	5.19	UFS & LR	12.8	17.53	26.98	16.45	28.54	17.49	36.64	/	/
LF19.5A	5.95	FC & LR	11.4	9.37	-21.66	8.76	-23.17	9.31	-18.33	9.99	6.62
LF19.5B	5.95	UFS & LR	10.6	13.49	21.42	12.58	18.66	13.37	26.13	/	/
Mean					13.31		12.53		19.62		
Standard deviation					21.56		24.66		26.21		

Note: % – the difference between test results and calculated values

/ – not available

† – frequency revised by reprocessing

5

Vibration of Lightweight Steel Floor Systems with Occupants

5.1 Introduction

Besides generating loads, human occupants also interact with a structure, and such interaction, known as human-structure interaction (HSI), can be significant if the mass of the occupants is comparable to that of the structure (Ellis and Ji, 1997). For lightweight floors, vibration analysis ought to consider a coupled system of the floor and occupants because the dynamic properties of the latter may influence the overall response of the system considerably (Foschi et al., 1995). One widely-known fact is that human occupants do not act merely as mass on the structure but behave as highly damped dynamical systems (20%-50% damping ratio) (Griffin, 1990). Two important issues must be borne in mind. Firstly, human bodies may have a considerable influence on the modal mass and damping in lightweight floor systems, and the dynamic characteristics therefore change with the location of human walking (Smith and Chui, 1989). Secondly, the traditional modal analysis where damping is ignored or assumed to be proportional is not valid (Ji, 2003) because floor-occupant systems consist of a lightly damped structure system and human bodies with high damping.

Most previous studies on HSI are based on two-degree-of-freedom (2-DOF) human-structure model (Zheng and Brownjohn, 2001; Sachse et al., 2004; Shahabpoor et al., 2013; Zhou et al., 2016). Such 2-DOF models were developed to describe coupled vibration

of the structure and human occupants, in which the human bodies and the structure were simulated as a SDOF model, respectively. Dynamic properties such as natural frequencies and damping ratios could be examined parametrically for a certain range of ratios of frequency, mass and damping coefficients of SDOF models of human occupants and the structure. The 2-DOF model considers only one structural mode based on the rule of superposition of the linear vibration, i.e., the total response can be obtained by summing up the contribution of each separate mode in modal analysis. However, human occupants may affect all the vibration modes of the structure, not just one mode solely. Furthermore, the 2-DOF model is inadequate without taking into account the spatial variation of human occupants on the structure. For instance, the influence of human occupants on floor vibration will vary with their locations on the floor. Based on tests of a concrete slab occupied by humans in various situations, Sachse (2002) concluded that the location of a human occupant affected the dynamic properties of the test structure and the influence of the occupant increased with the amplitude of the mode shape at the occupant's location. Same conclusions were also reported by Weckendorf and Smith (2012). Therefore, it is desirable to develop integrated human-structure models to obtain realistic properties and responses of structure.

Additionally, dynamic properties of the human body are strongly related to the intensity of vibration. Thus, the human models used in biomechanics may need to be modified before being adopted to model human occupants of building and bridge structures because the vibration intensities usually encountered in such structures are considerably less than those employed by biomechanics to derive dynamic human models (Griffin, 1990; Sachse et al., 2003). Furthermore, existing human models proposed for application in civil engineering are primarily developed based on the dynamic behaviour of human occupants on a simply-supported beam, one-way slab or a test rig under laboratory conditions (Ellis and Ji, 1997; Brownjohn, 1999; Falati, 1999; Sachse et al., 2003; Zhang, 2013). It is necessary to recalibrate the parameters of the human models by realistic full-scale test results and thus to model human occupants on lightweight floor systems to investigate the vibration of such coupled floor-occupant systems based on the parameters obtained from tests of lightweight floors.

Nicholson and Bergman (1986) adopted the Green's function of the vibrating plate to obtain the natural frequencies and mode shapes of the undamped plate–oscillator system.

The forced response of the combined system is also determined by modal analysis for both proportional damping and general damping. However, the dynamic properties of the undamped plate-oscillator system may not be applicable for floor-occupant systems. Based on a finite-strip formulation, Foschi and colleagues (Foschi and Gupta, 1987; Folz and Foschi, 1991) made an early effort to investigate the combined transient dynamic response of floor systems with occupants . The wood floor systems with various complexities commonly applied in construction were modeled by using finite strips combined into T-beam elements and the occupants were idealized as damped oscillators. Two human models were compared: a simple 2-DOF model and a more-detailed undamped 11-DOF model. Further applications were extended to develop the design criteria for residential wood floor systems and a SDOF human model was proposed by Foschi et al. (1995). Nevertheless, the finite-strip formulation might only be applicable for one-way stiffened floor systems without accounting for effects of the transverse elements such as blocking, bridging and strongbacks. Furthermore, Foschi et al. (Foschi and Gupta, 1987; Folz and Foschi, 1991; Foschi et al., 1995) applied the impulse due to heel drop impact for the dynamic response of floors but did not investigate the response induced by walking, although they recognised that the use of heel drop impacts to develop design guidelines for lightweight floors was questioned by Allen and Rainer (1989). In addition, considerable research was also conducted to develop the combined vibrational systems for investigation of human-structure interaction in other structures such as stadia and footbridges (Živanović, 2015).

In the present study, a damped plate-oscillator model is proposed to represent lightweight steel floor systems with occupants. The dynamic properties and responses obtained from the proposed model are compared with test results. The influence of human occupants on dynamic properties of floors is investigated in three scenarios: an unoccupied floor, a floor with one standing occupant and a floor with two standing occupants. Several existing human models are examined. Three loading models: moving force, moving damped-oscillator, and moving and stationary damped-oscillator, are subsequently proposed to obtain the dynamic responses of floors to human walking. Finally, parametric studies are conducted on the effects of step frequency, damping ratio, human-to-structure mass ratio, and walking path.

5.2 Damped plate-oscillator model

To simplify the presentation, occupants are modeled by SDOF oscillators and the floor is represented by an orthotropic plate. Then, the coupled floor-occupant system can be simulated by a damped plate-oscillator model as illustrated in Fig. 5.1, which is a rectangular orthotropic plate of constant thickness h connected to N_o linear, damped oscillators at locations of (ξ_i, η_i), $i = 1, 2, ..., N_o$. The dimensions of the plate are $0 \leqslant x \leqslant a$ and $0 \leqslant y \leqslant b$. The occupant-induced force, $f(x, y, t)$, is located at the position of one occupant, and $g(t)$ is an external force applied to the oscillator.

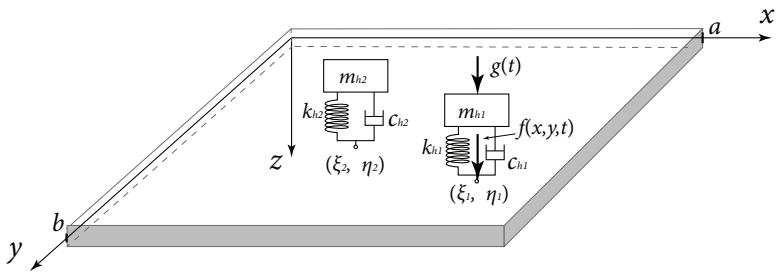

Figure 5.1 A damped plate-oscillator model.

5.2.1 Methodology and formulation

Using the dot denoting differentiation with respect to time t, the governing equation for the orthotropic plate is

$$\begin{aligned} &\nabla_o^4 w(x,y,t) + c\dot{w}(x,y,t) + \rho h\ddot{w}(x,y,t) = f(x,y,t) \\ &+ \sum_{i=1}^{N_p} \Big\{ k_{hi}\Big[z_i(t) - w(\xi_i,\eta_i,t)\Big] + c_{hi}\Big[\dot{z}_i(t) - \dot{w}(\xi_i,\eta_i,t)\Big] \Big\} \delta(x-\xi_i)\delta(y-\eta_i) \end{aligned} \tag{5.1}$$

where $w(x, y, t)$ is the vertical deflection of the plate; c is the viscous damping constant for the plate; ρ is the mass density; k_{hi}, c_{hi} and $z_i(t)$ are the stiffness, damping constant and displacement of ith oscillator; δ is the Dirac delta function; and ∇_o^4 is the biharmonic operator for orthotropic plates as defined in Eq. (3.4).

The equation of motion for each oscillator (i.e., human occupant) is

$$m_{hi}\ddot{z}_i(t) + c_{hi}\dot{z}_i(t) + k_{hi}z_i(t) = c_{hi}\dot{w}(\xi_i, \eta_i, t) + k_{hi}w(\xi_i, \eta_i, t) + g_i(t) \tag{5.2}$$

where m_{hi}, c_{hi} and k_{hi} are the mass, damping constant and spring stiffness of the ith human occupant, respectively. Divide both side of Eq. (5.2) by m_{hi} and rewrite Eq. (5.2) in terms of the circular frequency ω_{hi} and the damping ratio ζ_{hi} of the ith human occupant:

$$\ddot{z}_i(t) + 2\zeta_{hi}\omega_{hi}\dot{z}_i(t) + \omega_{hi}^2 z_i(t) = 2\zeta_{hi}\omega_{hi}\dot{w}(\xi_i, \eta_i, t) + \omega_{hi}^2 w(\xi_i, \eta_i, t) + \frac{1}{m_{hi}}g_i(t) \tag{5.3}$$

where

$$\zeta_{hi} = \frac{c_{hi}}{2m_{hi}\omega_{hi}},\ \omega_{hi} = \sqrt{\frac{k_{hi}}{m_{hi}}} \tag{5.4}$$

The plate-oscillator system in Fig. 5.1 can be treated as a plate constrained by attached oscillators. For a 'constrained' plate performing free vibration, the inertia forces of the concentrated masses and the restoring forces of the translational springs can be considered as the external exciting forces for the plate (Wu and Luo, 1997). Thus, the assumed-mode method or eigenfunction expansion (i.e., the mode superposition theory) adopted for the forced vibration of an 'unconstrained' plate (without any oscillator attached) may be used to determine the natural frequencies and mode shapes of the 'constrained' plate. Therefore, the vertical displacement of the plate $w(x, y, t)$ can be expressed as

$$w(x, y, t) = \sum_{n=1}^{\infty} W_n(x, y)q_n(t) \tag{5.5}$$

where $W_n(x, y)$ is the vibration modes of the 'unconstrained' plate with same boundary conditions and $q_n(t)$ is the time varying generalized coordinate. It can be obtained for $W_n(x, y)$ that (Leissa, 1969)

$$\nabla_o^4 W_n(x, y) - \omega_n^2 \rho h W_n(x, y) = 0 \tag{5.6}$$

where ω_n is the circular frequency of the n-th mode of the 'unconstrained' plate with same boundary conditions. If all edges are simply supported, W_n and ω_n can be determined from

$$W_n(x, y) = \sin\alpha_i x \sin\beta_j y \tag{5.7a}$$

$$\omega_n^2 = \frac{\Omega_{ij}}{\rho h} \tag{5.7b}$$

where

$$\Omega_{ij} = D_x \alpha_i^4 + 2H\alpha_i^2\beta_j^2 + D_y\beta_j^4 \tag{5.8a}$$

$$\alpha_i = i\pi/a,\ \beta_j = j\pi/b \tag{5.8b}$$

Substituting Eqs. (5.5) and (5.6) into Eq. (5.1) results in

$$\begin{aligned}\sum_{n=1}^{\infty}\omega_n^2\rho h W_n(x,y)q_n(t) + c\sum_{n=1}^{\infty}W_n(x,y)\dot{q}_n(t) + \rho h\sum_{n=1}^{\infty}W_n(x,y)\ddot{q}_n(t)\\ = f(x,y,t) + \sum_{i=1}^{N_o}\left\{k_{hi}\left[z_i(t) - \sum_{n=1}^{\infty}W_n(\xi_i,\eta_i)q_n(t)\right]\right.\\ \left. + c_{hi}\left[\dot{z}_i(t) - \sum_{n=1}^{\infty}W_n(\xi_i,\eta_i)\dot{q}_n(t)\right]\right\}\delta(x-\xi_i)\delta(y-\eta_i)\end{aligned} \tag{5.9}$$

Multiplying both sides of Eq. (5.9) by $W_m(x,y)$, integrating on area of the plate and applying the orthogonality relation yields

$$\begin{aligned}M_n\ddot{q}_n(t) + 2\zeta_n\omega_n M_n\dot{q}_n(t) + \omega_n^2 M_n q_n(t)\\ + \sum_{i=1}^{N_o}2\zeta_{hi}\omega_{hi}m_{hi}W_n(\xi_i,\eta_i)\sum_{j=1}^{\infty}W_j(\xi_i,\eta_i)\dot{q}_j(t) + \sum_{i=1}^{N_o}\omega_{hi}^2 m_{hi}W_n(\xi_i,\eta_i)\sum_{j=1}^{\infty}W_j(\xi_i,\eta_i)q_j(t)\\ - \sum_{i=1}^{N_o}2\zeta_{hi}\omega_{hi}m_{hi}\dot{z}_i(t)W_n(\xi_i,\eta_i) - \sum_{i=1}^{N_o}\omega_{hi}^2 m_{hi}z_i(t)W_n(\xi_i,\eta_i)\\ = \int_0^a\int_0^b f(x,y,t)W_n(x,y)dxdy\end{aligned} \tag{5.10}$$

where M_n is the n-th modal mass, represented as

$$M_n = \rho h\int_0^a\int_0^b W_n^2(x,y)dxdy \tag{5.11}$$

ζ_n is the n-th modal damping ratio, expressed by

$$\zeta_n = \frac{c}{2\rho h \omega_n} \tag{5.12}$$

Introducing the modal mass ratio $\gamma_{ni} = m_{hi}/M_n$, Eq. (5.10) can be rearranged as

$$\begin{aligned} &\ddot{q}_n(t) + 2\zeta_n\omega_n\dot{q}_n(t) + \omega_n^2 q_n(t) \\ &+ \sum_{i=1}^{N_o} 2\zeta_{hi}\omega_{hi}\gamma_{ni}W_n(\xi_i,\eta_i)\sum_{j=1}^{\infty} W_j(\xi_i,\eta_i)\dot{q}_j(t) + \sum_{i=1}^{N_o}\omega_{hi}^2\gamma_{ni}W_n(\xi_i,\eta_i)\sum_{j=1}^{\infty} W_j(\xi_i,\eta_i)q_j(t) \\ &- \sum_{i=1}^{N_o} 2\zeta_{hi}\omega_{hi}\gamma_{ni}\dot{z}_i(t)W_n(\xi_i,\eta_i) - \sum_{i=1}^{N_o}\omega_{hi}^2\gamma_{ni}z_i(t)W_n(\xi_i,\eta_i) = F_n(t) \end{aligned} \tag{5.13}$$

where

$$F_n(t) = \frac{1}{M_n}\int_0^a\int_0^b f(x,y,t)W_n(x,y)dxdy \tag{5.14}$$

Similarly, substituting Eq. (5.5) into Eq. (5.3), it gives

$$\begin{aligned} &\ddot{z}_i(t) + 2\zeta_{hi}\omega_{hi}\dot{z}_i(t) + \omega_{hi}^2 z_i(t) \\ &-2\zeta_{hi}\omega_{hi}\sum_{j=1}^{\infty} W_j(\xi_i,\eta_i)\dot{q}_j(t) - \omega_{hi}^2\sum_{j=1}^{\infty} W_j(\xi_i,\eta_i)q_j(t) = \frac{1}{m_{hi}}g_i(t) \end{aligned} \tag{5.15}$$

Eqs. (5.13) and (5.15) can be solved simultaneously and expressed in a matrix form as follows:

$$\mathbf{M}\ddot{\mathbf{U}} + \mathbf{C}\dot{\mathbf{U}} + \mathbf{K}\mathbf{U} = \mathbf{F} \tag{5.16}$$

where $\mathbf{M}$, $\mathbf{C}$ and $\mathbf{K}$ are the mass, damping and stiffness matrices, respectively; and $\mathbf{U}$, $\dot{\mathbf{U}}$, $\ddot{\mathbf{U}}$ and $\mathbf{F}$ are the displacement, velocity, acceleration and force vectors, respectively. $\mathbf{M}$ is an identity matrix of size $(N + N_o) \times (N + N_o)$. The expressions of the matrices and vectors are presented in Appendix B.

Since the high damping of human occupants, the damping matrix cannot be expressed as a linear combination of mass and stiffness matrices (Ji, 2003). Thus, the state-space method is employed in this study. Eq. (5.16) can be transformed into the state-space form as (Balachandran and Magrab, 2009)

$$\dot{\mathbf{V}} = \mathbf{A}\mathbf{V} + \mathbf{B} \tag{5.17}$$

where the state vector $\mathbf{V}$ and its time derivative $\dot{\mathbf{V}}$ are given by

$$\mathbf{V} = \begin{Bmatrix} \mathbf{U} \\ \dot{\mathbf{U}} \end{Bmatrix}_{2(N+N_o)\times 1} \qquad \dot{\mathbf{V}} = \begin{Bmatrix} \dot{\mathbf{U}} \\ \ddot{\mathbf{U}} \end{Bmatrix}_{2(N+N_o)\times 1} \tag{5.18}$$

In Eq. (5.17), the state matrices $\mathbf{A}$ and $\mathbf{B}$ are, respectively, expressed as

$$\mathbf{A} = \begin{bmatrix} \mathbf{0} & \mathbf{I} \\ -\mathbf{M}^{-1}\mathbf{K} & -\mathbf{M}^{-1}\mathbf{C} \end{bmatrix}_{2(N+N_o)\times 2(N+N_o)} \tag{5.19a}$$

$$\mathbf{B} = \begin{Bmatrix} \mathbf{0} \\ \mathbf{M}^{-1}\mathbf{F}(t) \end{Bmatrix}_{2(N+N_o)\times 1} \tag{5.19b}$$

For free vibration, $\mathbf{F}$(t) is the $(N + N_o)$–dimensional null vector $\mathbf{0}$. Thus, Eq. (5.17) becomes

$$\dot{\mathbf{V}} = \mathbf{A}\mathbf{V} \tag{5.20}$$

Since Eq. (5.20) is a set of linear ordinary differential equations with constant coefficients, a solution can be assumed as

$$\mathbf{V} = \mathbf{X}e^{\lambda t} \tag{5.21}$$

in which λ is a scalar constant and $\mathbf{X}$ is a constant $2(N + N_o)$ vector. Then, it can be obtained

$$q_n(t) = x_n e^{\lambda t} \qquad (n = 1, 2, 3, ..., N) \tag{5.22a}$$

$$z_i(t) = x_i e^{\lambda t} \qquad (i = N + 1, N + 2, ..., N + N_o) \tag{5.22b}$$

where x_n and x_i are elements of vector $\mathbf{X}$. Substituting Eq. (5.21) into Eq. (5.20) and canceling the common factor of $e^{\lambda t}$ on both sides of the equation, the following eigenvalue problem can be obtained

$$\mathbf{A}\mathbf{X} = \lambda\mathbf{X} \tag{5.23}$$

Since the state matrix $\mathbf{A}$ is not a symmetric matrix, the eigenvalues and eigenvectors of the matrix are complex valued. The solution of Eq. (5.23) consists of $2(N + N_o)$

eigenvalues λ_i (in complex conjugate pairs) and $2(N+N_o)$ corresponding eigenvectors $\mathbf{X}_i$ (also in complex conjugate pairs). Once the state-space eigenvalue problem is solved, the modal frequencies and damping ratios can be determined by (Inman, 2006)

$$\widetilde{\omega}_i = |\lambda_i|, \qquad \widetilde{\zeta}_i = -\frac{Re(\lambda_i)}{|\lambda_i|} \tag{5.24}$$

The ith mode shape of plate are given by

$$\widetilde{W}_i(x,y) = \sum_{n=1}^{N} W_n(x,y)x_n, \quad x_1,\ x_2 ... x_N \in \mathbf{X}_i \tag{5.25}$$

Meanwhile, the mode values of oscillators are taken as $x_j,\ (j = N+1, N+2, ..., N+N_o)$ in $\mathbf{X}_i$ for corresponding oscillators.

The dynamic responses of forced vibrations of occupant-floor systems can be obtained from Eq. (5.17) numerically by the Runge-Kutta method (Inman, 2006) or the Newmark-β method (Clough and Penzien, 2003). Then, the acceleration of occupant-floor systems is determined from (Qin et al., 2013)

$$\ddot{\mathbf{U}} = \mathbf{M}^{-1}\left(\mathbf{F} - \mathbf{C}\dot{\mathbf{U}} - \mathbf{K}\mathbf{U}\right) \tag{5.26}$$

The preceding process adopted the model of SDOF oscillator for human occupants. The extension of the process to multiple degrees-of-freedom (MDOF) oscillators for human occupants is straightforward. For instance, if a 2-DOF oscillator is adopted for a human occupant as that shown in Fig. 5.2, the corresponding Eq. (5.2) becomes

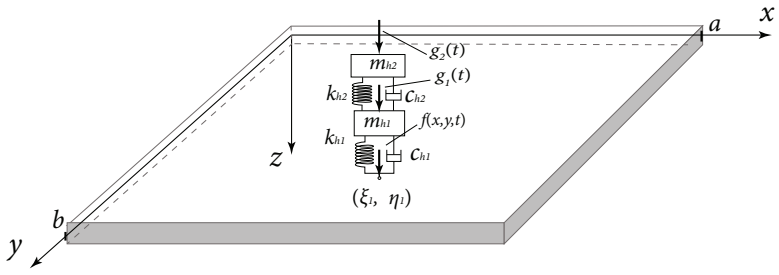

Figure 5.2 Occupant-floor systems: 2-DOF oscillators for human occupant.

$$\mathbf{M}_h\ddot{\mathbf{Z}} + \mathbf{C}_h\dot{\mathbf{Z}} + \mathbf{K}_h\mathbf{Z} = \mathbf{F}_h \tag{5.27}$$

in which

$$\begin{gathered}
\mathbf{M}_h = \begin{bmatrix} m_{h1} & 0 \\ 0 & m_{h2} \end{bmatrix},\ \mathbf{C}_h = \begin{bmatrix} c_{h1}+c_{h2} & -c_{h2} \\ -c_{h2} & c_{h2} \end{bmatrix},\ \mathbf{K}_h = \begin{bmatrix} k_{h1}+k_{h2} & -k_{h2} \\ -k_{h2} & k_{h2} \end{bmatrix} \\
\mathbf{F}_h = \begin{bmatrix} c_{h1}\dot{w}(\xi_1,\zeta_1,t) + k_{h1}w(\xi_1,\zeta_1,t) + g_1(t) \\ g_2(t) \end{bmatrix} \\
\ddot{\mathbf{Z}} = \begin{bmatrix} \ddot{z}_1 \\ \ddot{z}_2 \end{bmatrix},\ \dot{\mathbf{Z}} = \begin{bmatrix} \dot{z}_1 \\ \dot{z}_2 \end{bmatrix},\ \mathbf{Z} = \begin{bmatrix} z_1 \\ z_2 \end{bmatrix}
\end{gathered} \tag{5.28}$$

Eq. (5.10) turns into

$$\begin{gathered}
M_n\ddot{q}_n(t) + 2\zeta_n\omega_n M_n\dot{q}_n(t) + \omega_n^2 M_n q_n(t) \\
+2\zeta_{h1}\omega_{h1}m_{h1}W_n(\xi_1,\eta_1)\sum_{j=1}^{\infty}W_j(\xi_1,\eta_1)\dot{q}_j(t) + \omega_{h1}^2 m_{h1}W_n(\xi_1,\eta_1)\sum_{j=1}^{\infty}W_j(\xi_1,\eta_1)q_j(t) \\
-2\zeta_{h1}\omega_{h1}m_{h1}\dot{z}_1(t)W_n(\xi_1,\eta_1) - \omega_{h1}^2 m_{h1}z_1(t)W_n(\xi_1,\eta_1) \\
= \int_0^a\int_0^b f(x,y,t)W_n(x,y)dxdy
\end{gathered} \tag{5.29}$$

Consequently, the governing equation, Eq. (5.16), will be revised accordingly. The expressions of matrices and vectors in Eq. (5.16) are provided in Appendix B for a plate having N_o damped 2-DOF oscillators.

5.2.2 Model validation

The damped plate-oscillator model proposed herein is examined by the undamped plate-oscillator system developed in Nicholson and Bergman (1986). The frequencies are obtained by Eq. (5.24) and compared with results of Nicholson and Bergman (1986). The system consists of a simply supported rectangular isotropic plate ($\nu = 0.3$) with a SDOF undamped oscillator attached to the plate. Damping was considered only for forced response in Nicholson and Bergman (1986). The properties of the system provided in Nicholson and Bergman (1986) are nondimensional and they can be converted in terms

of the parameters defined in present study as:

$$\begin{gathered} b/a = 0.75,\ \xi = 0.225a,\ \eta = 0.275a, \\ \frac{m_o}{\rho h a^2} = 1,\ \frac{k_o a^2}{D} = 100, \\ c_o = 0.1 m_o \sqrt{\frac{D}{\rho h a^4}},\ c = 0.01 \rho h \sqrt{\frac{D}{\rho h a^4}}. \end{gathered} \tag{5.30}$$

where a, b and h is the length, width and thickness of the plate, respectively; ρ is the density of the plate; c is the damping constant of the plate; D is the flexural rigidity of the plate; ξ and η define the location of the oscillator on the plate; and m_o, k_o and c_o is the mass, stiffness and damping constant of the oscillator, respectively. The circular frequency of the SDOF oscillator can be obtained as

$$\omega_o = \sqrt{\frac{k_o}{m_o}} = 10\sqrt{\frac{D}{\rho h a^4}} \tag{5.31}$$

The first six frequencies in terms of frequency parameter ($\sqrt{D/(\rho h a^4)}$) of the plate-oscillator model and plate alone are listed in Table. 5.1. The present results obtained from the proposed model agree well with the results in Nicholson and Bergman (1986). It should be noted that the present results are calculated by setting the number of vibration modes in Eq. (5.5) as 100.

Table 5.1 Frequency parameter of simply supported plate coupled to a SDOF oscillator.

Mode	Frequency parameter ($\sqrt{D/(\rho h a^4)}$)			
	Uncoupled plate		Plate-oscillator model	
	Present	Reference*	Present	Reference*
1	27.41556	27.41556	8.09821	8.09799
2	57.02438	57.02437	30.13916	30.13446
3	80.05346	80.05346	60.46412	60.45673
4	106.37240	106.37239	80.83531	80.83303
5	109.66227	109.66227	107.36724	107.36171
6	159.01029	159.01028	111.57198	111.56776

∗–Nicholson and Bergman (1986)

5.3 Dynamic properties of coupled floor-occupant systems

In order to assess the proposed plate-oscillator model for its application on vibration of lightweight steel floor systems with occupants, the predicted dynamic properties are compared with the test results of the floors with/without human occupants. A variety of existing human models used in civil engineering application are examined in the proposed plate-oscillator model.

5.3.1 Laboratory tests

Full-scale lightweight CFS floor systems with different configurations were constructed and tested in the Structures Lab at the University of Waterloo by CCFSRG from 1999 to 2005. The details on the test apparatus and procedure were reported previously (Xu et al., 2000; Xu, 2000, 2001a; Liu, 2001; Tangorra et al., 2002; Tangorra, 2005; Xu and Tangorra, 2007). Both static and dynamic tests were carried out on the floor systems to identify the critical parameters that contribute to the control of floor vibration. The test results were then compared with those obtained from different design methods.

In addition to the published test results reported in Xu et al. (2000), Tangorra et al. (2002), and Xu and Tangorra (2007), the influence of occupants was also studied when conducting sandbag drop on floors without occupants and with one or two occupants standing at the center of the floor as shown in Fig. 5.3. The obtained natural frequencies and damping ratios are listed in Table 5.2. The acceleration time-history records of floor A in Table 5.2 and corresponding Fourier spectrum are illustrated in Fig. 5.4. It can be found from Fig. 5.4(a) that floor vibration decays faster when human occupants are standing on the floor. The more human occupants, the faster the rate of decay. Fig. 5.4(b) illustrates that due to human occupant's presence, the peaks of spectra are significantly reduced and the damping is increased. The damping ratios are evaluated by the bandwidth method. Additionally, the control tests were conducted for floors with furnitures which have same weight as the human occupants. The results of control tests are shown in Table 5.3.

Table 5.2 shows that the frequencies are slightly changed when there are occupants standing at the center of the floor whereas the damping ratios more than doubled. However,

the damping ratios are not increased proportionally with the number of the occupants. Furthermore, Fig. 5.4 shows that the rates of dissipation of the acceleration for the floor with occupants are much faster than that without occupants. As it can be observed in Table 5.3, the weight of furniture changes the first natural frequency much more than that by the occupant although the weight of the furniture is the same as that of a person. As it was expected, the addition of furniture does not improve the damping ratio to any great extent.

Figure 5.3 The sandbag drop test with two occupants on the floor.

Configuration and structural properties of the floor specimens listed in Table 5.2 and 5.3 are provided in Table 5.4. Floor layout and configuration details can be found in Tangorra et al. (2002). Floor structural properties can be calculated from equivalent rigidities provided in Zhang and Xu (2016). Since the shear modulus and the thickness of the OSB are very small, values of H in Table 5.4 are ignored.

5.3.2 Human models

The human body is a complex mechanical system and it is often modelled as a lumped parameter vibratory model consisting of an assemblage of discrete masses, linear springs, and viscous dashpots as shown in Fig. 5.5. The model has a point contact with the floor and maintains that contact as it walking or stay on the floor. Such a model may

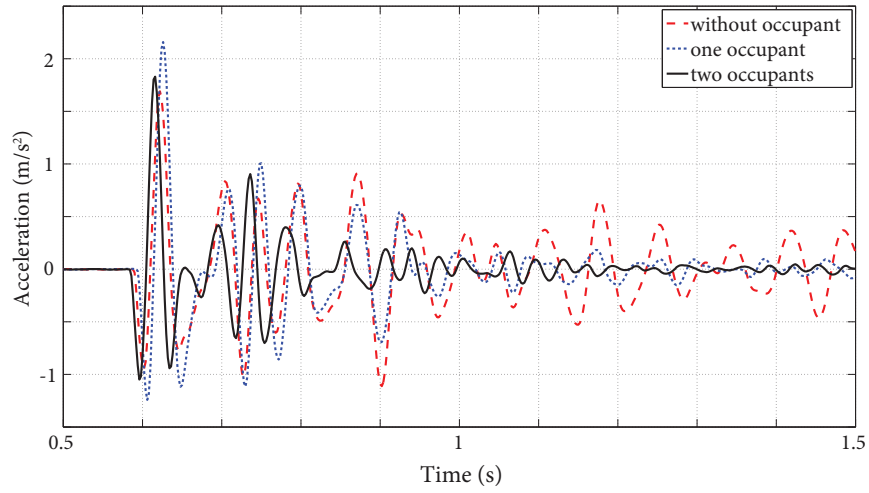

(a) Time history

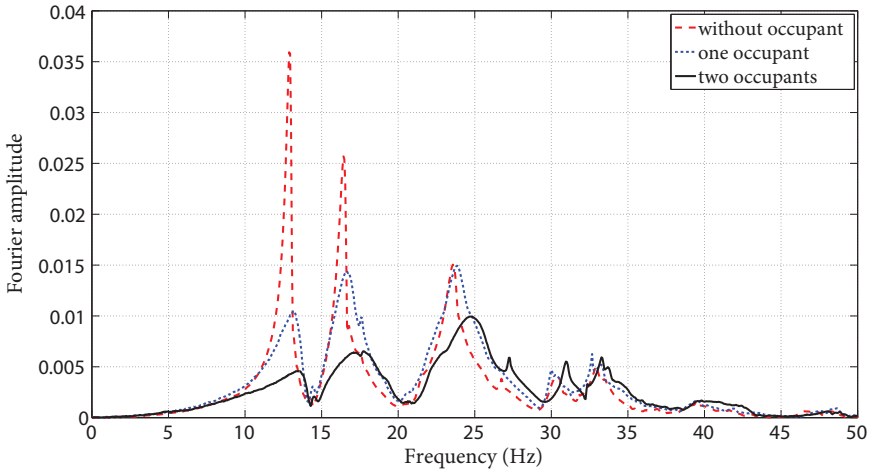

(b) Fourier spectrum

Figure 5.4 Acceleration of the floor A with and without occupants induced by sandbag drop.

Table 5.2 Influence of human occupants on dynamic properties of CFS floors (Liu, 2001).

Floor ID	No. of Occupants	Natural Frequencies			Damping ratio
		f_1 (Hz)	f_2 (Hz)	f_3 (Hz)	ζ_1 (%)
A	0	12.909	16.434	23.575	1.338
	1	13.123	16.632	23.85	5.506
	2	13.474	17.09	24.811	8.5
B	0	11.917	15.549	24.857	1.422
	1	11.765	15.71	25.238	7.95
	2	12.054	16.007	25.452	11.444
C	0	10.849	14.526	20.783	1.276
	1	10.849	14.786	20.996	8.687
	2	10.757	15.289	22.202	12.085

Table 5.3 Influence of furniture and human occupants on dynamic properties of CFS floors (Liu, 2001).

Floor ID	Furniture	No. of Occupants	Natural Frequencies			Damping ratio
			f_1 (Hz)	f_2 (Hz)	f_3 (Hz)	ζ_1 (%)
D	No	0	13.031	16.571	24.078	1.398
	No	1	13.046	16.846	24.643	5.825
	Yes	0	11.429	16.266	24.323	2.476
	Yes	1	11.398	16.327	25.208	6.447
E	No	0	13.519	17.975	24.597	1.088
	No	1	13.656	18.265	24.841	4.767
	Yes	0	11.932	17.334	24.658	2.154
	Yes	1	11.551	17.181	24.78	5.153

vary from a simple SDOF model (Foschi et al., 1995) to a more complex multi-degree-of-freedom model (e.g., 15-DOF in Nigam and Malik (1987)), the choice of which may be determined in terms of the effects of frequency, activity and posture when the human body is subjected to certain level of vibration. A considerable number of properties of human models are reported by biomechanical scientists in widely differing values. Detailed reviews on dynamic models of human body in civil engineering can be found in Sachse et al. (2003) and Shahabpoor et al. (2016b).

For representing the dynamic properties of the human body, the most common,

Table 5.4 CFS floor configurations in Liu (2001).

Floor	Floor configuration	Span (m)	Width (m)	Density (kg/m^2)	D_x (Nm)	D_y (Nm)	H
A	**fl-6.114-2-6"-1/5-B0-S6-2b**	6.114	4.5	25.22	2.655×10^6	1.694×10^4	0
B	**fl-6.114-2-6"-1/5-B0-S6-2b-Ce**	6.114	4.5	35.62	2.656×10^6	1.694×10^4	0
C	**fl-6.754-2-6"-1/5-B0-S6-2b-g**	6.754	4.5	25.11	2.655×10^6	1.533×10^4	0
D	**fl-6.114-2-6"-1/5-B0-S6-2b-g**	6.114	4.5	25.22	2.655×10^6	1.694×10^4	0
E	**fl-6.114-2-6"-1/5-B2-S6-2b-g**	6.114	4.5	25.22	2.655×10^6	1.694×10^4	0

convenient and simple reasonable model is a SDOF model (Griffin, 1990). Sachse et al. (2003) summarized that vertical vibrations of the whole-body of sitting or standing people are dominated by a heavily damped mode with a natural frequency between 4 and 6 Hz and a damping ratio ranging from 20% to 50%. Shahabpoor et al. Shahabpoor et al. (2016b) suggested ranges of 1.85-3.5 Hz and 20-50% for a SDOF model of a walking human. Four typical SDOF models of human walking, sitting and standing are presented in Table 5.5.

Furthermore, 2-DOF human models are also commonly used. One of most well-known 2-DOF human models for standing position might be the one proposed by Coermann (1962). This model was adopted by the ISO 5982 (1981) and employed by Folz and Foschi (1991) to predict the vibration response of wood-framed floors subjected to heel-drop impact. Farah (1977) reevaluated the experimental data of Coermann (1962) and provided the properties of 2-DOF models of standing human. These two 2-DOF human models for standing position are tabulated in Table 5.6.

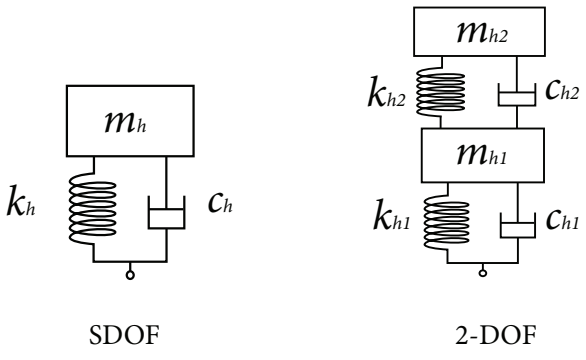

Figure 5.5 Dynamical models of a human occupant.

Table 5.5 Properties of SDOF models of a human body subjected to vertical vibrations.

Human models	References	Mass	Frequency (Hz)	Damping ratio
Sitting	Coermann (1962)*	m_t	5.0	32%
Standing	Zheng and Brownjohn (2001)	m_t	5.24±0.40	39%±0.05
	Falati (1999)	$m_t/3$	10.43	50%
Walking	Shahabpoor et al. (2016a)	m_t	2.75∽3.00	27.5%∽30%

∗– unit converted by Sachse et al. (2003)

m_t–total mass of human body

Table 5.6 Properties of 2-DOF models of a standing human body subjected to vertical vibrations.

References	Mass	Frequency (Hz)	Damping ratio
Coermann (1962); ISO 5982 (1981)	$m_{h1} = 62m_t/75$	$f_{h1} = 5.0$	$\zeta_{h1} = 37\%$
	$m_{h2} = 13m_t/75$	$f_{h2} = 12.5$	$\zeta_{h2} = 46\%$
Farah (1977)	$m_{h1} = 5.1m_t/5.6$	$f_{h1} = 6.9$	$\zeta_{h1} = 25\%$
	$m_{h2} = 0.5m_t/5.6$	$f_{h2} = 7.6$	$\zeta_{h2} = 31\%$

m_t–total mass of human body

5.3.3 Numerical results

The weights of human occupants are both 80 kg. The natural frequencies and damping ratios are obtained by the proposed damped plate-oscillator model for different human models and compared with the test results. The human occupants are modelled to be located at the center of the floor even though for the case of two occupants are not exactly standing at the center of the floor in the tests (Fig. 5.3). Four human dynamical models in standing position, two SDOF human models presented in Zheng and Brownjohn (2001) and Falati (1999) and two 2-DOF human models described in Coermann (1962) and Farah (1977), are adopted and the corresponding model properties are listed in Table 5.5 and 5.6. The models are denoted in present study as Brownjohn SODF model (Zheng and Brownjohn, 2001), Falati SDOF model (Falati, 1999), Coermann 2-DOF model (Coermann, 1962) and Farah 2-DOF model (Farah, 1977).

Firstly, natural frequencies are determined for unoccupied floors (i.e., no occupants on the floors). Although only two joist-end edges were supported in the tests, the boundary

conditions are assumed as simply-supported for all four edges for the sake of simplicity in this study. Such simplification is reasonable because the tested CFS lightweight floors are one-way floors of which the transverse stiffness of the floor is contributed only by 20mm thick OSB subfloor and is much less than the stiffness of the joists. The test and present results of frequencies of unoccupied floors are listed in Table 5.7. Good agreements on the results obtained from the tests and proposed models can be observed. Since test results only provide the damping ratio of the first vibration shape, present damping ratios for higher vibration modes of the unoccupied floors are assumed to be 1.5%.

Then, the dynamic properties of the coupled floor-occupant systems are evaluated by the proposed damped plate-oscillator model with adoption of the Brownjohn SDOF human model and the Falati SDOF human model, respectively. In this evaluation, the first 100 vibration modes are adopted in numerical computations. Table 5.7 lists the test results and the evaluated results for the floors occupied by one person at the floor center. The evaluated results by the foregoing different human models shows an additional lower frequency and a corresponding very large damping ratio, which are introduced by human SDOF models and denoted as f_0 and ζ_0, respectively. These additional vibration modes are associated with presence of human occupants and might be not observed directly from the data measured from floor tests (Ellis and Ji, 1997; Sachse et al., 2004). For illustration, the first and second mode shapes of floor specimen A obtained by the proposed plate-oscillator model with adoption of the Brownjohn SDOF human are presented in Fig. 5.6. The magnitudes of the complex mode shapes obtained from Eq. (5.25) are normalized with the mode value of human occupant, and the normalized first and second mode shapes ($|\widetilde{W}_1(x,y)|$ and $|\widetilde{W}_2(x,y)|$) of floor specimen A with one occupant are plotted in Fig. 5.6. It can be observed that the first and second modes are dominated by the occupant and the floor, respectively. The extra mode introduced by the human occupant may not be detected by accelerometers placed on the floors in tests, therefore, test results of floors with one person in Table 5.7 do not contain f_0 and ζ_0, but they are included in the evaluated results from the damped plate-oscillator models.

Furthermore, from the comparison shown in Table 5.7, frequencies and damping ratios of the second and fourth vibration modes of unoccupied floors (i.e., f_2, f_4, ζ_2 and ζ_4 highlighted in Table 5.7) are not affected by the human occupants. This is because the human occupants were located at the nodal point of the second and fourth vibration

modes, which is the center of the floors. It can be concluded that the influence of the human occupants on the floor vibration are associated with the human location on the floor. The dynamic properties of a vibration mode may not be much affected by human occupants if they are standing at the nodal points of the mode. Additionally, it is also observed that the first natural frequencies f_1 of the floor A and B with one occupant evaluated by the Falati SDOF human model are less the ones evaluated for the floors without occupants, which contradicts the test results shown in Table 5.7.

Table 5.7 Comparison between tested and evaluated dynamic properties of floor specimens with/without human occupants.

Floor	Occupant	Method	Frequency (Hz)					Damping ratio (%)				
			f_0	f_1	f_2	f_3	f_4	ζ_0	ζ_1	ζ_2	ζ_3	ζ_4
A	0	test	/	12.909	16.434	23.575	/	/	1.338	/	/	/
		present	/	13.781	**15.829**	22.655	**34.936**	/	1.338	1.500	1.500	1.500
	1	test	/	13.123	16.632	23.850	/	/	5.506	/	/	/
		present-I	5.124	14.101	**15.829**	22.670	**34.936**	33.795	8.038	**1.500**	6.106	**1.500**
		present-II	10.847	13.388	**15.829**	22.481	**34.936**	41.157	9.972	**1.500**	5.815	**1.500**
B	0	test	/	11.917	15.549	24.857	/	/	1.422	/	/	/
		present	/	11.596	**13.319**	19.061	**29.396**	/	1.422	1.500	1.500	1.500
	1	test	/	11.765	15.710	25.238	/	/	7.950	/	/	/
		present-I	5.129	11.830	**13.319**	19.093	**29.396**	33.529	7.401	**1.500**	5.484	**1.500**
		present-II	11.012	11.104	**13.319**	18.891	**29.396**	6.999	43.250	**1.500**	5.325	**1.500**
C	0	test	/	10.849	14.526	20.783	/	/	1.276	/	/	
		present	/	11.360	**13.570**	20.565	**32.646**	/	1.276	1.500	1.500	1.500
	1	test	/	10.849	14.786	20.996	/	/	8.687	/	/	/
		present-I	5.091	11.682	**13.570**	20.598	**32.646**	32.104	9.688	**1.500**	6.172	**1.500**
		present-II	10.509	11.405	**13.570**	20.381	**32.646**	8.538	41.114	**1.500**	5.954	**1.500**

/–Not available

present-I–Results from the proposed damped plate-oscillator model by applying Brownjohn SDOF human model

present-II–Results from the proposed damped plate-oscillator model by applying Falati SDOF human model

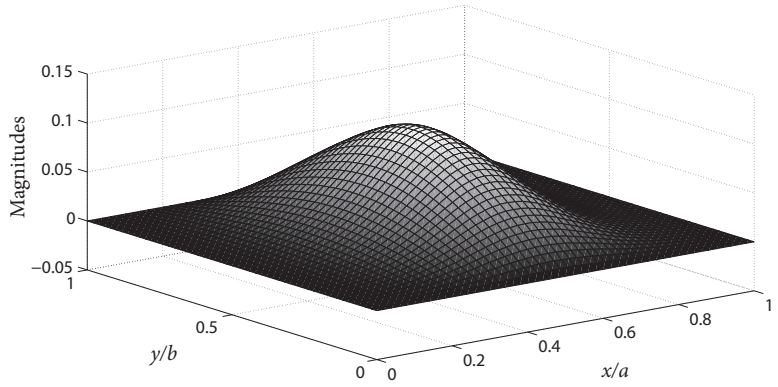

(a) First mode

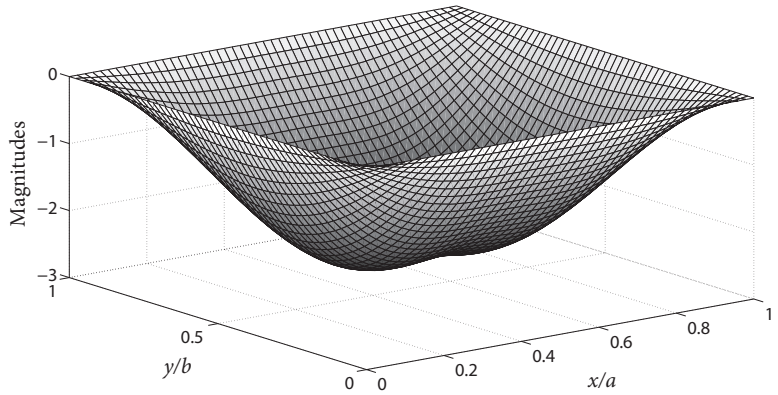

(b) Second mode

Figure 5.6 The normalized first and second mode shapes of floor A with one occupant.

Dynamic properties of floors with two occupants are also evaluated by the proposed damped plate-oscillator model with adoption of Brownjohn SDOF human model and Falati SDOF human model, respectively. Both occupants are modelled individually and the evaluated results are listed in Table 5.8. Similar to those in the Table 5.7, f_{01} and f_{02} are two additional frequencies introduced by human SDOF models and their corresponding damping ratios are ζ_{01} and ζ_{02}. However, f_{02} and ζ_{02} are same as the human models. The comparison in Table 5.8 illustrates that the effects of human occupants is overestimated considerably when modelling each occupant separately for the case that two occupants closely standing on the floor. As a results, the obtained damping ratios become extremely large. Since the damping ratios obtained from tests are not increased proportionally with the number of the occupants, it may suggest that closely standing human occupants

should be modeled by one SDOF model instead of modelling each occupant as a SDOF model individually.

Lastly, 2-DOF human models (i.e., Coermann (1962) and Farah (1977)) are adopted into the proposed plate-oscillator model to predict the dynamic properties of floors with one occupant and corresponding results are shown in Table 5.9. Comparing the results shown in Table 5.7 and 5.9, it can be found that the results obtained from the 2-DOF human models are not better than those from SDOF models. The 2-DOF models, however, introduce two extra vibration modes in the floor-occupant systems. These extra modes will cause some difficulties to recognise the dominant modes of floor-occupant systems. Thus, it requires more efforts to identify the dominant modes from the results obtained using Coermann 2-DOF model (Coermann, 1962) and Farah 2-DOF model (Farah, 1977) for floor B and C. Therefore,a SDOF model of human is sufficient to obtain dynamic properties of floor-occupant systems.

Table 5.8 Comparison between tested and evaluated dynamic properties of floor specimens with human occupants.

Floor	Occupant	Method	Frequency (Hz)					Damping ratio (%)				
			f_{01}	f_{02}	f_1	f_2	f_3	ζ_{01}	ζ_{02}	ζ_1	ζ_2	ζ_3
A	2	test	/	/	13.474	17.090	24.811	/	/	8.500	/	/
		present-I	4.964	**5.240**	14.790	15.829	22.491	29.096	**39.000**	14.630	**1.500**	11.130
		present-II	10.382	**10.430**	14.350	15.829	22.081	25.109	**50.000**	26.334	**1.500**	11.213
B	2	test	/	/	12.054	16.007	25.452	/	/	11.444	/	/
		present-I	4.964	**5.240**	12.336	13.319	19.013	28.581	**39.000**	13.455	**1.500**	9.827
		present-II	9.909	**10.430**	12.629	13.319	18.560	13.325	**50.000**	36.535	**1.500**	9.299
C	2	test	/	/	10.757	15.289	22.202	/	/	12.085	/	/
		present-I	4.868	**5.240**	12.382	13.570	20.485	26.232	**39.000**	17.312	**1.500**	11.297
		present-II	9.228	**10.430**	13.334	13.570	20.004	12.400	**50.000**	37.824	**1.500**	10.705

/–Not available

present-I–Results from the proposed damped plate-oscillator model by applying Brownjohn SDOF human model

present-II–Results from the proposed damped plate-oscillator model by applying Falati SDOF human model

Table 5.9 Comparison between tested and evaluated dynamic properties of floor specimens with human occupants.

Floor	Occupant	Method	Frequency (Hz)					Damping ratio (%)				
			f_{01}	f_{02}	f_1	f_2	f_3	ζ_{01}	ζ_{02}	ζ_1	ζ_2	ζ_3
A	1	test	/	/	13.123	16.632	23.850	/	/	5.506	/	/
		present-III	4.394	13.955	14.017	15.829	22.699	29.411	52.914	5.565	1.500	4.822
		present-IV	5.802	8.450	14.477	15.829	22.959	18.472	32.327	6.768	1.500	5.436
B	1	test	/	/	11.765	15.710	25.238	/	/	7.950	/	/
		present-III	4.395	11.793	13.319	13.940	19.112	29.271	4.996	1.500	52.945	4.332
		present-IV	5.6790	8.454	12.186	13.319	19.333	18.054	32.011	6.860	1.500	5.038
C	1	test	/	/	10.849	14.786	20.996	/	/	8.687	/	/
		present-III	4.366	11.623	13.570	13.950	20.619	28.391	6.492	1.500	52.992	4.845
		present-IV	5.701	8.419	12.156	13.570	20.883	16.900	31.663	8.790	1.500	5.556

/–Not available

present-III–Results from the proposed damped plate-oscillator model by applying Coermann 2-DOF human model

present-IV–Results from the proposed damped plate-oscillator model by applying Farah 2-DOF human model

5.3.4 Discussion and remarks

2-DOF model of human-structure system

An integrated 2-DOF model of a human-structure system was investigated as a reasonable way to simplify the dynamic analysis of human-structure interaction (Sachse et al., 2004; Shahabpoor et al., 2013). The 2-DOF model could be sufficient for qualitative analysis of human-structure interaction to explain damping increases, additional vibration modes as well as the insignificant changes of natural frequencies observed on structures due to human occupancy. However, caution is advised when employing the 2-DOF human-structure model to evaluate the dynamic properties and responses of floor-occupant systems because the model considers only one structural mode. Alternatively, the proposed plate-oscillator model can be reduced to a 2-DOF human-structure model through the selection of one certain vibration mode using Eq. (5.5) instead of adding many modes together. For instance, Table. 5.10 shows the results evaluated by the proposed plate-oscillator model and the 2-DOF human-structure model. The Brownjohn SDOF human model is adopted to simulate the presence of human and 100 vibration modes are considered for the damped plate-oscillator model, whereas only first vibration mode is taken for the 2-DOF human-structure model. Differences between the results evaluated by the two models can be observed in Table 5.10.

Table 5.10 Dynamic properties evaluated by proposed plate-oscillator model and 2-DOF model.

Floor	Model	Frequencies (Hz)		Damping ratio (%)	
		f_1 (Hz)	f_2 (Hz)	ζ_1	ζ_2
A	Plate-oscillator	5.121	14.108	33.796	9.407
	2-DOF	5.171	13.965	35.44	9.738
B	Plate-oscillator	5.126	11.838	33.526	8.759
	2-DOF	5.176	11.737	35.208	9.049
C	Plate-oscillator	5.088	11.692	32.105	11.502
	2-DOF	5.149	11.56	33.896	11.466

Non-existence of the "bubble mode"

In 1998, Talja and Kullaa (Talja and Kullaa, 1998; Kullaa and Talja, 1998) performed modal testing on the lightweight steel joist floors with use of a 5 kg impact hammer. The person who applied the hammer impact was resting his knees on a soft mat near the center of the floor. Surprisingly, results from experimental modal analysis illustrated that the first mode of the structure was a full sine wave in the vertical direction instead of a half-sine wave (i.e., "bubble mode"), a mode that could not be found from the test results. The so-called "bubble mode" was found only for the floor specimens with concrete topping and the associated damping ratios are abnormally high (i.e., around 10%). However, the reasons for not being able to find the the 'bubble mode' and the high damping ratios were unclear.

From the analysis of the damped plate-oscillator model, human occupants can increase the first frequency slightly and damping ratio substantially, but have no influence on vibration modes when located at the nodal points. In the tests by Talja and Kullaa (Talja and Kullaa, 1998; Kullaa and Talja, 1998), the presence of the test person at the floor center increased the damping ratios and the first natural frequency, but the second frequency was expected to be unchanged because the person was located at the nodal point of the second mode. If the first two natural frequencies of unoccupied floors are closely spaced, the presence of a person on the floor would result in the frequency associated with the half-sine wave mode (i.e., the first frequency of the unoccupied floor) being greater than that of sine wave mode (i.e., the second frequency of the unoccupied floor). Consequently, the first mode from test results was the one with a full sine wave.

Nested frequencies

It is generally accepted that the natural frequencies of the combined plate-oscillator systems are nested among the natural frequencies of the plate alone (Nicholson and Bergman, 1986; Folz and Foschi, 1991). Extensive studies of human-structure interaction also conclude that the frequencies of the human and unoccupied structure are always between those of the coupled human-structure system if only considering the first frequency of the unoccupied structure (Ellis and Ji, 1997). The relationship can be expressed as

$$f_1 < (f_h,\ f_{s1}) < f_2 \tag{5.32}$$

in which f_h and f_{s1} are the natural frequency of the human and the first frequency of the unoccupied structure, respectively; and f_1 and f_2 are the first and second frequency of coupled human-structure system, respectively. However, Eq. (5.32) may not always be true. The issue of the "bubble mode" in Section 5.3.4 is a notable example. Sachse (2002) (page 107-108) also discussed this equation (5.32) based on the parametrical study of 2-DOF model of a human-structure system.

Based on the findings of Sachse (2002), Eq. (5.32) is studied in more detail in this study, using the proposed damped plate-oscillator model. Only the first two frequencies, f_1 and f_2, of the combined floor-occupant system are considered, and SDOF human models with two different modal masses, m_h, and their corresponding mass ratios $\gamma = m_h/M$ (M is the mass of the floor) are used, as listed in Table 5.11. Then, the natural frequencies f_1 and f_2 are determined for floor A with a human standing at the floor center. The results are plotted in Fig. 5.7(a) and 5.7(b). It is found that f_1 or f_2 is within the range bound by the natural frequencies of the human model and structure (i.e., f_h and the first frequency of structure f_{s1}), which can be described as

$$f_h < f_1 < f_2 < f_{s1} \tag{5.33}$$

or

$$f_h < f_1 < f_{s1} < f_2 \tag{5.34}$$

In particular, the frequency relationship of Eq. (5.33) can be observed in Fig. 5.7(a) for the mass ratio $\gamma = 0.038$ with a human damping ratio of 50%. Similarly, the frequency relationship of Eq. (5.34) can be noticed in Fig. 5.7(b) for the mass ratio $\gamma = 0.115$, with a human damping ratio of 50%. The nested-frequency relationship (i.e., Eq. (5.32)) occurs in the case of human damping ratio of 30%, as shown in both Fig. 5.7(a) and 5.7(b).

In summary, the issue of Eq. (5.32) not always being true occurs for the case with smaller mass ratios (i.e., $\gamma < 0.1$) and a higher human damping ratio ($\zeta_h \geqslant 50\%$ in this study). Therefore, it can be concluded that human occupants will introduce additional vibration modes, but the frequencies of combined floor-occupant systems are not always nested among the natural frequencies of the unoccupied floors, especially for the case

with smaller mass ratios (i.e., $\gamma < 0.1$) and a higher human damping ratio ($\zeta_h \geqslant 50\%$ in this study).

Table 5.11 SDOF human models for parametrical study.

Model	m_h	$\gamma = m_h/M$	ζ_h	f_h(Hz)
A	$m_t/3$	0.038	30% or 50%	$0.8f_{s1} \backsim 1.1f_{s1}$
B	m_t	0.115	30% or 50%	$0.8f_{s1} \backsim 1.1f_{s1}$

m_t–total mass of human body assumed as 80kg

Human model in standing position

Through the numerical results in Section 5.3.3, the Brownjohn SDOF human model (Zheng and Brownjohn, 2001) for standing position is verified and can be adopted for the application of lightweight steel floor systems. However, it is observed that the evaluated damping ratios are larger than those for the tested results. Thus, it is necessary to recalibrate the Brownjohn SDOF human model for its application in lightweight steel floor systems. Table. 5.12 demonstrates the dynamic properties of floor specimen A by applying Brownjohn SDOF human model with different modal mass m_h. The frequency f_1 and corresponding damping ratio ζ_1 of the combined floor-occupant system increase along with m_h. Same observation was also for other floor specimens. Ji and Ellis (1995) proposed the human body model in a standing position as a continuous system and derived its modal mass and $m_h = 2m_t/3$ was suggested. Therefore, when applying Brownjohn SDOF human model, the mass m_h may be less than the human total mass m_t.

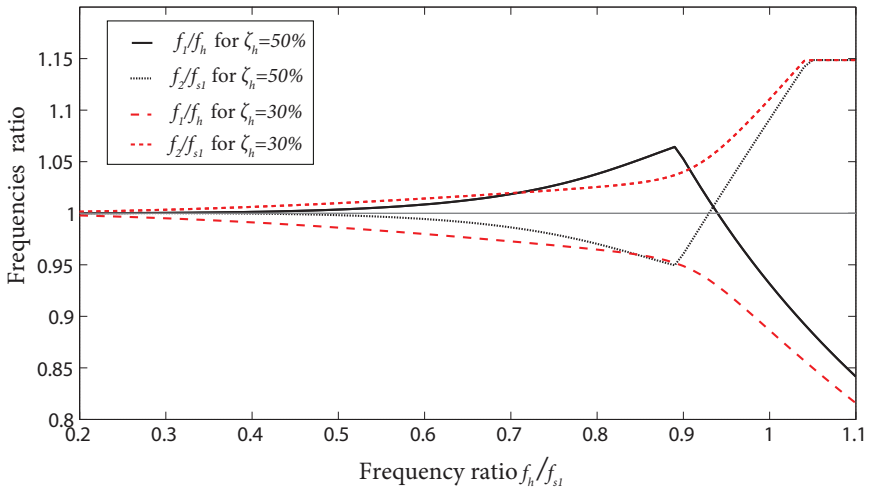

(a) $m_h = m_t/3$ and $\gamma = 0.038$)

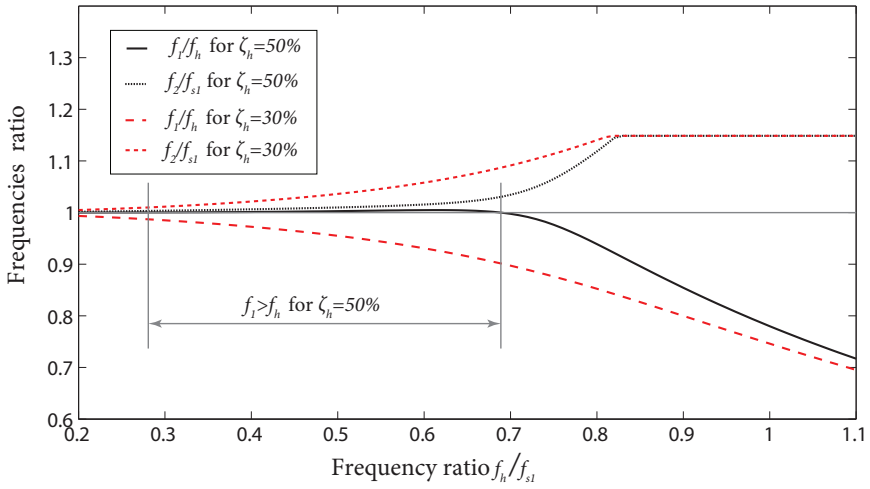

(b) $m_h = m_t$ and $\gamma = 0.115$

Figure 5.7 Natural frequencies f_1 and f_2 of floor-occupant systems with SDOF human model.

Table 5.12 Brownjohn SDOF human model with different mass m_h.

		f_0	f_1	ζ_0	ζ_1
tested		/	13.123	/	5.506
m_h	$m_t/3$	5.206	13.849	37.235	4.239
	$m_t/2$	5.187	13.899	36.361	5.575
	$0.6m_t$	5.175	13.934	35.839	6.363
	$0.7m_t$	5.163	13.972	35.322	7.141
	$0.8m_t$	5.149	14.014	34.809	7.908
	$0.9m_t$	5.136	14.059	34.230	8.664
	m_t	5.121	14.108	33.796	9.407

/–Not available

m_t–total mass of human body

5.4 Dynamic responses induced by human walking

A variety of approaches exist in the literature for modelling human-induced vibration (Caprani and Ahmadi, 2016). The simplest one only considers the concentrated force induced by human walking without taking into account the HSI during walking. This model is denoted as moving force (MF) model. A more realistic model can be established based on the proposed plate-oscillator model in which human occupants are represented by damped oscillators. Thus, a moving damped-oscillator (MDO) model is proposed.

Furthermore, human occupants do not only excite the floor systems but also receive the vibration response. As illustration in Fig. 1.2, human occupants that perform walking can be referred to as active occupants. Other humans sitting or standing on the structure may be the passive ones who are referred to as stationary occupants (Pedersen, 2011). Besides difference in loading, the dynamic properties of human body also differ between the active and stationary occupants as well as acceptability of vibrations. It is known that a walking person accepts much larger vibrations than a stationary person (Ohlsson, 1986). In residential occupancies, the thresholds of vibrations are determined by a seated person rather than one that is standing or in motion (Onysko et al., 2000). Thus, the model of moving and stationary damped-oscillators (MSDO) is desirable to determinate the vibrations felt by a stationary person (receiver), sitting or standing on the floor, when another person (impactor) applies a footfall impact at any other point on the floor.

It should be noted that although the damped–oscillator models may not be the best to model human walking in terms of reflecting the gait cycle as the bipedal model reported by Qin et al. (2013), the simplicity of its dynamics also allows a comprehensive investigation of coupled human-structure system under different loading conditions (Shahabpoor et al., 2013).

5.4.1 Moving force model

As shown in Fig. 5.8, human walking is modelled using a single-footfall force loading on the footprints (i.e., the position of the feet during walking) in a sequence of footsteps. For the location of a footprint is (ξ_i, η_i), the single-footfall force $f(x, y, t)$ can be expressed as

$$f(x, y, t) = F(t)\delta(x - \xi_i)\delta(y - \eta_i) \tag{5.35}$$

where $F(t)$ is the force from a single footfall and δ is the Dirac delta function. The vertical force produced by humans walking has been paid much attention by researchers in last several decades (Živanović et al., 2005; Racic et al., 2009). In present research, the single footfall force model developed by Li et al. (2010) based on Young's equation (Young, 2001) is adopted. The force model is given by

$$F(t) = G\sum_{n=1}^{+\infty} A_n \sin(\frac{n\pi}{t_e}t),\ \ t_e = \frac{1}{0.76f_s},\ \ 0 \leqslant t \leqslant t_e \tag{5.36}$$

where G is the weight of a human body, A_n is the Fourier coefficient, f_s is walking step rate and t_e is the duration of single foot step. The first five order Fourier coefficients are determined by

$$\begin{aligned}
A_1 &= \begin{cases} -0.0698f_s + 1.211,\ \ 1.6Hz \leqslant f_s \leqslant 2.32Hz \\ -0.1784f_s + 1.463,\ \ 2.32Hz \leqslant f_s \leqslant 2.4Hz \end{cases} \\
A_2 &= \begin{cases} 0.1052f_s - 0.1284,\ \ 1.6Hz \leqslant f_s \leqslant 2.32Hz \\ -0.4716f_s + 1.210,\ \ 2.32Hz \leqslant f_s \leqslant 2.4Hz \end{cases} \\
A_3 &= \begin{cases} 0.3002f_s - 0.1534,\ \ 1.6Hz \leqslant f_s \leqslant 2.32Hz \\ -0.0118f_s + 0.5703,\ \ 2.32Hz \leqslant f_s \leqslant 2.4Hz \end{cases} \\
A_4 &= \begin{cases} 0.0416f_s - 0.0288,\ \ 1.6Hz \leqslant f_s \leqslant 2.32Hz \\ -0.2600f_s + 0.6711,\ \ 2.32Hz \leqslant f_s \leqslant 2.4Hz \end{cases} \\
A_5 &= \begin{cases} -0.0275f_s + 0.0608,\ \ 1.6Hz \leqslant f_s \leqslant 2.32Hz \\ 0.0906f_s - 0.2132,\ \ 2.32Hz \leqslant f_s \leqslant 2.4Hz \end{cases}
\end{aligned} \tag{5.37}$$

Fig. 5.9 illustrates the single-footfall force with 2 Hz walking frequency.

The dynamic responses of floor systems due to footfall forces can be determined by the proposed plate-oscillator model discussed in Section 5.2 by setting $N_o = 0$ and solving Eq. (5.16) numerically. Alternatively, the analytical solutions can also be obtained by

$$\nabla_o^4 w(x,y,t) + c\dot{w}(x,y,t) + \rho h\ddot{w}(x,y,t) = f(x,y,t) \tag{5.38}$$

By applying the assumed-mode method (Meirovitch, 1967), it can be obtained that

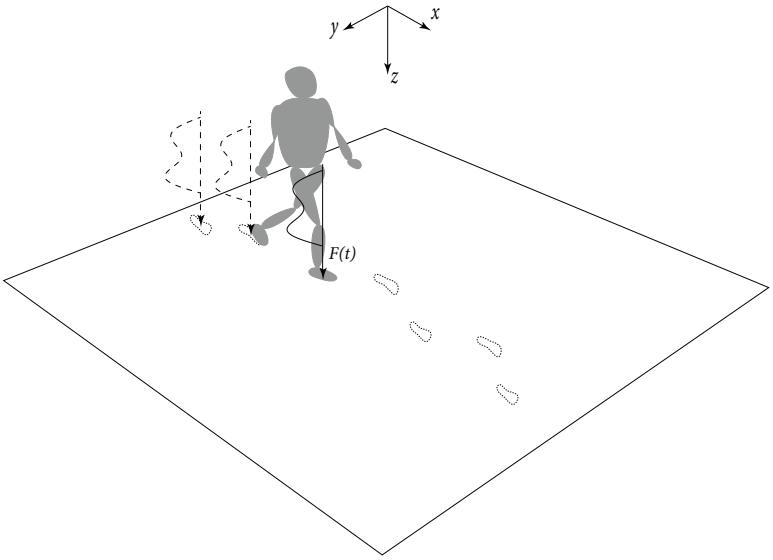

Figure 5.8 Moving force model.

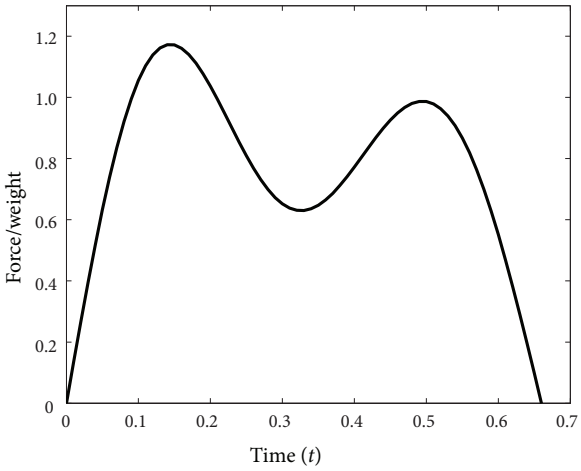

Figure 5.9 Single footfall force.

$$\ddot{q}_n(t) + 2\zeta_n\omega_n\dot{q}_n(t) + \omega_n^2 q_n(t) = F_n(t) \tag{5.39}$$

$$F_n(t) = \frac{W_n(\xi_i, \eta_i)}{M_n} F(t) \tag{5.40}$$

Then, the solution of Eq. (5.39) can be solved by using Laplace transform as

$$q_n(t) = W_n(\xi_i, \eta_i) \int_0^t F(\tau) h(t-\tau) d\tau \tag{5.41}$$

in which $h(t-\tau)$ is the impulse response function of the floor as

$$h(t-\tau) = \frac{1}{\omega_{nd} M_n} e^{-\zeta_n \omega_n (t-\tau)} \sin \omega_{nd}(t-\tau) \tag{5.42}$$

It is known that there are some short time periods when both feet are on the ground which gives an overlapping between the left and right foot during walking (Živanović et al., 2005). Then, the duration of single footfall t_e will be greater than period of human walking $t_s = 1/f_s$. When considering the overlap periods, the loading scheme is illustrated in Fig. 5.10. The response of the floor during interval $it_s < t < (i+1)t_s$ is

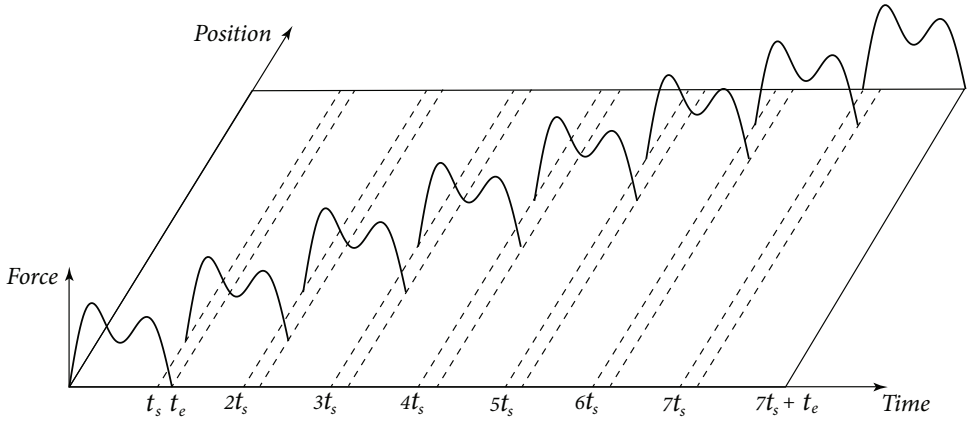

Figure 5.10 Loading scheme of single-footfall forces.

$$\begin{aligned} w(x,y,t) = &\sum_{n=1}^{N} W_n(x,y) W_n(\xi_1,\eta_1) \int_0^{t_e} F(\tau) h(t-\tau) d\tau \\ &+ \sum_{n=1}^{N} W_n(x,y) W_n(\xi_2,\eta_2) \int_0^{t_e} F(\tau) h(t-t_s-\tau) d\tau + \dots \\ &+ \sum_{n=1}^{N} W_n(x,y) W_n(\xi_i,\eta_i) \int_0^{t-it_s} F(\tau) h(t-it_s-\tau) d\tau \end{aligned} \tag{5.43}$$

Applying Liebnitz's rule (De Silva, 2007), the velocity and acceleration responses can be obtained by successive differentiation of Eq. (5.43) with respect to time as follows:

$$v(x,y,t) = \frac{\partial w(x,y,t)}{\partial t} = \sum_{n=1}^{N} W_n(x,y) W_n(\xi_1,\eta_1) \int_0^{t_e} F(\tau)\dot{h}(t-\tau)d\tau + \sum_{n=1}^{N} W_n(x,y) W_n(\xi_2,\eta_2) \int_0^{t_e} F(\tau)\dot{h}(t-t_s-\tau)d\tau + \ldots + \sum_{n=1}^{N} W_n(x,y) W_n(\xi_i,\eta_i) \int_0^{t-it_s} F(\tau)\dot{h}(t-it_s-\tau)d\tau \tag{5.44}$$

$$a(x,y,t) = \frac{\partial^2 w(x,y,t)}{\partial t^2} = \sum_{n=1}^{N} W_n(x,y) W_n(\xi_1,\eta_1) \int_0^{t_e} F(\tau)\ddot{h}(t-\tau)d\tau + \sum_{n=1}^{N} W_n(x,y) W_n(\xi_2,\eta_2) \int_0^{t_e} F(\tau)\ddot{h}(t-t_s-\tau)d\tau + \ldots + \sum_{n=1}^{N} W_n(x,y) W_n(\xi_i,\eta_i) \left[\frac{F(t-it_s)}{M_n} + \int_0^{t-it_s} F(\tau)\ddot{h}(t-it_s-\tau)d\tau \right] \tag{5.45}$$

where

$$\dot{h}(t-\tau) = \frac{e^{-\zeta_n\omega_n(t-\tau)}}{\omega_{nd}M_n}\Big[\omega_{nd}\cos\omega_{nd}(t-\tau) - \zeta_n\omega_n\sin\omega_{nd}(t-\tau)\Big] \tag{5.46}$$

$$\ddot{h}(t-\tau) = \frac{e^{-\zeta_n\omega_n(t-\tau)}}{\omega_{nd}M_n}\Big[(\zeta_n^2\omega_n^2 - \omega_{nd}^2)\sin\omega_{nd}(t-\tau) - 2\zeta_n\omega_n\omega_{nd}\cos\omega_{nd}(t-\tau)\Big] \tag{5.47}$$

Since the forcing function $F(t)$ is expressed by Fourier series in Eq. (5.36), the closed-form solutions of Eqs. (5.43), (5.44) and (5.45) can be derived explicitly. Alternatively, numerical methods can also be applied to obtain an approximate evaluation of the Duhamel's integral in the solutions, e.g., the trapezoidal method (Humar, 2002).

5.4.2 Moving damped-oscillator model

In order to consider HSI during human walking, the human body can be simulated as a heavily damped oscillator (i.e., a SDOF mass-spring-damper) moving on a structure as shown in Fig. 5.11. The proposed damped-oscillator model can be adopted to determine the floor responses due to human walking. Eq. (5.16) can be adopted to obtained the dynamic responses for every footprint. Then, the total responses during human walking on the floor can be obtained from the principle of superposition.

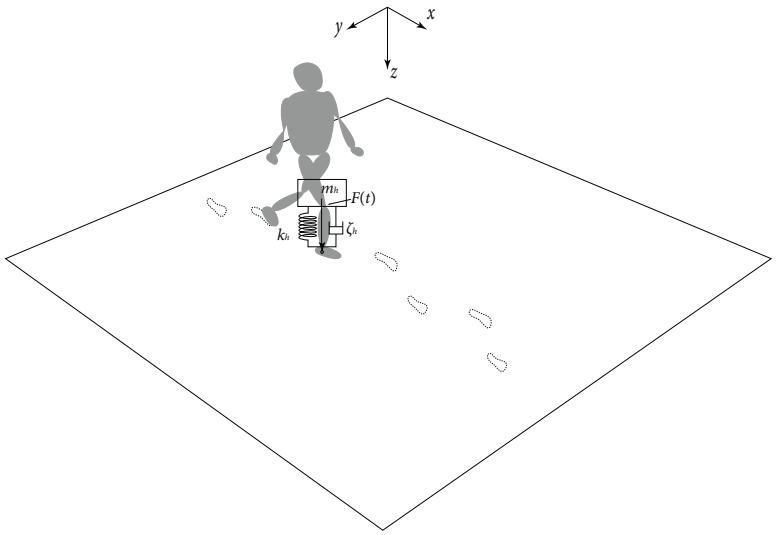

Figure 5.11 Moving damped-oscillator model.

5.4.3 Model of moving and stationary damped-oscillators

If there are stationary occupants on the floor, both moving and stationary occupants need to be modelled separately in the proposed damped plate-oscillator model. As illustrated in Fig. 5.12, moving and stationary occupants are modelled as the damped oscillator moving on the floor from one footprint to next footprint and staying at a fixed location, respectively. The properties of the moving oscillator and the stationary oscillator are selected from Table 5.5 for sitting human model (Coermann, 1962) and walking human model (Shahabpoor et al., 2016a). Similar to that of MDO model, Eq. (5.16) and the principle of superposition can be applied to obtain the total response at the location of the stationary occupant while the other occupant is walking on the floor.

5.4.4 Comparison with test results

The three models, MF, MDO and MSDO, are assessed by comparing with the test results. In these comparisons, two types of tests conducted in structures laboratory at University of Waterloo are selected. The first type is walking tests which were performed by a 82 kg man walking perpendicular and parallel to the direction of the joists at 2007 (Davis, 2008; Parnell, 2008). MF and MDO models are examined by results of walking tests. The second one are human evaluation tests which were conducted at 2001 (Liu, 2001;

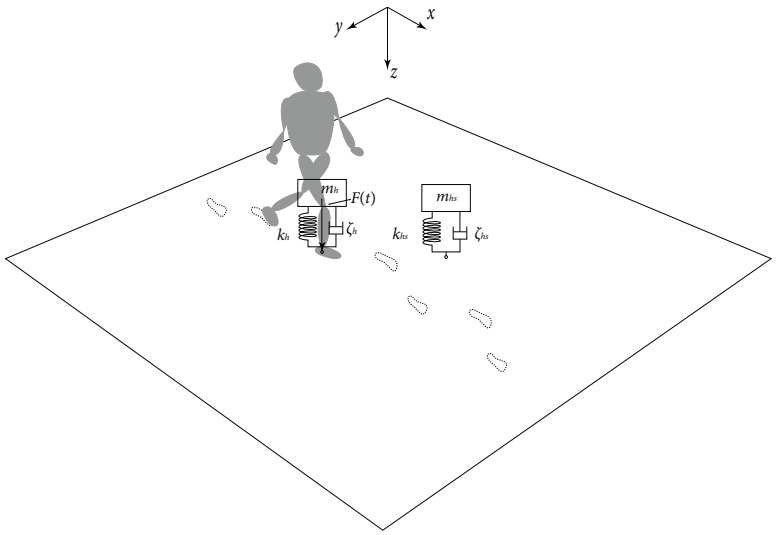

Figure 5.12 Model of moving and stationary damped-oscillators.

Tangorra, 2005). In these tests, an evaluator sitting on a stool while a 82.5 kg (i.e., 185 lb) man walked in the directions of parallel, perpendicular and diagonal to the joist as shown in Fig. 5.13. Then, MDO and MSDO models are analyzed through comparing with the human evaluation tests. The damp ratios of all these floors are 0.015.

Figure 5.13 Human evaluation of floor vibration induced by human walking.

Numerical procedure

Dynamic responses of floors due to human walking can be obtained numerically through MF, MDO and MSDO models in the following steps:

1) Input the geometric parameters and structural properties of floors and the mechanical characteristics of human occupants with their positions;
2) Determine the parameters of human walking and footprints;
3) Obtain the natural frequencies and damping ratios of the unoccupied floors;
4) Solve the Eq. (5.17) numerically for each footprint (i.e., the Runge-Kutta method) and determine the corresponding acceleration of the floor by Eq. (5.26); and
5) Sum the dynamic responses of each footprint based on the principle of superposition for linear vibration system.

In this research, the step frequency of human walking are assumed to be normal, i.e., $f_s = 2$ Hz. The step length l_s is 0.7 m.

Walking tests

Three lightweight floors constructed with CFS C-shape joists with different spans are selected from Davis (2008) and Parnell (2008) and the structural properties and the fundamental frequency are listed in Table 5.13. It is observed that the fundamental frequencies obtained from tests and the proposed method in Section 4.5.1 is in good agreement with floor LF 14.5B. However, considerable discrepancy can be found on the results for floors LF17.0A and LF19.5B which needs to be further investigated in the future. Applying the structural properties in Table 5.13, the dynamic responses induced by human walking can be predicted by models of MF and MDO. The obtained acceleration time histories are compared with test results for human walking parallel to the joists as illustrated in Fig. 5.14.

It can be found from Fig. 5.14(a) that acceleration predicted by MDO model agrees well with test results and is more accurate than that of MF model although the predicted maximum accelerations are almost the same for both models. However, the good

agreement between the predicted and test results are not encountered for floors LF17.0A and LF19.5B, as shown in Fig. 5.14(b) and 5.14(c). The build-up resonant responses associated with low-frequency floors (Brownjohn and Middleton, 2008; Middleton and Brownjohn, 2010) may become an issue as such resonance cannot be found from the test results. Moreover, the magnitudes of the maximum acceleration obtained by MDO model are less than those by MF model. The large differences on the magnitudes of the acceleration between predicted and tested may result from the discrepancies of the frequencies in Table 5.13. For instance, the test results reflect LF19.5B is a high-frequency floor (i.e., $f_1 > 10Hz$) while the predicted results show LF19.5B as a low-frequency floor (i.e., $f_1 < 10Hz$) based on the clarification of high-frequency floors and low-frequency floors by Brownjohn and Middleton (2008). As a result, Fig. 5.14(c) demonstrates the distinction between the impulsive response obtained by tests and the resonance response predicted by MF and MDO models.

Table 5.13 CFS floor configurations of walking tests.

Floor	Span (m)	Width (m)	Density (kg/m^2)	D_x (Nm)	D_y (Nm)	H	Fundamental frequency (Hz)	
							test	present
LF14.5B	4.42	4.88	31.2347	2260000	234000	0	22.5	22.4
LF17.0A	5.18	4.88	80.1629	2930000	199612	0	14.9	11.7
LF19.5B	5.95	4.88	103.4151	2966000	174000	0	11.4	7.98

Human evaluation tests

Further information of human evaluation tests can be found in Liu (2001) and Tangorra (2005). Fig. 5.15 illustrates the acceleration histories obtained from the test and predicted by MDO and MSDO models for floor C in Table 5.4 subjected to one person walking parallel to the joists and the other siting on the floor center to conduct subjective evaluation. It should be noted that the restraining beams were placed on the floor at the support ends of the joists in the test to simulate the possible end rotational restraints provided by the end walls on the floor, but the boundary conditions in both models are still assumed as simply supported in numerical prediction. As a result, the magnitudes of predicted acceleration histories are greater than that of the test. The maximum acceleration magnitudes predicted by both MDO and MSDO models are the same but

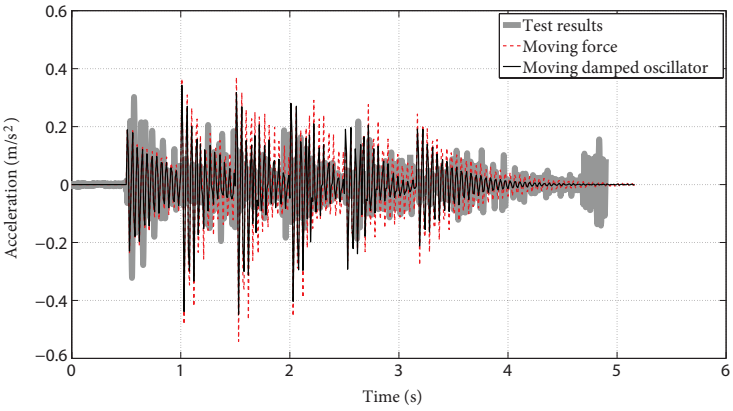

(a) LF14.5B

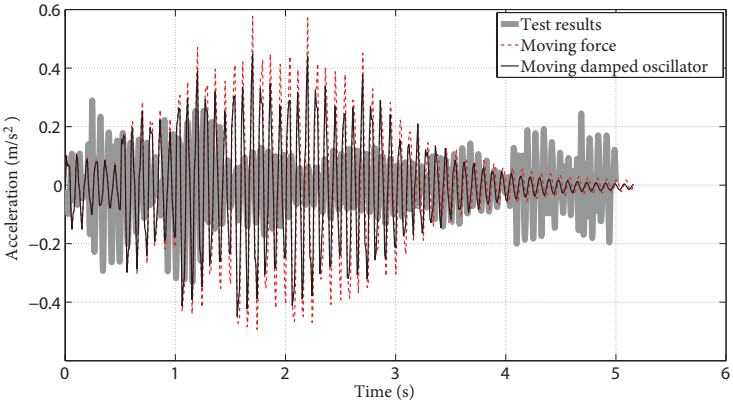

(b) LF17.0A

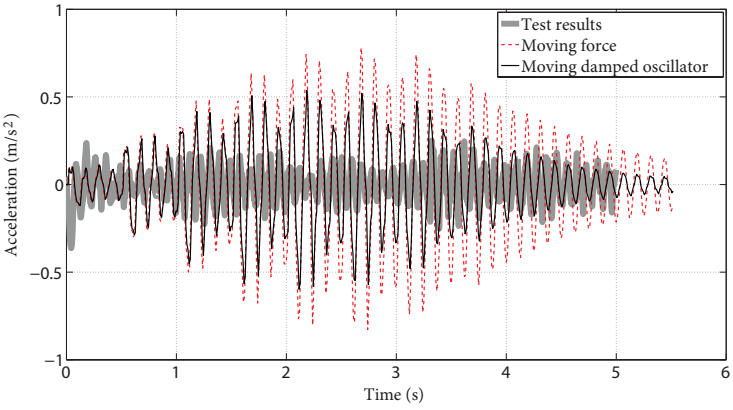

(c) LF19.5B

Figure 5.14 Comparisons of floor responses induced by human walking parallel to the joists.

the decay rate of the response after each footfall is faster for MSDO model due to the consideration of the evaluator at the floor center.

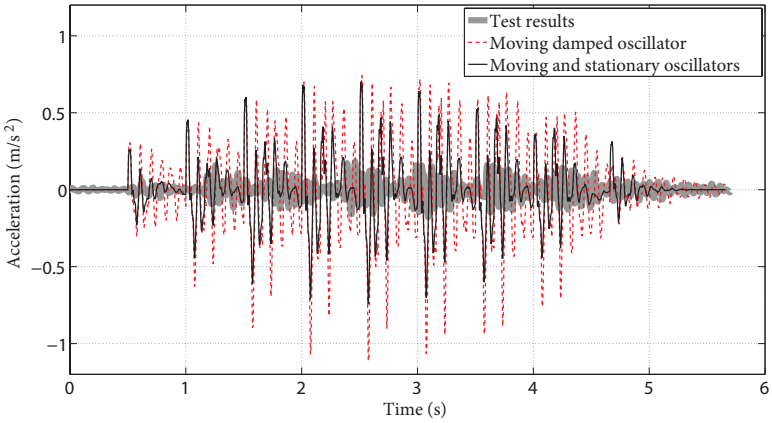

Figure 5.15 Human evaluation of floor vibration induced by human walking.

5.5 Parametric study

Floor vibration due to human walking is primarily influenced by four parameters: step frequency, floor damping ratio, mass ratio of human to floor, and the walking paths. Parametric studies are conducted in the following by means of the foregoing three loading models and the test results.

5.5.1 Step frequency

The step frequency (i.e., footfall rate) dominates the resulting dynamic load. For normal walk on a horizontal surface, the frequency range was found between 1.5 and 2.5 Hz (Bachmann and Ammann, 1987). In general, the peak of the force of single-footfall shown in Fig. 5.9 increases with the step frequency (Wheeler, 1982). Thus, for relatively higher step frequency, larger dynamic response will be induced. On the other hand, if the natural frequencies of floors are in coincidence with one multiple of the step frequency, resonance response will occur and the magnitude may be larger than that of the higher step frequency.

The influence of the step frequency on the dynamic response of the lightweight floors induced by human walking is investigated by MF, MDO and MSDO models respectively. LF14.5B is selected and with a 80 kg human walking parallel to the joists. The damping ratio of the floor is assumed as 0.015 and the step length is 0.7 m. The step frequency varies from 1.5 Hz to 2.5 Hz. The RMS values of acceleration history are illustrated in Fig. 5.16 for three loading models. It can be found that the RMS values have an upward tendency with the increase of the step frequency. However, sudden significant increases can be observed at the step frequencies of 1.7 Hz and 2.2 Hz, which may result from their multiples are close to the fundamental frequency of the floor of LF14.5B (i.e., 22.4 Hz in Table 5.13).

5.5.2 Damping ratio

For floor LF14.5B with same values of the parameters specified in Section 5.4.4, the influence of damping ratios of floors is investigated within the range of 0.005 to 0.06 and the step frequency is 2 Hz. RMS accelerations obtained from three loading models are shown in Fig. 5.17. The RMS accelerations from MF model decrease rapidly with the

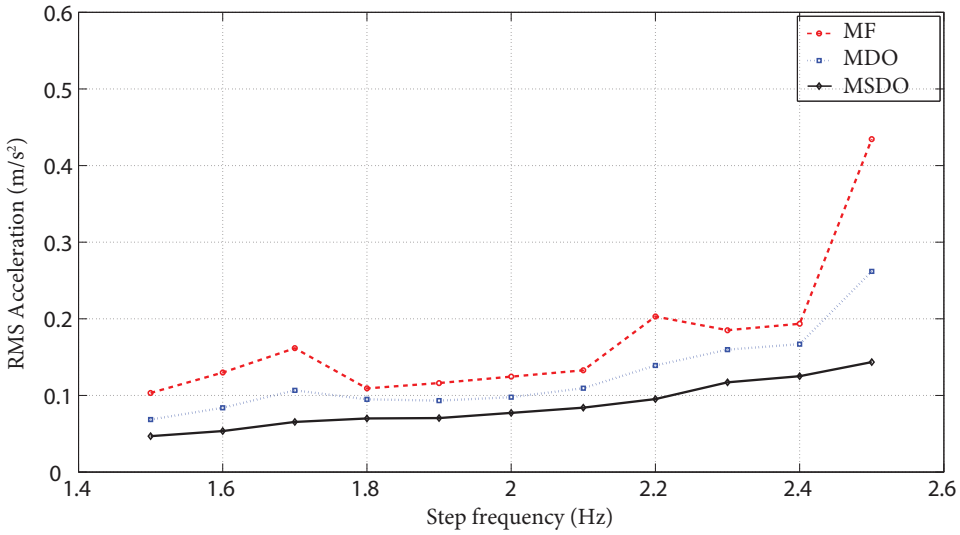

Figure 5.16 The influence of the step frequency on the dynamic response of floor.

increase of the damping ratio in the range between 0.005 and 0.02. However, for MDO and MSDO models, the decrease is much slower and insignificant. It can be concluded that the damping ratio of the floor may not play a important role in the floor vibration when HSI is considered. This finding may bring many benefits to design practice. Damping is a headache issue because the damping capability of a structure is difficult to assess and the scatter in quantification of damping parameters for lightweight floors reported in the literature is large (Weckendorf et al., 2015). Moreover, on-site measurements of floor responses have reflected damping to be significant higher than that in laboratory conditions (Toratti and Talja, 2006; Xu and Tangorra, 2007). However, Fig. 5.17 implies that the damping ratios of unoccupied floors may not play an important role in the vibration of lightweight floors as the human occupants will increase the floor damping considerably. Consequently, the inconsistencies between the laboratory and field studies will be reduced. This would be a trade-off for lightweight steel floors which are significantly influenced by human occupants.

5.5.3 Mass ratio

The intensity of the dynamic interaction between the structure and human occupants is influenced by the mass ratio of human to structure. The HSI is significant if the human mass is comparable to that of the structure but is negligible when the human mass is

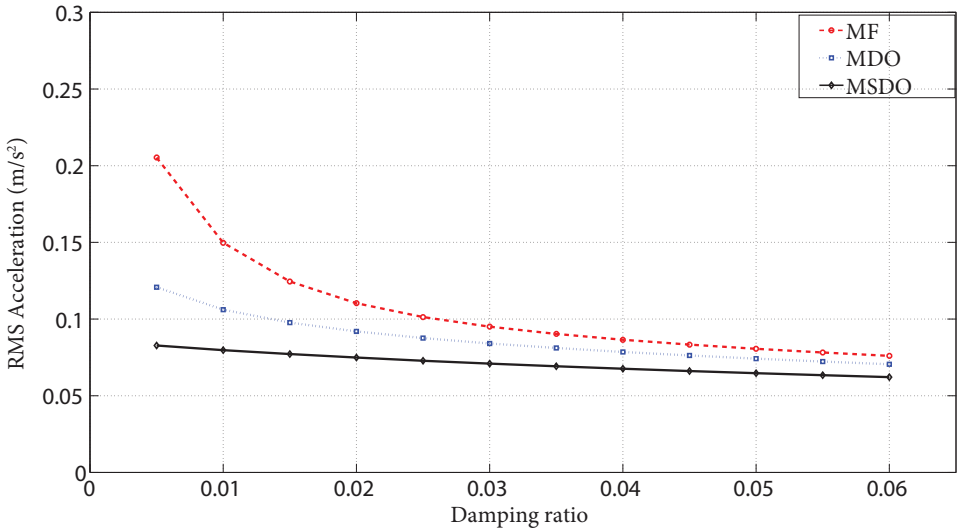

Figure 5.17 The influence of damping ratio on the dynamic response of floor induced by human walking.

relatively small comparing to the structure mass. Thus, the influence of the mass ratios on the HSI is investigated through applying human models with different masses on floor LF14.5B. Two loading models: MF and MDO are adopted and the RMS values of the acceleration are calculated. The comparison is illustrated in Fig. 5.18. It can be found that the influence of HSI becomes more significant as the increase of the mass ratio.

5.5.4 Walking path

Human occupants may walk randomly on structures and change path direction frequently, which can be either unexpected or unanticipated in advance. For the reason of simplicity, the occupants are assumed to walk across the structures along a certain path suitable for producing maximum responses even though it is rarely encountered in everyday life. In the context of residential and office floors, it is widely accepted that footfall loading induced by a single human has proved to be the major source of vibration disturbance (Pavic and Reynolds, 1999). The goal of this investigation is to determine the difference of the floor responses of four different walking paths: parallel and perpendicular to the floor joists, diagonal path and circular path as shown in Fig. 5.19. Both test results and analytical predictions obtained from the proposed loading models are presented.

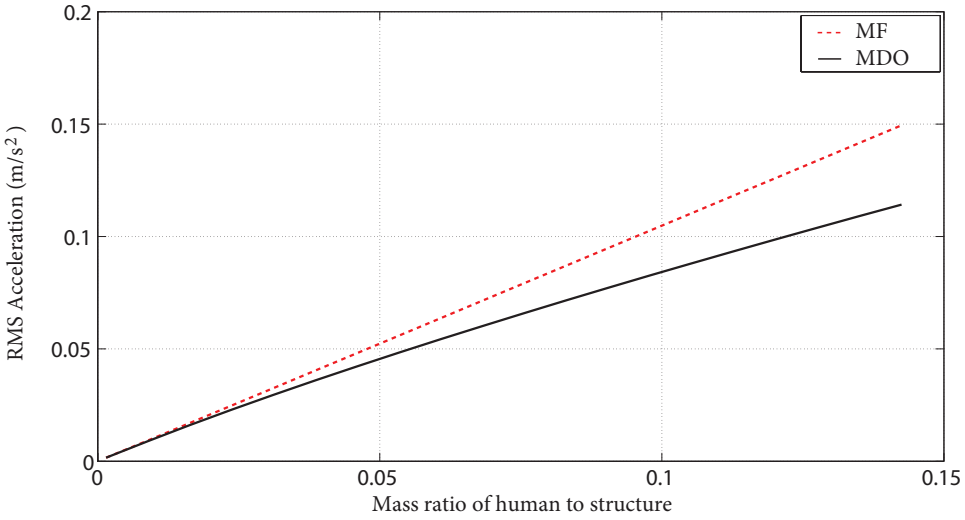

Figure 5.18 The influence of mass ratio on the dynamic response of floor induced by human walking.

Walking tests conducted by Parnell (2008) and Davis (2008) were performed at the University of Waterloo by a 82 kg man walking perpendicular and parallel to the direction of the floor joists. Test results of LF14.5B and LF19.5B, the typical of a high-frequency and a low-frequency floor, respectively, are plotted in Fig. 5.20. It can be observed that human walking perpendicular to the joists produces greater acceleration responses in both cases of LF14.5B and LF19.5B. This results may be because only edges at joist ends are supported and the edges perpendicular to the joists are free.

The second comparison is performed for human evaluation tests on the floor C in Table 5.4 with edges at the joist ends restrained. Acceleration histories of three walking paths: parallel, perpendicular and diagonal path are illustrated in Fig. 5.21. Acceleration responses induced by human walking perpendicular to the joists are found to be close to those of human walking along diagonal path. Similar to waht was found in floor LF14.5B and LF19.5B, perpendicular to floor joist direction yield large response.

What was not investigated in the tests of Parnell (2008) and Davis (2008) is walking with a circular path on the floor, as shown in Fig. 5.19(d). The circular path can be investigated by the proposed loading models either MDO or MSDO. Fig. 5.22 illustrates the dynamic responses induced by human walking perpendicular to the joists as well as walking along the circular paths on the floor of LF14.5B. The acceleration responses are

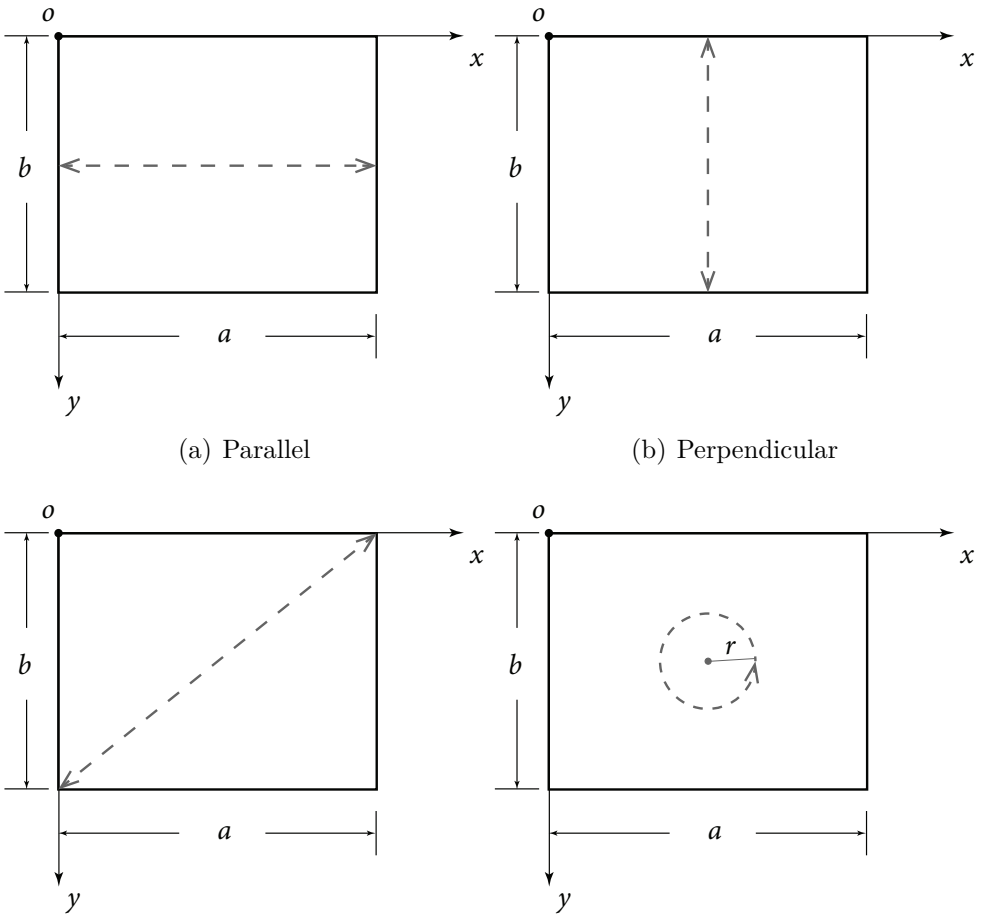

(a) Parallel (b) Perpendicular

(c) Diagonal (d) Circular

Figure 5.19 Walking paths on the floor.

obtained by MDO model and the radius of the circular path shown in Fig. 5.19(d) is set as same as the step length. It can be observed from Fig. 5.22 that the response of circular path is almost the same as that of perpendicular path.

5.6 Summary

In this chapter, a damped plate-oscillator model is proposed to investigate the dynamic properties of lightweight steel floor systems with occupants and predict the dynamic responses of floors due to human walking. The influence of stationary occupants on dynamic properties of lightweight floors was studied. The predicted results by the proposed

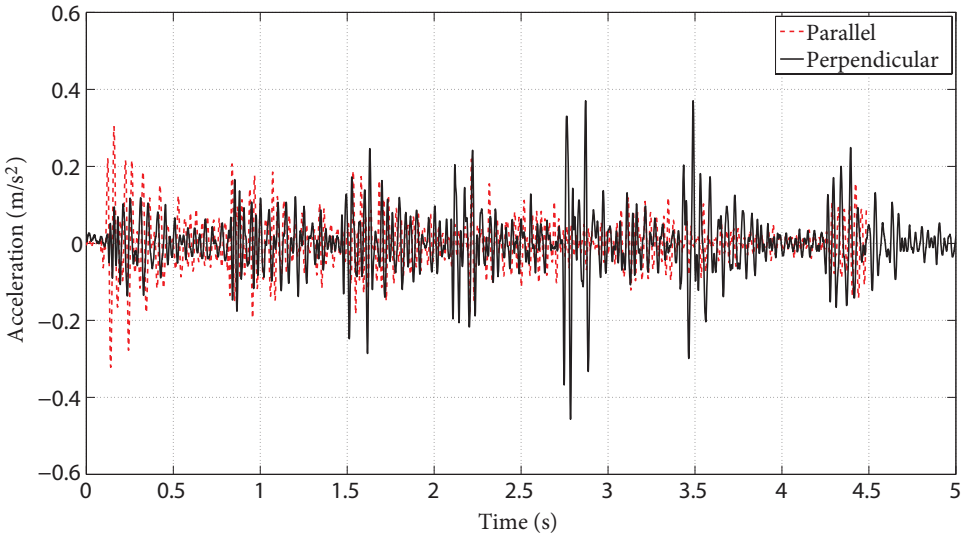

(a) LF14.5B

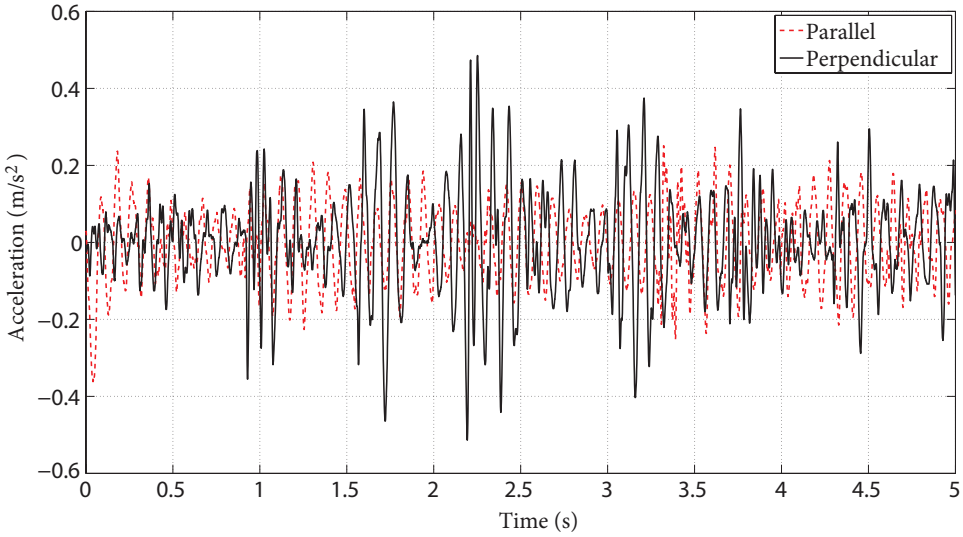

(b) LF19.5B

Figure 5.20 Floor responses induced by human walking parallel and perpendicular to the joists.

damped plate-oscillator model were compared with results of the laboratory tests on CFS floor systems with and without occupants. Three models used for predicting dynamic response: MF, MDO and MSDO are examined by the test results. At last, parametric studies are conducted on the influence of step frequencies, damping ratios, mass ratios and walking paths.

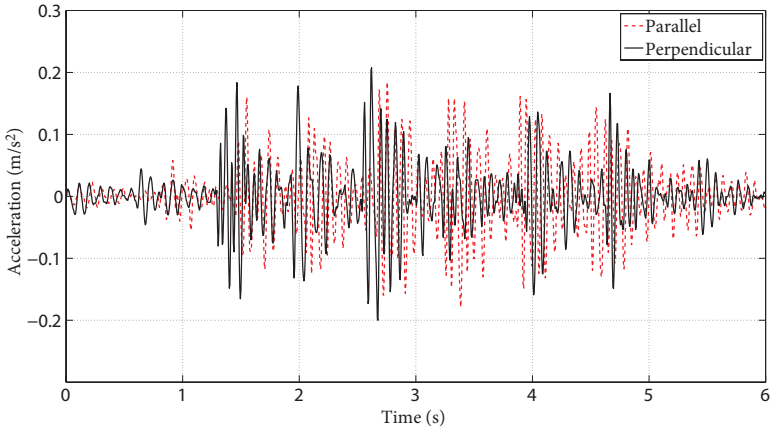

(a)

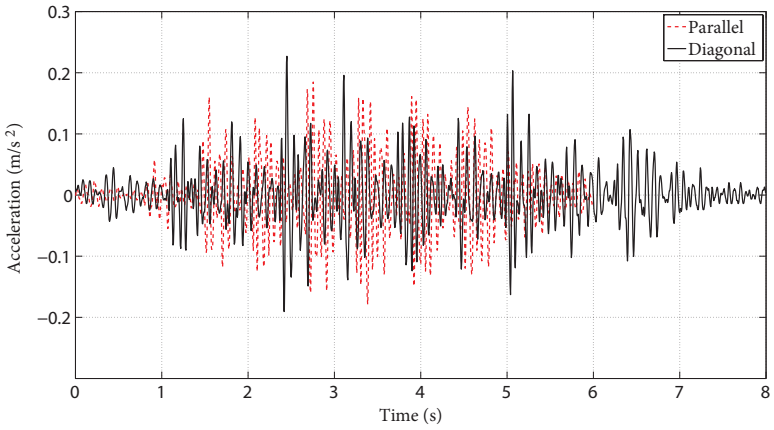

(b)

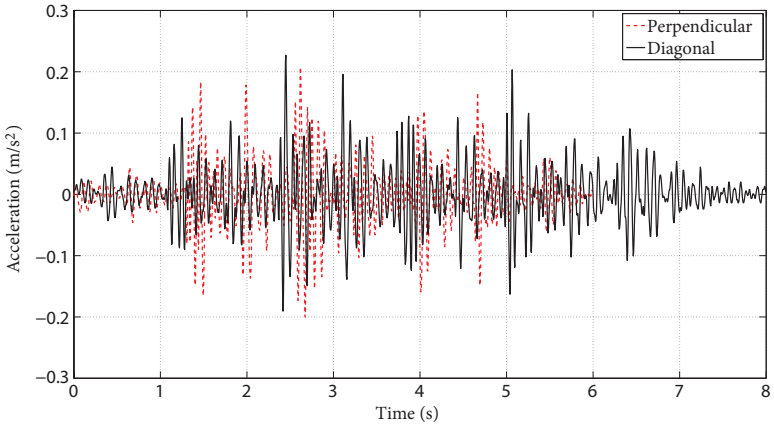

(c)

Figure 5.21 Floor responses induced by human walking along different paths.

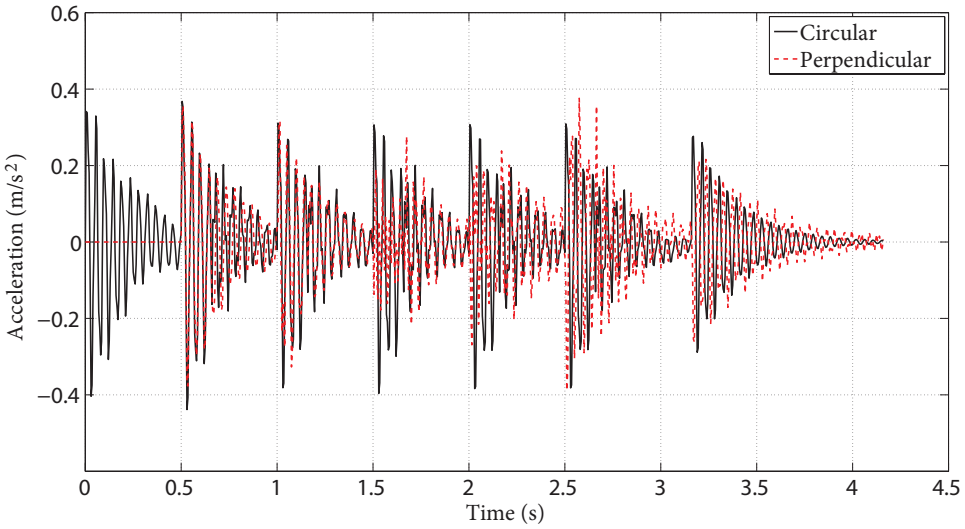

Figure 5.22 Dynamic responses induced by human walking along different paths on LF14.5B.

6

Performance criteria and design methods for Residential Construction

6.1 Introduction

Traditionally, in design practice, floor vibration is controlled by ensuring the adequacy of floor stiffness when a floor is subjected to a distributed load. Approaches have included limiting the maximum floor deflection under the combination of dead load and a uniformly distributed live load to span/360 or even span/480, along with restricting the ratio of the span to depth of a supporting steel beam to 24 or under. However, many examples have shown that this approach may not be sufficient (Allen and Rainer, 1976; Ohlsson, 1986; Murray et al., 1997), in part, perhaps, because the stiffness due to a distributed load is essentially equivalent to the floor's fundamental frequency. This frequency can be calculated by

$$f = 0.18\sqrt{\frac{g}{\Delta}} \tag{6.1}$$

where g is the acceleration of gravity and Δ is the mid-span deflection under the distributed load. Thus, limiting stiffness under a distributed load is intended to restrict the fundamental frequency such that the possible resonance induced by human walking can be avoided. Lightweight floors, however, rarely experience resonance, due to their higher fundamental frequencies (Hu et al., 2006).

Currently, the most widely used design standard for lightweight floor systems is the

static stiffness criterion adopted by ATC Design Guide 1 (Allen et al., 1999), which limits the floor deflection under a 1 kN concentrated load. This criterion relates more directly to vibration performance of floor systems subjected to human walking. It can be traced back to subjective surveys of wood floors in residential construction, conducted in Canada in the 1980s (Onysko, 1988a), which reported that the static deflection under a concentrated load applied at the centre of a floor correlated very well with occupant acceptabnce of various types of wood floors. Nevertheless, this standard does not take account of the mass of floors and other properties unique to floor transient response such as damping (Onysko et al., 2000). Furthermore, since the database of the subjective surveys of Onysko (1988a) did not include floors with concrete toppings, and most of the floor spans in the surveys were far shorter than 6.0 m, the criterion may be unreliable for floors with heavy toppings (Smith and Chui, 1988) or with long spans. It is also questionable whether it can be applied to lightweight CFS floors.

In essence, the aforementioned two approaches do not directly deal with dynamic responses due to human activities. It would desirable to have alternative methods characterized by the dynamic nature of loads and relatively simple to implement practically. The design guidelines proposed in this chapter are primarily applicable for residential construction.

6.2 Basis of design guidelines

A design guideline for floor vibration serviceability normally consists of two parts: a design criterion related to human tolerance of floor vibration (i.e., a human acceptance criterion) and a design method to evaluate the parameters specified in the design criterion. Prior to developing the design guidelines for vibration serviceability of lightweight floors, it is necessary to discuss some important issues associated with the vibration serviceability.

6.2.1 Human perception of vibration

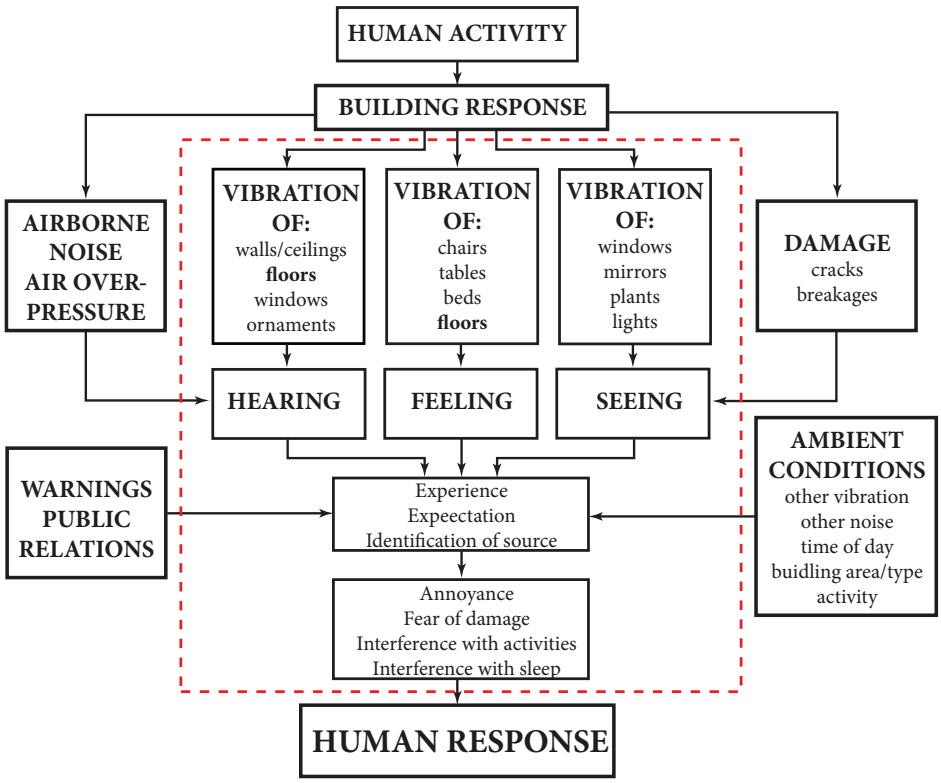

Figure 6.1 Factors affecting the acceptability of building vibrations induced by human activity (Griffin, 1990).

Human perception of vibration in a building relates to a large number of parameters, as shown in Fig. 6.1. In many circumstances, the degree of annoyance and complaint cannot be explained directly by the magnitude of vibration alone but also depends on audio and visual impressions. To evaluate human perception, many additional effects need

to be considered, such as the environment surrounding the person, the person's activity, as well as the psychological reaction of the person. Under some conditions of amplitude and frequency, adverse comments may arise even though the measured amplitude is lower than the perception level (ISO 2631-2, 2003). For instance, people can be aware of a low-level vibration in a quiet apartment, which may not be perceived in a busy workplace. It is known that the vibration perception is greatest in a seated person rather than one standing or in motion (Onysko et al., 2000). Humans who are moving may experience hundred times greater vibration magnitude than stationary people. Thus, the current edition of ISO 2631-2 (2003) deviated from the first edition (ISO 2631-2, 1989) by not specifying the acceptable magnitudes of vibration; instead, it provides guidelines for collecting data concerning complaints about building vibration to develop corresponding design criteria. Clearly, it is unrealistic to assume that human sensitivity to a given vibration amplitude will be predicted precisely. Vibration levels can be considered as general indicators of serviceability rather than precise assessments (Ellis, 2001).

6.2.2 Direct criteria and correlative criteria

Existing design criteria to control floor vibration can be classified into two categories: direct and correlative (i.e., indirect). Direct criteria relate one aspect of human perception of whole body vibration (e.g., acceleration) to floor vibration serviceability, and require correct predictions or suitable measurements of human responses to vibration and absolute thresholds for human sensitivity to vibrations. However, the criteria for deciding the acceptability of building vibration will vary from situation to situation (Griffin, 2007). Efforts to determine the individual acceptance levels of occupants of a building would produce inconsistent results.

Extensive attempts were made to quantify human responses to floor vibrations last century (Wright and Green, 1959; Allen and Murray, 1993). One direct criterion still widely used in North America is the acceptance criterion recommended in Steel Design Guide Series 11 (Murray et al., 1997) of AISC/CISC. The AISC/CISC criterion was developed using acceleration limits provided by ISO 2631-2 (1989), as shown in Fig. 6.2. A base curve of RMS acceleration was given in ISO 2631-2 (1989) as the average level of human perception to constant sinusoidal vertical vibration at different frequencies. The design criteria for different occupancies can be obtained from multiples of the base curve by

referring to experiences and practices. For instance, in the case of residential construction in day time, a multiplier of 2 to 4 is suggested for continuous or intermittent vibrations, and 60 to 90 for transient vibrations. Since walking vibration is intermittent and low frequency in nature, the multiplier for walking vibration in residence can be estimated in the range of 5 to 8 (Allen and Murray, 1993). Based on the RMS acceleration criteria, the AISC/CISC criterion was developed by using peak acceleration, which was transferred from RMS limits by an estimated ratio of approximately 1.7 for typical walking vibration. Finally, a value of 0.5 percent of the acceleration of gravity for 4-8Hz is recommended as the peak acceleration limit used in AISC/CISC Steel Design Guide Series 11 (Murray et al., 1997) as illustrated in Fig. 6.2.

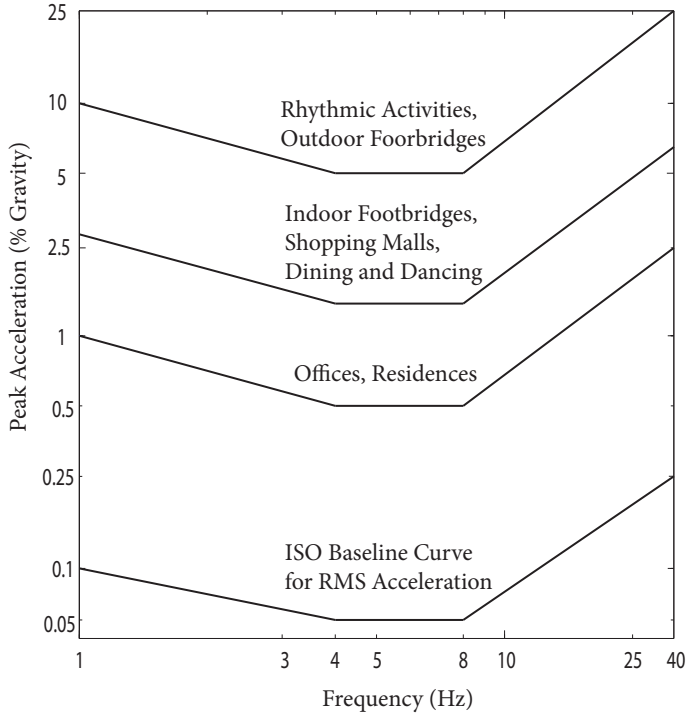

Figure 6.2 Peak acceleration criteria for different occupancies (Murray et al., 1997).

Unfortunately, the acceptance criterion in ISO 2631-2 (1989) was withdrawn, as the range of potential applications was too widespread for that standard (ISO 10137, 2007). Therefore, the AISC/CISC criterion based on the acceptance criterion of ISO 2631-2 (1989) collapsed immediately. Furthermore, the method of evaluating floor responses due

to occupant activities associated with the AISC/CISC criterion may be overly simplified and is often inaccurate and inappropriate, as discussed extensively by Middleton and Brownjohn (2011). It is noticed that the recently published guideline by the Steel Joist Institute (SJI) (Murray and Davis, 2015) still recommends the tolerance acceleration limits of the AISC/CISC criterion. The SCI Standard P354 (Smith et al., 2009) of the UK Steel Construction Institute (SCI) has adopted the human tolerance criterion which are similar to that of the AISC/CISC but are in terms of a multiplying factor, R. Optimistically, the predicted peak acceleration response and the AISC/CISC criterion in Murray et al. (1997) were compared to the subjective evaluations for human occupants in quiet spaces and the comparison results show excellent agreement between subjective and predicted evaluations (Murray and Davis, 2015). This validation by subjective evaluations is the technique applied by the other type of criteria, i.e., correlative criteria.

Correlative criteria relate the acceptability of a floor to its engineering-performance characteristics not exactly the vibration experienced by occupants (e.g., static deflection under a concentrated load). In contrast to direct criteria involving accurate predictions of floor responses due to human activities, as well as the subjectivity of human perception to one single parameter, correlative criteria derive some empirical links by correlating on human acceptability of floors to measured or computed parameters from tested floors and subjective evaluations of the same floors. In particular, the parameters must be conveniently addressed in design. The correlation studies can be conducted by statistical analysis such as logistic regression (Hu, 2002). The complex calculation of floor responses induced by human walking will not necessarily be considered. The limitations of maximum deflection under a 1 kN concentrated load recommended by Onysko (1988a) and Hu (2002) come under this category. The static deflection limitations corresponding to a 1 kN concentrated load are still widely used and are preferred by the wood floor industry (Weckendorf et al., 2015). The application of the limitations on lightweight steel floors will be validated by subjective evaluations of CFS floors in the following sections.

Above all, direct criteria require accurate prediction of floor responses under human activities and thresholds of human sensitivity to vibration, which is theoretically impossible and difficult to apply in daily engineering practice. On the other hand, correlative criteria would be more practical, although subjective evaluations may result in some uncertainty. Such uncertainty will be reduced if the subjective surveys are fairly adequate. If the exact

floor responses cannot be accurately predicted, direct criteria are essentially correlative criteria to some extent, even though the absolute thresholds for human sensitivity of vibrations exist. For instance, since the floor response due to occupant activity is predicted by simplified methods by Murray et al. (1997) with questionable accuracy in some cases, the AISC/CISC criterion was developed as a direct criterion initially, but becomes a correlative criterion after its results were compared with those of subjective evaluations.

6.2.3 Lightweight high-, mid- and low-frequency floors

It is convenient to have different approaches for different types of floors based on their vibration characteristics under human activities. Building floors are commonly classified into two categories when vibration serviceability is the focus: high- and low-frequency (ISO 10137, 2007). This classification was originally introduced by Wyatt (1989), who suggested that low-frequency floors responded harmonically, with a resonant response, and high-frequency floors acted impulsively with a transient response (Middleton and Brownjohn, 2010, 2011). More specifically, floors with a fundamental frequency less than four times the step frequency will most likely resonate with one of the harmonics, and the resonance will be constantly maintained by subsequent footfalls. On the other hand, when the natural frequency of a floor is above four times the step frequency, the response generated by an individual footfall decays to a comparatively small value by the time the successive footfall begins due to damping. Resonance is thus unlikely to occur, and the vibration will most likely be dominated by a transient response. Hence, the fourth harmonic of the step frequency is commonly used to set the threshold frequency as approximately 10 Hz (Brownjohn and Middleton, 2008). Different design methods have been developed for the calculation of resonance and transient responses in floor vibration serviceability, such as Arup's methods by Willford and Young (2006).

However, the classification of high- and low-frequency floors needs to be refined for lightweight floors because most of them have a fundamental frequency greater than 10 Hz or even more than 20 Hz. The dynamic responses of high-frequency floors (over 10 Hz) comprise two parts: transient vibrations generated by higher harmonic components of the footstep forces and motions produced by the varying static floor deflection caused by the low-frequency components of the footstep forces and their varying location (Allen and Rainer, 1989). If a high-frequency floor has a fundamental frequency of considerably

greater than 10 Hz, say over 20 Hz, vibrations in the higher modes generally damp out quickly and might not cause discomfort. It is the varying static deflection that causes much of the discomfort. Therefore, the stiffness of the floor under concentrated load will be sufficient to control floor vibrations. For high-frequency floors with a fundamental frequency between 10 Hz and 20 Hz, transient vibrations should be taken into account. For instance, based on a database of 112 field wood floors, Hu (2002) developed a criterion using the combination of 1 kN deflection and fundamental frequency, as shown in Fig. 6.3. The fundamental frequency of misclassified floors in Fig. 6.3 are primarily in the range of 10 Hz to 20 Hz.

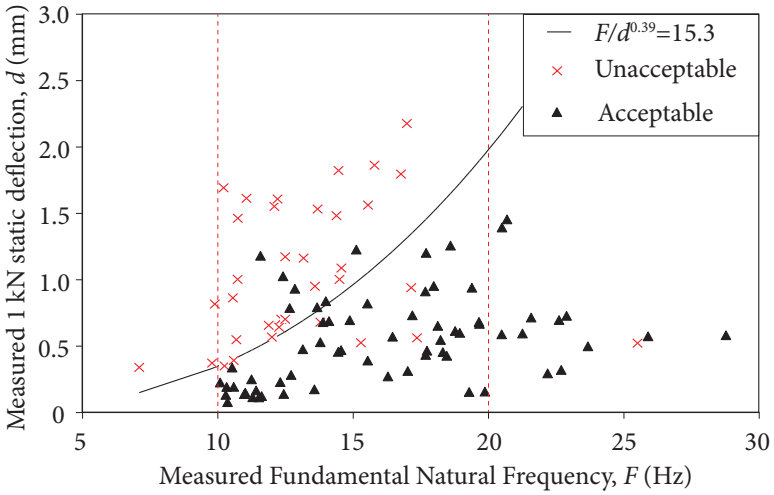

Figure 6.3 Proposed criterion by Hu (2002).

Thus, for lightweight floors, the category “high-frequency floor" can be further classified into two groups: lightweight mid-frequency floors (between 10 Hz and 20 Hz) and lightweight high-frequency floors (over 20 Hz). It should be pointed out that the threshold frequencies of 10 Hz and 20 Hz are preliminary assumptions for lightweight floors in this study and need further investigation. From the governing vibration characteristics of lightweight high-, mid- and low-frequency floors, three simple vibration models can be developed: a resonance model for lightweight low-frequency floors, an impulse-vibration model for lightweight mid-frequency floors, and a point-deflection model for lightweight high-frequency floors. These three simple models of floor vibration were first proposed in ATC DG 1 (Allen et al., 1999).

Additionally, it has been noticed that the natural frequencies of lightweight high-

frequency floors can be within the audible frequency range of humans (roughly 20 Hz–20000 Hz). A thump-like response to footfalls will be primarily audible, and is distinct from perceptible deflection or vibration. Given the high rigidity of most lightweight floors, this characteristic appears to reflect a drum-like ability to radiate sound in response to impacts, especially for wood floors (Bernard, 2008). As a consequence, those floors satisfying existing vibration design criteria may fail to display satisfactory performance with respect to vibrational disturbances such as drumminess. However, this issue is beyond the scope of this research.

6.2.4 Damping

Damping is one of most important factors in vibration serviceability evaluation but is always excluded in existing design guidelines. Onysko et al. (2000) stated that the computed response of a floor subjected to an arbitrary dynamic impulse load resulted in equally successful discrimination between acceptable and unacceptable floors as the maximum static deflection under 1 kN concentrated load. However, evaluation of damping was problematic, which inhibited their attempts to develop design guidelines based on dynamic response. Similarly, zero damping was assumed by Dolan et al. (1999) in their derivation of a design criterion that requires the fundamental frequency of a floor system be greater than 15 Hz for unoccupied conditions and greater than 14 Hz for occupied conditions.

In general, two troublesome problems have impeded the application of damping in design. First, damping is difficult to assess, and the scatter in quantification is large. Second, results show many inconsistencies between laboratory and field studies. Damping in on-site measurements has been significantly higher than that under laboratory conditions (Xu and Tangorra, 2007; Weckendorf and Smith, 2012). However, the problem can be compensated for by the presence of human occupants. Since human occupants can increase the damping of unoccupied floors several fold, the wide range of damping and the inconsistencies between laboratory and field floors have little effect on human acceptability of floors, assuming single values in a design, which was discussed in the parametric studies of Section 5.5.2.

6.2.5 Development of design guidelines

It should be acknowledged that complex engineering problems such as floor vibration may not have final or universal solutions, and such complex problems need to be reduced and simplified to achieve a clearer picture of the governing relations. Design criteria and methods for floor vibration serviceability should capture the most-important features, and the corresponding performance parameters of the criteria should be measurable, calculable and explainable. Based on the foregoing discussion of the four important issues in the vibration serviceability of lightweight floors, it can be recognised that predicting human acceptability of floors through a given vibration amplitude is unreliable. Correlative criteria are likely more practical than direct criteria in residential constructions.

Based on the above discussion, a comprehensive subjective evaluation should be conducted for each type of particular structure based on its intended occupancies and structural characteristics. The subjective evaluations involve more actual conditions and can aggregate the effects of experience gained under multiple scenarios. Moreover, with the significant increase of damping introduced by human occupants, the damping ratios obtained based on laboratory floors and field floors may not have large inconsistencies if HSI is considered.

Once the results of subjective evaluations are available, simple parameters should be proposed for reflecting the governing structural properties and characterizing the dynamic performance of each type of floor under human activities rather than calculating the responses induced by human activities. In particular, these parameters must be conveniently addressed in design and involve the most important factors. After that, design criteria can be proposed by correlating studies that use subjective evaluations of human acceptability of floors with computed parameters. Then, design methods need to be developed for calculation of the parameters.

Finally, the previous investigation in Chapter 5 has illustrated that HSI is an important issue that needs to be considered in the evaluation of serviceability performance, especially for lightweight floors. However, for correlative criteria, it is not necessary to calculate the exact responses induced by human activities. A carefully selected design parameter is sufficient to characterize the vibration performance of floors. A floor is unacceptable owing to its structural properties. Even though human occupants can affect

the dynamic properties of structures, such as their natural frequencies and damping ratios, the vibration serviceability may not be improved significantly. Therefore, HSI has been taken into account in previous analytical studies of floor vibration but not considered in the development of design guidelines.

6.3 Static criterion for lightweight mid- and high-frequency floors

In this research, limiting the maximum deflection of floors under a 1 kN concentrated load applied at the centre is referred to as a static criterion. Two forms of static criteria are reviewed in Section 2.2: the first in ATC Design Guide 1 (Allen et al., 1999) and CWC et al. (1997) developed based on Onysko (1988a,b), and the other proposed by Hu (2002) and Hu and Chui (2004). These two forms are herein designated as Onysko criteria and Hu criteria, respectively. For the sake of consistency with criteria for lightweight low-frequency floors, the form of Hu criteria, combining the fundamental frequency and 1 kN deflection, is adopted to propose a static criterion for lightweight mid- and high-frequency CFS floors.

6.3.1 Test database and logistic regression

A total of 65 floors tested in a laboratory forms the main database used to find a static criterion. The tests were conducted by Wiss et al. (1977), Kraus (1997), Samuelsson and Sandberg (1998), Talja and Kullaa (1998), and Liu (2001). Wiss et al. (1977) measured the maximum deflection caused by a 300 lb (1.334 kN) concentrated load at mid-span of the centerline joist. Since the load-deflection curves in Wiss et al. (1977) indicate that floor systems behave linearly under a concentrated load within this range, the deflections under 1 kN (225 lb) concentrated load can be obtained from the test results for these deflections of 1.334 kN (300 lb). As mentioned in Section 2.3, Kraus (1997) and Liu (2001) conducted similar subjective evaluations on CFS floor systems in the laboratory. Four lightweight steel joist floors (designated SBI in the tables) tested at the laboratory of the Swedish Institute of Steel Construction (Samuelsson and Sandberg, 1998) and nine similar floors (designated VTT in the tables) tested at VTT Building Technology in Finland (Kullaa and Talja, 1998; Talja and Kullaa, 1998). The test results for these SBI and VTT

floors were also collected by Hu (2000) to validate her static criteria of wood floors.

Binary logistic regression analysis in SPSS® statistical analysis software (Norušis, 2003) is performed on the database to determine the correlation of the subjective evaluations with fundamental frequencies and deflections under 1 kN concentrated load. The background and methods are given in Hu (2000). It is noted that the binary logistic regression is restricted to two categories (i.e., acceptable and unacceptable). However, in the database, the subjective evaluations have three categories: acceptable, marginal and unacceptable. Given that all the floors were built in a laboratory and that the acceptable floors are far fewer than the unacceptable floors, the marginal floors in the database are merged with the acceptable floors in the binary logistic regression analysis. Thus, in total, 65 floors consisting of 35 unacceptable floors and 31 acceptable floors are used in the analysis. The cut-off point is equal to 0.5.

6.3.2 Proposed static criterion

From the results of the regression analysis, the criterion for acceptable floors can be obtained as the fundamental frequency, F, and the deflection under 1 kN concentrated load, d, satisfying the relationship:

$$\frac{F}{d^{0.44}} > 15.9 \tag{6.2}$$

Table 6.1 summarises classification of floor acceptability as predicted by Eq. (6.2) and their comparisons with subjective evaluations. In the 31 acceptable floors, 15 floors are marginal and 16 acceptable in the subjective evaluations. As illustrated in Figs. 6.4 and 6.5, the subjective evaluations in the database are compared with predictions using the Onysko criterion (i.e., Eq. (2.1)), Hu criteria (i.e., Eqs. (2.3) and (2.4)), and the proposed criteria in Eq. (6.2). The details of comparisons for each floor in the database can be found in Tables C.1, C.2, C.3, and C.4 of Appendix C. Although the accuracy of the prediction using Eq. (6.2) is 64.5% in Table 6.1, only 3 of 16 acceptable floors are misclassified, which can be observed in Fig. 6.5. Thus, the accuracy for predicting acceptable floors in the database becomes 81.2%.

Furthermore, the static criteria are also validated using test results for field floors by Kraus (1997) and CCFSRG, and the comparisons are tabulated in Tables C.5 and C.6

Table 6.1 Classification by logistic regression analysis in SPSS®.

Subjective evaluations	Predicted results		Accuracy
	Unacceptable	Acceptable	
34 unacceptable floors	27	7	79.4%
31 acceptable floors†	11	20	64.5%
Overall accuracy			72.3%

†–15 marginal floors and 16 acceptable floors

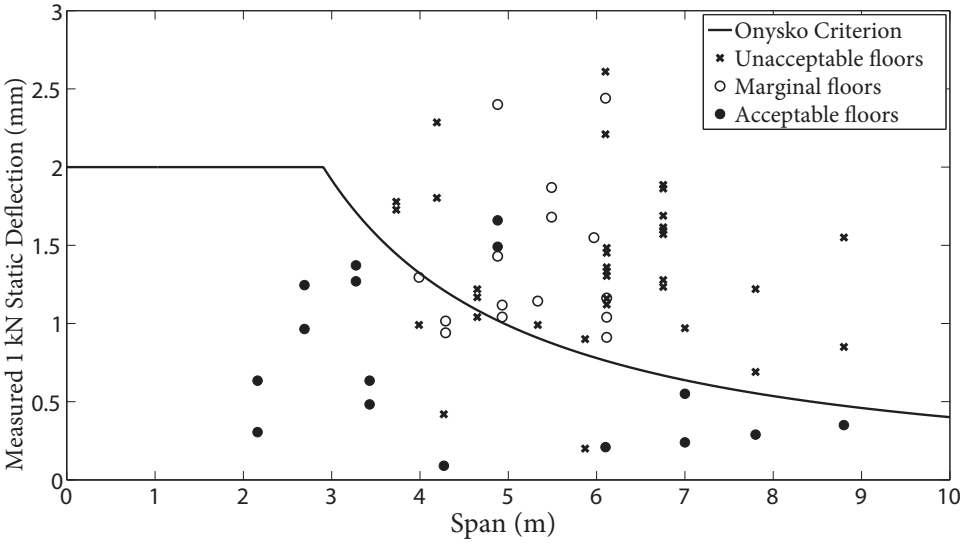

Figure 6.4 Comparison of Onysko criterion with subjective evaluations.

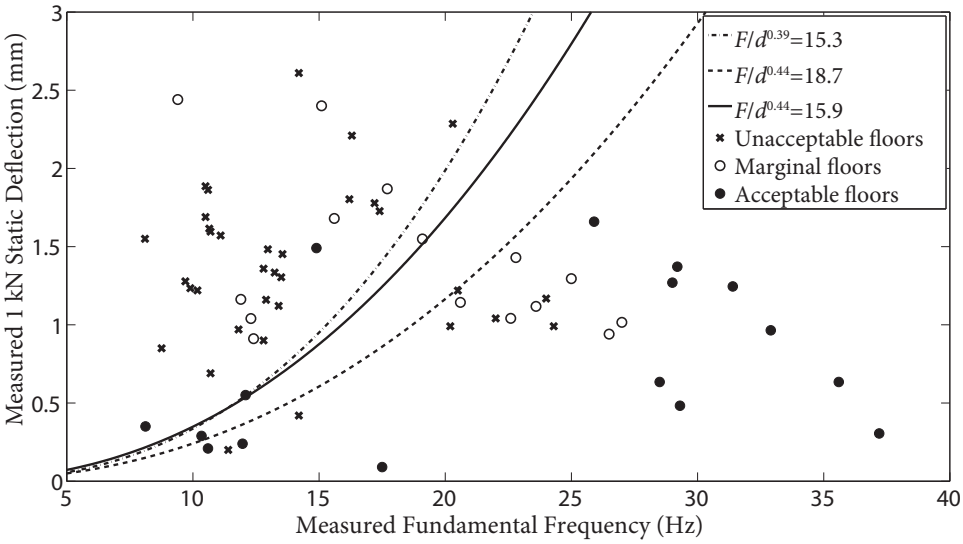

Figure 6.5 Comparison of Hu criteria and proposed criterion with subjective evaluations.

of Appendix C. As can be observed, the acceptance of floors predicted by all four static criteria match well with the subjective evaluations in tests. However, the Onysko criterion provides the best predictions, followed by the proposed static criterion of Eq. (6.2). Thus, both these criteria are recommended for design criteria for the vibration serviceability of lightweight mid- and high-frequency CFS floor systems. Such criteria may be sufficient for lightweight high-frequency floors but the dynamic criteria associated with the transient response of lightweight mid-frequency floors may need to be considered as well, and so is presented in the following sections.

6.4 Impulsive criterion for lightweight mid-frequency floors

The static criteria do not directly deal with the dynamic response due to human activities. A design criterion should be developed based on the transient vibration of lightweight mid-frequency floors. In this section, a simple parameter is proposed to represent transient properties of these floors, and then used to develop the design criterion for such floors. This criterion is termed as the impulsive criterion.

6.4.1 Floor impulsive factor

The dominant feature of the transient vibration of lightweight mid-frequency floors is that the floor response is a series of impulses, wherein the impulse due to one footstep dies away before the next footstep impulse takes place. This feature can be illustrated by either test results or analytical modelling. Thus, a single impulse due to a footstep will be sufficient to represent the dynamic response of a lightweight mid-frequency floor under human walking, as shown in Fig. 6.6. Furthermore, from the parametric study of walking paths, it can be found that the maximum response always occurs when the position of the footstep is close to the center of the floor, regardless of walking paths. As a consequence, the single impulse due to a footstep at the floor center should be selected; the time window is the period of a walking stride, t_s. Given that it is not necessarily to calculate the exact response of a floor under a footstep, a unit impulse (1 Ns) can be assumed to excite the floor at the center. If only the first vibration mode is considered, the deflection response of the floor at the center will be reduced to a SDOF oscillator under a unit impulse and can be expressed as in Kelly (2012)

$$x(t) = \frac{1}{M_1 \omega_d} e^{-\zeta \omega t} \sin \omega_d t \tag{6.3}$$

where M_1 is the modal mass of the first mode of a floor structure, ζ is the damping ratio of the first mode, ω and ω_d are the first circular frequency and the damped frequency, respectively. The acceleration response can be obtained by taking the second derivative with respect to the time. It gives

$$a(t) = \frac{e^{-\zeta \omega t}}{\omega_d M_1} \Big[(\zeta^2 \omega^2 - \omega_d^2) \sin \omega_d t - 2\zeta \omega \omega_d \cos \omega_d t \Big] \tag{6.4}$$

Since the damping ratios of unoccupied CFS floor systems are unlikely to exceed 0.06, the damped frequency ω_d is approximately equal to ω. Then, substituting $\omega = 2\pi f$ yields

$$a(t) = -\frac{2\pi f e^{-2\pi \zeta f t}}{M_1} \Big(\sin 2\pi f t + 2\zeta \cos 2\pi f t \Big) \tag{6.5}$$

The duration of the single impulse is the period of the stride, t_s. The RMS value can be used to assess the vibration serviceability, which can be expressed as

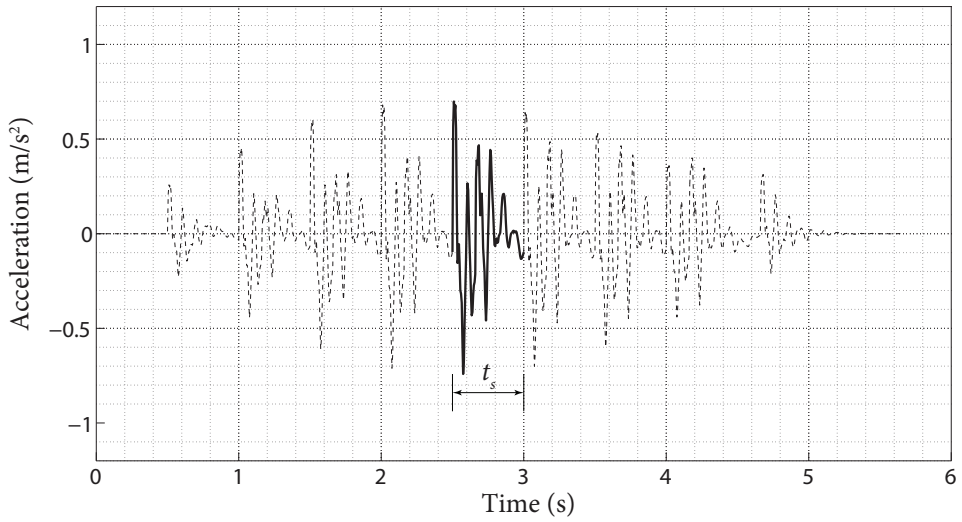

Figure 6.6 Selection of the time window t_s for a typical transient response.

$$a_{rms} = \sqrt{\frac{1}{t_s}\int_0^{t_s} a^2(t)dt} \tag{6.6}$$

The faster the walking speeds, the greater the floor responses (Willford and Young, 2006). However, it is not necessary to perform the calculation for the fastest anticipated walking speed. Having the same step frequency for all floors is sufficient; for instance, the step frequency of normal walking, $f_s = 2$ Hz, and the corresponding period, $t_s = 0.5$ s. The setting of the sampling frequency is 200 Hz. The floor impulsive factor, I_F, which is introduced to represent the transient properties of lightweight mid-frequency floors, is defined as the RMS, with a duration of $t_s = 0.5$ s:

$$I_F = \sqrt{\frac{1}{100}\sum_{i=1}^{100} a_i^2} \tag{6.7}$$

where

$$a_i = \frac{2\pi f e^{i\pi\zeta f/200}}{M_1}\left(\sin\left(\frac{i\pi f}{200}\right) + 2\zeta\cos\left(\frac{i\pi f}{200}\right)\right), \qquad i = 1, 2, 3, \ldots, 100 \tag{6.8}$$

6.4.2 Modal mass and damping ratio

As discussed in Section 4.4, the rotational fixity factors are very small. Thus, it can be assumed that all edges are simply supported when calculating the modal mass. From the calculation methods in Feldmann et al. (2009), the modal mass is obtained from

$$M = \frac{M_t}{4} \tag{6.9}$$

where M is the modal mass and M_t is the total mass. If span a is much larger than width b, the modal mass can be determined from

$$M = \frac{M_t}{4}\left(2 - \frac{b}{a}\right) \tag{6.10}$$

For field floors, the portion of live load should be added to the total mass. As recommended in ATC Design Guide 1 by Allen et al. (1999) and AISC/CISC Design Guide 11 by Murray et al. (1997), the live load for residential construction is 0.25 kPa.

Based on test data and other design guides such as from Willford and Young (2006), Feldmann et al. (2009), and Smith et al. (2009), damping values for floor systems can be determined as suggested in Table 6.2 for different construction materials, furnishings and conditions of use.

Table 6.2 Suggested damping ratio for CFS floor systems.

Type	Damping ratio
Structural damping D_1	
wood joists with subfloor	0.03
CFS joists with subfloor	0.01
Damping due to topping and Ceiling D_2	
Topping or covering	0.005
Ceiling	0.005
Concrete topping	0.015
Damping due to furnishings D_3	
a small amount of furnishings	0.01
fully furnished	0.02
Total damping $D = D_1 + D_2 + D_3$	

6.4.3 Proposed impulsive criterion

The RMS acceleration levels tolerated by humans tend to increase for flooring with higher fundamental frequencies (de Andrade and de Andrade, 2000), as can be observed from the limits in ISO 2631-2 (1989). Thus, limiting floor impulsive factors for acceptable floors depends on the fundamental frequency. The relationship between the floor impulsive factors, I_F, and the fundamental frequency, F, can be developed by correlation studies on the subjective evaluations of lightweight mid-frequency floors.

The database built in Section 6.3.1 for static criteria is employed again, but only floors with a fundamental frequency in the range of 9Hz to 24Hz are selected. Then, floor impulsive factors can be calculated for every floor, based on Eq. (6.7). As mentioned in Section 6.3.1, the binary logistic regression analysis in SPSS® statistical analysis software can be employed to obtain the correlation of the subjective evaluations with fundamental frequencies and floor impulsive factors. After merging the marginal floors to acceptable floors in the database, a total of 49 floors, consisting of 31 unacceptable floors and 18 acceptable floors, is used in the analysis. The cut-off point is also equal to 0.5.

From the result of the regression analysis, the criterion for acceptable floors can be obtained as the fundamental frequency, F, and the floor impulsive factors, I_F, satisfying the relationship:

$$\frac{F}{I_F^{0.24}} > 22.5 \tag{6.11}$$

Table 6.3 summarises the classification of floor acceptability as predicted by Eq. (6.11) and their comparisons with subjective evaluations. Fig. 6.7 illustrates the subjective evaluations in the database and predictions by the impulsive criterion proposed in Eq. (6.11). It can be observed that 2 of 6 acceptable floors in the database are misclassified, and the accuracy of predictions is 66.7%. For comparison, the vibration performance of the floors is also evaluated by the static criterion proposed in Eq. (6.2), as shown in Fig. 6.8. The details of the predictions by both proposed static criterion and impulsive criterion can be found in Tables D.1, D.2, and D.3 from Appendix D.

Furthermore, the proposed impulsive criterion is also validated using test results for field floors by Parnell (2008) and Davis (2008). Meanwhile, test results of wood floors collected by Hu (2000) are also adopted for validation. The comparison of the subjective

Table 6.3 Classification by logistic regression analysis in SPSS®.

Subjective evaluations	Predicted results		Accuracy
	Unacceptable	Acceptable	
31 unacceptable floors	25	6	80.6%
18 acceptable floors†	10	8	44.4%
Overall accuracy			67.3%

†–12 marginal floors and 6 acceptable floors

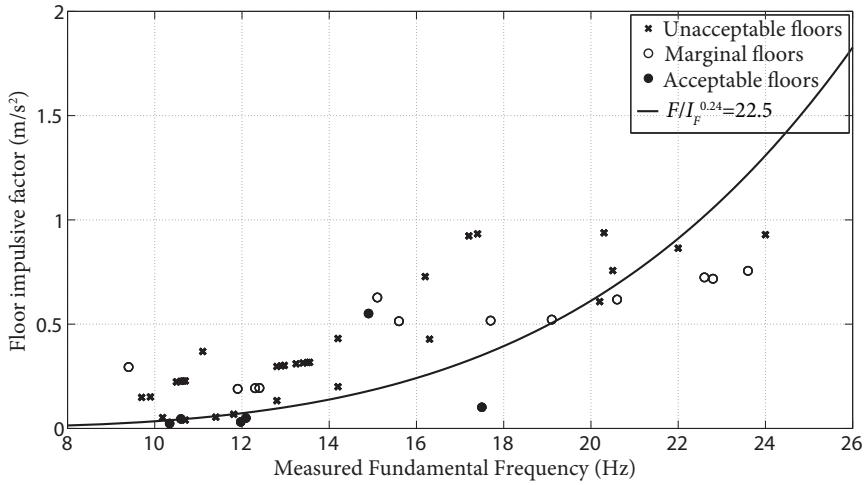

Figure 6.7 Proposed impulsive criterion with the subjective evaluations.

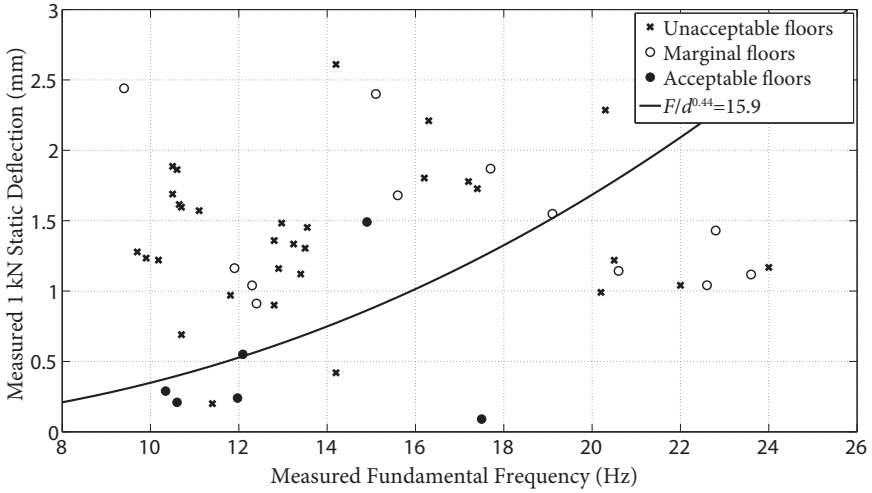

Figure 6.8 Proposed static criterion with the subjective evaluations.

evaluations with predictions using the proposed criteria are tabulated in Tables D.4 and D.5 in Appendix D. As can be observed, the acceptance of floors predicted by the proposed static and impulsive criteria are in excellent agreement with each other, and both criteria match well with the subjective evaluations in tests.

6.5 Resonance criterion for lightweight low-frequency floors

6.5.1 Floor resonance factor

Resonance is the dominant floor vibration in lightweight low-frequency floors, and it occurs when a harmonic component of a periodic force introduced by footsteps corresponds to the natural frequency of the floor. Since all other harmonic vibrations are small in comparison to the harmonic associated with resonance, only one harmonic component of the footstep force is adopted (Murray et al., 1997). If only the first vibration mode is accounted for, a SDOF oscillator under the sinusoidal force corresponding to the resonance can be adopted to characterise the resonant nature of lightweight low-frequency floors. The unit sinusoidal force can be expressed as

$$F(t) = \sin 2\pi f t \tag{6.12}$$

where f is the forcing frequency, which is equal to the fundamental frequency of the floor. To determine dynamic response to the sinusoidal loading of Eq. (6.12) of a SDOF oscillator, the dynamic deflection of the oscillator under a steady-state response is given by (Inman, 2007):

$$x(t) = AF\frac{\sin 2\pi f t}{k} \tag{6.13}$$

where k is the stiffness of the oscillator, and AF is the amplification factor as in

$$AF = \frac{1}{\sqrt{\left[1-\left(\frac{f}{f_o}\right)^2\right]^2 + \left(2\zeta\frac{f}{f_o}\right)^2}} \tag{6.14}$$

where f is the forcing frequency and f_o is the frequency of the oscillator. Under resonance conditions ($f = f_o$), the amplification factor will be

$$AF = \frac{1}{2\zeta} \tag{6.15}$$

Substituting Eq. (6.15) and $(2\pi f)^2 = k/M_1$, where M_1 is the modal mass corresponding to the first vibration mode, into Eq. (6.13) gives

$$x(t) = \frac{1}{2\zeta} \frac{\sin 2\pi f t}{(2\pi f)^2 M_1} \tag{6.16}$$

The acceleration response can be determined by taking the second derivative with respect to time t on Eq. (6.16), yielding

$$a(t) = -\frac{\sin 2\pi f t}{2\zeta M_1} \tag{6.17}$$

The RMS values of the acceleration response can be employed to evaluate the vibration serviceability. Given that the maximum value is approximately 0.7 times the RMS value for the sinusoidal response, it gives

$$a_{rms} = 0.35 \frac{1}{\zeta M_1} \tag{6.18}$$

Thus, a floor resonance factor R_F is proposed for lightweight low-frequency floors as

$$R_F = \frac{1}{\zeta M_1} \tag{6.19}$$

It should be noted that the unit sinusoidal force of Eq. (6.12) is inspired from one harmonic component of footstep forces associated with resonance, which will decrease with increasing frequencies. As a result, the floor resonance factor, R_F, for acceptable lightweight low-frequency floors is related to the fundamental frequencies of floors. This issue will be reflected in the development of the design criterion.

6.5.2 Resonance criterion

In view of the correlative criteria, subjective evaluations of CFS floor systems should be conducted on-site or in a laboratory. However, there are no existing subjective evolutions available for lightweight low-frequency floors built with CFS joists. Fortunately, as discussed in Section 6.2.2, subjective evaluations have been reported recently (Murray and Davis, 2015) for open-web steel-joist and joist-girder supported concrete slab floor systems. The subjective evaluations show excellent agreement with evaluations predicted by applying the method of Murray and Davis (2015), which has minor revisions to the approach proposed by Murray et al. (1997). The floor response due to occupant activity was predicted by simplified methods (Murray et al., 1997) which might not be able to provide accurate responses in some cases. As a consequence, the AISC/CISC criterion was initially developed as a direct criterion, but it eventually becomes a correlative criterion. Since it is known that the design criterion is independent of the construction material, the AISC/CISC criterion can be applied as a tentative criterion for lightweight low-frequency floors. Validation studies should be conducted if the subjective evaluations exist for such floors in the future.

The AISC/CISC criterion is expressed as

$$\frac{P_o exp(-0.35 f_n)}{\beta W} \leqslant \frac{a_o}{g} \tag{6.20}$$

where P_0 is a constant force equal to 0.29 kN for floors, f_n is the fundamental natural frequency of a floor, β is modal damping ratio, and W is the modal mass of its fundamental mode of vibration. The acceleration limit, a_o/g, for office and residential building occupancies is taken as 0.5%. Rearranging Eq. (6.20) gives

$$\frac{1}{\beta W} \leqslant \frac{a_o}{g} \frac{1}{P_o exp(-0.35 f_n)} \tag{6.21}$$

Therefore, resonance criterion–that is, the design criterion for lightweight low-frequency floors, plotted in Fig. 6.9, will be derived as

$$R_F = \frac{1}{\zeta M_1} \leqslant \frac{1}{5800 e^{-0.35 f}} \tag{6.22}$$

where f, ζ and M_1 are the fundamental frequency, the damping ratio and the modal mass of the first vibration mode of the floor.

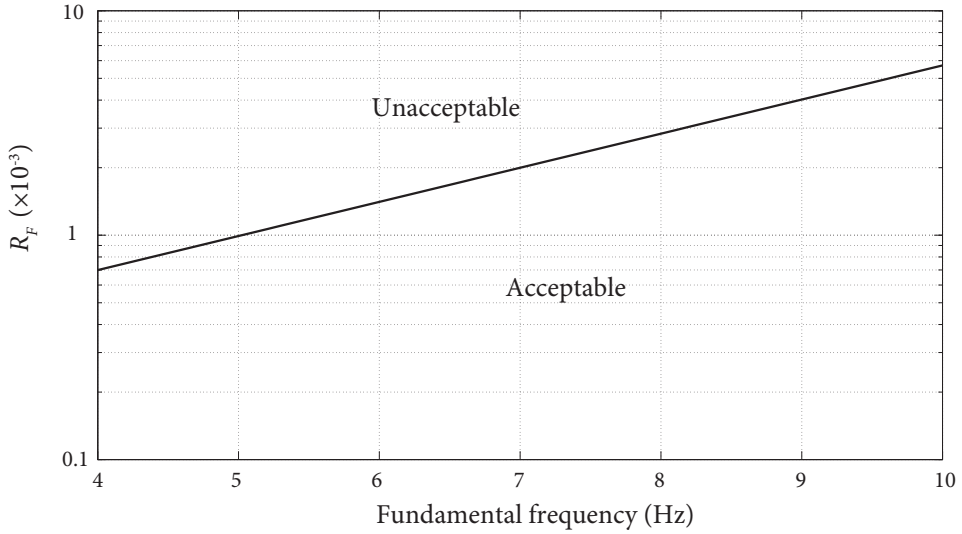

Figure 6.9 Resonance criterion for lightweight low-frequency floors.

6.6 Design procedure

The design procedure is set out step-by-step below:

1) Calculate the fundamental frequency, F;

2) Determine the floor type based on F;

3) Compute floor resonance factors, R_F, for lightweight low-frequency floors or deflection under 1 kN concentrated load, d, for lightweight high- and mid-frequency floors, and check the resonance criterion or static criterion.

4) Evaluate the floor impulsive factors, I_F, for lightweight mid-frequency floors if they satisfy the static criterion.

The flowchart of the design procedure is illustrated in Fig. 6.10.

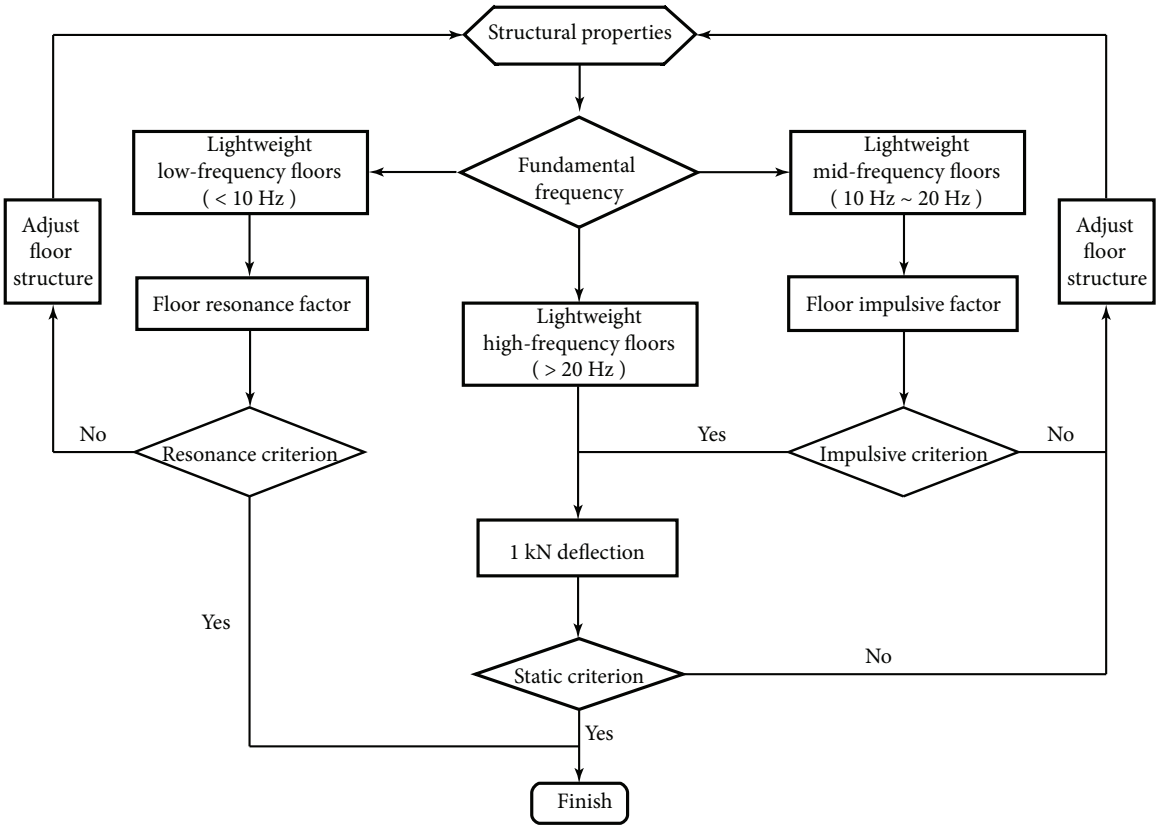

Figure 6.10 Flowchart of the design guideline.

6.7 Examples

The following examples illustrate the application of proposed design procedures to evaluate vibration performance of CFS floor systems.

Example 1: A CFS floor with OSB sheathing

As shown in Fig. 6.11, a residential floor, spanning 4.27 m and 4.5 m wide, is designed for strength criteria with 800S162–43 CFS C-shape joists at 400 mm spacing. The subfloor and ceiling of the floor are 16 mm (5/8 in.) OSB and 13 mm (1/2 in.) gypsum ceiling board, respectively. One row of steel strapping (58×1.44 mm) are located at mid-span with a 600S162–43 CFS channel blocking placed at every five joist-spacing. The joist ends are connected to a CFS rim-track section and are simply supported.

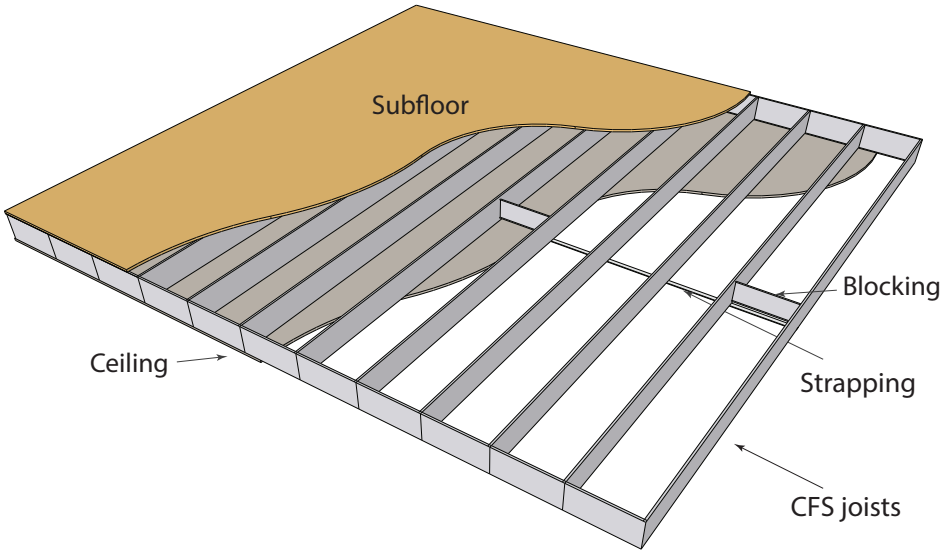

Figure 6.11 A CFS floor with OSB sheathing.

Geometry

Span: $L = 4.27\ m$ Width: $b = 4.5\ m$ Joist spacing: $s = 400\ mm$

Structural properties

Structural properties of joists and blockings are obtained from SSMA (2015), and those of OSB and gypsum board are from Allen et al. (1999).

CFS joists 800S162-43 C-shape

Depth: $d_j = 203\ mm$ Area: $A_j = 346\ mm^2$ Density: $\rho = 2.723\ kg/m$

Mass: $m_j = \rho L = 11.63\ kg$

Flexural stiffness: $EI_j = 3.914 \times 10^5\ Nm^2$

Axial stiffness: $EA_j = 7.024 \times 10^7\ N$

Blocking

Area: $A_b = 288\ mm^2$ Moment of inertia: $9.64 \times 10^5\ mm^4$

Flexural stiffness: $EI_b = 1.957 \times 10^5\ Nm^2$

Mass: $m_b = 2.26\ kg/m \times s \times 3$=2.712 kg

OSB panel

Depth: $d_o = 16\ mm$ Mass $m_o = 199.84\ kg$

Flexural stiffness (parallel to joists): $EI_{oj} = 361.6\ Nm^2$

Flexural stiffness per unit width (transverse to joists): $EI_{ot} = 3051\ Nm$

Axial stiffness (parallel to joists): $EA_{oj} = 2.468 \times 10^7\ N$

Ceiling

Mass: $m_c = 162.37\ kg$

Effective flexural stiffness

Slip modulus: $k = 4.14 \times 10^6\ N/m^2$ (Allen et al., 1999)
Modified axial stiffness of the OSB (Eq. (4-3b) of Allen et al. (1999)):

$$EA'_{oj} = \frac{EA_{oj}}{1 + 10\frac{EA_{oj}}{kL^2}} = 5.78 \times 10^6\ N$$

Effective flexural stiffness:

$$h = \frac{d_j + d_o}{2} = 109.6 \ mm$$

From Eq. (4-3a) of Allen et al. (1999), it can be obtained that

$$EI_{eff} = EI_j + EI_{oj} + \frac{EA'_{oj} \cdot EA_j}{E\bar{A}_{oj} + EA_j} h^2 = 4.559 \times 10^5 \ Nm^2$$

From Section 4.5.1, the equivalent rigidities and fundamental frequency can be determined as follows:

Equivalent rigidities

$$D_x = \frac{EI_{eff}}{s} = 1.14 \times 10^6 \ Nm$$

$$D_y = \frac{1}{L}\left(EI_{ot} + 2\frac{3}{11}EI_b\right) = 2.57 \times 10^4 \ Nm$$

where 3/11 is used for discrete blockings because only three blockings are installed in the eleven joist spacings.

$$H = 0$$

Fundamental frequency

Mass

$$m = m_o + m_c + m_j(N_j - 1) + m_b = 492.8 \ kg$$

Fundamental frequency

$$F = \frac{\pi}{2}\sqrt{\frac{Lb}{m}}\sqrt{\frac{D_x}{L^4} + 2\frac{H}{L^2 b^2} + \frac{D_y}{L^4}} = 18.33 \ Hz$$

Since

$$10 \ Hz < F < 20 \ Hz$$

the floor is a lightweight mid-frequency floor. The static criterion and impulsive criterion should be checked for vibration serviceability. For the reason of demonstration, only the

impulsive criterion is checked here. The evaluation of floor deflection subjected to 1 kN concentrated load at the center of the floor can be referred to ATC Design Guide 1 by Allen et al. (1999).

Checking the impulsive criterion

Modal mass: $M_1 = m/4 = 123.2\ kg$ Damping ratio: $\zeta = 0.015$
Floor impulsive factor (Eq. (6.7))

$$I_F = \sqrt{\frac{1}{100}\sum_{i=1}^{100} a_i^2} = 0.4565\ m/s^2$$

Check the impulsive criterion (Eq. (6.11))

$$\frac{F}{I_F^{0.24}} - 22.5 = -0.3783 < 0$$

The floor is unacceptable for vibration serviceability.

Ledger or balloon framing

If the floor is ledger or balloon framing, the restraint coefficient $c_1 = 1.13$, $c_2 = 1$ and $c_4 = 1$ for the transverse elements located at the mid-span. Then, the fundamental frequency will be

$$F = \frac{\pi}{2}\sqrt{\frac{Lb}{m}}\sqrt{\frac{c_1 D_x}{L^4} + 2\frac{c_2 H}{L^2 b^2} + \frac{D_y}{L^4}} = 19.46\ Hz$$

Floor impulsive factor

$$I_F = \sqrt{\frac{1}{100}\sum_{i=1}^{100} a_i^2} = 0.4783\ m/s^2$$

Check the impulsive criterion

$$\frac{F}{I_F^{0.24}} - 22.5 = 0.7298 > 0$$

After considering the rotational restraints of ledger or balloon framing, the floor is acceptable for vibration serviceability.

Example 2: A CFS floor with steel deck and lightweight concrete topping

A CFS floor system (Fig. 6.12) is constructed using nine 1200S2000–68 CFS C-shape joists at 610 mm (24 in.) spacing, and the span length is 5.95 m. The subfloor is 22 gauge (0.76 mm) metal form deck (UFS) with lightweight concrete topping: USG LevelRock® 3500 floor underlayment. The ceiling is 15.9 mm (5/8 in.) type C gypsum board. Two rows of 1200S200–54 CFS channel blockings are placed at every four joist-spacing at the 3/4 and 1/4 of the span. The joist ends are connected to a CFS rim-track section and are simply supported.

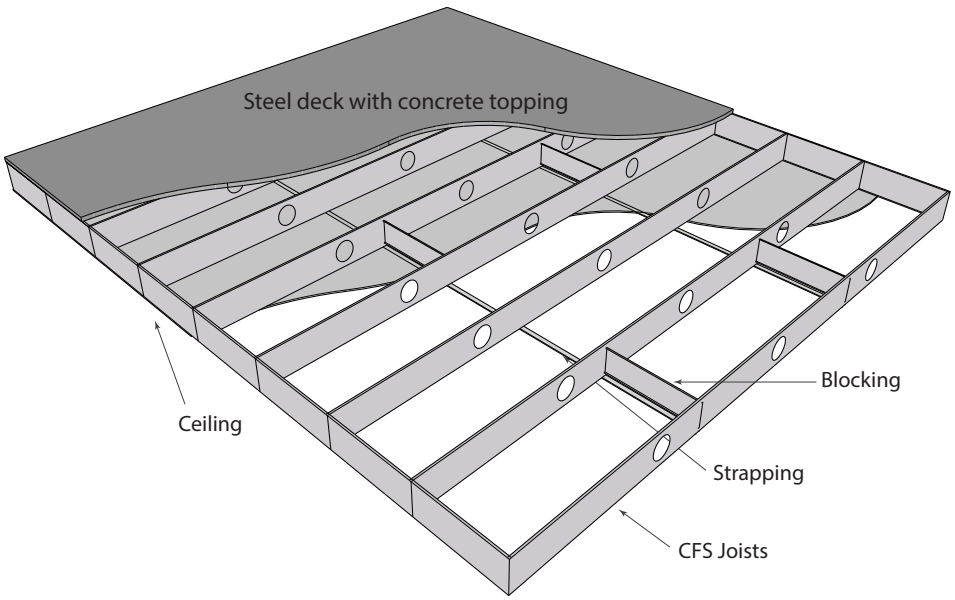

Figure 6.12 A CFS floor with steel deck and concrete topping.

Geometry

Span: $L = 5.95\ m$ Width: $b = 4.88\ m$ Joist spacing: $s = 610\ mm$

Structural properties

Structural properties of joists and blockings are obtained from SSMA (2015), and those of OSB and gypsum board are from Allen et al. (1999). Properties of steel deck and

concrete topping LevelRock® can be referred to the manufacturer.

CFS joists

Depth: $d_j = 305\ mm$ Area: $A_j = 769\ mm^2$ Density: $\rho = 6.041\ kg/m$

Mass: $m_j = \rho L = 39.87\ kg$

Flexural stiffness: $EI_j = 1.854 \times 10^6\ Nm^2$

Axial stiffness: $EA_j = 1.561 \times 10^8\ N$

Blocking

Area: $A_b = 615\ mm^2$ Moment of inertia: $7.35 \times 10^{-6}\ m^4$

Flexural stiffness: $EI_b = 1.376 \times 10^6\ Nm^2$

Mass: $m_b = 4.82\ kg/m \times s \times 6$=17.6 kg

Steel deck

22 gauge UFS form deck Thickness: $t_d = 0.7\ mm$ Mass: $m_d = 212.63\ kg$

LevelRock®

Thickness (parallel to joists): $t_{lj} = 23.8\ mm$ Mass $m_d = 1727.58\ kg$

Thickness (transverse to joists): $t_{lt} = 31\ mm$

Young's modulus (ACI Committee 318, 2008): $E_c = 16.6\ Gpa$

Flexural stiffness (parallel to joists): $EI_{cj} = 11393.88\ Nm^2$

Based on ANSI/SDI C-2011 (2012), flexural stiffness per unit width (transverse to joists): $EI_{ct} = 84001\ Nm$

Axial stiffness (parallel to joists): $EA_{cj} = 24.11 \times 10^7\ N$

Ceiling

Mass: $m_c = 311.84\ kg$

Effective flexural stiffness

Slip modulus is assumed as $k = 100 \times 10^6\ N/m^2$ from test results of Erdélyi and Dunai (2009).

Modified axial stiffness of the subfloor:

$$EA'_{oj} = \frac{EA_{cj}}{1 + 10\frac{EA_{cj}}{kL^2}} = 143.43 \times 10^6 \ \ N$$

Effective flexural stiffness:

$$h = \frac{d_j + t_{lj}}{2} + 0.5 \times 0.0254 = 0.1778 \ \ m$$

$$EI_{eff} = EI_j + EI_{cj} + \frac{EA'_{cj} \cdot EA_j}{E\bar{A}_{cj} + EA_j} h^2 = 4.208 \times 10^6 \ \ Nm^2$$

From Section 4.5.1, the equivalent rigidities and fundamental frequency can be determined as follows:

Equivalent rigidities

$$D_x = \frac{EI_{eff}}{s} = 6.899 \times 10^6 \ \ Nm$$

From Eq. (4.50),

$$D_y = \frac{1}{L}\left(EI_{ot} + 2 \times 2 \times 0.5 \times \frac{3}{8} EI_b\right) = 1.88 \times 10^5 \ \ Nm$$

where 3/8 is used for discrete blockings because only three blockings are installed in the eight joist spacings. Two rows of blockings are installed at the 1/4 and 3/4 of the span. For each location, the restraint coefficient $c_4 = 0.5$.

$$H = 0$$

Fundamental frequency

Mass

$$m = m_d + m_l + m_c + m_j(N_j - 1) + m_b = 2557.26 \ \ kg$$

Fundamental frequency

$$F = \frac{\pi}{2}\sqrt{\frac{Lb}{m}}\sqrt{\frac{D_x}{L^4} + 2\frac{H}{L^2b^2} + \frac{D_y}{L^4}} = 12.78\ Hz$$

Since

$$10\ Hz < F < 20\ Hz$$

the floor is a lightweight mid-frequency floor. The static criterion and impulsive criterion should be checked for vibration serviceability. For the reason of demonstration, only the impulsive criterion is checked here. The evaluation of floor deflection subjected to 1 kN concentrated load at the center of the floor can be referred to ATC Design Guide 1 by Allen et al. (1999).

Checking the impulsive criterion

Modal mass: $M_1 = m/4 = 639.32\ kg$ Damping ratio: $\zeta = 0.03$
Floor impulsive factor in Eq. (6.19)

$$I_F = \sqrt{\frac{1}{100}\sum_{i=1}^{100} a_i^2} = 0.0679\ m/s^2$$

Check the impulsive criterion of Eq. (6.22)

$$\frac{F}{I_F^{0.24}} - 22.5 = 1.88 > 0$$

The floor is acceptable for vibration serviceability.

Ledger or balloon framing

If the floor is ledger or balloon framing, the restraint coefficient $c_1 = 1.13$, $c_2 = 1$ and $c_4 = 0.5$ for the transverse elements located at the 1/4 and 3/4 span. Then, the fundamental frequency will be

$$F = \frac{\pi}{2}\sqrt{\frac{Lb}{m}}\sqrt{\frac{c_1 D_x}{L^4} + 2\frac{c_2 H}{L^2b^2} + \frac{D_y}{L^4}} = 13.54\ Hz$$

Floor impulsive factor in Eq. (6.19)

$$I_F = \sqrt{\frac{1}{100}\sum_{i=1}^{100} a_i^2} = 0.0714 \ m/s^2$$

Check the impulsive criterion of Eq. (6.22)

$$\frac{F}{I_F^{0.24}} - 22.5 = 3.0227 > 0$$

The floor is acceptable for vibration serviceability.

Example 3: A long-span CFS floor

Fig. 6.13 illustrates a long-span CFS floor system with span of 7.2 m. Floor configurations are the same as the floor in Example 2 except that one strongback of 362S125-54 is installed at the mid-span.

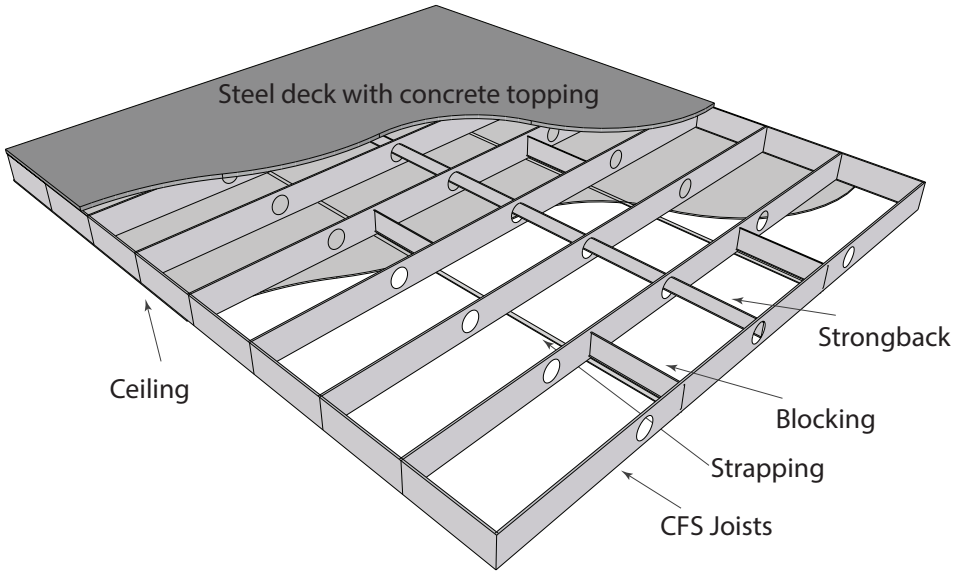

Figure 6.13 A long-span CFS floor with steel deck and concrete topping.

Structural properties

Structural properties are the same in Example 2.

Strongback

Area: $A_s = 222\ mm^2$

Flexural stiffness: $EI_s = 5.58 \times 10^5\ Nm^2$

Mass: $m_s = 1.74\ kg/m \times b$=8.5 kg

From Section 4.5.1, the equivalent rigidities and fundamental frequency can be determined as follows:

Equivalent rigidities

$$D_x = \frac{EI_{eff}}{s} = 7.17 \times 10^6 \ Nm$$

From Eq. (4.50),

$$D_y = \frac{1}{L}\left(EI_{ot} + 2 \times 2 \times 0.5 \times \frac{3}{8}EI_b + 2 \times EI_s\right) = 1.81 \times 10^5 \ Nm$$

$$H = 0$$

Fundamental frequency

Mass

$$m = m_d + m_l + m_c + m_j(N_j - 1) + m_b + m_s = 3099.3 \ kg$$

Fundamental frequency

$$F = \frac{\pi}{2}\sqrt{\frac{Lb}{m}}\sqrt{\frac{D_x}{L^4} + 2\frac{H}{L^2b^2} + \frac{D_y}{L^4}} = 9.14 \ Hz$$

Since

$$F < 10 \ Hz$$

the floor is a lightweight low-frequency floor. The resonance criterion should be checked for vibration serviceability.

Checking the resonance criterion

Modal mass: $M_1 = m/4 = 774.8 \ kg$ Damping ratio: $\zeta = 0.03$
Floor resonance factor (Eq. (6.19)) (Eq. (6.22))

$$R_F = \frac{1}{\zeta M_1} = 0.043 \ m/s^2$$

Check the impulsive criterion (Eq. (6.22))

$$R_F - \frac{1}{5800e^{-0.35F}} = 0.0379 > 0$$

The floor is unacceptable for vibration serviceability.

6.8 Summary

In this chapter, existing design criteria for the evaluation of the performance of floor vibration are classified into two categories: direct and correlative. The correlative criteria are developed for CFS floor systems in residential construction. Based on the fundamental frequency of the floor, CFS floors are divided into three types: lightweight high-, mid- and low-frequency floors. A static criterion is proposed for lightweight high- and mid-frequency floors, and the existing static criteria are also validated with the test results. From the validation studies, the Onysko criterion provides the best predictions, followed by the proposed static criterion of Eq. (6.2). Thus, both are recommended as design criteria for the vibration serviceability of lightweight mid- and high-frequency CFS floor systems. Static criteria are not sufficient for lightweight mid-frequency floors (between 10 Hz and 20 Hz), and an impulsive criterion is needed. By introducing the floor impulse and resonance factors, impulse criterion and resonance criterion are respectively developed for the evaluation vibration performance of mid- and low-frequency floors. Lastly, a design procedure is proposed together the presentation of three examples to illustrate the proposed procedure.

7

Conclusions and Recommendations

7.1 Conclusions

This research has produced numerous results and findings related to rotational restraints along floor edges and human-structure interaction. These findings have been used to evaluate the vibration performance of lightweight steel floors affected by human walking, and led to recommendations on performance criteria and corresponding methods for vibration serviceability in residential construction. The key conclusions are as follows.

7.1.1 Method of finite integral transform

The finite integral transforms are remarkable methods, which simply convert differential equations to algebraic equations. The resulting equations can be solved without much difficulty, and solutions for the original differential equations can be obtained using the inverse integral transform. This procedure is straightforward in concept and systematic in formulation.

The method of finite integral transform has been applied to flexural and vibration analysis of a rectangular orthotropic plate with rotationally restrained edges. A new rotational fixity factor has been introduced to define rotational restraints to reflect the relative stiffness of the plate and the restraints. Thus, the present approach for plates with rotationally restrained edges can be applied for plates with general boundary conditions– from simply supported to fully clamped–by using the corresponding rotational fixity

factors. The present method is validated through numerical examples by comparing the results with available exact solutions and approximate solutions. It can be concluded that

- The proposed rotational fixity factor is simple and convenient for design practice as it results in an approximately linear relationship between the factor and the moment or deflection.
- The method of finite integral transform is simple and straightforward, can be calculated with the desired accuracy, and has general applicability. However, this unified and systematic method only provides approximate values for vibration analysis of plates due to the issue of slow convergence.
- Two different formulations exist for the method when applying it to flexural and vibration analysis of plates. The right one must be carefully chosen for free vibration analysis of plates with rotational restrained edges; otherwise, the numerical results may not be available.

7.1.2 Equivalent orthotropic plates for CFS floor systems

An analytical approach based on the Rayleigh method has been presented for calculating the fundamental frequency of a CFS floor system while considering the effect of the rotational restraints along two opposite edges. The beam characteristic function has been obtained using the method of finite integral transform and used as the admission function. The equivalent rigidities and mass of equivalent orthotropic plates for CFS floor systems were developed. The effects of transverse elements such as blocking, strapping and stongbacks are discussed. Some conclusions can be drawn from the study:

- The rotational fixity factor needs to be considered when calculating the fundamental frequency, and the recommended values can be adopted as 0.1 for ledger-framed or balloon-framed CFS floor systems and 0 for platform framing.
- The proposed method makes more-accurate evaluations of the transverse flexural stiffness that significantly influences the floor's structural properties.
- A design equation has been developed for calculating the fundamental frequency of CFS floors.

7.1.3 Damped plate-oscillator models

A damped plate-oscillator model has been proposed to investigate the dynamic behaviors of lightweight steel floor systems with occupants and predict the dynamic responses of floors affected by human walking. The influence of stationary occupants on dynamic properties of lightweight floors has been studied. The results predicted by the proposed damped plate-oscillator model were compared with results of the laboratory tests on CFS floor systems with and without occupants. Three models used for predicting dynamic response induced by human walking–MF, MDO and MSDO–were proposed and examined against the test results. Finally, parametric studies have been conducted on the effects of step frequencies, damping ratios, mass ratios and walking paths. The analyses show that

- The influence of the human occupants on floor vibration are dependent on the humans' location on the floor. The dynamic properties of a vibration mode will not be affected by the presence of occupants who are located at the nodal points of the mode.
- It may not be necessary to adopt 2-DOF human models to evaluate dynamic properties of floor-occupant system as a SDOF model appears to be sufficient for design practice.
- The Falati SDOF model (Falati, 1999) may not be appropriate for simulating occupants on lightweight steel floor systems. Human occupants standing close together should be modelled as one SDOF model instead as individuals.
- Human occupants will introduce additional vibration modes, but the frequencies of combined floor-occupant systems are not always nested among the natural frequencies of unoccupied floors, especially for cases with small mass ratios (i.e., $\gamma < 0.1$) and high human damping ratios ($\zeta_h \geqslant 50\%$ in this study).
- A 2-DOF human-structure model may be sufficient for qualitative analysis of human-structure interaction, but it is not recommended for evaluating the dynamic properties and responses of floor-occupant systems because the model considers only one structural mode. The damped plate-oscillator model provides more- accurate results.
- The Brownjohn SDOF human model can be adopted for lightweight steel floor systems but the modal mass m_h may be less than the human total mass m_t.
- Given that the significant influence of human occupants, the model of moving and

stationary damped-oscillators is appropriate for predicting floor responses induced by human walking.

- Damping ratios of lightweight steel floors are significantly increased by human occupants, and the uncertainties and inconsistencies between the laboratory and field studies will be reduced.

7.1.4 Design criteria and methods in residential construction

Design criteria were classified as either direct or correlative, with the correlative criteria being developed for lightweight steel floor systems in residential constructions. For simplicity, lightweight floors are divided into three types: lightweight high-, mid-, and low-frequency. Existing static criteria were validated for lightweight steel floors. A static criterion has been developed by logistic regression. Impulse and resonance criteria were proposed by introducing the floor impulse factor and resonance factor, respectively. Lastly, a design procedure was presented along with three demonstrated examples. It can be concluded that

- Static criteria are not sufficient for lightweight mid-frequency floors (between 10 Hz and 20 Hz), and an impulsive criterion is needed.
- From the validation studies, the Onysko criterion provides the best predictions, followed by the proposed static criterion of Eq. (6.2). Thus, both are recommended as design criteria for the vibration serviceability of lightweight mid- and high-frequency CFS floor systems.
- The proposed impulsive criterion and resonance criterion are both tentative, and so future investigations and validations may be needed.

7.2 Recommendations for future research

Recommendations for future work include:

- Partial composite action and load sharing action of CFS floor systems should be investigated for calculating the maximum deflection under 1 kN concentrated load. The slip modulus between subfloor and CFS joists need to be determined. The exact

series solutions obtained by the finite integral transform method can be adopted to develop the load sharing action.

- The equivalent rigidities of CFS floors in Chapter 4 are used for vibration analysis. The structural properties of equivalent orthotropic plates of CFS floors under static load should be determined.
- Retrofit techniques to improve the vibration performance of lightweight steel floors should be investigated using the analytical tools developed in this research.

Bibliography

ACI Committee 318, 2008. ACI 318-08: Building Code Requirements for Structural Concrete and Commentary. American Concrete Insitute.

AISI S100, 2012. North American Specification for the Design of Cold-Formed Steel Structural Members. American Iron and Steel Institute, Washington, D. C.

Allen, D. E., Murray, T. M., 1993. Design criterion for vibrations due to walking. Engineering Journal-American Institute of Steel Construction 30 (4), 117–129.

Allen, D. E., Onysko, D. M., Murray, T. M., 1999. Minimizing floor vibration. ATC Design Guide 1. Applied Technology Council, Redwood City, California.

Allen, D. E., Rainer, J. H., 1976. Vibration criteria for long-span floors. Canadian Journal of Civil Engineering 3 (2), 165–173.

Allen, D. E., Rainer, J. H., 1989. Discussion: Design of lightweight wooden floors to avoid human discomfort. Canadian Journal of Civil Engineering 16 (2), 202–202.

Amba-Rao, C. L., 1964. On the vibration of a rectangular plate carrying a concentrated mass. Journal of applied Mechanics 31 (3), 550–551.

An, C., Gu, J., Su, J., 2016. Exact solution of bending problem of clamped orthotropic rectangular thin plates. Journal of the Brazilian Society of Mechanical Sciences and Engineering 38 (2), 601–607.

Anderson, G., 1969. On the determination of finite integral transforms for forced vibrations of circular plates. Journal of Sound and Vibration 9 (1), 126–144.

ANSI/SDI C-2011, 2012. Standard for Composite Steel Floor Deck–Slabs. American National Standards Institute/Steel Deck Institute.

AS 3623, 1993. Domestic metal framing. Standards Association of Australia, Homebush, NSW, Australia.

Ayhan, D., Schafer, B. W., 2016a. The effect of m/v ratio on ledger-framing performance of cold-formed steel buildings. In: Proceedings of the International Colloquium on Stability and Ductility of Steel Structures. Timisoara, Romania.

Ayhan, D., Schafer, B. W., 2016b. Stiffness, stability, and strength of floor-to-wall connections in ledger-framed cold-framed steel construction. In: Proceedings of the Annual Stability Conference, Structural Stability Research Council. Orlando, Florida.

Ayhan, D., Schafer, B. W., 2017. Floor-to-wall connection behavior in ledger-framed cold-framed steel construction. In: Proceedings of the World Conference on Earthquake Engineering, 16WCEE 2017. Santiago, Chile.

Bachmann, H., Ammann, W., 1987. Vibrations in structures: induced by man and machines. Vol. 3. IABSE.

Balachandran, B., Magrab, E. B., 2009. Vibrations, 2nd Edition. Cengage Learning.

Bapat, A. V., Venkatramani, N., Suryanarayan, S., 1988. Simulation of classical edge conditions by finite elastic restraints in the vibration analysis of plates. Journal of Sound and Vibration 120 (1), 127–140.

Bauchau, O. A., Craig, J. I., 2009. Structural analysis: with applications to aerospace structures. Vol. 163. Springer Science & Business Media.

Bernard, E. S., 2008. Dynamic serviceability in lightweight engineered timber floors. Journal of structural engineering 134 (2), 258–268.

Bhaskar, K., Kaushik, B., 2004. Simple and exact series solutions for flexure of orthotropic rectangular plates with any combination of clamped and simply supported edges. Composite structures 63 (1), 63–68.

Bhaskar, K., Sivaram, A., 2008. Untruncated infinite series superposition method for accurate flexural analysis of isotropic/orthotropic rectangular plates with arbitrary edge conditions. Composite Structures 83 (1), 83–92.

Bromwich, T. J. I., 1965. An introduction to the theory of infinite series, 2nd Edition. Macmillan and Company, limited.

Brown, H. K., 1943. The resolution of boundary value problems by means of the finite fourier transformation: general vibration of a string. Journal of Applied Physics 14 (11), 609–618.

Brownjohn, J. M. W., 1999. Energy dissipation in one-way slabs with human participation. In: Proceedings of the Asia-Pacific Vibration Conference, Nanyang Technological University, Singapore, 11-13 December. Vol. 1. pp. 155–160.

Brownjohn, J. M. W., Middleton, C. J., 2008. Procedures for vibration serviceability assessment of high-frequency floors. Engineering Structures 30 (6), 1548–1559.

Burstrand, H., Talja, A., 2001. Design guide for light weight steel floors due to human induced vibrations. Swedish Institute of Steel Construction and VTT Building Technology, Steel and Composite Structures, Stockholm/Espoo/Lulea.

Caprani, C. C., Ahmadi, E., 2016. Formulation of human–structure interaction system models for vertical vibration. Journal of Sound and Vibration 377, 346–367.

Carmichael, T., 1959. The vibration of a rectangular plate with edges elastically restrained against rotation. The Quarterly Journal of Mechanics and Applied Mathematics 12 (1), 29–42.

Chui, Y. H., 1987. Vibrational performance of wooden floors in domestic dwellings. Ph.D. dissertation, Brighton Polytechnic.

Chui, Y. H., 2002. Application of ribbed-plate theory to predict vibrational serviceability of timber floor systems. In: The Proceedings of 7 th World Conference on Timber Engineering WCTE. Vol. 4. pp. 87–93.

Churchill, R. V., 1972. Operational mathematics, 3rd Edition. McGraw-Hill, Inc.

Clough, R. W., Penzien, J., 2003. Dynamics of structures, 3rd Edition. Computers & Structures, Inc.

Cobble, M., Fang, P., 1967. Finite transform solution of the damped cantilever beam equation having distributed load, elastic support, and the wall edge elastically restrained against rotation. Journal of Sound and Vibration 6 (2), 187–198.

Coermann, R. R., 1962. The mechanical impedance of the human body in sitting and standing position at low frequencies. Human Factors: The Journal of the Human Factors and Ergonomics Society 4 (5), 227–253.

Cunnigham, R., 1990. Some aspects of semi-rigid connections in structural steelwork. The Structural Engineer 68 (5), 85–92.

CWC, DMO Associates, Quaile Engineering Ltd., Forintek Canada Corp, 1997. Design guide for light weight steel floors due to human induced vibrations. Concluding report, Canadian Construction Materials Centre and Consortium of Manufacturers of Engineered Wood Products Used In Repetitive Member Situations, Ottawa, Canada.

Davis, B. W., 2008. Influence of construction details on vibration characteristics of cold-formed steel floor systems. Master's thesis, University of Waterloo, Waterloo, ON, Canada.

de Andrade, C. F., de Andrade, J. C., 2000. Disscussion: Preventing annoying wood floor vibrations. Journal of Structural Engineering 126 (3), 425–426.

De Silva, C. W., 2007. Vibration: fundamentals and practice, 2nd Edition. CRC press.

Debnath, L., Bhatta, D., 2014. Integral transforms and their applications. CRC press.

Dolan, J. D., Murray, T. M., Johnson, J. R., Runte, D., Shue, B. C., 1999. Preventing annoying wood floor vibrations. Journal of structural engineering 125 (1), 19–24.

Du, J., Li, W. L., Jin, G., Yang, T., Liu, Z., 2007. An analytical method for the in-plane vibration analysis of rectangular plates with elastically restrained edges. Journal of Sound and Vibration 306 (3), 908–927.

Ebrahimpour, A., Sack, R. L., 2005. A review of vibration serviceability criteria for floor structures. Computers & Structures 83 (28), 2488–2494.

Ellis, B. R., 2001. Serviceability evaluation of floor vibration induced by walking loads. Structural Engineer 79 (21), 30–36.

Ellis, B. R., Ji, T., 1997. Human–structure interaction in vertical vibrations. Proceedings of the Institution of Civil Engineers - Structures and Buildings 122 (1), 1–9.

Erdélyi, S., Dunai, L., 2009. Light-gauge composite floor beam with self-drilling screw shear connector: experimental study. Steel and Composite Structures 9 (3), 255–274.

Falati, S., 1999. The contribution of non-structrual components to the overall dynamic behaviour of concrete floor slabs. Ph.D. dissertation, University of Oxford.

Farah, A., 1977. Human response: A criterion for the assessment of structural serviceability. Ph.D. dissertation, University of Waterloo, Ontario, Canada.

Feldmann, M., Heinemeyer, C., Butz, C., Caetano, E., et al., 2009. Design of floor structures for human induced vibrations. JRC–ECCS joint report.

Folz, B., Foschi, R. O., 1991. Coupled vibrational response of floor systems with occupants. Journal of engineering mechanics 117 (4), 872–892.

Foschi, R. O., Gupta, A., 1987. Reliability of floors under impact vibration. Canadian Journal of Civil Engineering 14 (5), 683–689.

Foschi, R. O., Neumann, G. A., Yao, F., Folz, B., 1995. Floor vibration due to occupants and reliability-based design guidelines. Canadian Journal of Civil Engineering 22 (3), 471–479.

Gorman, D. J., 1999. Vibration analysis of plates by the superposition method. Vol. 3. World Scientific.

Gorman, D. J., Yu, S. D., 2012. A review of the superposition method for computing free vibration eigenvalues of elastic structures. Computers & Structures 104, 27–37.

Green, A. E., 11 1944. Double fourier series and boundary value problems. Mathematical Proceedings of the Cambridge Philosophical Society 40 (3), 222–228.

Greif, R., Mittendorf, S., 1976. Structural vibrations and Fourier series. Journal of Sound and Vibration 48 (1), 113–122.

Griffin, M. J., 1990. Handbook of human vibration. Academic press.

Griffin, M. J., 2007. Predicting the feeling of vibration in buildings. Proceedings of the Institute of Acoustics 29 (2), 15pp.

Hagberg, K. G., Tommy, P., Matilda, H., 2009. Design of light weight constructions-risks and opportunities. In: 38th International Congress and Exposition on Noise Control Engineering 2009 (INTER-NOISE 2009). Ottawa, Canada.

Hearmon, R. F. S., 1959. The frequency of flexural vibration of rectangular orthotropic plates with clamped or supported edges. Journal of applied Mechanics 26 (3-4), 537–540.

Hernández, S. A. M., Chui, Y. H., 2014. Effect of end support conditions on the vibrational performance of cross-laminated timber floors. In: World Conference on Timber Engineering. Quebec City, Canada.

Hu, L. J., 1998. Effects of solutions for sound isolation and fire resistance on serviceability performance of engineered wood floors. In: The Proceedings of 5 th World Conference on Timber Engineering, WCTE. Vol. 2. pp. 446–453.

Hu, L. J., 2000. Serviceability design criteria for commericial and multi-family floors. Project No. 1092, Canadian Forest Serice No. 04, Forintek Canada Corp.

Hu, L. J., 2002. Development of a performance criterion for controlling vibration in wood-based floors. In: Proceedings of the 7th World Conference on Timber Engineering. Vol. 5. Shah Alam, Malaysia.

Hu, L. J., Chui, Y. H., 2004. Development of a design method to control vibrations induced by normal walking action in wood-based floors. In: Proceedings of the 8th World Conference on Timber Engineering. Vol. 2. Lahti, Finland, pp. 217–222.

Hu, L. J., Chui, Y. H., Onysko, D. M., 2001. Vibration serviceability of timber floors in residential construction. Progress in Structural Engineering and Materials 3 (3), 228–237.

Hu, L. J., Desjardins, R., Chui, Y. H., 2006. Nature of vibrations induced by footsteps in lightweight and heavyweight floors. In: 9th World Conference of Timber Engineering. Portland, USA.

Huffington, Jr., N., 1956. Theoretical determination of rigidity properties of orthogonally stiffened plates. Journal of Applied Mechanics 23 (1), 15–20.

Humar, J., 2002. Dynamics of structures, 2nd Edition. CRC Press.

Hurlebaus, S., Gaul, L., Wang, J. T.-S., 2001. An exact series solution for calculating the eigenfrequencies of orthotropic plates with completely free boundary. Journal of Sound and Vibration 244 (5), 747–759.

Hutchinson, J. R., 1992. On the bending of rectangular plates with two opposite edges simply supported. Journal of applied mechanics 59 (3), 679–681.

Inman, D. J., 2006. Vibration with control. John Wiley & Sons, Ltd.

Inman, D. J., 2007. Engineering Vibration, 3rd Edition. Pearson Education, inc.

ISO 10137, 2007. Bases for design of structures–Serviceability of buildings and walkways against vibrations. International Organization for Standardization, Geneva, Switzerland.

ISO 2631-2, 1989. Mechanical vibration and shock: Evaluation of human exposure to whole-body vibration-Part 2: Vibration in buildings (1 Hz to 80 Hz). International Organization for Standardization, Geneva, Switzerland.

ISO 2631-2, 2003. Mechanical vibration and shock: Evaluation of human exposure to whole-body vibration-Part 2: Vibration in buildings (1 Hz to 80 Hz), 2nd Edition. International Organization for Standardization, Geneva, Switzerland.

ISO 5982, 1981. Vibration and shock – Mechanical driving point impedance of the human body, 1st Edition. International Organization for Standardization, Geneva, Switzerland.

Iyengar, K. T. S. R., Iyengar, R. N., 1967. Determination of the orthotropic plate parameters of stiffened plates and grillages in free vibration. Applied Scientific Research 17 (6), 422–438.

Jaramillo, T. J., 1950. Deflections and moments due to a concentrated load on a cantilever plate of infinite length. Journal of Applied Mechanics-Transactions of the ASME 17 (1), 67–72.

Ji, T., 2003. Understanding the interactions between people and structures. Structural Engineer 81 (14), 12–13.

Ji, T., Ellis, B., 1995. A continuous model for the vertical vibration of the human body in a standing position. In: UK Informal Group Meeting on Human Response to Vibration. Silsoe, UK, pp. 1–12.

Johnson, J. R., 1994. Vibration acceptability in wood floor systems. Master's thesis, Virginia Polytechnic Institute and State University, Blacksburg, VA, USA.

Kelly, S. G., 2012. Mechanical vibrations: theory and applications. Cengage Learning.

Khalili, M. R., Malekzadeh, K., Mittal, R., 2005. A new approach to static and dynamic analysis of composite plates with different boundary conditions. Composite Structures 69 (2), 149–155.

Khov, H., Li, W. L., Gibson, R. F., 2009. An accurate solution method for the static and dynamic deflections of orthotropic plates with general boundary conditions. Composite Structures 90 (4), 474–481.

Kim, H. K., Kim, M. S., 2001. Vibration of beams with generally restrained boundary conditions using fourier series. Journal of Sound and Vibration 245 (5), 771–784.

Kirk, C. L., 1970. Natural frequencies of stiffened rectangular plates. Journal of Sound and Vibration 13 (4), 375–388.

Kitterman, S. S., 1994. Investigation of several aspects of the vibration characteristics of steel member-supported floors. Master's thesis, Virginia Polytechnic Institute and State University, Blacksburg, VA, USA.

Kraus, C. A., 1997. Floor vibration design criterion for cold-formed C-Shaped supported residential floor systems. Master's thesis, Virginia Polytechnic Institute and State University, Blacksburg, VA, USA.

Kshirsagar, S., Bhaskar, K., 2008. Accurate and elegant free vibration and buckling studies of orthotropic rectangular plates using untruncated infinite series. Journal of Sound and Vibration 314 (3), 837–850.

Kullaa, J., Talja, A., 1998. Vibration tests for lightweight steel joist floors–subjective perceptions of vibrations and comparisons with design criteria. Finnish R&D conference on steel structure (Teräsrakenteiden tutkimus-ja kehityspäivät), Lappeenranta, Finland.

Kullaa, J., Talja, A., 1999. Vibration performance tests for light-weight steel-joist floors. In: Light-Weight Steel and Aluminium Structures: ICSAS '99. Espoo, Finland, pp. 719–726.

Laura, P., Grossi, R., 1979. Transverse vibrations of rectangular anisotropic plates with edges elastically restrained against rotation. Journal of Sound and Vibration 64 (2), 257–267.

Laura, P., Luisoni, L., Ficcadenti, G., 1978. On the effect of different edge flexibility coefficients on transverse vibrations of thin, rectangular plates. Journal of Sound and Vibration 57 (3), 333–340.

Laura, P., Romanelli, E., 1974. Vibrations of rectangular plates elastically restrained against rotation along all edges and subjected to a bi-axial state of stress. Journal of Sound and Vibration 37 (3), 367–377.

Leissa, A. W., 1969. Vibration of plates. NASA SP-160, National Aeronautics and Space Administration, Washington, D.C.

Leissa, A. W., 2005. The historical bases of the rayleigh and ritz methods. Journal of Sound and Vibration 287 (4), 961–978.

Leissa, A. W., Laura, P. A. A., Gutierrez, R. H., 1980. Vibrations of rectangular plates with nonuniform elastic edge supports. Journal of Applied Mechanics 47 (4), 891–895.

Li, Q., Fan, J., Nie, J., Li, Q., Chen, Y., 2010. Crowd-induced random vibration of footbridge and vibration control using multiple tuned mass dampers. Journal of Sound and Vibration 329 (19), 4068–4092.

Li, R., Tian, B., Zhong, Y., 2013. Analytical bending solutions of free orthotropic rectangular thin plates under arbitrary loading. Meccanica 48 (10), 2497–2510.

Li, R., Zhong, Y., 2011. On a new symplectic geometry method for exact bending solutions of orthotropic rectangular plates with two opposite sides clamped. Acta Mechanica 216 (1-4), 333–343.

Li, R., Zhong, Y., Tian, B., Liu, Y., 2009a. On the finite integral transform method for exact bending solutions of fully clamped orthotropic rectangular thin plates. Applied Mathematics Letters 22 (12), 1821–1827.

Li, W. L., 2000. Free vibrations of beams with general boundary conditions. Journal of Sound and Vibration 237 (4), 709–725.

Li, W. L., 2002. Comparison of fourier sine and cosine series expansions for beams with arbitrary boundary conditions. Journal of sound and vibration 255 (1), 185–194.

Li, W. L., 2004. Vibration analysis of rectangular plates with general elastic boundary supports. Journal of Sound and Vibration 273 (3), 619–635.

Li, W. L., Daniels, M., 2002. A fourier series method for the vibrations of elastically restrained plates arbitrarily loaded with springs and masses. Journal of Sound and Vibration 252 (4), 768–781.

Li, W. L., Zhang, X., Du, J., Liu, Z., 2009b. An exact series solution for the transverse vibration of rectangular plates with general elastic boundary supports. Journal of Sound and Vibration 321 (1), 254–269.

Lim, C. W., Cui, S., Yao, W., 2007. On new symplectic elasticity approach for exact bending solutions of rectangular thin plates with two opposite sides simply supported. International journal of solids and structures 44 (16), 5396–5411.

Liu, W., 2001. Vibration of floors supported by cold-formed steel joists. Master's thesis, University of Waterloo, Waterloo, ON, Canada.

Magrab, E. B., 1968. Vibration of a rectangular plate carrying a concentrated mass. Journal of Applied Mechanics 35 (2), 411–412.

Maurizi, M., Robledo, G., 1998. A further note on the "dynamic analysis of generally suppported beams using fourier series". Journal of sound and vibration 214 (5), 972–973.

Mbakogu, F., Pavlović, M., 2000. Bending of clamped orthotropic rectangular plates: a variational symbolic solution. Computers & Structures 77 (2), 117–128.

Meirovitch, L., 1967. Analytical Methods In Vibrations. The Macmillan Co, London.

Middleton, C. J., Brownjohn, J. M. W., 2010. Response of high frequency floors: A literature review. Engineering Structures 32 (2), 337–352.

Middleton, C. J., Brownjohn, J. M. W., 2011. Simplified methods for estimating the response of floors to a footfall. In: ASCE Proceedings of the 2011 Structures Congress. American Society of Civil Engineers, Las Vegas, Nevada, USA, pp. 383–403.

Monforton, G., Wu, T. H., 1963. Matrix analysis of semi-rigid connected frames. Journal of the Structural Division 89 (6), 13–24.

Morley, L. S. D., 1966. Bending of rectangular orthotropic plates under concentrated load with two opposite edges simply supported. Schweizerische Bauzeitung 84 (48), 843–848.

Mukhopadhyay, M., 1979. Free vibration of rectangular plates with edges having different degrees of rotational restraint. Journal of Sound and Vibration 67 (4), 459–468.

Mukhopadhyay, M., 1989. Vibration and buckling of rectangular plates with varying degrees of rotational restraint along the edges. Computers & structures 32 (2), 341–346.

Murray, T. M., Allen, D. E., Ungar, E. E., 1997. Floor Vibrations Due to Human Activities. Steel Design Guide Series 11. American Institute of Steel Construction/Canadian Institute of Steel Construction, Chicago, Illinois, USA.

Murray, T. M., Davis, B., 2015. Vibration of steel joist–concrete slab floors. Technical Digest 5, Steel Joist Institute, Florence, South Carolina, USA.

Newmark, N. M., Siess, C. P., Viest, I., et al., 1951. Tests and analysis of composite beams with incomplete interaction. Proceedings of the Society of Experimental Stress Analysis 9 (1), 75–92.

Nicholson, J. W., Bergman, L. A., 1986. Vibration of damped plate-oscillator systems. Journal of Engineering Mechanics 112 (1), 14–30.

Nigam, S., Malik, M., 1987. A study on a vibratory model of a human body. Journal of biomechanical engineering 109 (2), 148–153.

Norušis, M. J., 2003. SPSS® 12.0 Statistical Procedures Companion. Prentice Hall.

Odley, E. G., 1947. Deflections and moments of a rectangular plate clamped on all edges and under hydrostatic pressure. Journal of Applied Mechanics-Transactions of the ASME 14 (4), A289–A299.

Ohlsson, S. V., 1986. Stiffness criteria and dynamic serviceability of light-weight steel floors. In: Proceddings of IABSE Colloquium: Thin-Walled Metal Structures in Buildings. International Association for Bridge and Structural Engineering, Stockholm, pp. 427–433.

Ohlsson, S. V., 1988a. Springiness and human-induced floor vibrations: a design guide. Swedish council for building research, Stockholm, Sweden, translated by L. J. Gruber.

Ohlsson, S. V., 1988b. Ten years of floor vibration research-a review of aspects and some results. In: Proceedings of the Symposium/Workshop on Serviceability of Buildings (Movements, Deformations, Vibrations). Vol. 1. Ottawa, Canada, pp. 419–434.

Onysko, D. M., 1988a. Performance and acceptability of wood floors-forintek studies. In: Proceedings of Symposium/Workshop on Serviceability of Buildings. Vol. 1. National Research Council, University of Ottawa, Ottawa, Ontario, Canada, pp. 477–494.

Onysko, D. M., 1988b. Performance criteria for residential floors based on consumer responses. In: Proceedings of 1988 International conference on timber engineering. Vol. 1. Seattle, Washington, USA, pp. 736–745.

Onysko, D. M., Hu, L. J., Jones, E. D., Di Lenardo, B., 2000. Serviceability design of residential wood framed floors in canada. In: Proceedings of the World Conference on Timber Engineering.

Parnell, R., Davis, B., Xu, L., 2009. Vibration performance of lightweight cold-formed steel floors. Journal of Structural Engineering 136 (6), 645–653.

Parnell, R. A., 2008. Vibration serviceability and dynamic modeling of cold-formed steel floor systems. Master's thesis, University of Waterloo, Waterloo, ON, Canada.

Pavic, A., Reynolds, P., 1999. Experimental assessment of vibration serviceability of existing office floors under human-induced excitation. Experimental Techniques 23 (5), 41–45.

Pavic, A., Reynolds, P., 2002. Vibration serviceability of long-span concrete building floors. part 1: Review of background information. Shock and Vibration Digest 34 (3), 191–211.

Pedersen, L., 2011. Interaction between structures and their occupants. In: Modal Analysis Topics, Volume 3, Proceedings of the 29th IMAC, A Conference and Exposition on Structural Dynamics. Springer, pp. 445–450.

Qin, J., Law, S., Yang, Q., Yang, N., 2013. Pedestrian–bridge dynamic interaction, including human participation. Journal of Sound and Vibration 332 (4), 1107–1124.

Racic, V., Pavic, A., Brownjohn, J. M. W., 2009. Experimental identification and analytical modelling of human walking forces: Literature review. Journal of Sound and Vibration 326 (1), 1–49.

Rack, W., Lange, J., 2009. Human induced vibrations of lightweight steel floor systems. In: Proceedings of the eleventh Nordic Steel Construction Conference, NSCC2009. Malmö, Sweden, pp. 502–509.

Ramsay, A., Maunder, E., 2016. An error in timoshenko's 'theory of plates and shells'. NAFEMS Benchmark Magazine.

Rao, S. S., 2007. Vibration of continuous systems. John Wiley & Sons.

Rehman, Q., 2014. Serviceability and flexural strength of lightweight floor made of cold formed steel joists. Ph.D. dissertation, Ryerson University, Toronto, Canada.

Sachse, R., 2002. The influences of human occupants on the dynamic properties of slender structures. Ph.D. dissertation, University of Sheffield.

Sachse, R., Pavic, A., Reynolds, P., 2003. Human-structure dynamic interaction in civil engineering dynamics: A literature review. Shock and Vibration Digest 35 (1), 3–18.

Sachse, R., Pavic, A., Reynolds, P., 2004. Parametric study of modal properties of damped two-degree-of-freedom crowd–structure dynamic systems. Journal of Sound and Vibration 274 (3), 461–480.

Samuelsson, M., Sandberg, J., 1998. Vibrations in lightweight steel floors. Report 190.4, Swedish Institute of Steel Construction, Stockholm.

Shahabpoor, E., Pavic, A., Racic, V., 2013. Using MSD model to simulate human-structure interaction during walking. In: Topics in Dynamics of Civil Structures, Volume 4: Proceedings of the 31st IMAC, A Conference on Structural Dynamics. Springer, pp. 357–364.

Shahabpoor, E., Pavic, A., Racic, V., 2016a. Identification of mass–spring–damper model of walking humans. In: Structures. Vol. 5. Elsevier, pp. 233–246.

Shahabpoor, E., Pavic, A., Racic, V., 2016b. Interaction between walking humans and structures in vertical direction: A literature review. Shock and Vibration 2016, Article ID 3430285.

Sharp, G. R., 1967a. Finite transform solution of the symmetrically vibrating annular membrane. Journal of Sound and Vibration 5 (1), 1–8.

Sharp, G. R., 1967b. Finite transform solution of the vibrating annular membrane. Journal of Sound and Vibration 6 (1), 117–128.

Smith, A. L., Hicks, S. J., Devine, P. J., 2009. Design of floors for vibration: A new approach. SCI Standard P354, Revised edition, Steel Construction Institute, Ascot, Berkshire, UK.

Smith, I., Chui, Y. H., 1988. Design of lightweight wooden floors to avoid human discomfort. Canadian Journal of Civil Engineering 15 (2), 254–262.

Smith, I., Chui, Y. H., 1989. Design of lightweight wooden floors to avoid human discomfort: Reply. Canadian Journal of Civil Engineering 16 (2), 202–203.

Sneddon, I. N., 1972. The use of integral transforms. McGraw-Hill, Inc.

Sneddon, I. N., 1975. Application of integral transforms in the theory of elasticity. Springer-Verlag New York.

SSMA, 2001. Product Technical Information. ICBO ER-4943P. Steel Stud Manufacturers Association, Chicago, IL.

SSMA, 2015. Product technical guide. Steel Stud Manufacturers Association.

Talja, A., Kullaa, J., 1998. Vibration tests for lightweight steel joist floors–dynamic properties and vibrations due to walking. Finnish R&D conference on steel structure (Teräsrakenteiden tutkimus-ja kehityspäivät), Lappeenranta, Finland.

Tangorra, F. M., 2005. A design procedure for floor supported by cold-formed steel joists. Master's thesis, University of Waterloo, Waterloo, ON, Canada.

Tangorra, F. M., Xu, L., Xie, W. C., 2002. Vibration characteristics of lightweight floors using cold-formed steel joist. In: 16th International Specialty Conference on Cold-Formed Steel Structures. Orlando, Florida, USA, pp. 573–588.

Tian, B., Li, R., Zhong, Y., 2015. Integral transform solutions to the bending problems of moderately thick rectangular plates with all edges free resting on elastic foundations. Applied Mathematical Modelling 39 (1), 128–136.

Tian, B., Zhong, Y., Li, R., 2011. Analytic bending solutions of rectangular cantilever thin plates. Archives of Civil and Mechanical Engineering 11 (4), 1043–1052.

Timoshenko, S., Woinowsky-Krieger, S., 1959. Theory of plates and shells, 2nd Edition. McGraw-Hill, Inc., New York.

Timoshenko, S. P., Gere, J. M., 1961. Theory of elastic stability, 2nd Edition. McGraw-Hill, inc., New York.

Tolstov, G. P., 1962. Fourier Series. Dover Publications, New York.

Toratti, T., Talja, A., 2006. Classification of human induced floor vibrations. Building acoustics 13 (3), 211–221.

Troitsky, M. S., 1976. Stiffened plates: bending, stability, and vibrations. Elsevier Scientific Pub. Co.

Wang, J. T.-S., Lin, C.-C., 1996. Dynamic analysis of generally supported beams using fourier series. Journal of Sound and Vibration 196 (3), 285–293.

Wang, J. T.-S., Lin, C.-C., 1999. A method for exact series solutions in structural mechanics. Journal of applied mechanics 66 (2), 380–387.

Warburton, G. B., 1954. The vibration of rectangular plates. Proceedings of the Institution of Mechanical Engineers 168 (1), 371–384.

Warburton, G. B., 1983. This week's citation classic. Current Contents/Engineering, Technology & Applied Sciences (44), 20.

Warburton, G. B., Edney, S. L., 1984. Vibrations of rectangular plates with elastically restrained edges. Journal of Sound and Vibration 95 (4), 537–552.

Watanabe, K., 2014. Integral transform techniques for green's function. Springer.

Weaver Jr, W., Timoshenko, S. P., Young, D. H., 1990. Vibration problems in engineering, 5th Edition. John Wiley & Sons.

Weckendorf, J., Smith, I., 2012. Dynamic characteristics of shallow floors with cross-laminated-timber spines. In: World Conference of Timber Engineering, WCTE 2012. Auckland, New Zealand.

Weckendorf, J., Toratti, T., Smith, I., Tannert, T., 2015. Vibration serviceability performance of timber floors. European Journal of Wood and Wood Products, 1–15.

Wheeler, J. E., 1982. Prediction and control of pedestrian-induced vibration in footbridges. Journal of the structural division, ASCE 108 (ST-9), 2045–2065.

Willford, M. R., Young, P., 2006. A design guide for footfall induced vibration of structures. The Concrete Center, London, UK.

Wiss, J. F., Linehan, P. W., Kudder, R. J., 1977. Report of laboratory tests and analytical studies of structural characteristics of cold-formed steel-joist floor systems. WJE NO. 73345, American Iron and Steel Institute, Project 1201-412.

Wolfram Research, Inc., 2016. Mathematica. Champaign, Illinois, version 10.4 Edition.

Wright, D. T., Green, R., 1959. Human sensitivity to vibration. Report NO. 7, Queen's Univeristy, Kingston, Ontario, Canada.

Wu, J.-S., Luo, S.-S., 1997. Free vibration analysis of a rectangular plate carrying any number of point masses and translational springs by using the modified and quasi-analytical and numerical combined methods. International journal for numerical methods in engineering 40 (12), 2171–2193.

Wyatt, T. A., 1989. Design guide on the vibration of floors. SCI Standard P076, Steel Construction Institute, Ascot, Berkshire, UK.

Xu, L., 2000. Dynamic behaviour of residential floor systems using cold-formed steel joists. Phase I, Final Report Prepared for the Canadian Sheet Steel Building Institute, University of Waterloo, Waterloo, ON, Canada.

Xu, L., 2001a. Dynamic behaviour of residential floor systems using cold-formed steel joists. Phase II, Interim Report Prepared for the Canadian Sheet Steel Building Institute, University of Waterloo, Waterloo, ON, Canada.

Xu, L., 2001b. Second-order analysis for semirigid steel frame design. Canadian Journal of Civil Engineering 28 (1), 59–76.

Xu, L., 2005. Site investigation of the dynamic behaviour of the iSPAN floor system. University of Waterloo, Waterloo, ON, Canada.

Xu, L., 2011. Floor vibration in lightweight cold-formed steel framing. Advances in Structural Engineering 14 (4), 659–672.

Xu, L., Ling, Z., Xie, W.-C., Schuster, R. M., 2000. Dynamic behaviour of floors with cold-formed steel joists. In: 15th International Specialty Conference on Cold-Formed Steel Structures. St. Louis, Missouri, USA, pp. 377–392.

Xu, L., Tangorra, F., 2007. Experimental investigation of lightweight residential floors supported by cold-formed steel C-shape joists. Journal of Constructional Steel Research 63 (3), 422–435.

Young, P., 2001. Improved floor vibration prediction methodologies. In: ARUP vibration seminar on Engineering for Structural Vibration—Current Developments in Research and Practice. London, UK.

Yu, C., July 12th 2016. personal communication between Dr. L. Xu and Dr. C. Yu.

Yu, C., Yousof, M., Mahdavian, M., 2015. Load bearing clip angle design. A Research Report Submitted to the American Iron and Steel Institute, Report No. UNT-GP6351, University of North Texas, Denton, Texas.

Zhang, Q., 2013. Models of a standing human body in structural vibration. Ph.D. dissertation, University of Manchester, Manchester, UK.

Zhang, S., Xu, L., 2016. Fundamental frequency of lightweight cold-formed steel floor systems. In: Dynamics of Coupled Structures, Volume 4, Proceedings of the 34th IMAC, A Conference and Exposition on Structural Dynamics. Springer, Orlando, FL, USA, pp. 137–145.

Zhang, X., Li, W. L., 2009. Vibrations of rectangular plates with arbitrary non-uniform elastic edge restraints. Journal of Sound and Vibration 326 (1), 221–234.

Zheng, X., Brownjohn, J. M. W., 2001. Modeling and simulation of human-floor system under vertical vibration. In: SPIE's 8th Annual International Symposium on Smart Structures and Materials. International Society for Optics and Photonics, pp. 513–520.

Zhong, Y., Yin, J.-H., 2008. Free vibration analysis of a plate on foundation with completely free boundary by finite integral transform method. Mechanics Research Communications 35 (4), 268–275.

Zhou, D., Han, H., Ji, T., Xu, X., 2016. Comparison of two models for human-structure interaction. Applied Mathematical Modelling 40 (5), 3738–3748.

Živanović, S., 2015. Modelling human actions on lightweight structures: experimental and numerical developments. In: MATEC Web of Conferences. Vol. 24. EDP Sciences.

Živanović, S., Pavic, A., Reynolds, P., 2005. Vibration serviceability of footbridges under human-induced excitation: a literature review. Journal of sound and vibration 279 (1), 1–74.

Appendix A

Bending of R-F-R-F Orthotropic Plates

A.1 Formulation and methodology

Consider a rectangular orthotropic thin plate with length a and width b having two opposite edges free (i.e., $y = 0$ and $y = b$) and the others elastically restrained against rotations (i.e., $x = 0$ and $x = a$) as shown in Fig. A.1.

Denoting partial differentiation by a comma, the boundary conditions of the plate can be written as

$$w = 0,\ M_x = -D_x\left(w_{,xx} + \nu_y w_{,yy}\right) = -R_{x0} w_{,x}\ \ at\ x = 0 \tag{A.1a}$$

$$w = 0,\ M_x = -D_x\left(w_{,xx} + \nu_y w_{,yy}\right) = R_{xa} w_{,x}\ \ at\ x = a \tag{A.1b}$$

$$M_y = -D_y\left(w_{,yy} + \nu_x w_{,xx}\right) = 0\ at\ y = 0,\ b \tag{A.1c}$$

$$V_y = -D_y w_{,yyy} - \left(H + 2D_{xy}\right) w_{,yxx} = 0\ at\ y = 0,\ b \tag{A.1d}$$

where M_x and M_y are the bending moments, V_y is the effective shear force, and R_{x0} and R_{xa} are rotational spring constants shown in Fig. A.1. Based on Eqs. (3.41), a rotational fixity factor r was introduced as

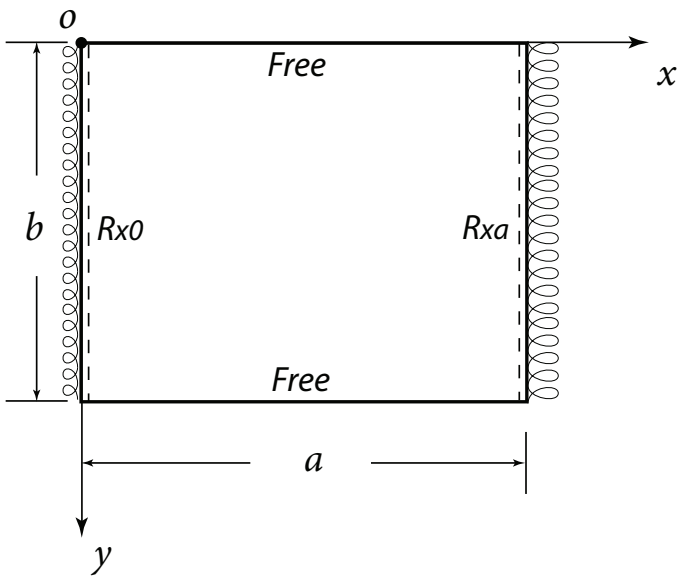

Figure A.1 Orthotropic plate with opposite free and rotationally restrained edges.

$$3r_{x0}D_x = (1 - r_{x0})R_{x0}a \tag{A.2a}$$

$$3r_{xa}D_x = (1 - r_{xa})R_{xa}a \tag{A.2b}$$

Then, a general boundary condition can be simulated by different values of rotational fixity factors with range from 0 to 1. The simply supported and fully clamped boundary conditions will be treated as the limiting cases with $r = 0$ and $r = 1$, respectively. Taking the finite cosine transform of the boundary conditions in Eqs. (A.1a) and (A.1b) with respect to y, and the finite sine transform of the boundary condition in Eqs. (A.1c) and (A.1d) with respect to x, it results the following

$$D_x \widehat{w}_{,xx}(0,n) = R_{x0}\widehat{w}_{,x}(0,n) \tag{A.3a}$$

$$D_x \widehat{w}_{,xx}(a,n) = -R_{xa}\widehat{w}_{,x}(a,n) \tag{A.3b}$$

$$\bar{w}_{,yy}(m,y) = \nu_x \alpha_m^2 \bar{w}(m,y), \ \ for\ y = 0, b \tag{A.3c}$$

$$\bar{w}_{,yyy}(m,y) = \frac{H + 2D_{xy}}{D_y}\alpha_m^2 \bar{w}_{,y}(m,y), \ \ for\ y = 0, b \tag{A.3d}$$

Subsequently, the method of finite integral transform will be applied to solve Eq. (3.3). First of all, the joint finite integral transform is defined by applying finite sine transform with respect to x with m as the subsidiary variable and the finite cosine transform with respect to y with n as the subsidiary variable. It can be expressed as

$$\widehat{\bar{w}}(m,n) = \int_0^a \int_0^b w(x,y) \sin \alpha_m x \cos \beta_n y dx dy \tag{A.4}$$

where

$$\alpha_m = \frac{m\pi}{a},\ \beta_n = \frac{n\pi}{b}\ (m = 1,2,3,...,n = 0,1,2,3,...) \tag{A.5}$$

The inversion of Eq. (A.4) can be obtained as (Sneddon, 1972)

$$w(x,y) = \frac{4}{ab} \sum_{m=1}^{\infty} \sum_{n=0}^{\infty} \varepsilon_n \widehat{\bar{w}}(m,n) \sin \alpha_m x \cos \beta_n y \tag{A.6}$$

where

$$\varepsilon_n = \begin{cases} 1/2, & n = 0 \\ 1, & n \neq 0 \end{cases} \tag{A.7}$$

Similarly, the joint finite sine and cosine transforms of the fourth derivatives in Eq. (3.3) are given by

$$\begin{aligned} \int_0^a \int_0^b w_{,xxxx} \sin \alpha_m x \cos \beta_n y dx dy =& \alpha_m^4 \widehat{\bar{w}}(m,n) \\ & - \alpha_m \Big[(-1)^m \widehat{w}_{,xx}(a,n) - \widehat{w}_{,xx}(0,n) \Big] \end{aligned} \tag{A.8a}$$

$$\begin{aligned} \int_0^a \int_0^b w_{,xxyy} \sin \alpha_m x \cos \beta_n y dx dy =& \alpha_m^2 \beta_n^2 \widehat{\bar{w}}(m,n) \\ & - \alpha_m^2 \Big[(-1)^n \bar{w}_{,y}(m,b) - \bar{w}_{,y}(m,0) \Big] \end{aligned} \tag{A.8b}$$

$$\begin{aligned} \int_0^a \int_0^b w_{,yyyy} \sin \alpha_m x \cos \beta_n y dx dy =& \beta_n^4 \widehat{\bar{w}}(m,n) \\ & + \Big[(-1)^n \bar{w}_{,yyy}(m,b) - \bar{w}_{,yyy}(m,0) \Big] \\ & - \beta_n^2 \Big[(-1)^n \bar{w}_{,y}(m,b) - \bar{w}_{,y}(m,0) \Big] \end{aligned} \tag{A.8c}$$

where coefficients $\widehat{w}_{,xx}(0,n)$ and $\widehat{w}_{,xx}(a,n)$ are determined from the finite cosine transform with respect to y at the rotationally restrained edges ($x=0$ and $x=a$). Similarly, $\bar{w}_{,y}(m,0)$ and $\bar{w}_{,y}(m,b)$ are determined from the finite-sine transformed boundary conditions at two free edges, separately. Then, it can be obtained from Eq. (A.3d) that

$$\Big[(-1)^n\bar{w}_{,yyy}(m,b)-\bar{w}_{,yyy}(m,0)\Big]=\frac{H+2D_{xy}}{D_y}\alpha_m^2\Big[(-1)^n\bar{w}_{,y}(m,b)-\bar{w}_{,y}(m,0)\Big] \tag{A.9}$$

Substituting Eq. (A.9) into Eq. (A.8c) yields

$$\begin{aligned}&\int_0^a\int_0^b w_{,yyyy}\sin\alpha_m x\cos\beta_n y dxdy\\ =&\beta_n^4\widehat{w}(m,n)+\left[\frac{H+2D_{xy}}{D_y}\alpha_m^2-\beta_n^2\right]\Big[(-1)^n\bar{w}_{,y}(m,b)-\bar{w}_{,y}(m,0)\Big]\end{aligned} \tag{A.10}$$

Taking the joint finite sine and cosine transform of the governing equation Eq. (3.3) and making use of Eqs. (A.8a), (A.8b) and (A.10) yields

$$\begin{aligned}\widehat{\bar{w}}(m,n)=\frac{1}{\Omega_{mn}}\Bigg\{&\widehat{\bar{q}}(m,n)+\alpha_m D_x\Big[(-1)^m\widehat{w}_{,xx}(a,n)-\widehat{w}_{,xx}(0,n)\Big]\\ &+D_y(\nu_x\alpha_m^2+\beta_n^2)\Big[(-1)^n\bar{w}_{,y}(m,b)-\bar{w}_{,y}(m,0)\Big]\Bigg\}\end{aligned} \tag{A.11}$$

where

$$\Omega_{mn}=D_x\alpha_m^4+2H\alpha_m^2\beta_n^2+D_y\beta_n^4 \tag{A.12}$$

$$\widehat{\bar{q}}(m,n)=\int_0^a\int_0^b q(x,y)\sin\alpha_m x\cos\beta_n y dxdy \tag{A.13}$$

Taking the inverse finite cosine transform with respect to y of Eq. (A.11), it is obtained

$$\bar{w}(m,y)=\frac{2}{b}\sum_{n=0}^{\infty}\varepsilon_n\widehat{\bar{w}}(m,n)\cos\beta_n y \tag{A.14}$$

Taking second-order derivative of Eq. (A.14) with respect to y and using the Stokes's transformation gives

$$\bar{w}_{,yy}(m,y) = \frac{2}{b}\sum_{n=0}^{\infty}\varepsilon_n\left\{\left[(-1)^n\bar{w}_{,y}(m,b) - \bar{w}_{,y}(m,0)\right] - \beta_n^2\widehat{\bar{w}}(m,n)\right\}\cos\beta_n y \tag{A.15}$$

Substituting Eqs. (A.3c) and (A.14) into Eq. (A.15), it is arrived at

$$\sum_{n=0}^{\infty}\varepsilon_n\left\{\left[(-1)^n\bar{w}_{,y}(m,b) - \bar{w}_{,y}(m,0)\right] - (\nu_x\alpha_m^2 + \beta_n^2)\widehat{\bar{w}}(m,n)\right\} = 0 \tag{A.16a}$$

$$\sum_{n=0}^{\infty}(-1)^n\varepsilon_n\left\{\left[(-1)^n\bar{w}_{,y}(m,b) - \bar{w}_{,y}(m,0)\right] - (\nu_x\alpha_m^2 + \beta_n^2)\widehat{\bar{w}}(m,n)\right\} = 0 \tag{A.16b}$$

Then, taking the inverse finite sine transform of Eq. (A.11) with respect to x yields

$$\widehat{w}(x,n) = \frac{2}{a}\sum_{m=1}^{\infty}\widehat{\bar{w}}(m,n)\sin\alpha_m x \tag{A.17}$$

Taking the derivative of Eq. (A.17) with respect to x and using Stokes's transformation, it is found

$$\widehat{w}_{,x}(x,n) = \frac{2}{a}\sum_{m=1}^{\infty}\alpha_m\widehat{\bar{w}}(m,n)\cos\alpha_m x \tag{A.18}$$

Substituting Eq. (A.3a) and (A.3b) into Eq. (A.18) and replacing constants R_{x0} and R_{xa} by the corresponding rotational fixity factors r_{x0} and r_{xa} based on Eqs. (A.2), the following equations can be obtained

$$a^2(1-r_{x0})\widehat{w}_{,xx}(0,n) = 6r_{x0}\sum_{m=1}^{\infty}\alpha_m\widehat{\bar{w}}(m,n) \tag{A.19a}$$

$$a^2(1-r_{xa})\widehat{w}_{,xx}(a,n) = -6r_{xa}\sum_{m=1}^{\infty}(-1)^m\alpha_m\widehat{\bar{w}}(m,n) \tag{A.19b}$$

Substituting Eq. (A.11) into Eqs. (A.16) and (A.19), it yields four infinite systems of linear Eqs. (A.20), (A.21), (A.22) and (A.23) with respect to coefficients $\widehat{w}_{,xx}(0,n)$, $\widehat{w}_{,xx}(a,n)$, $\bar{w}_{,y}(m,0)$, and $\bar{w}_{,y}(m,b)$.

$$\begin{aligned}\sum_{n=0}^{\infty}\varepsilon_n\Phi_{mn}\widehat{\bar{q}}(m,n) = &\sum_{n=0}^{\infty}(-1)^n\varepsilon_n(1-\Psi_{mn}D_y)\bar{w}_{,y}\,(m,b)\\ &-\sum_{n=0}^{\infty}\varepsilon_n(1-\Psi_{mn}D_y)\bar{w}_{,y}\,(m,0)\\ &-\sum_{n=0}^{\infty}(-1)^m\varepsilon_n\alpha_m\Phi_{mn}D_x\widehat{w}_{,xx}\,(a,n)\\ &+\sum_{n=0}^{\infty}\varepsilon_n\alpha_m\Phi_{mn}D_x\widehat{w}_{,xx}\,(0,n)\end{aligned} \tag{A.20}$$

$$\begin{aligned}\sum_{n=0}^{\infty}(-1)^n\varepsilon_n\Phi_{mn}\widehat{\bar{q}}(m,n) = &\sum_{n=0}^{\infty}\varepsilon_n\left(1-\Psi_{mn}D_y\right)\bar{w}_{,y}\,(m,b)\\ &-\sum_{n=0}^{\infty}(-1)^n\varepsilon_n\left(1-\Psi_{mn}D_y\right)\bar{w}_{,y}\,(m,0)\\ &-\sum_{n=0}^{\infty}(-1)^{n+m}\varepsilon_n\alpha_m\Phi_{mn}D_x\widehat{w}_{,xx}\,(a,n)\\ &+\sum_{n=0}^{\infty}(-1)^n\varepsilon_n\alpha_m\Phi_{mn}D_x\widehat{w}_{,xx}\,(0,n)\end{aligned} \tag{A.21}$$

$$\begin{aligned}6r_{x0}\sum_{m=1}^{\infty}\frac{\alpha_m}{\Omega_{mn}}\widehat{\bar{q}}(m,n) = &-6r_{x0}\sum_{m=1}^{\infty}(-1)^n\alpha_m\Phi_{mn}D_y\bar{w}_{,y}\,(m,b)\\ &+6r_{x0}\sum_{m=1}^{\infty}\alpha_m\Phi_{mn}D_y\bar{w}_{,y}\,(m,0)\\ &-6r_{x0}\sum_{m=1}^{\infty}\frac{(-1)^m\alpha_m^2D_x}{\Omega_{mn}}\widehat{w}_{,xx}\,(a,n)\\ &+\left[a^2(1-r_{x0})+6r_{x0}\sum_{m=1}^{\infty}\frac{\alpha_m^2D_x}{\Omega_{mn}}\right]\widehat{w}_{,xx}\,(0,n)\end{aligned} \tag{A.22}$$

$$\begin{aligned}6r_{xa}\sum_{m=1}^{\infty}\frac{(-1)^m\alpha_m}{\Omega_{mn}}\widehat{\bar{q}}(m,n) = &-6r_{xa}\sum_{m=1}^{\infty}(-1)^{m+n}\alpha_m\Phi_{mn}D_y\bar{w}_{,y}\,(m,b)\\ &+6r_{xa}\sum_{m=1}^{\infty}(-1)^m\alpha_m\Phi_{mn}D_y\bar{w}_{,y}\,(m,0)\\ &-\left[a^2(1-r_{xa})+6r_{xa}\sum_{m=1}^{\infty}\frac{\alpha_m^2D_x}{\Omega_{mn}}\right]\widehat{w}_{,xx}\,(a,n)\\ &+6r_{xa}\sum_{m=1}^{\infty}\frac{(-1)^m\alpha_m^2D_x}{\Omega_{mn}}\widehat{w}_{,xx}\,(0,n)\end{aligned} \tag{A.23}$$

where

$$\Phi_{mn} = \frac{\nu_x \alpha_m^2 + \beta_n^2}{\Omega_{mn}} \tag{A.24a}$$

$$\Psi_{mn} = \frac{\left(\nu_x \alpha_m^2 + \beta_n^2\right)^2}{\Omega_{mn}} \tag{A.24b}$$

For each combination of m and n, Eqs. (A.20), (A.21), (A.22) and (A.23) produce $2m + 2(n+1)$ equations with $2m + 2(n+1)$ unknown coefficients. This set of equations can be solved to find the coefficients in Eq. (A.11). Once these coefficients have been computed, the deflection $w(x, y)$ can be obtained by substituting Eq. (A.11) into Eq. (A.6). Furthermore, the bending moments along the edges $x = 0$ and $x = a$ can be obtained as following:

$$M_x\Big|_{x=0} = -D_x \left(w_{,xx} + \nu_y w_{,yy}\right)\Big|_{x=0} = -\frac{2}{b} D_x \sum_{n=0}^{\infty} \widehat{w}_{,xx}\left(0, n\right) \cos \beta_n y \tag{A.25a}$$

$$M_x\Big|_{x=a} = -D_x \left(w_{,xx} + \nu_y w_{,yy}\right)\Big|_{x=a} = -\frac{2}{b} D_x \sum_{n=0}^{\infty} \widehat{w}_{,xx}\left(a, n\right) \cos \beta_n y \tag{A.25b}$$

For any position not along the edges, the bending moments can be obtained by

$$M_x = -D_x \left(w_{,xx} + \nu_y w_{,yy}\right) \tag{A.26a}$$

$$M_y = -D_y \left(w_{,yy} + \nu_x w_{,xx}\right) \tag{A.26b}$$

where $w_{,xx}$ can be given by using Stokes's transformation as

$$w_{,xx} = -\frac{4}{ab} \sum_{m=1}^{\infty} \sum_{n=0}^{\infty} \alpha_m^2 \varepsilon_n \widehat{\bar{w}}(m, n) \sin \alpha_m x \cos \beta_n y \tag{A.27}$$

and $w_{,yy}$ can be expressed by substituting $\bar{w}_{,yy}\left(m, y\right)$ of Eq. A.15 as

$$w_{,yy} = \frac{2}{a} \sum_{m=1}^{\infty} \bar{w}_{,yy}\left(m, y\right) \sin \alpha_m x \tag{A.28}$$

In addition, for a rectangular orthotropic plate with two opposite edges simply supported and the others free (S-F-S-F), the solution can be easily obtained by setting $r_{x0} = r_{xa} = 0$. For the orthotropic plate with two opposite edges fully clamped and the

others free (C-F-C-F), rotational fixity factors are equal to 1. Alternatively, for S-F-S-F orthotropic plates, the following can also be obtained from the foregoing procedure:

$$\widehat{\bar{w}}(m,n)=\frac{1}{\Omega_{mn}}\left\{\widehat{\bar{q}}(m,n)+D_y(\nu_x\alpha_m^2+\beta_n^2)\Big[(-1)^n\bar{w}_{,y}\,(m,b)-\bar{w}_{,y}\,(m,0)\Big]\right\} \tag{A.29}$$

Substituting Eq. (A.29) into Eqs. (A.16) yields two infinite systems of linear equations with respect to coefficients $\bar{w}_{,y}\,(m,0)$ and $\bar{w}_{,y}\,(m,b)$. Consequently, the corresponding deflection $w(x,y)$ can be obtained by the preceding procedure.

A.2 Numerical results and discussion

The presented numerical results are obtained by using MATLAB® software. For the sake of convenience, the numbers of double series terms are chosen to be same and denoted by N (i.e., $m=1,2,3,...,N$, $n=0,1,2,3,...,N$) and the two restrained edges have the same elastic fixity factor (i.e., $r_{x0}=r_{xa}=r$). The results are theoretically exact when $N\to\infty$ while convergent solutions with satisfactory accuracy can be acquired by a finite number of terms. In this study N is taken to be 300. Furthermore, although the proposed method is valid for arbitrary loading, numerical results are presented here only for two common cases: uniform distributed load q and concentrated load P at the center.

The first example validates the solution of a S-F-S-F isotropic plate subjected to a uniform distributed load. The numerical results are compared with those of Timoshenko and Woinowsky-Krieger (1959),Hutchinson (1992) and Lim et al. (2007). The obtained displacement of a square plate is plotted as shown in Fig. A.2. As it can be seen in Table. A.1, the results obtained from the proposed method agree well with those of the references with exactly four and five significant digits for flexural moments and deflections, respectively. In addition, it needs to point out, the result of M_y at $x=a/2,\ y=b/2$ of Timoshenko and Woinowsky-Krieger (1959) for $b/a=0.5$ is inaccurate which was discovered by Ramsay and Maunder (2016) and reconfirmed by this study.

The second example validates the proposed method with a C-F-C-F isotropic plate loaded by a concentrated load P at the center with results of Timoshenko and Woinowsky-Krieger (1959). Four different aspect ratios are investigated. Form Table. A.2, considerable differences between the results of the present study and Timoshenko and Woinowsky-

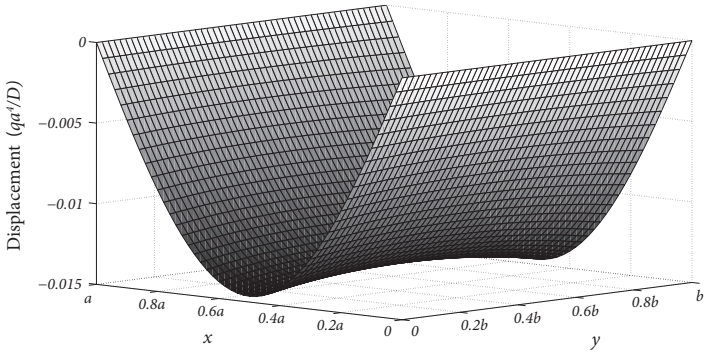

Figure A.2 Displacement of an isotropic plate under a uniform distributed load.

Krieger (1959) are observed in cases of aspect ratio, i.e., $b/a = 1$ and $b/a = 0.5$. However, it is known that the deflection will increase with the decrease of the aspect ratios such as results shown in Table. A.2. This tendency is illustrated by present results but not the ones of Timoshenko and Woinowsky-Krieger (1959). Further validation with other methods is desirable to verify present results.

The third investigation is performed for a C-F-C-F orthotropic plate loaded with a uniform distributed load q with results from the symplectic geometry method Li and Zhong (2011). As shown in Table. A.3, excellent agreements in both flexural deflections and moments can be found between the proposed method and Li and Zhong (2011). In addition, numerical results of R-F-R-F orthotropic plates obtained from the proposed method are also presented in Table. A.3.

Finally, as shown in Table. A.4, present numerical results are compared with the ones from Morley (1966) for case of a S-F-S-F orthotropic plate subjected to a concentrated load P at the center of the plate. The singular solution of the bending of an infinitely long simply supported orthotropic strip under concentrated load was employed to accelerate the convergence rate in Morley (1966) where the results were obtained by summing the series up to $n = 100$. As expected, present results agree well with those of Morley (1966). Additionally, a convergence study is conducted and plotted in Fig. A.3. Generally, it is known that the single series solution (e.g., Levy's solution) presents much faster convergence rates than the double series solution (e.g., Navier's solution) (Bauchau and Craig, 2009). Nevertheless, it can be found that the convergence rate of the present

Table A.1 Deflection and bending moment for a S-F-S-F isotropic rectangular plate under uniform distributed load q ($\nu = 0.3$).

b/a	Present	References		
		I	II	III
	$w(0.01qa^4/D)$ at $x = a/2,\ y = b/2$			
0.5	1.37138	1.377	N.A.	1.37131
1.0	1.30939	1.309	N.A.	1.30937
2.0	1.28867	1.289	N.A.	1.28873
	$M_x(0.1qa^2)$ at $x = a/2,\ y = b/2$			
0.5	1.23641259	1.235	1.23642359	1.23642
1.0	1.22539461	1.225	1.22545398	1.22545
2.0	1.23460079	1.235	1.23467772	1.23468
	$M_y(0.1qa^2)$ at $x = a/2,\ y = b/2$			
0.5	0.12122895	**0.102**	0.12147577	0.121476
1.0	0.27051852	0.271	0.27078215	0.270782
2.0	0.36382430	0.364	0.36388775	0.363888
	$w(0.01qa^4/D)$ at $x = a/2,\ y = 0$ *or* b			
0.5	1.4643483	1.443	1.4644623	N.A.
1.0	1.5009268	1.509	1.5011257	N.A.
2.0	1.5199052	1.521	1.5202171	N.A.
	$M_x(0.1qa^2)$ at $x = a/2,\ y = 0$ *or* b			
0.5	1.27802858	1.259	1.27812536	N.A.
1.0	1.31070797	1.318	1.31087659	N.A.
2.0	1.32776004	1.329	1.32801999	N.A.

Note: N.A.–Not available
Reference I–Timoshenko and Woinowsky-Krieger (1959)
Reference II–Hutchinson (1992)
Reference III–Lim et al. (2007)

double trigonometric series solution is not that much slower than that of the single series solution of Morley (1966). Five-figure precision is given for $m = n = 200$.

Table A.2 Displacement $w(0.01Pa^2/D)$ at the center $(x = a/2,\ y = b/2)$ for a C-F-C-F isotropic rectangular plate under a concentrated load P at the center ($\nu = 0.3$).

b/a	Rotational fixity factor $r_{x0} = r_{xa} = r$						References
	0.5	0.9	0.99	0.999	0.9999	1	I
3	1.18789	0.81738	0.73194	0.72323	0.72236	0.72226	0.72404
2	1.19453	0.81873	0.73279	0.72403	0.72315	0.72306	0.72243
1	1.38961	0.87631	0.77377	0.76353	0.76250	0.76239	**0.70308**
0.5	2.36970	1.32296	1.12901	1.11005	1.10814	1.10793	**0.38379**

Note: Reference I–Page 191 of Timoshenko and Woinowsky-Krieger (1959)

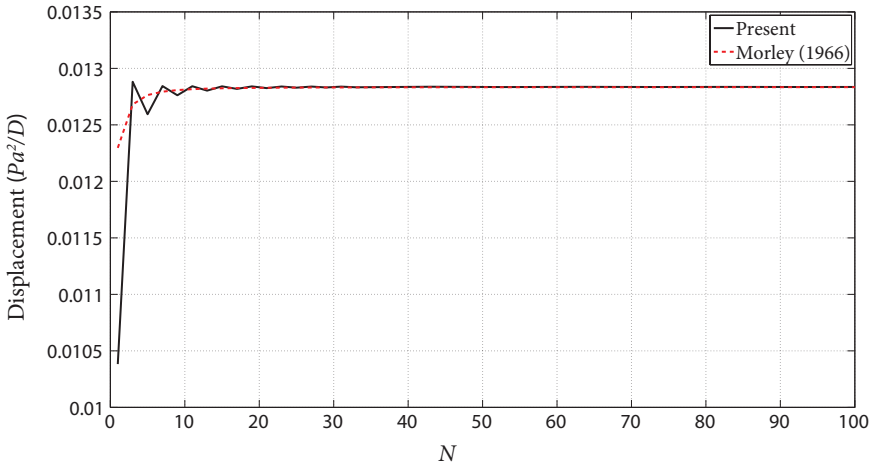

Figure A.3 Convergence of displacement results for a S-F-S-F orthotropic plate under a concentrated load.

Table A.3 Deflection and bending moment for a C-F-C-F orthotropic rectangular plate under uniform distributed load q.

b/a	Rotational fixity factor $r_{x0} = r_{xa} = r$						References
	0.5	0.9	0.99	0.999	0.9999	1	I
	$w(0.01qa^4/D_x)$ at $x = a/2,\ y = b/2$						
1.0	0.671805	0.328095	0.263622	0.257377	0.256754	0.256684	0.2578
1.1	0.670831	0.327779	0.263401	0.257165	0.256543	0.256647	0.2577
1.4	0.669132	0.327451	0.263245	0.257027	0.256407	0.256338	0.2574
1.7	0.668867	0.327759	0.263574	0.257358	0.256738	0.256670	0.2578
2.0	0.669471	0.328354	0.264089	0.257866	0.257246	0.257177	0.2584
	$M_x(-0.1qa^2)$ at $x = a,\ y = b/2$						
1.0	0.496628	0.768778	0.819177	0.823473	0.822484	0.821155	0.8223
1.1	0.495898	0.767942	0.818555	0.822881	0.821976	0.820994	0.8216
1.4	0.494713	0.767578	0.819054	0.823464	0.822860	0.822429	0.8225
1.7	0.494635	0.768913	0.821041	0.825504	0.825162	0.824952	0.8250
2.0	0.495178	0.770726	0.823178	0.827667	0.827518	0.827410	0.8274
	$M_x(0.1qa^2)$ at $x = a/2,\ y = b/2$						
1.0	0.743949	0.469830	0.418472	0.413497	0.413000	0.412944	0.4101
1.1	0.743156	0.469624	0.418347	0.413379	0.412882	0.412827	0.4103
1.4	0.741837	0.469546	0.418431	0.413476	0.412981	0.412926	0.4112
1.7	0.741783	0.470056	0.418991	0.414043	0.413548	0.413493	0.4123
2.0	0.742543	0.470879	0.419775	0.414825	0.414330	0.414275	0.4133

Note: Reference I–Page 191 of Li and Zhong (2011)

Table A.4 Deflection $w(0.01Pa^2/D)$ at loaded point for a S-F-S-F orthotropic square plate under a concentrated load P.

Position	Present	Morley (1966)
$x = a/2,\ y = b/2$	1.28343	1.28335
$x = a/4,\ y = b/2$	0.779029	0.778973

Appendix B

Matrices and vectors for the damped plate-oscillator model

For SDOF oscillators, $\mathbf{M}$ is an identity matrix of size $(N + N_o) \times (N + N_o)$. $\mathbf{C}$ and $\mathbf{K}$ can be represented as

$$\mathbf{C} = \begin{bmatrix} c_{(1,1)} & c_{(1,2)} & \cdots & c_{(1,N)} & c_{(1,N+1)} & \cdots & c_{(1,N+N_o)} \\ c_{(2,1)} & c_{(2,2)} & \cdots & c_{(2,N)} & c_{(2,N+1)} & \cdots & c_{(2,N+N_o)} \\ \vdots & \vdots & \vdots & \vdots & \vdots & \vdots & \vdots \\ c_{(N,1)} & c_{(N,2)} & \cdots & c_{(N,N)} & c_{(N,N+1)} & \cdots & c_{(N,N+N_o)} \\ c_{(N+1,1)} & c_{(N+1,2)} & \cdots & c_{(N+1,N)} & c_{(N+1,N+1)} & \cdots & c_{(N+1,N+N_o)} \\ \vdots & \vdots & \vdots & \vdots & \vdots & \vdots & \vdots \\ c_{(N+N_o,1)} & c_{(N+N_o,2)} & \cdots & c_{(N+N_o,N)} & c_{(N+N_o,N+1)} & \cdots & c_{(N+N_o,N+N_o)} \end{bmatrix} \tag{B.1a}$$

$$\mathbf{K} = \begin{bmatrix} k_{(1,1)} & k_{(1,2)} & \dots & k_{(1,N)} & k_{(1,N+1)} & \dots & k_{(1,N+N_o)} \\ k_{(2,1)} & k_{(2,2)} & \dots & k_{(2,N)} & k_{(2,N+1)} & \dots & k_{(2,N+N_o)} \\ \vdots & \vdots & \vdots & \vdots & \vdots & \vdots & \vdots \\ k_{(N,1)} & k_{(N,2)} & \dots & k_{(N,N)} & k_{(N,N+1)} & \dots & k_{(N,N+N_o)} \\ k_{(N+1,1)} & k_{(N+1,2)} & \dots & k_{(N+1,N)} & k_{(N+1,N+1)} & \dots & k_{(N+1,N+N_o)} \\ \vdots & \vdots & \vdots & \vdots & \vdots & \vdots & \vdots \\ k_{(N+N_o,1)} & k_{(N+N_o,2)} & \dots & k_{(N+N_o,N)} & k_{(N+N_o,N+1)} & \dots & k_{(N+N_o,N+N_o)} \end{bmatrix} \tag{B.1b}$$

in which

$$\begin{aligned} c_{(i,i)} &= 2\zeta_i\omega_i + \sum_{k=1}^{N_o} 2\zeta_{hk}\omega_{hk}\gamma_{ik}W_i^2(\xi_k,\eta_k) \\ c_{(i,j)} &= \sum_{k=1}^{N_o} 2\zeta_{hk}\omega_{hk}\gamma_{ik}W_i(\xi_k,\eta_k)W_j(\xi_k,\eta_k) \\ c_{(i,N+k)} &= -2\zeta_{hk}\omega_{hk}\gamma_{ik}W_i(\xi_k,\eta_k) \\ c_{(N+k,i)} &= -2\zeta_{hk}\omega_{hk}W_i(\xi_k,\eta_k) \\ c_{(N+k,N+k)} &= 2\zeta_{hk}\omega_{hk} \\ k_{(i,i)} &= \omega_i^2 + \sum_{k=1}^{N_o} \omega_{hk}^2\gamma_{ik}W_i^2(\xi_k,\eta_k) \\ k_{(i,j)} &= \sum_{k=1}^{N_o} \omega_{hk}^2\gamma_{ik}W_i(\xi_k,\eta_k)W_j(\xi_k,\eta_k) \\ k_{(i,N+k)} &= -\omega_{hk}^2\gamma_{ik}W_i(\xi_k,\eta_k) \\ k_{(N+k,i)} &= -\omega_{hk}^2W_i(\xi_k,\eta_k) \\ k_{(N+k,N+k)} &= \omega_{hk}^2 \\ i &= 1,2,...,N \qquad i \neq j \leqslant N \\ k &= 1,2,...,N_o \qquad k \neq l \leqslant N_o \end{aligned} \tag{B.2}$$

Note that elements of $\mathbf{C}$ and $\mathbf{K}$ above not specified are zero. The displacement vector $\mathbf{U}$ and the force vector $\mathbf{F}$ are given by

$$\mathbf{U} = [q_1(t), q_2(t), ..., q_N(t), z_1(t), ..., z_{N_o}(t)]$$
$$\mathbf{F} = \left[F_1(t), F_2(t), ..., F_N(t), \frac{1}{m_{h1}} g_1(t), ..., \frac{1}{m_{hN_o}} g_{N_o}(t)\right]_{(N+N_o)} \tag{B.3}$$

For 2-DOF oscillators, $\mathbf{M}$, $\mathbf{C}$ and $\mathbf{K}$ are matrices of size $(N + 2N_o) \times (N + 2N_o)$ and can be represented as

$$\mathbf{M} = \begin{bmatrix} M_1 & 0 & \dots & 0 & 0 & 0 & \dots & 0 \\ 0 & M_2 & \dots & 0 & 0 & 0 & \dots & 0 \\ \vdots & \vdots & \vdots & \vdots & \vdots & \vdots & \vdots & \vdots \\ 0 & 0 & \dots & M_N & 0 & 0 & \dots & 0 \\ 0 & 0 & \dots & 0 & m_{h11} & 0 & \dots & 0 \\ 0 & 0 & \dots & 0 & 0 & m_{h12} & \dots & 0 \\ \vdots & \vdots & \vdots & \vdots & \vdots & \vdots & \vdots & \vdots \\ 0 & 0 & \dots & 0 & 0 & \dots & m_{hN_o1} & 0 \\ 0 & 0 & \dots & 0 & 0 & \dots & 0 & m_{hN_o2} \end{bmatrix} \tag{B.4a}$$

$$\mathbf{C} = \begin{bmatrix} c_{(1,1)} & c_{(1,2)} & \dots & c_{(1,N)} & c_{(1,N+1)} & \dots & c_{(1,N+2N_o)} \\ c_{(2,1)} & c_{(2,2)} & \dots & c_{(2,N)} & c_{(2,N+1)} & \dots & c_{(2,N+2N_o)} \\ \vdots & \vdots & \vdots & \vdots & \vdots & \vdots & \vdots \\ c_{(N,1)} & c_{(N,2)} & \dots & c_{(N,N)} & c_{(N,N+1)} & \dots & c_{(N,N+2N_o)} \\ c_{(N+1,1)} & c_{(N+1,2)} & \dots & c_{(N+1,N)} & c_{(N+1,N+1)} & \dots & c_{(N+1,N+2N_o)} \\ \vdots & \vdots & \vdots & \vdots & \vdots & \vdots & \vdots \\ c_{(N+2N_o,1)} & c_{(N+2N_o,2)} & \dots & c_{(N+2N_o,N)} & c_{(N+2N_o,N+1)} & \dots & c_{(N+2N_o,N+2N_o)} \end{bmatrix} \tag{B.4b}$$

$$\mathbf{K} = \begin{bmatrix} k_{(1,1)} & k_{(1,2)} & \dots & k_{(1,N)} & k_{(1,N+1)} & \dots & k_{(1,N+2N_o)} \\ k_{(2,1)} & k_{(2,2)} & \dots & k_{(2,N)} & k_{(2,N+1)} & \dots & k_{(2,N+2N_o)} \\ \vdots & \vdots & \vdots & \vdots & \vdots & \vdots & \vdots \\ k_{(N,1)} & k_{(N,2)} & \dots & k_{(N,N)} & k_{(N,N+1)} & \dots & k_{(N,N+2N_o)} \\ k_{(N+1,1)} & k_{(N+1,2)} & \dots & k_{(N+1,N)} & k_{(N+1,N+1)} & \dots & k_{(N+1,N+2N_o)} \\ \vdots & \vdots & \vdots & \vdots & \vdots & \vdots & \vdots \\ k_{(N+2N_o,1)} & k_{(N+2N_o,2)} & \dots & k_{(N+2N_o,N)} & k_{(N+2N_o,N+1)} & \dots & k_{(N+2N_o,N+2N_o)} \end{bmatrix} \tag{B.4c}$$

where

$$\begin{gathered} c_{(i,i)} = 2\zeta_i\omega_i M_i + \sum_{k=1}^{N_o} 2\zeta_{hk1}\omega_{hk1}m_{hk1}W_i^2(\xi_k,\eta_k) \\ c_{(i,j)} = \sum_{k=1}^{N_o} 2\zeta_{hk1}\omega_{hk1}m_{hk1}W_i(\xi_k,\eta_k)W_j(\xi_k,\eta_k) \\ c_{(i,N+2k-1)} = -2\zeta_{hk1}\omega_{hk1}m_{hk1}W_i(\xi_k,\eta_k) \\ c_{(N+2k-1,i)} = -2\zeta_{hk1}\omega_{hk1}m_{hk1}W_i(\xi_k,\eta_k) \\ c_{(N+2k-1,N+2k-1)} = 2\zeta_{hk1}\omega_{hk1}m_{hk1} + 2\zeta_{hk2}\omega_{hk2}m_{hk2} \\ c_{(N+2k-1,N+2k)} = -2\zeta_{hk2}\omega_{hk2}m_{hk2} \\ c_{(N+2k,N+2k)} = 2\zeta_{hk2}\omega_{hk2}m_{hk2} \\ c_{(N+2k,N+2k-1)} = -2\zeta_{hk2}\omega_{hk2}m_{hk2} \\ i = 1,2,...,N \qquad i \neq j \leqslant N \end{gathered} \tag{B.5}$$

$$
\begin{aligned}
k_{(i,i)} &= \omega_i^2 M_i + \sum_{k=1}^{N_o} \omega_{hk1}^2 m_{hk1} W_i^2(\xi_k, \eta_k) \\
k_{(i,j)} &= \sum_{k=1}^{N_o} \omega_{hk1}^2 m_{hk1} W_i(\xi_k, \eta_k) W_j(\xi_k, \eta_k) \\
k_{(i,N+2k-1)} &= -\omega_{hk1}^2 m_{hk1} W_i(\xi_k, \eta_k) \\
k_{(N+2k-1,i)} &= -\omega_{hk1}^2 m_{hk1} W_i(\xi_k, \eta_k) \\
k_{(N+2k-1,N+2k-1)} &= \omega_{hk1}^2 m_{hk1} + \omega_{hk2}^2 m_{hk2} \\
k_{(N+2k-1,N+2k)} &= -\omega_{hk2}^2 m_{hk2} \\
k_{(N+2k,N+2k)} &= \omega_{hk2}^2 m_{hk2} \\
k_{(N+2k,N+2k-1)} &= -\omega_{hk2}^2 m_{hk2} \\
k = 1, 2, ..., N_o & \qquad k \neq l \leqslant N_o
\end{aligned}
\tag{B.6}
$$

Elements in $\mathbf{C}$ and $\mathbf{K}$ which are not specified above are zero. The displacement vector $\mathbf{U}$ and the force vector $\mathbf{F}$ are given by

$$
\begin{aligned}
\mathbf{U} &= [q_1(t), q_2(t), ..., q_N(t), z_{11}(t), z_{12}(t), ..., z_{N_o 1}(t), z_{N_o 2}(t)]_{(N+2N_o)} \\
\mathbf{F} &= [F_1(t), F_2(t), ..., F_N(t), g_{11}(t), g_{12}(t), ..., g_{N_o 1}(t), g_{N_o 2}(t)]_{(N+2N_o)}
\end{aligned}
\tag{B.7}
$$

in which

$$
F_n(t) = \int_0^a \int_0^b f(x, y, t) W_n(x, y) dx dy \tag{B.8}
$$

Appendix C

Floor evaluations by static criteria

Table C.1 Comparison of floor acceptability by subjective evaluations and predictions from static criteria for laboratory floors in Wiss et al. (1977).

Floor ID	Span	F	d	Floor acceptability				
	(m)	(Hz)	(mm)	Tested	Onysko	Hu-I	Hu-II	Proposed
A1	6.1	9.4	2.44	M	U	U	U	U
A2	5.49	15.6	1.68	M	U	U	U	U
A3	4.88	14.9	1.49	A	U	U	U	U
B1	6.1	14.2	2.61	U	U	U	U	U
B3	4.88	25.9	1.66	A	U	A	A	A
C	6.1	10.6	0.21	A	A	A	A	A
E1	6.1	16.3	2.21	U	U	U	U	U
E2	5.49	17.7	1.87	M	U	U	U	U
E3	4.88	22.8	1.43	M	U	A	A	A
F	4.88	15.1	2.4	M	U	U	U	U

F–Measured fundamental frequency; d–Measured deflection under 1 kN concentrated load
U–Unacceptable; M–Marginal; A–Acceptable
Hu-I–$F/d^{0.39} > 15.3$ in Hu (2002); Hu-II–$F/d^{0.44} > 18.7$ in Hu and Chui (2004)
Tested–Subjective evaluations

Table C.2 Comparison of floor acceptability by subjective evaluations and predictions from static criteria for laboratory floors in SBI and VTT.

Institute	Floor ID	Span (m)	F (Hz)	d (mm)	Floor acceptability				
					Tested	Onysko	Hu-I	Hu-II	Proposed
SBI	SBI-1a	4.27	14.2	0.42	U	A	A	A	A
	SBI-1b	5.87	12.8	0.9	U	U	U	U	U
	SBI-2a	4.27	17.5	0.09	A	A	A	A	A
	SBI-2b	5.87	11.4	0.2	U	A	A	A	A
VTT	VP1-a	7	11.81	0.97	U	U	U	U	U
	VP1-b	7.8	10.18	1.22	U	U	U	U	U
	VP1-c	8.8	8.1	1.55	U	U	U	U	U
	VP2-a	7	12.09	0.55	A	A	U	U	U
	VP2-b	7.8	10.7	0.69	U	U	U	U	U
	VP2-c	8.8	8.76	0.85	U	U	U	U	U
	VP3-a	7	11.97	0.24	A	A	A	U	A
	VP3-b	7.8	10.34	0.29	A	A	A	U	A
	VP3-c	8.8	8.12	0.35	A	A	U	U	U

F–Measured fundamental frequency; d–Measured deflection under 1 kN concentrated load

U–Unacceptable; A–Acceptable

Hu-I–$F/d^{0.39} > 15.3$ in Hu (2002); Hu-II–$F/d^{0.44} > 18.7$ in Hu and Chui (2004)

Tested–Subjective evaluations

Table C.3 Comparison of floor acceptability by subjective evaluations and predictions from static criteria for laboratory floors in Kraus (1997).

Floor ID	Parameters	Span	F	d	Floor acceptability				
		(m)	(Hz)	(mm)	Tested	Onysko	Hu-I	Hu-II	Proposed
8A	Blocking	4.191	20.300	2.286	U	U	U	U	U
	Drywall	4.191	16.200	1.803	U	U	U	U	U
8B	Strap	3.731	17.200	1.778	U	U	U	U	U
	Blocking	3.731	17.400	1.727	U	U	U	U	U
8C	Strap	3.276	29.200	1.372	A	A	A	A	A
	Blocking	3.276	29.000	1.270	A	A	A	A	A
8D	Strap	2.692	32.900	0.965	A	A	A	A	A
	Blocking	2.692	31.400	1.245	A	A	A	A	A
8E	Strap	2.160	37.200	0.305	A	A	A	A	A
	Blocking	2.160	35.600	0.635	A	A	A	A	A
10C	Strap	4.648	24.000	1.168	U	U	A	A	A
	Blocking	4.648	22.000	1.041	U	A	A	A	A
	Drywall	4.648	20.500	1.219	U	U	A	A	A
10D	Strap	3.988	24.300	0.991	U	A	A	A	A
	Blocking	3.988	25.000	1.295	M	A	A	A	A
12A	Strap	5.969	19.100	1.549	M	U	A	U	U
12B	Strap	5.334	20.200	0.991	U	U	A	A	A
	Blocking	5.334	20.600	1.143	M	U	A	A	A
12C	Strap	4.930	23.600	1.118	M	U	A	A	A
	Blocking	4.930	22.600	1.041	M	U	A	A	A
12D	Strap	4.290	27.000	1.016	M	A	A	A	A
	Blocking	4.290	26.500	0.940	M	A	A	A	A
12E	Strap	3.430	29.300	0.483	A	A	A	A	A
	Blocking	3.430	28.500	0.635	A	A	A	A	A

F–Measured fundamental frequency; d–Measured deflection under 1 kN concentrated load

U–Unacceptable; M–Marginal; A–Acceptable

Hu-I–$F/d^{0.39} > 15.3$ in Hu (2002); Hu-II–$F/d^{0.44} > 18.7$ in Hu and Chui (2004)

Tested–Subjective evaluations

Table C.4 Comparison of floor acceptability by subjective evaluations and predictions from static criteria for laboratory floors in Liu (2001).

Floor ID	Span	F	d	Floor acceptability				
	(m)	(Hz)	(mm)	Tested	Onysko	Hu-I	Hu-II	Proposed
fl-6.754-2-6-1/5-B0-S12-2b	6.754	10.500	1.886	U	U	U	U	U
fl-6.754-2-6-1/5-B2-S12-2b	6.754	10.600	1.863	U	U	U	U	U
fl-6.754-2-6-1/5-B0-S6-2b	6.754	10.500	1.689	U	U	U	U	U
fl-6.754-2-6-1/5-B2-S6-2b	6.754	10.700	1.596	U	U	U	U	U
fl-6.754-2-6-1/1-B0-S12-2b	6.754	10.650	1.615	U	U	U	U	U
fl-6.754-2-6-1/5-B0-S6-2b-Ce	6.754	9.700	1.278	U	U	U	U	U
fl-6.754-2-6-1/5-B2-S6-2b-Ce	6.754	9.900	1.234	U	U	U	U	U
fl-6.754-2-6-1/5-B2-S6-2b-g	6.754	11.100	1.571	U	U	U	U	U
fl-6.114-2-6-1/5-B0-S12-2b	6.114	12.970	1.483	U	U	U	U	U
fl-6.114-2-6-1/5-B2-S12-2b	6.114	13.550	1.452	U	U	U	U	U
fl-6.114-2-6-1/5-B0-S6-2b	6.114	12.800	1.359	U	U	U	U	U
fl-6.114-2-6-1/5-B2-S6-2b	6.114	13.240	1.334	U	U	U	U	U
fl-6.114-2-6-1/1-B0-S6-2b	6.114	12.900	1.160	U	U	U	U	U
fl-6.114-2-6-1/1-B2-S6-2b	6.114	13.400	1.121	U	U	U	U	U
fl-6.114-2-6-1/5-B0-S6-2b-Ce	6.114	11.900	1.163	M	U	U	U	U
fl-6.114-2-6-1/5-B2-S6-2b-ce	6.114	12.300	1.040	M	U	U	U	U
fl-6.114-2-6-1/5-B2-S6-2b-g-Ce	6.114	12.400	0.911	M	U	U	U	U
fl-6.114-2-6-1/5-B2-S6-2b-g	6.114	13.500	1.304	U	U	U	U	U

F–Measured fundamental frequency; d–Measured deflection under 1 kN concentrated load

U–Unacceptable; M–Marginal

Hu-I–$F/d^{0.39} > 15.3$ in Hu (2002); Hu-II–$F/d^{0.44} > 18.7$ in Hu and Chui (2004)

Tested–Subjective evaluations

Table C.5 Comparison of floor acceptability by subjective evaluations and predictions from static criteria for field floors in Kraus (1997).

Floor ID	Span (m)	F (Hz)	d (mm)	Floor acceptability				
				Tested	Onysko	Hu-I	Hu-II	Proposed
S1LR	4.7752	22.5	0.3048	A	A	A	A	A
S1FYR	3.6449	/	0.2286	/	A	/	/	/
S1MBR	3.6322	27.25	/	A	/	/	/	/
S1GR	4.7752	13	0.254	A	A	A	A	A
S1BR#3	4.7752	17.5	/	A	/	/	/	/
S1BR#4	4.7752	17.5	/	A	/	/	/	/
S2DIN	4.9784	19.3	0.6858	A	A	A	A	A
S2LR	4.7752	14.5	0.635	A	A	A	U	A
S2MBR	5.4864	15.5	1.3716	A	U	U	U	U
S3LR	4.1656	25.5	/	A	/	/	/	/
S3BR	3.2004	11.5	/	U	/	/	/	/

/–not available; U–Unacceptable; A–Acceptable
F–Measured fundamental frequency; d–Measured deflection under 1 kN concentrated load
Hu-I–$F/d^{0.39} > 15.3$ in Hu (2002); Hu-II–$F/d^{0.44} > 18.7$ in Hu and Chui (2004)
Tested–Subjective evaluations

Table C.6 Comparison of floor acceptability by subjective evaluations and predictions from static criteria for field floors by CCFSRG.

References	Floor ID	Span (m)	F (Hz)	d (mm)	Floor acceptability				
					Tested	Onysko	Hu-I	Hu-II	Proposed
[1]	iSPAN	5.45	20.3	0.36	A	A	A	A	A
[2]	House 1 lot 9	5.91	18	0.97	U	U	A	U	A
		5.3	14.9	1.2	U	U	U	U	U
	House 2 lot 15	5.09	15.4	0.91	U	A	A	U	A
[3]	CG601	5.33	14.4	0.46	A	A	A	A	A
	CG604	4.51	16.3	0.28	A	A	A	A	A
	CGMH6	5.12	15.7	0.36	A	A	A	A	A
[4]	DDG1	6	12	0.39	A	A	A	U	A
	DDG2	6	14	0.37	A	A	A	A	A
	DDG3	6	13.2	0.2	A	A	A	A	A
	DDG4	6	16.1	0.08	A	A	A	A	A

[1]–Xu (2005); [2]–Xu and Tangorra (2007); [3]–Parnell et al. (2009); [4]–Parnell (2008)
F–Measured fundamental frequency; d–Measured deflection under 1 kN concentrated load
U–Unacceptable; A–Acceptable
Hu-I–$F/d^{0.39} > 15.3$ in Hu (2002); Hu-II–$F/d^{0.44} > 18.7$ in Hu and Chui (2004)
Tested–Subjective evaluations

Appendix D

Floor evaluations by proposed static and impulsive criteria

Table D.1 Comparisons of floor acceptability by subjective evaluations with predictions from proposed criteria for laboratory floors in Kraus (1997).

Floor	Parameters	F (Hz)	ζ^*	M_1 (kg)	d (mm)	I_F (m/s^2)	Subjective evaluations	Proposed criteria	
								Static	Impulsive
8A	Blocking	20.300	0.010	82.437	2.286	0.938	U	U	U
	Drywall	16.200	0.015	82.437	1.803	0.728	U	U	U
8B	Strap	17.200	0.010	82.437	1.778	0.923	U	U	U
	Blocking	17.400	0.010	73.389	1.727	0.933	U	U	U
10C	Strap	24.000	0.010	39.451	1.168	0.929	U	A	A
	Blocking	22.000	0.010	96.199	1.041	0.864	U	A	A
	Drywall	20.500	0.015	96.199	1.219	0.757	U	A	U
12A	Strap	19.100	0.010	82.539	1.549	0.522	M	U	U
12B	Strap	20.200	0.010	141.856	0.991	0.608	U	A	A
	Blocking	20.600	0.010	126.765	1.143	0.618	M	A	A
12C	Strap	23.600	0.010	126.765	1.118	0.756	M	A	A
	Blocking	22.600	0.010	117.163	1.041	0.724	M	A	A

F–Measured fundamental frequency; ζ–Damping ratio; M_1–Modal mass of the first mode;
d–Measured deflection under 1 kN concentrated load; I_F–Floor impulsive factors
U–Unacceptable; M–Marginal; A–Acceptable
$*$–the damping ratio are assumed based on the floor configuration.

Table D.2 Comparisons of floor acceptability by subjective evaluations with predictions from proposed criteria for laboratory floors in Wiss et al. (1977), SBI and VTT.

Test	Floor ID	F (Hz)	ζ^*	M_1 (kg)	d (mm)	I_F (m/s^2)	Subjective evaluations	Proposed criteria	
								Static	Impulsive
Wiss	A1	9.400	0.010	134.531	2.440	0.294	M	U	U
	A2	15.600	0.010	121.078	1.680	0.514	M	U	U
	A3	14.900	0.010	107.625	1.490	0.551	A	U	U
	B1	14.200	0.010	130.895	2.610	0.431	U	U	U
	C	10.600	0.020	868.996	0.210	0.046	A	A	U
	E1	16.300	0.010	149.075	2.210	0.428	U	U	U
	E2	17.700	0.010	134.167	1.870	0.517	M	U	U
	E3	22.800	0.010	119.260	1.430	0.718	M	A	A
	F	15.100	0.010	95.989	2.400	0.628	M	U	U
SBI	SBI-1a	14.200	0.015	269.010	0.420	0.200	U	A	U
	SBI-1b	12.800	0.015	369.810	0.900	0.133	U	U	U
	SBI-2a	17.500	0.030	538.020	0.090	0.102	A	A	A
	SBI-2b	11.400	0.030	739.620	0.200	0.054	U	A	A
VTT	VP1-a	11.810	0.033	650.720	0.970	0.062	U	U	A
	VP1-b	10.180	0.040	743.680	1.220	0.046	U	U	U
	VP2-a	12.090	0.017	862.400	0.550	0.053	A	U	A
	VP2-b	10.700	0.021	985.600	0.690	0.041	U	U	A
	VP3-a	11.970	0.018	1332.800	0.240	0.034	A	A	A
	VP3-b	10.340	0.018	1523.200	0.290	0.026	A	A	A

F–Measured fundamental frequency; ζ–Damping ratio; M_1–Modal mass of the first mode;
d–Measured deflection under 1 kN concentrated load; I_F–Floor impulsive factors
U–Unacceptable; M–Marginal; A–Acceptable
$*$–the damping ratio are assumed based on the floor configuration except the floors of VTT

Table D.3 Comparisons of floor acceptability by subjective evaluations with predictions from proposed criteria for laboratory floors in Liu (2001).

Floor ID	F (Hz)	ζ	M_1 (kg)	d (mm)	I_F (m/s^2)	Subjective evaluations	Proposed criteria	
							Static	Impulsive
fl-6.754-2-6-1/5-B0-S12-2b	10.500	0.019	190.818	1.886	0.209	U	U	U
fl-6.754-2-6-1/5-B2-S12-2b	10.600	0.021	190.818	1.863	0.208	U	U	U
fl-6.754-2-6-1/5-B0-S6-2b	10.500	0.022	190.818	1.689	0.205	U	U	U
fl-6.754-2-6-1/5-B2-S6-2b	10.700	0.021	190.818	1.596	0.210	U	U	U
fl-6.754-2-6-1/1-B0-S12-2b	10.650	0.017	190.818	1.615	0.215	U	U	U
fl-6.754-2-6-1/5-B0-S6-2b-Ce	9.700	0.022	262.351	1.278	0.142	U	U	U
fl-6.754-2-6-1/5-B2-S6-2b-Ce	9.900	0.021	262.351	1.234	0.144	U	U	U
fl-6.754-2-6-1/5-B2-S6-2b-g	11.100	0.015	190.818	1.571	0.230	U	U	U
fl-6.114-2-6-1/5-B0-S12-2b	12.970	0.016	173.464	1.483	0.286	U	U	U
fl-6.114-2-6-1/5-B2-S12-2b	13.550	0.017	173.464	1.452	0.296	U	U	U
fl-6.114-2-6-1/5-B0-S6-2b	12.800	0.013	173.464	1.359	0.289	U	U	U
fl-6.114-2-6-1/5-B2-S6-2b	13.240	0.013	173.464	1.334	0.301	U	U	U
fl-6.114-2-6-1/1-B0-S6-2b	12.900	0.012	173.464	1.160	0.295	U	U	U
fl-6.114-2-6-1/1-B2-S6-2b	13.400	0.011	173.464	1.121	0.311	U	U	U
fl-6.114-2-6-1/5-B0-S6-2b-Ce	11.900	0.014	244.998	1.163	0.191	M	U	U
fl-6.114-2-6-1/5-B2-S6-2b-ce	12.300	0.013	244.998	1.040	0.197	M	U	U
fl-6.114-2-6-1/5-B2-S6-2b-g-Ce	12.400	0.012	244.998	0.911	0.200	M	U	U
fl-6.114-2-6-1/5-B2-S6-2b-g	13.500	0.011	173.464	1.304	0.313	U	U	U

F–Measured fundamental frequency; ζ–Damping ratio; M_1–Modal mass of the first mode;
d–Measured deflection under 1 kN concentrated load; I_F–Floor impulsive factors
U–Unacceptable; M–Marginal; A–Acceptable

Table D.4 Comparisons of floor acceptability by subjective evaluations with predictions from proposed criteria for field floors in Parnell (2008) and Davis (2008).

Floor ID	F (Hz)	ζ	M_1 (kg)	d (mm)	I_F (m/s^2)	Subjective evaluations	Proposed criteria	
							Static	Impulsive
CG601	14.4	0.036	466.5276	0.46	0.0965	A	A	A
CG604	16.3	0.042	499.1868	0.28	0.0934	A	A	A
CG805	15.2	0.036	1107.464	/	0.0425	A	/	A
CGMH6	15.7	0.073	736.8732	0.36	0.0501	A	A	A
CGMH7	16.6	0.062	736.8732	/	0.0552	A	/	A
CW707	16.1	0.038	952.0721	/	0.0503	A	/	A
CW708	18.7	0.036	907.767	/	0.0593	A	/	A
CW709	9.9	0.038	1297.069	/	0.0262	A	/	A
CW805	11.9	0.050	1149.196	/	0.0313	A	/	A
OK401	22.3	0.045	1101.454	/	0.0499	A	/	A
OK402	23.7	0.060	1101.454	/	0.0455	A	/	A

F–Measured fundamental frequency; ζ–Damping ratio; M_1–Modal mass of the first mode;
d–Measured deflection under 1 kN concentrated load; I_F–Floor impulsive factors
U–Unacceptable; M–Marginal; A–Acceptable
/–not available

Table D.5 Comparisons of floor acceptability by subjective evaluations with predictions from proposed criteria for wood floors in Hu (2000).

Test	Floor ID	F (Hz)	ζ^*	$M_1^\star$ (kg)	d (mm)	I_F (m/s^2)	Subjective evaluations	Proposed criteria	
								Static	Impulsive
Field	newf5	16.8	0.035	256.693	0.880	0.197	A	A	A
	newf6	20.5	0.030	173.760	0.170	0.349	A	A	A
	newf7	13.3	0.050	678.627	0.540	0.057	A	A	A
	newf8	17.0	0.040	258.582	0.510	0.189	A	A	A
	newf9	10.1	0.040	258.107	1.610	0.131	U	U	U
	newf10	13.5	0.035	127.949	0.450	0.342	A	A	U
	newf11	10.7	0.035	307.872	0.680	0.119	U	U	U
	newf15	10.5	0.035	428.563	0.870	0.084	U	U	U
	newf16	10.1	0.040	427.873	1.010	0.079	U	U	U
	newf17	11.4	0.035	428.563	0.850	0.090	U	U	U
	newf18b	16.1	0.030	1526.080	0.320	0.034	A	A	A
	newf18c	15.1	0.030	1526.080	0.270	0.032	A	A	A
	newf18d	15.4	0.040	403.273	0.700	0.114	A	A	A
Lab	I-F2a	8.5	0.030	147.544	1.960	0.211	U	U	U
	I-F2b	9.1	0.030	147.544	1.360	0.227	U	U	U
	TR-Fa	11.2	0.030	128.124	2.080	0.309	U	U	U
	TR-Fb	11.5	0.030	128.124	1.120	0.315	U	U	U
	TR-Fc	11.5	0.030	128.124	0.970	0.315	U	U	U
	TR-Fd	11.6	0.030	128.124	1.270	0.317	U	U	U
	TR-Fe	9.2	0.030	330.532	0.590	0.103	U	U	U
	IF1b	14.3	0.030	99.105	1.630	0.475	U	U	U
	IF1g	11.3	0.040	218.063	0.810	0.170	U	U	U
	IF2lc	9.8	0.050	396.459	0.460	0.079	U	U	U
	IF3nc	22.9	0.030	146.521	0.970	0.446	A	A	A
	IF3b	12.2	0.050	674.081	0.300	0.054	A	A	A
	IF4b	15.5	0.030	227.074	1.270	0.222	U	U	U
	IF4nc	8.0	0.050	1044.671	0.530	0.026	U	U	U

F–Measured fundamental frequency; ζ–Damping ratio; M_1–Modal mass of the first mode;
d–Measured deflection under 1 kN concentrated load; I_F–Floor impulsive factors
U–Unacceptable; A–Acceptable
$*$–the damping ratio are assumed based on the floor configuration
$\star$–modal mass of field floors includes a 0.25 kpa live load